1 OF 4

ADA080486

REPORT 15068.2

COMMUNICATIONS DATA BASE ANALYSIS FOR MILITARY
OPERATIONS IN A BUILT-UP AREA (MOBA/COBA)

DR. LEONARD EHRMAN
DR. ALFONSO MÁLAGA
DR. FREDRIC ZIOLKOWSKI

SIGNATRON, INC.
12 HARTWELL AVENUE
LEXINGTON, MASSACHUSETTS 02173

9 AUGUST 1979

80

DISCLAIMER NOTICE

THIS DOCUMENT IS BEST QUALITY PRACTICABLE. THE COPY FURNISHED TO DDC CONTAINED A SIGNIFICANT NUMBER OF PAGES WHICH DO NOT REPRODUCE LEGIBLY.

The findings of this Report are not to be
construed as an official Department of the
Army position, unless so designated by
other authorized documents.

ii

REPORT DOCUMENTATION PAGE		READ INSTRUCTIONS BEFORE COMPLETING FORM
1. REPORT NUMBER	2. GOVT ACCESSION NO.	3. RECIPIENT'S CATALOG NUMBER
4. TITLE (and Subtitle) Communications Data Base Analysis for Military Operations in a Built-up Area (MOBA/COBA)		5. TYPE OF REPORT & PERIOD COVERED Final Report 4/18/77 - 9/8/79
		6. PERFORMING ORG. REPORT NUMBER A223F
7. AUTHOR(s) Dr. Leonard Ehrman Dr. Alfonso Malaga Dr. Fredric Ziolkowski		8. CONTRACT OR GRANT NUMBER(s) DAAG29-77-C-0020
9. PERFORMING ORGANIZATION NAME AND ADDRESS SIGNATRON, Inc. 12 Hartwell Avenue Lexington, Massachusetts 02173		10. PROGRAM ELEMENT, PROJECT, TASK AREA & WORK UNIT NUMBERS N/A
11. CONTROLLING OFFICE NAME AND ADDRESS U.S. Army Research Office Post Office Box 12211 Research Triangle Park, NC 27709		12. REPORT DATE 9 August 1979
		13. NUMBER OF PAGES 386
14. MONITORING AGENCY NAME & ADDRESS(if different from Controlling Office) SAME		15. SECURITY CLASS. (of this report) Unclassified
		15a. DECLASSIFICATION DOWNGRADING SCHEDULE N/A

16. DISTRIBUTION STATEMENT (of this Report)

Approved for Public Release; distribution unlimited

17. DISTRIBUTION STATEMENT (of the abstract entered in Block 20, if different from Report)

N/A

18. SUPPLEMENTARY NOTES

The findings in this report are not to be construed as an official Department of the Army position unless so designated by other authorized documents.

19. KEY WORDS (Continue on reverse side if necessary and identify by block number)

MOBA
COBA
UHF Radio Communications
VHF Radio Communications
Mobile Radio Communications
Active Antennas

20. ABSTRACT (Continue on reverse side if necessary and identify by block number)

This report concludes a two-year investigation into the limitations of VHF/UHF radio communications during military operations in a built-up area (MOBA/COBA). VHF/UHF propagation measurements, made in a suburban and an urban area, are presented and analyzed. A prediction model for mobile radio path loss in built-up areas when using ground level antennas is presented. Data are also given for path loss

DD FORM 1473 EDITION OF 1 NOV 65 IS OBSOLETE

within and between buildings. Space and field diversity measurement data are given and correlation coefficients are analyzed. An approach to active antenna design is presented.

Accession For		
NTIS GRA&I		☑
DDC TAB		
Unannounced		
Justification		
By		
Distribution		
Availability		
Dist	Avail and/or special	
A	23 CP	

FOREWORD

EXECUTIVE SUMMARY

This report, along with the Interim Report [1] issued by SIGNATRON in 1977, constitutes the Final Report on Contract DAAG29-77-C-0020, "Communications Data Base Analysis for Military Operations in a Built-Up Area (MOBA/COBA)". The objectives of this study were, broadly, (i) to assess the state-of-the-art for radio communications in built-up areas; (ii) to determine the capabilities of the military to maintain reliable communications in built-up areas; and (iii) recommend further research efforts with the goal of improved military communications. In performing (i) through (iii), we found that information concerning propagation between low-height antennas in a MOBA environment was not available in the current data base. We also determined that the most significant single means of improving MOBA radio performance is to utilize diversity reception. We therefore embarked on an experimental program to measure and analyze low-height antenna MOBA propagation at VHF and UHF, and to determine feasible means of implementing diversity reception.

The experimental program consisted of propagation measurements at three frequencies, namely 27 MHz, 49.8 MHz, and 446 MHz. The measurements were made in an urban area, Boston, Massachusetts, and in a suburban area, Lexington, Massachusetts. At each frequency, measurements were made of:

 a.   street-to-street path loss between low elevation (~5 ft) antennas

 b.   street-to-building path loss

c. building-to-building path loss

d. intrabuilding path loss

e. correlation between signals received on two
    whip antennas spaced a half-wavelength apart.

In addition, at 27 MHz and 49.8 MHz, measurements were
made of

f. correlation between signals received on
    collocated whip and loop antennas.

The most significant results, from an operational
viewpoint, are as follows:

a. The maximum transmission range (with typical Army
    radios) in either an urban or a suburban environ-
    ment is approximately one mile. In order to
    achieve this, one or possibly both of the radios
    must be in the middle of the street. If both
    radios are on the sidewalk, surrounded by high
    buildings, the maximum range can be as low as
    500 feet at VHF, while UHF cannot be received
    unless the two radios are in line-of-sight of
    each other.

b. Short distance (100 meters) street-to-building
    communications can be reliably established at
    VHF and UHF as long as the radio inside the
    building is not too far in the building interior.
    When the radio is deep in the building, low VHF
    is superior to UHF or high VHF.

c. Building-to-building communications cannot be
    reliably established at either VHF or UHF unless
    one of the radios is near a window facing the
    other building.

d. Communications can be reliably established at both VHF and UHF between nearly any floors in a building providing the radios are in a stairwell or near an elevator shaft. Communications are possible, although with a higher path loss, away from stairwells and shafts, as well as between the lower floor and the basement. Of the three frequencies used, 49.8 MHz had the best performance, i.e., least path loss, in between-floor tests.

e. The communications range along corridors in a building is dependent on the corridor geometry and interior wall construction. UHF is superior to VHF in straight corridors, but has a greater path loss when the corridors have corners. The VHF range may be as great as 100 meters in a cinder block or concrete-walled corridor, and reduced by a factor of two to four in a gypsum walled corridor.

f. When either the receiver on the transmitter is moved, the received signal level will vary according to the Rayleigh probability distribution. Correlation measurements made with collocated whip and loop antennas, as well as whip antennas separated by 0.5 wavelengths, show sufficient decorrelation such that a dual diversity MOBA radio would have its range increased by a factor of 1.4 to 1.8.

The most significant results from a technical viewpoint are concerned with models of the transmission loss for low elevation antennas at VHF and UHF. This model extends the

usefulness of the Okumura model [2], and is in excellent
numerical agreement with it at 446 MHz. The model is
easier to use than the Okumura model, and is similar in
certain respects to the Allsebrook/Parsons model [3].
Our model takes the form:

$$L = L_p(d) + L_D(f) - H_t(h_t,f) - H_r(h_r,f) +$$

$$K_{u,s}(f,d) + L_b(f)$$

where

$L_p(d)$ is the plane-earth path loss between
two 2-meters high antennas

$L_D(f)$ is an environmental clutter factor
which varies with frequency. Our
estimate of this factor from our
data is shown in Figure 3.3-7.

$H_t(h_t,f)$ and $H_r(h_r,f)$ are the classical antenna
height-gain factors relative to a
2-meter antenna

$K_{u,s}(f,d)$ is a highly-built-up (urban) or
medium-built-up (suburban or along-
street urban) correction factor.
The urban correction factor K_u is
frequency independent but varies
depending on the transmitter
and receiver locations. The medium-
built-up area correction factor K_s
also applies to transmission along
urban streets and varies with fre-
quency. Our estimate of this factor
from our data is shown in Figure 3.3-9.
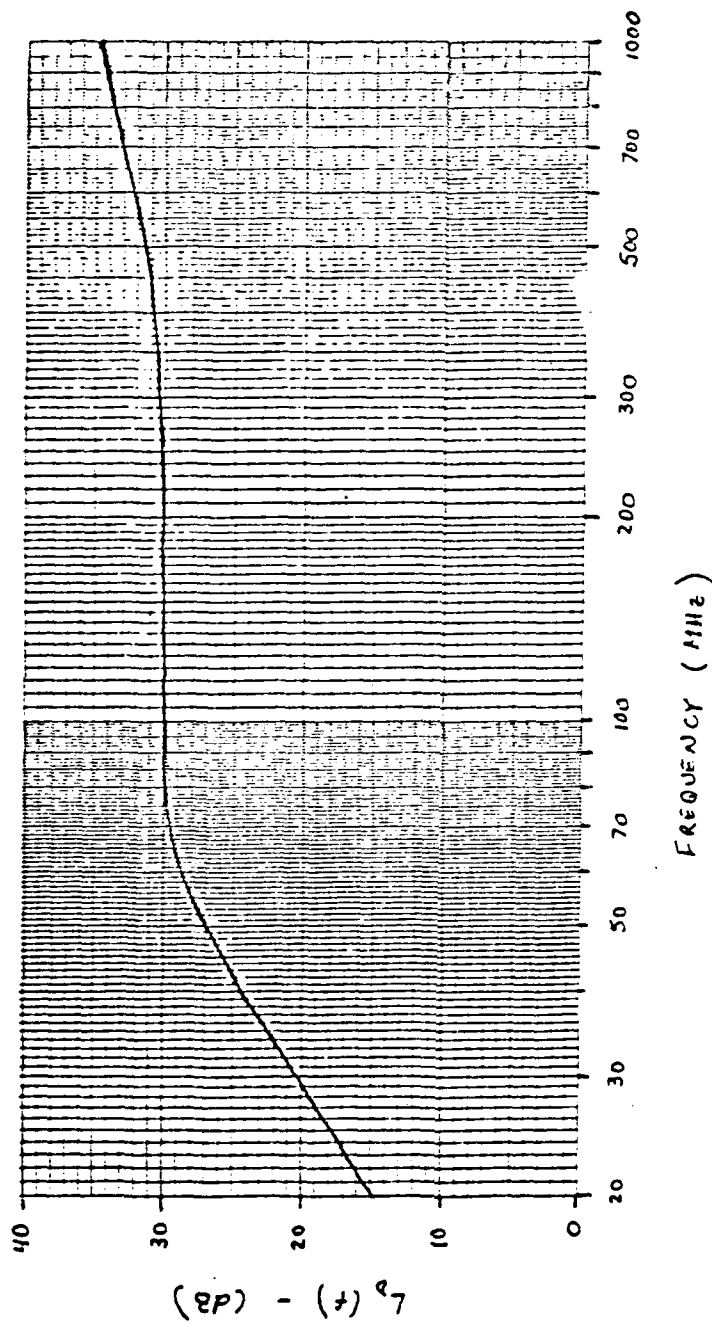
<center>x</center>

FIGURE 3.3-7   Environmental Clutter Factor for VHF and UHF Propagation
in Built-up Areas (Poorly Conducting Soil) and for
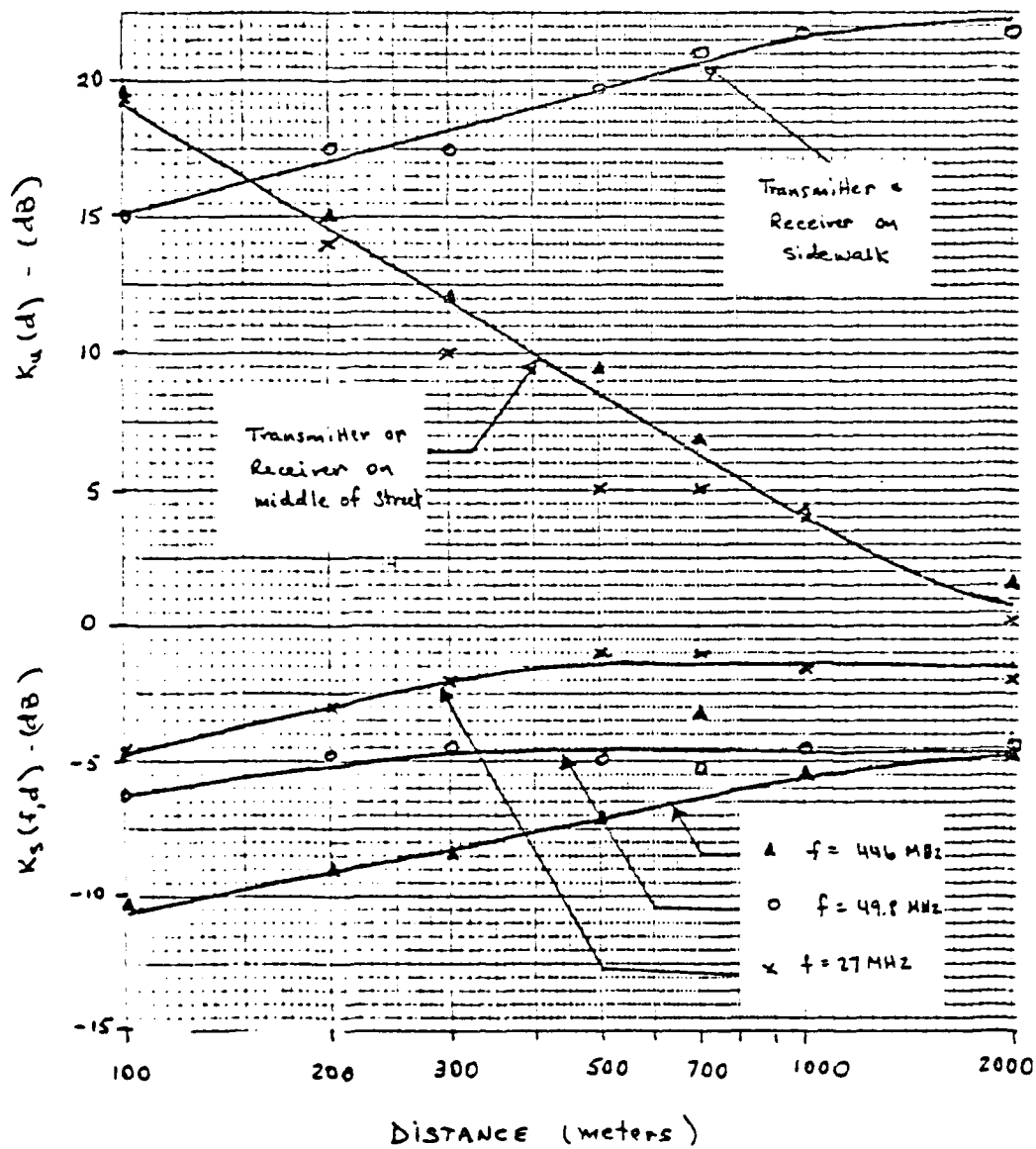Antenna Heights of 2 Meters (from SIGNATRON Data)

FIGURE 3.3-9   Urban (K_u) and Suburban (K_s) Correction Factors
              (from SIGNATRON Data)

The theoretical plane-earth path loss increases at a rate of 40 dB per decade of separation between the transmitter and receiver. Figure 3.3-6 shows the average path loss measured by SIGNATRON at 27 MHz, 49.8 MHz, and 446 MHz. All of our experimental data were used to compute these losses; the 27 MHz and 49.8 MHz data include both in-street and on-sidewalk measurements, while the 446 MHz data are for in-street measurements only. In all cases, the data are seen to show the theoretical 40 dB/decade slope. Also shown on the figure is a point from Okumura's model for the urban path loss at 446 MHz and 1 kM separation. Our measurement differs from his prediction by 1.4 dB. Therefore our model can be used to smoothly extend the Okumura model to VHF propagation at distances less than 1 km.

Based on the results of this program, two recommendations were made. First, a development program should be started to build and test a VHF diversity receiver using an active loop antenna as the auxiliary antenna. Second, a research program should be started to determine means of extending the range of MOBA radio communications. This should include consideration of relay techniques, externally deployed antennas, and the use of other frequencies, most notably HF.
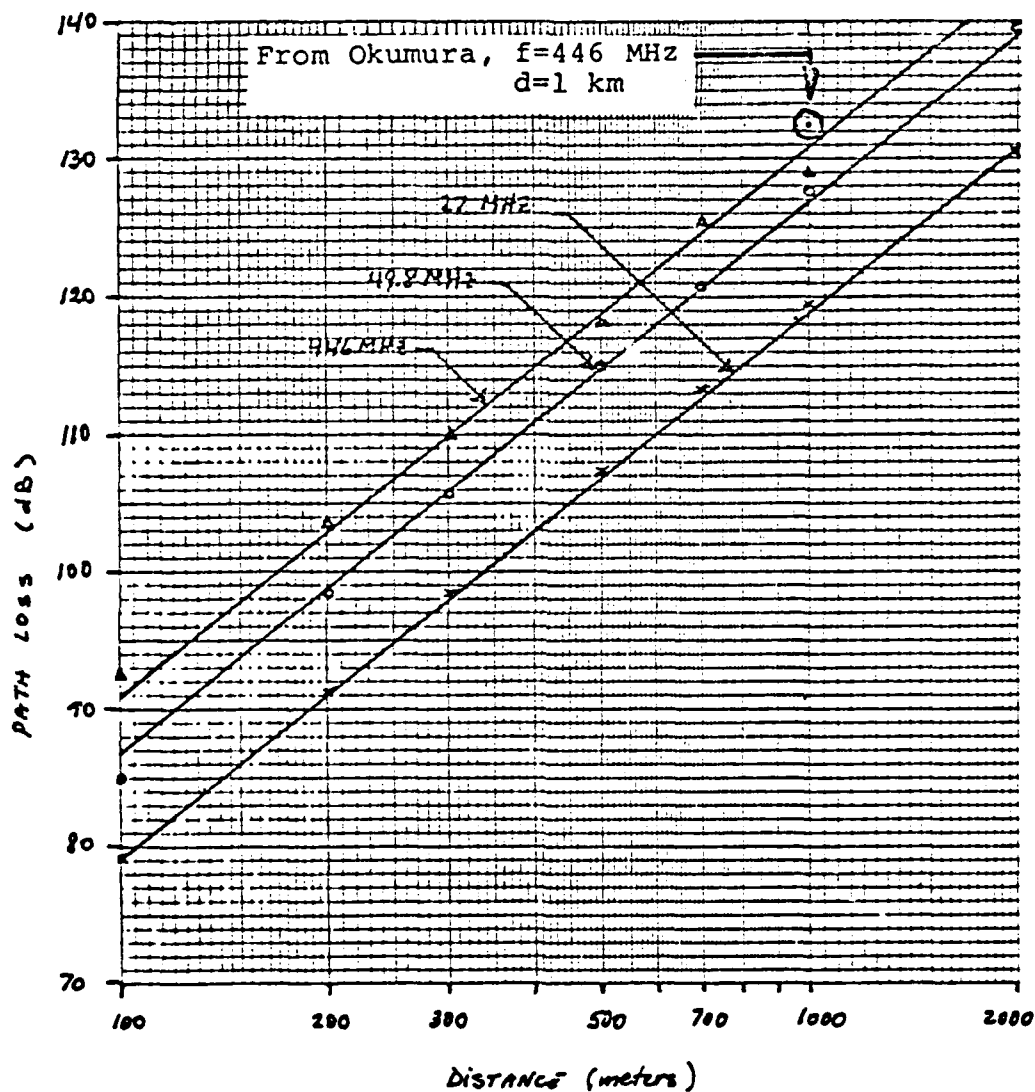
FIGURE 3.3-6   SIGNATRON Data for the Average Path Loss
at 27 MHz, 49.8 MHz, and 446 MHz in Built-
up Areas

References for Executive Summary

[1]   Ehrman, L., S. Parl, "Communications Data Base
        Analysis for Military Operations in a Built-up
        Area (MOBA/COBA)", Interim Report for Period
        18 Apr 1977 - 9 Dec 1977, Report 15068.1, Con-
        tract DAAG29-77-C-0020, SIGNATRON, Inc.,
        9 Dec 1977.

[2]   Okumura, Y., E. Ohmori, T. Kawano, K. Fukuda,
        "Field Strength and Its Variability in VHF
        and UHF Land-Mobile Radio Service", Review
        of the Electrical Communication Laboratory,
        Tokyo, Vol. 16, Nos. 9-10, Sep-Oct 1968,
        pp 825-873.

[3]   Allsebrook, K., J.D. Parsons, "Mobile Radio
        Propagation in British Cities at Frequencies
        in the VHF and UHF Bands", IEEE Trans. Vehic.
        Tech., Vol. VT-26, No. 4, pp 313-323, 1977.

TABLE OF CONTENTS

TABLE OF CONTENTS (CONT)

TABLE OF CONTENTS (CONT)

LIST OF ILLUSTRATIONS

LIST OF ILLUSTRATIONS (CON'T)

LIST OF ILLUSTRATIONS (CON'T)

LIST OF ILLUSTRATIONS (CON'T)

LIST OF ILLUSTRATIONS (CON'T)

LIST OF ILLUSTRATIONS (CON'T)

LIST OF ILLUSTRATIONS (CON'T)

LIST OF ILLUSTRATIONS (CON'T)

LIST OF ILLUSTRATIONS (CON'T)

LIST OF ILLUSTRATIONS (CON'T)

LIST OF TABLES

LIST OF TABLES (CON'T)

SECTION 1

INTRODUCTION AND SUMMARY

1.1   Introduction

This document is the final report on Contract DAAG29-77-C-0020, "Data Base Analysis for Military Operations in a Built-Up Area (MOBA)". The background of this work is as follows. Military operations have classically taken place in open areas, and tactical radio communication systems have been developed to work in that type of environment. It has been found that when conducting military operations in a built-up area (MOBA), radio communications become erratic, with even short distance communications being impaired. A considerable body of literature on VHF and UHF radio transmission and propagation in the urban environment is in existence. However, no compilation or analysis of the operational impact of this data base had been performed prior to this study.

The objectives of SIGNATRON's study were originally to review and expand the data base and (i) assess the state-of-the-art for communications in built-up areas; (ii) determine the capabilities of the military to maintain reliable communications in built-up areas; and (iii) recommend further research efforts with the goal of improved military communications. All of these objectives have been fulfilled and are documented in our Interim Report 15068.1: "Communications Data Base Analysis for Military Operations in a Built-Up Area (MOBA/COBA)". In the course of our research we discovered certain data to be lacking in the existing MOBA data base. We also determined that the most significant single means of improving MOBA radio performance is to utilize diversity reception. The objective of the present contract to SIGNATRON was to gather the lacking data, perform diversity propagation research measurements, and analyze the results so that they could be used to augment the existing data base and give direction to future MOBA radio development. The current program

consisted of MOBA data base augmentation, MOBA data base up-
dating and research for long-term improvements.

i)   MOBA Data Base Augmentation

The MOBA data base which we reviewed in the original
study has two shortcomings. First, the data were primarily taken
with elevated base-station antennas. Secondly, there is little
quantitative information concerning building-to-building, short-
distance street-to-street, and street-to-building propagation.
Thus, the present contract was intended to allow us to perform
experiments to acquire data in the VHF and UHF bands which would
fill in the gaps in the existing data base. The data reduction
and analysis were designed so that the results would be similar
in form to those of the existing data base, e.g., Okumura,
allowing them to be used in a unified propagation analysis.

ii)   MOBA Data Base Updating

A significant data base was established and analyzed
in the interim report. As part of the continuing effort the
technical literature was monitored, on an on-going basis,
and the data base periodically updated. In addition, contact
was made with researchers in other countries, in order to
obtain the most recent and unpublished results for inclusion in
the data base.

iii)   Research for Long-Term Performance Improvement

A primary conclusion of the data base analysis was
that MOBA radio communications can be best improved by use of
diversity. We recommend two techniques which require neither
transmitter modification nor extra frequency allocation. These
are polarization or field diversity and space diversity. Thus
a diversity measurement program was included in our MOBA
data base augmentation experiments. The purpose of these measure-
ments was to determine the strength and correlation of the
signals received on space diversity receiving antennas and on
two field diversity receiving antennas, thereby providing a
MOBA diversity data base.

Antenna development was included as part of the
experimental program. The original study indicated that space
diversity would be more practical and desirable at UHF than at
VHF, and that field diversity using vertically polarized whip
and loop antennas would be the most practical means of achieving
diversity with manpack radios at VHF. The correlation data was
analyzed to give the performance of a selection diversity combiner.

All of these objectives have been met and are reported
in this document.

This report is divided into five sections. Section 2
contains a description of the propagation and correlation measure-
ments made, the sites where the measurements were made, the equip-
ment used to make the measurements, and the 'raw' data
(measurements). The analysis and results of the analysis of the
data are presented in Section 3. Section 4 contains the results
of the MOBA data base updating as well as an introduction to
active antennas, a new development which may be in use in future
MOBA diversity radios. Section 5 contains our conclusions and
recommendations.

In the remainder of this section we provide a summary
of the results of Sections 2 through 5.

1.2 Summary of Section 2: VHF and UHF Propagation Measurements in MOBA Environments

In Section 2 we give a detailed description of the types of measurements made, the locations were the measurements were made, the equipment used to make the measurements, the frequencies at which the measurements were made and the results of the measurements.

The frequencies chosen for the measurements were 27 MHz, 49.8 MHz and 446 MHz. The choice was dictated by frequency allocation (49.8 MHz) and the availability of equipment to make the measurements (27 MHz and 446 MHz). The characteristics of the equipment (radios, antennas and detectors) are discussed in Section 2.1. Different transceivers with different output powers and antenna gains were used at the three frequencies. The output power and other characteristics of the three transceivers are given in Table 2.1-1 while the antenna characteristics and their estimated gains are given in Tables 2.1-2 and 2.1-3.

The types of measurements made and the sites (locations) where they were made are discussed in Section 2.2. As discussed in the introduction, two types of measurements were made: path (or transmission) loss measurements and diversity (or correlation) measurements. The path loss measurements can be grouped into four different types of measurements:

a)   Short distance street-to-street propagation between low elevation (~5 ft) antennas;

b)   street-to-building propagation;

c)   building-to-building propagation; and

d)   intrabuilding propagation.

The correlation measurements were made with the purpose of investigating two types of diversity reception:

a)   field diversity which uses two receiving antennas to detect the electric field (whip antenna) and the magnetic field (loop antenna) components of the received electromagnetic field; and

b)   space diversity which uses two antennas placed far
       enough apart (a half-wavelength) so that the signals
       captured by the two antennas are sufficiently
       decorrelated.

The street-to-street propagation measurements were made in
two areas: the business district of Boston, Massachusetts, and
the center of Lexington, Massachusetts. The various propagation
paths (transmit-receive-location) used in each area are described
in detail in Section 2.2. The Boston business district is typical
of an urban area while Lexington Center is more typical of a
dense suburban area. The results of these measurements (raw data)
are given in Section 2.3 in graphical form as a function of the
transmitter-receiver separation. Some of the trends observed are:

1)   the maximum range, under favorable transmitter/receiver
       siting, when the transmitted power is in the order of
       2 watts (at 27 MHz and 49.8 MHz) to 10 watts (at 446 MHz)
       is about 5,000 ft (~ 1.5 Km) in both urban and suburban
       areas;

2)   the range is reduced to 2000 ft where both transmitter
       and receiver are surrounded by very high buildings
       (>10 stories high) provided the transmitter and receiver
       are not too close to the buildings (e.g. middle of the
       street);

3)   where both transmitter and receiver are surrounded by
       high buildings and both are on the sidewalk close to
       the buildings, the range is as low as 500 ft; and

4)   when the transmit location is moved from a location
       close to a building to the middle of the street, the
       received signal level increases by as much as 20 dB.

The street-to-building, building-to-building, and intra-
building measurements were made for the most part in two reinforced
concrete office buildings located in the business district of
Boston. One of the buildings was 24 stories high while the other

was 5 stories high. Both of them were located on the same side of the street, roughly 100 ft apart. A floor map of the two buildings is given in Section 2.2. In addition, some of the measurements were made in the SIGNATRON building which is located in Lexington, MA. The outside walls of this building are made of cinder block with brick veneer, while the interior consists of a wooden frame with gypsum walls.

The street-to-building measurements were made both along a floor and in various floors (including a basement) as a function of elevation. The results of these measurements are given in Section 2.4 in graphical form as a function of receiver floor location (for one set of measurements) and as a function of distance from the transmitter (for the other). Some of the observations made were:

1)   the received signal level in general decreases as the floor height increases; and

2)   the received signal decreases as the location inside the building is farther away from the other location outside the building.

The building-to-building propagation measurements were made with the receiver located in a fixed location in one building while the transmitter position was varied from floor to floor in the other building. The relative positions of the transmit and receive locations are shown in a scaled drawing in Section 2.2. The results of the measurements are given graphically in Section 2.5 as a function of the difference in floor levels between the transmit and receive locations. The measurements exhibited no height dependance. Reception was possible only when the transmitter was located near a window and no reception was possible when the receiver was in the basement.

The intrabuilding propagation measurements tested for the following effects:

a)   transmission along straight and winding corridors;

b)   transmission between above ground floors;

1-6

c)   transmission between a basement and above-ground
        floors; and

d)   transmission in stairwells and elevator shafts.

The results of these measurements are given in Section 2.6 in
graphical form as a function of distance along the corridors
and the number of floors between transmitter and receiver. The
height of each floor was estimated to be 15 feet. Some of the
observations made are:

a)   the received signal in corridors drops off exponentially
        with distance indicating waveguide type of propagation;

b)   in the transmissions between above-ground floors,
        basement to above-ground floors and in stairwells,
        the received signal decreases as the nth power of
        the number of floors transmitted through (the value
        of n varies from one frequency to another and from
        one type of transmission to another);

c)   in the transmissions along elevator shafts, the received
        signal decreases exponentially with the number of
        floors transmitted through;

d)   in general, for transmission through a fixed number
        of floors, the received signal is stronger in a stair-
        well than in elevator shafts and weakest where trans-
        mission is through the ceilings.

In addition to the path loss measurements, data was gathered
to determine whether diversity reception could be useful or not.
The data was obtained simultaneously and consisted of the received
signal levels from the diversity antennas while the receiver
remained in a fixed position. Two types of diversity reception
were investigated:

a)   field diversity at 27 MHz and 49.8 MHz, and

b)   space diversity at 49.8 MHz and 446 MHz.

1-7

The field diversity measurements were made using a standard whip antenna which measures the electric field component of the received signal, and a multiturn loop antenna which measures the magnetic field component of the received signal. The amount of correlation between the two signals determines the diversity gain.

The space diversity measurements at 49.8 MHz were made by correlating the received signal levels at locations 10 ft. apart $(.506\lambda)$. Similarly, the space diversity measurements at 446 MHz were made by correlating the received signal levels at distances of 1.67 ft $(.75\lambda)$ and 3.3 ft (1.5λ).

1.3   Summary of Section 3:   VHF and UHF Data Analysis

In Section 3, path loss and correlation analysis of the
data are presented. The path loss is defined as the average
attenuation introduced by the propagation (transmission) medium
independent of the transmitted power and the transmitting and
receiving antenna gains. The correlation analysis is done by
determining the correlation coefficient (defined in Section 3.2)
between the signals measured with the two diversity antennas
(field or space diversity).

The results of the path loss analysis are given in graphical
form in Sections 3.1.1 to 3.1.4 for the four types of propagation
conditions described earlier. The average path loss for the
various street-to-street propagation paths tested are given in
Section 3.1.1. In general the path loss (attenuation) increases
with frequency for all locations (paths) tested. The difference
between the path loss at 27 MHz and the path loss at 49.8 MHz
is on the average 8 dB, while the difference in path loss between
49.8 MHz and 446 MHz is on the average 4 dB. Furthermore the path
loss for the various urban and suburban locations (paths) tested
increases with distance at rates ranging from 20 dB/decade to
47 dB/decade. The average rate of increase of the path loss with
distance is, however, 40 dB/decade for all three frequencies
tested as shown in Fig. 1.3-1. The difference in the average path
loss between a medium built-up area (suburban Lexington) and a
highly built-up are (Boston) ranges from 2.5 dB at distances
greater than 1 Km to 30 dB at distances less than 100 meters.
These trends, and others discussed in Section 3.1.1, were used
to derive a path loss prediction model applicable to short
distance propagation (up to 2 Km) between low elevation antennas
located in built-up areas. The path loss prediction model is
described in detail in Section 3.3 and is more suitable than
other models previously described in the literature for the
situation just described.
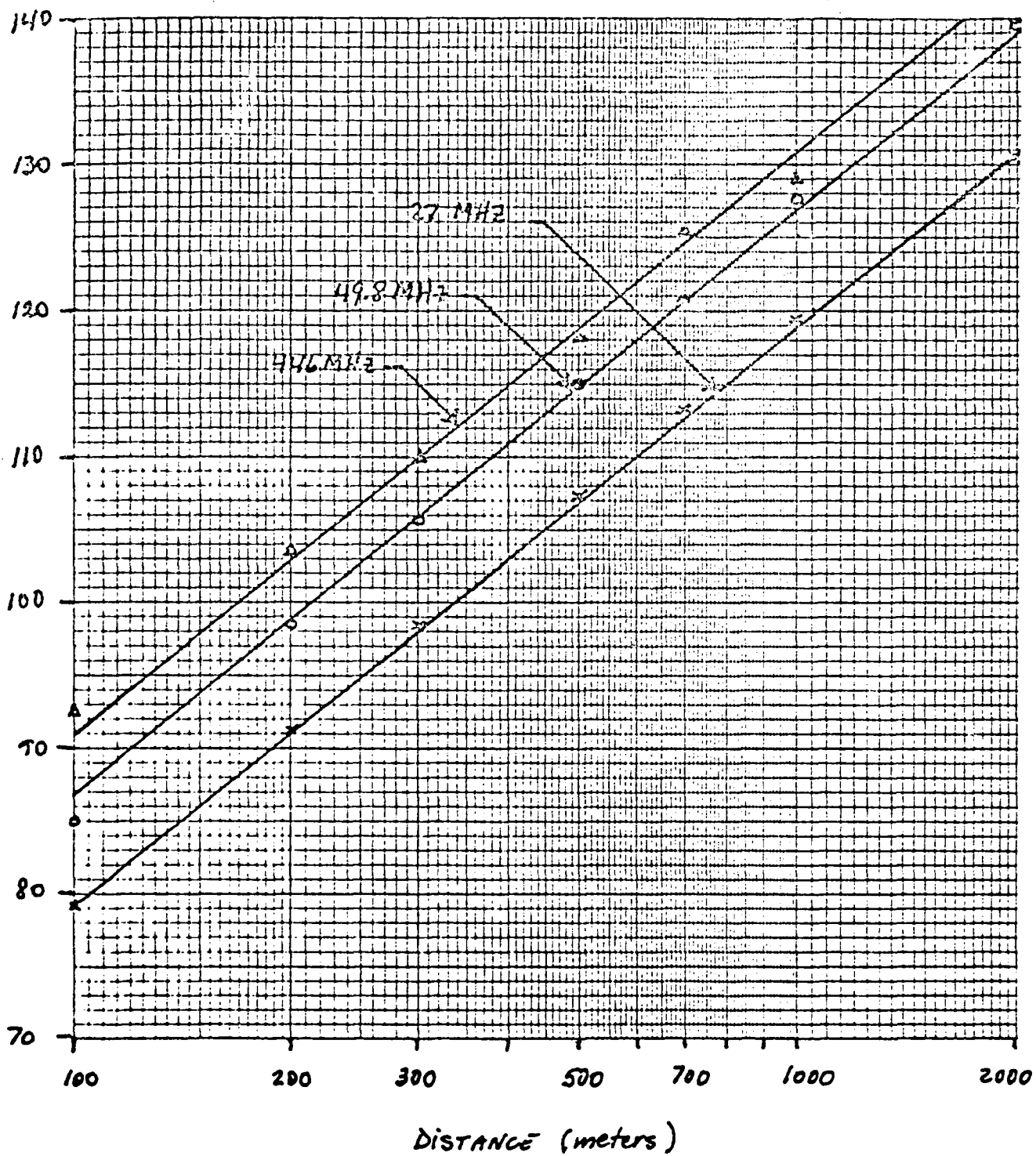
Fig. 1.3-1 Path loss at 27 MHz, 49.8 MHz and 446 MHz for
all Locations in Built-Up Areas (From SIGNATRON
Measurements).

1-10

The (average) transmission losses for the street-to-building propagation measurements are discussed in Section 3.1.2. The effect of the building is discussed in terms of the building penetration loss, which is defined as the difference (in dB) between the average transmission loss and the free-space loss for a transmitter and receiver located at an equal distance in free space. The building penetration loss in general decreases with frequency. However, since the free-space loss increases with frequency (6 dB/octave), the average street-to-building transmission loss reaches a minimum at a frequency estimated to be around 50 MHz. The building penetration loss varies randomly from floor-to-floor so that no height-gain (decrease in the penetration loss as the receiver floor location increases) is observed. More specifically, the street-to-above-ground-floor penetration loss for a concrete wall building ranges from 54 dB to 80 dB at 27 MHz, from 54 dB to 68 dB at 49.8 MHz, and from 38 dB to 48 dB at 446 MHz. The street-to-basement penetration loss for a concrete wall building is 67.5 dB at 27 MHz, 58 dB at 49.8 MHz and 52 dB at 446 MHz. For a building with outer cinder block walls and inside gypsum walls, the penetration loss is 61 dB at 27 MHz, 44 dB to 48 dB at 49.8 MHz, and 40 dB to 58 dB at 446 MHz.

The (average) transmission losses for the building-to-building propagation measurements are discussed in Section 3.1.3. The effects of the two buildings are discussed in terms of the two-building penetration loss which is defined as the difference (in dB) between the building-to-building transmission loss and the free-space loss for a transmitter and receiver located at an equal distance in free space. From the transmission loss analysis it was found that the two-building penetration loss exhibits no height dependance, i.e., on the average it is independent of the difference in floor levels at the transmitting and receiving ends. The two-building penetration loss ranges from 57.5 dB to 86 dB at 27 MHz, from 65 dB to 77 dB at 49.8 MHz, and from 58 dB to 64.5 dB at 446 MHz.

The (average) transmission losses for the various intrabuilding propagation measurements are discussed in Section 3.1.4. The transmission loss (in dB) along corridors varies linearly with distance. Its rate of increase varies with the dimensions of the corridor, whether the corridor is straight or not, and with frequency. When the corridor is straight, the transmission loss and the rate at which the transmission loss increases (with distance) decrease with frequency. However, the converse is true when the corridor has one or more turns. Table 1.1 summarizes the average transmission loss at a distance of 20 meters along various corridors and the rate of increase for longer distances. The transmission loss (in dB) between above ground floors, between a basement and above-ground floors, and in stairwells increases linearly with the log of the number of floors transmitted through. The transmission loss (in dB) along elevator shafts increases linearly with the number of floors transmitted through at the VHF frequencies and linearly with the log of the number of floors transmitted through at 446 MHz. Table 1.2 summarizes the average loss due to transmission through one floor and the rate of increase in the average loss due to transmission through a greater number of floors for the various cases mentioned above at the three test frequencies.

The results of the correlation analysis are discussed in Section 3.2. The envelope (amplitude) correlation coefficients for the field diversity measurements at 27 MHz and 49.8 MHz are summarized in Tables 3.2-1 through 3.2-4. They vary from a value of .14 (little correlation) to .90 (high correlation) from one set of measurements at 27 MHz to another. At 49.8 MHz, they vary from .07 (no correlation) to .90 (high correlation). Similarly, the envelope correlation coefficients for the space diversity measurements are

Table 1.1

Transmission Losses in Intrabuilding Propagation Along Corridors

	27 MHz		49.8 MHz		446 MHz	
	transmission loss at 20 meters	rate of increase in transmission loss	transmission loss at 20 meters	rate of increase in transmission loss	transmission loss at 20 meters	rate of increase in transmission loss
Straight corridor (cinder block walls)	64.5 dB	0.69 dB/meter	63 dB	0.69 dB/meter	51.8 dB	0.54 dB/meter
Winding corridor (cinder block walls). First turn at 10 meters	70 dB	0.83 dB/meter	68.1 dB	0.98 dB/meter	82.5 dB	1.02 dB/meter
straight corridor (gypsum walls)	84 dB	34.00 dB/meter				
L shaped corridor (gypsum walls) turn at 15 meters	108 dB	48.00 dB/meter				

Table 1.2

Transmission Losses in Intrabuilding Propagation Between Floors

	27 MHz		49.8 MHz		446 MHz	
	average loss due to transmission through one floor	rate of increase in transmission loss	average loss due to transmission through one floor	rate of increase in transmission loss	average loss due to transmission through one floor	rate of increase in transmission loss
transmission between above ground floors	83 dB	51.3 dB/decade	83 dB	25.5 dB/decade	88 dB	30.2 dB/decade
transmission between basement and above ground floors	77 dB	56 dB/decade	83 dB	44.5 dB/decade	82 dB	50. dB/decade
transmission near (or along) elevator shafts	40 dB	60 dB/decade	45.6 dB	27.5 dB/decade	59.4 dB	38. dB/decade
transmission near (or along) elevaton shafts	64.4 dB	3.4 dB/floor	73.3 dB	4.3 dB/floor	52 dB	52.6 dB/decade

summarized in Tables 3.2-5 through 3.2-11. At 49.8 MHz,
the spatial correlation varies from .003 (uncorrelated) to
.72 for a separation distance between antennas of 3 meters.
At 446 MHz, the spatial correlation varies from .10 to .79
for a separation distance between antennas of 50 cm and from
.02 to .71 for antennas 100 cm apart.

The diversity gain resulting from the use of
field or spatial diversity is usually explained in terms
of a decrease in the outage rate (the fraction of time that
the received signal is below a usable level). However, in
the case of street-to-street propagation, the diversity
gain is directly related to an increase in the range of a
fixed output power transmitter. Thus, we have plotted in
Figure 1.3-2 the increase in the range of a radio which
uses dual selection diversity (either field or space) as a
function of the path loss rate of increase with distance
and for various values of the 'complex' (amplitude and phase)
correlation coefficient r between the two diversity branches.
When the signals received with the two diversity antennas
are Rayleigh fading (as they are in this case), the ampli-
tude (envelope) correlation coefficients are approximately
equal to the square of the complex correlation coefficient, r.
Keeping this in mind, it can be seen from Figure 1.3-2 that the
use of field diversity at VHF and space diversity at VHF
and UHF will result in an increase in the range of the
transmitter by at least a factor of 1.3 and up to a factor
of 1.8 times the range of a similar system which does not
use diversity, when the path loss increases at a rate of
40 dB/decade (inverse fourth power law). When the path
loss increases at a lower rate, the increase in range can
be greater. Measurements by other workers indicate that
the higher the antenna elevation the lower the rate of
increase in path loss.
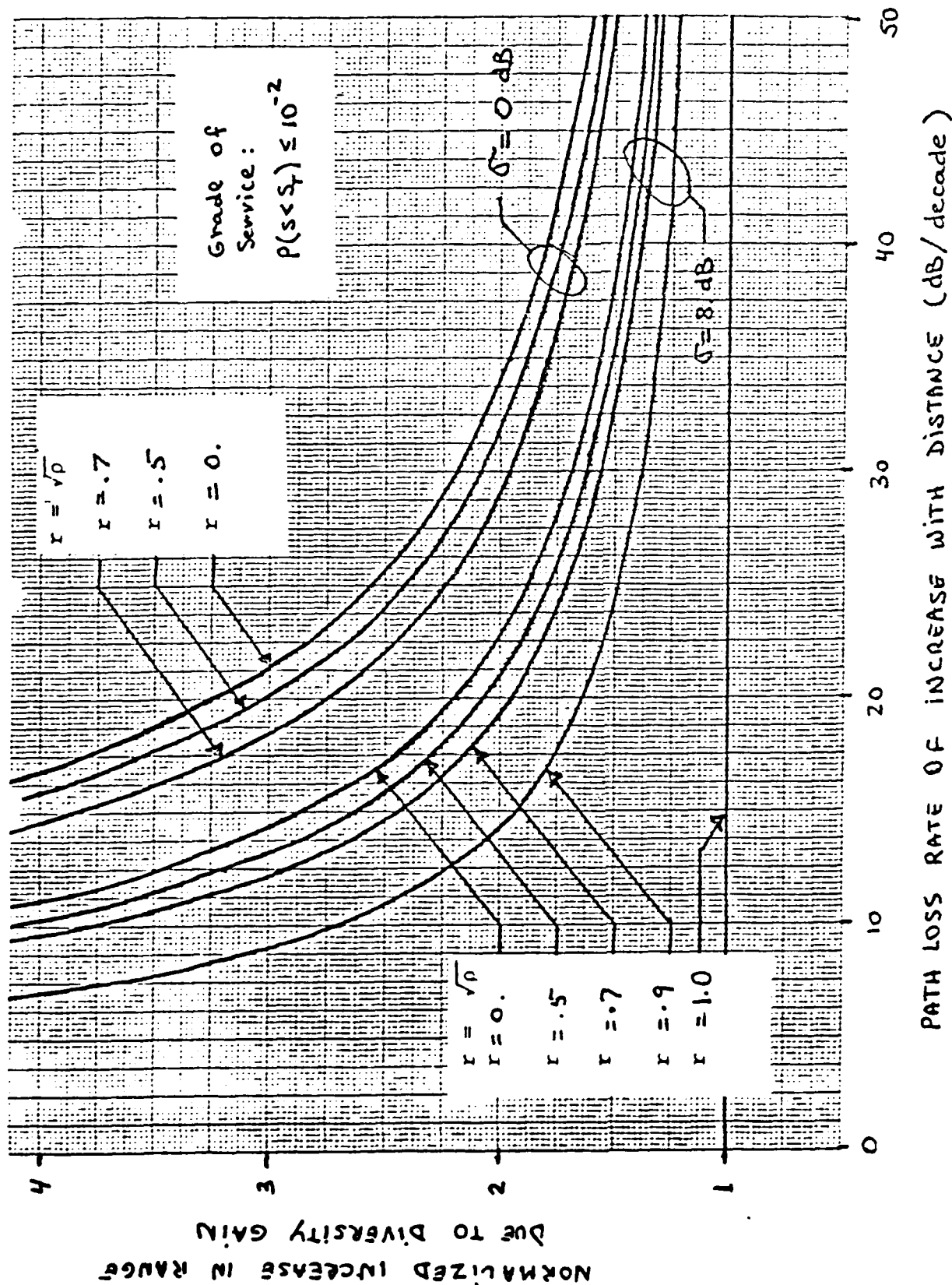
FIGURE 1.3-2 Increase in Range due to Diversity Gain as a Function of Path Loss Rate (Power Law) and Correlation

1.4 Summary of Section 4: MOBA/COBA Data Base Update

In Section 4, we discuss a series of topics which
are related to the MOBA/COBA problem but which are indepen-
dent from the measurements we made. In Section 4.1 we give
a summary of a series of meetings held with European re-
searchers with the purpose of incorporating their findings
into the MOBA/COBA data base. Basically, all of the British
German, and Swedish researchers that we talked with have
conducted experiments with similar results to ours showning
that the received signal level in an urban environment
follows an inverse fourth power law, i.e., the path loss
increases at a rate of 12 dB/octave or 40 dB/decade. Most
of them, also agree that urban radio communications can
be improved by using diversity reception and by employing
elevated antennas. In addition, the German scientists
have been successfully employing active antennas in di-
versity configurations.

Section 4.2 summarizes work which has recently
appeared in the literature and which is related to the MOBA/
COBA problem. Among the recently published work are the
results of propagation measurements made in British cities
by a group of British workers at frequencies in the VHF
and UHF range using medium elevation antennas (20 to 50
meters). Their measurements exhibit the same distance de-
pendence as ours (inverse fourth power law) and further
reinforce our prediction model. In addition, we also re-
port on some man-made (ignition) noise measurements made
by the same group of workers. The other work reported on
deals with the analysis of the performance of a two-branch
equal-gain combining diversity receiver with applications
to mobile communications. These latter results are com-
pared with the performance calculations we have done for

a two-branch selection-diversity receiver and which we discuss in the context of diversity gain in Section 3.2.3.

Finally, in Section 4.3 we discuss the performance and some design aspects of an active loop antenna for implementation of a VHF (30-80 MHz) field diversity system. An active loop antenna offers an advantage over the multi-turn loop (MTL) antenna originally chosen for this purpose, namely that an active antenna can be designed to be very broadband (and thus require no tuning) while a multiturn loop antenna is inherently very narrowband and requires automatic tuning. The automatic tuning makes the MTL extremely bulky and heavy for use with manpack radios. The resulting active antenna has a lower profile and smaller size and weight than the corresponding passive antenna.

1.5   Summary of Section 5:   Conclusions and Recommendations

The following conclusions are based on the results of our propagation research.

1.   Communications Range

The communications range in an urban or suburban environment is limited. If both the transmitter and receiver are located on a sidewalk, the VHF range may be less than 500 feet in highly-built-up areas (average building height of 5 stories or more), while UHF is unusable. If both the transmitter and receiver are in the center of the street, the range may be as great as one mile for both VHF and UHF. The urban area has a shorter communications range than the suburban area. For a given transmitter power, the communication range can be extended by a factor of approximately 1.4 to 1.8 if diversity reception is used.

2.   Communications Between and Within Buildings

Communications within a building are possible at both VHF and UHF, with the communications range being dependent on the corridor structure, building material, and number of floors separating the transmitter and receiver. Communications between the street and a building are possible at VHF and UHF, although the attenuation increases rapidly at UHF when one terminal moves into the interior of the building. Communications between two adjacent buildings is not possible unless one terminal is near a window. Communications inside a building along a straight corridor is better at UHF than at VHF, but the converse is true when the corridor has turns. Communications be-

tween floors is enhanced at both VHF and UHF if within
a stairwell or near an elevator.

3. Path Loss Prediction Model

When low elevation antennas are used, our
experimental data indicate that the path loss in dB can
be approximated by Eq. (3.3-2):

$$L = L_p(d) + L_D(f) - H_e(h_t, f) - H_r(h_t, f) \quad (3.3-2)$$

$$+ K_{u,s}(f,d) + L_b(f)$$

where L_p is the plane-earth path loss for 2-meter antenna
height and separation d; $L_D(f)$ is a frequency-dependent
environmental clutter factor; H_t and H_r are antenna
height-gain factors; $K_{u,s}(f,d)$ is a frequency and distance
dependent urban/suburban clutter factor; and $L_b(f)$ is a
frequency dependent building penetration loss, applicable
when one terminal is within a building and the other is
in the street. This model is in excellent agreement with
that of Okumura at 446 MHz, but shows less of a frequency
dependence than his at VHF. It is similar to the Allsebrook
and Parsons model, but more complete in the inclusion of
$K_{u,s}$ and L_b.

4. Propagation Phenomenological Model

The path loss measured in urban and suburban
environments showed distance relations from inverse square-
law to inverse fourth-power law. The inverse square-law
is associated with a single predominant diffraction path,
and the inverse fourth-power is associated with (near)
equal strength multiple reflected (or diffracted) signals.

The single diffraction path is important when a terminal is located on the sidewalk, next to a building; however, the diffraction loss may be so great that the received signal is unusable. The multiple-reflected (or diffracted) signal case, which is the more reliable means of communication, requires that one of the terminals be away from the building.

    5.   Selection of MOBA Radio Operating Frequency

        The measurements show, and the modeling explains, that communications are best when the building heights are small compared to a wavelength. This implies that urban communications would be better, from a path-loss point of view, at HF than at VHF. It further implies that UHF should not be considered for MOBA use by the Army in highly built-up areas as it requires that radio operators be in exposed positions. However, use of UHF in suburban areas (average building height of two stories or less) may be more desirable than VHF if antenna profile (height) is a factor.

    6.   Fading and Correlation Properties of the
          Received Signal

        The received signal has been shown by our measurements, as well as by the measurements made by numerous other researchers, to be a fading signal. Thus, improved performance can best be achieved by diversity reception. Our correlation measurements show that both field diversity, using collocated loop and whip antennas, and space diversity, using two whip antennas spaced approximately one-half wavelength apart, are possible. From a practical point of view, only the field diversity approach is feasible for a manpack VHF radio.

7. Antenna Developments

Active antennas appear to have significant application to military radios. First, because they are broadband, they can be used as auxiliary receiving antennas in diversity receivers without requiring additional tuning sections. Secondly, because they are physically small, they have good low-profile capabilities. Third, because they are decoupled from their environment by the unilateral transistors, they do not require ground planes and, when used in arrays, they do not cross-couple. An active loop antenna would be a practical means of implementing an appliqué for a diversity VHF receiver.

The following recommendations are based on the conclusions of this study.

1. A development program be started to build and test a VHF diversity receiver using an active loop antenna as the auxiliary antenna.

2. A research program be started to determine means of extending the range of MOBA radio communications. This should include both consideration of relay techniques and the use of other frequencies, most notably HF.

3. Consideration should be given to externally deployed antennas for use with radios in the interior of a building.

SECTION 2
VHF AND UHF PROPAGATION MEASUREMENTS
IN MOBA ENVIRONMENTS

2.0 Introduction

In this section we present the results of propagation
measurements made in typical MOBA environments at three fre-
quencies: 27 MHz, 49.8 MHz, and 446 MHz. The purpose of making
these measurements was to determine and quantify the effects of
the medium (environment) on radio communications in the VHF and
UHF bands. The types of propagation media selected were typical
of those found during Military Operations in Built-up Areas
(MOBA). Thus we obtained measurements of received signal level
in a highly built-up area with a high density of tall buildings
(urban environments) and also in a less built-up area with a
higher density of one and two story buildings (suburban environ-
ments). From these measurements we are then able to de-
termine the path loss as a function of the environment as well
as the potential for improving the performance of a radio
communications link through the use of diversity. The potential
for performance improvement can be determined from measurements
made with two types of receiving antennas - a whip and a loop
antenna - which measure different components of the received
electromagnetic field (Field Diversity). In order to com-
pletely determine the effects of MOBA environments, measure-
ments of the received signal level inside buildings were also made.
Thus the type of measurements made and described in this section
may be grouped into: street-to-street propagation measurements
between low elevation antennas; street-to-building transmission;
building-to-building transmission; and intrabuilding propagation
measurements.

The choice of frequencies was dictated by frequency allo-
cation and the availability of equipment to make measurements.

in these bands. Because we are mostly interested in quantifying the effects of the propagation medium, we must take into account the effects of the measuring equipment before comparing the measurements at the various frequencies. Since different transceivers were used to make the measurements at 27 MHz, 49.8 MHz, and 446 MHz, special care must be taken to determine the transmitted power and antenna gains of the various transceivers before a meaningful comparison of the measurements can be made.

Hence, Section 2.1 discusses the equipment used in making the measurements. The types of measurements made and the sites of the measurements are described in Section 2.2. The measurements of received signal level for the various types of propagation conditions are given in Sections 2.3 to 2.6. The trends of the measurements are also discussed in these subsections but a more thorough analysis of the data is deferred to Section 3. Finally, Section 2.7 summarizes the measurements and preliminary conclusions reached from the trends exhibited by the data.

2.1 The Measuring Equipment

A block diagram of the measuring system used in making the propagation measurements is shown in Figure 2.1-1. A calibrated detector is used to obtain an estimate of the path loss due to propagation through a MOBA environment by measuring a DC voltage at the detector output. This requires knowledge of the transmitted power and antenna gains, as well as the receiver plus detector input-output characteristics. Thus, in this section we discuss the pertinent characteristics of the equipment that we used to make the measurements at 27 MHz, 49.8 MHz, and 446 MHz.
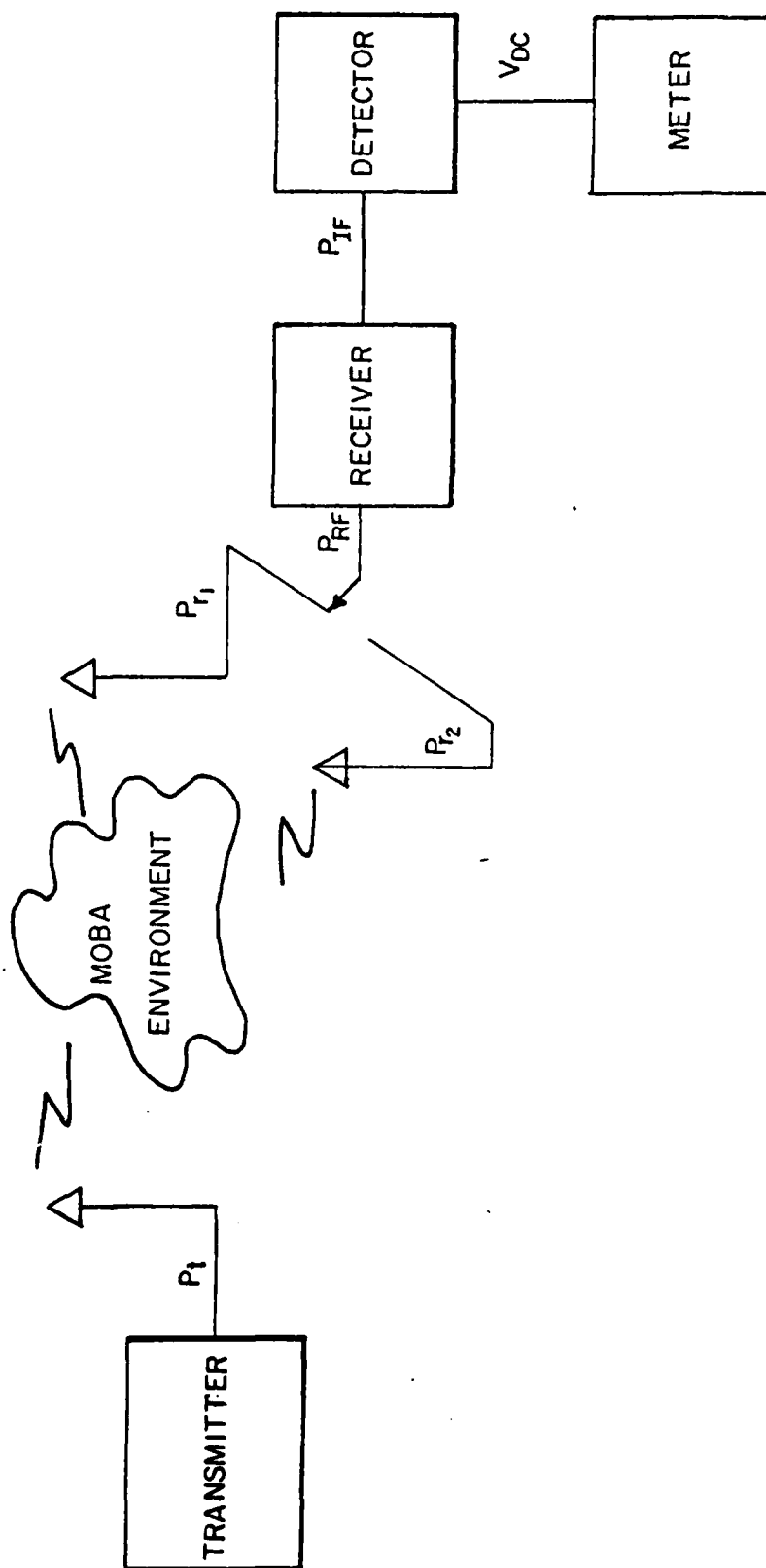
FIGURE 2.1-1   Measurement Set up

2.1.1 Transceiver Characteristics

The primary characteristics of the transceivers used in the measurements are shown in Table 2.1-1. Two of the radios are FM, and one is AM. The AM receiver had an AGC system which, after calibration, was used as the received signal level monitor. The FM radios used conventional limiter/discriminator receivers. Therefore it was necessary to build a wide dynamic range detector and interface it at a low-level point in the FM receivers so that the dynamic range is not degraded at high signal levels. The detector circuit is described in Appendix I.

Figures 2.1-2 through 2.1-4 show the calibration curves for the three receivers. This measurement is from the input antenna port to the AGC or external detector output. The AGC covers the input signal range of -30 to -110 dBm without switching while the external detectors used in the FM measurements required a switched design to cover a sufficiently wide dynamic range for useful measurements.

All of the transceivers are normally operated with whip antennas. The Dyna-Com and PRC-77 use short whips while the Kenwood used a quarter-wave whip. In addition, the Dyna-Com and PRC-77 have 50 ohm antenna input connectors. These antenna ports were used for making measurements with loop antennas.

TABLE 2.1-1

Transceiver Characteristics

	Dyna-Com 40	PRC-77	Kenwood TR-8300
Frequency Range	27 MHz Band	30-80 MHz	445-450 MHz
Modulation	AM	FM	FM
Output Power	2.25 W	2.50 W	1 & 10 W*
Channel Spacing	10 KHz	50 KHz	100 KHz
IF Bandwidth	6 KHz	18 KHz	20 KHz
AGC or Limiter	AGC	Limiter	Limiter
Sensitivity	1 μv (10 dB SNR)	.5 μv (12 dB SNR)	.5 μv (20 dB SNR)
Receiver Calibrated Measurement Range	-30 to -110 dBm	-30 to -100 dBm	-40 to -95 dBm
Minimum Detectable Signal	-110 dBm	-105 dBm	-100 dBm
Antennas	5' Whip +50 Ω External	3' Whip +50 Ω External	λ/4 Whip

*The 10W output power setting was used in all measurements
except for the intrabuilding measurements along corridors.
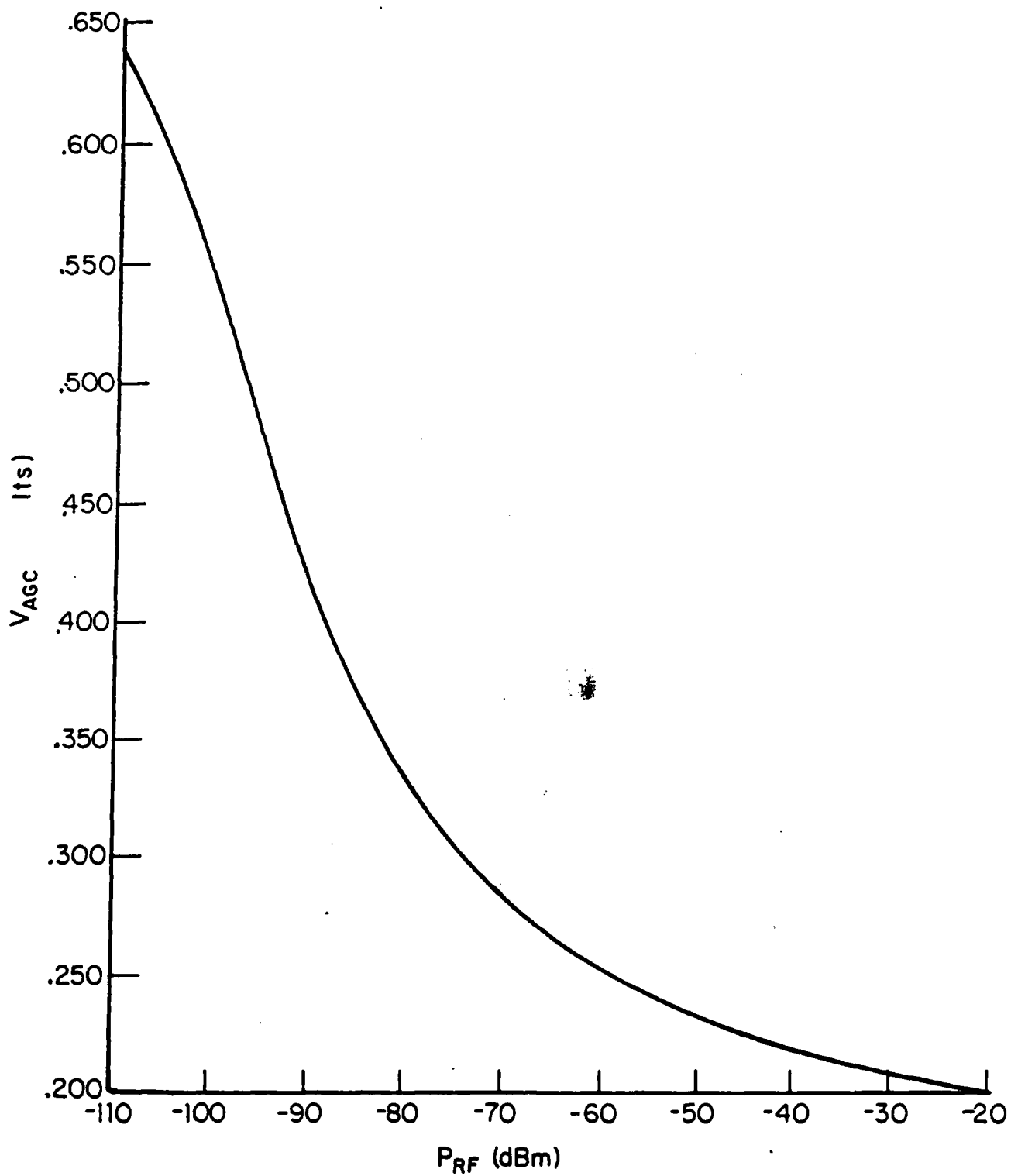
FIGURE 2.1-2 Dynacom 40 Receiver Front End Plus Detector
Input-Output Characteristics

2-6
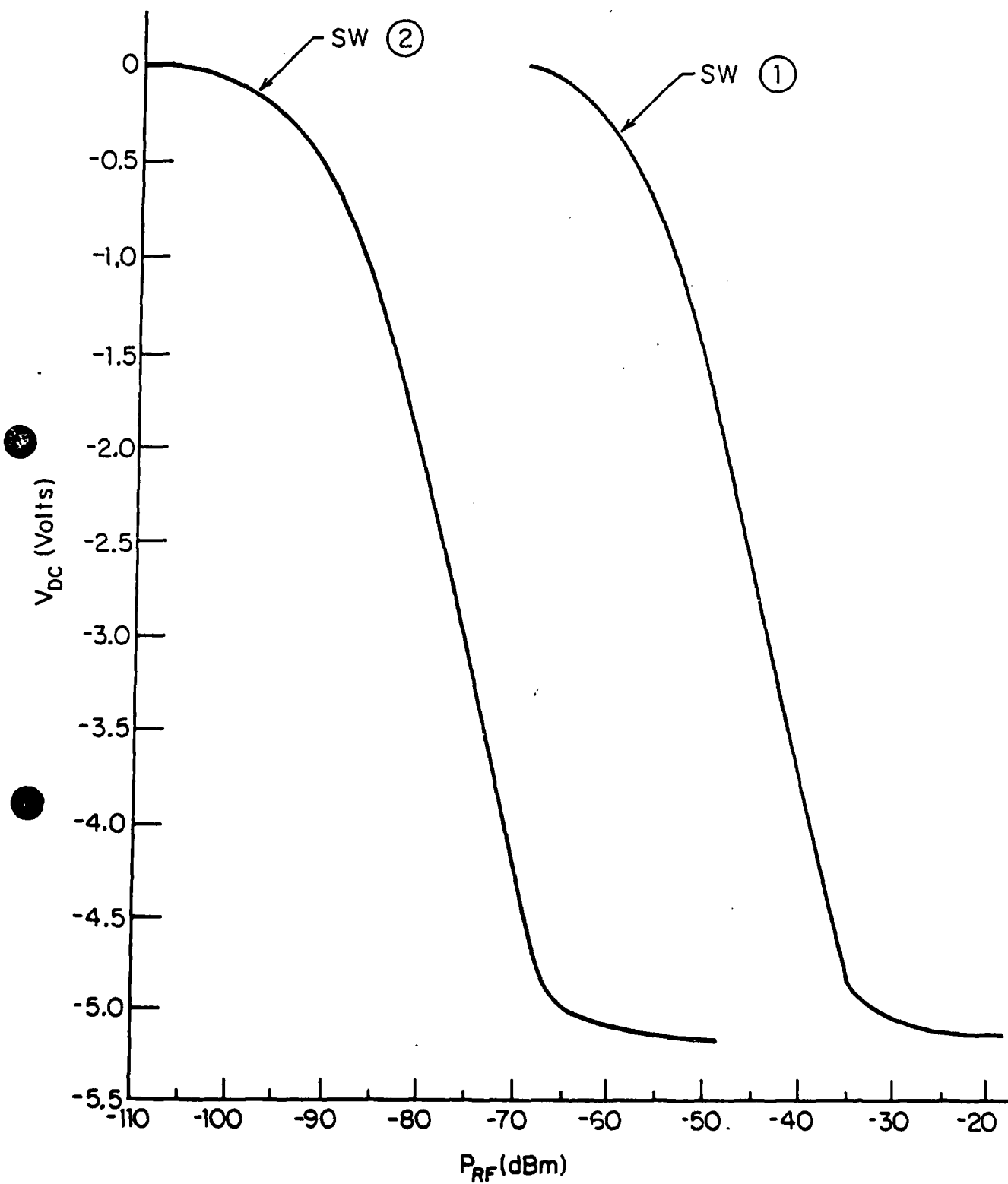
FIGURE 2.1-2   AN/PRC-77 Receiver Front End Plus Detector
Input-Output Characteristics

2-7
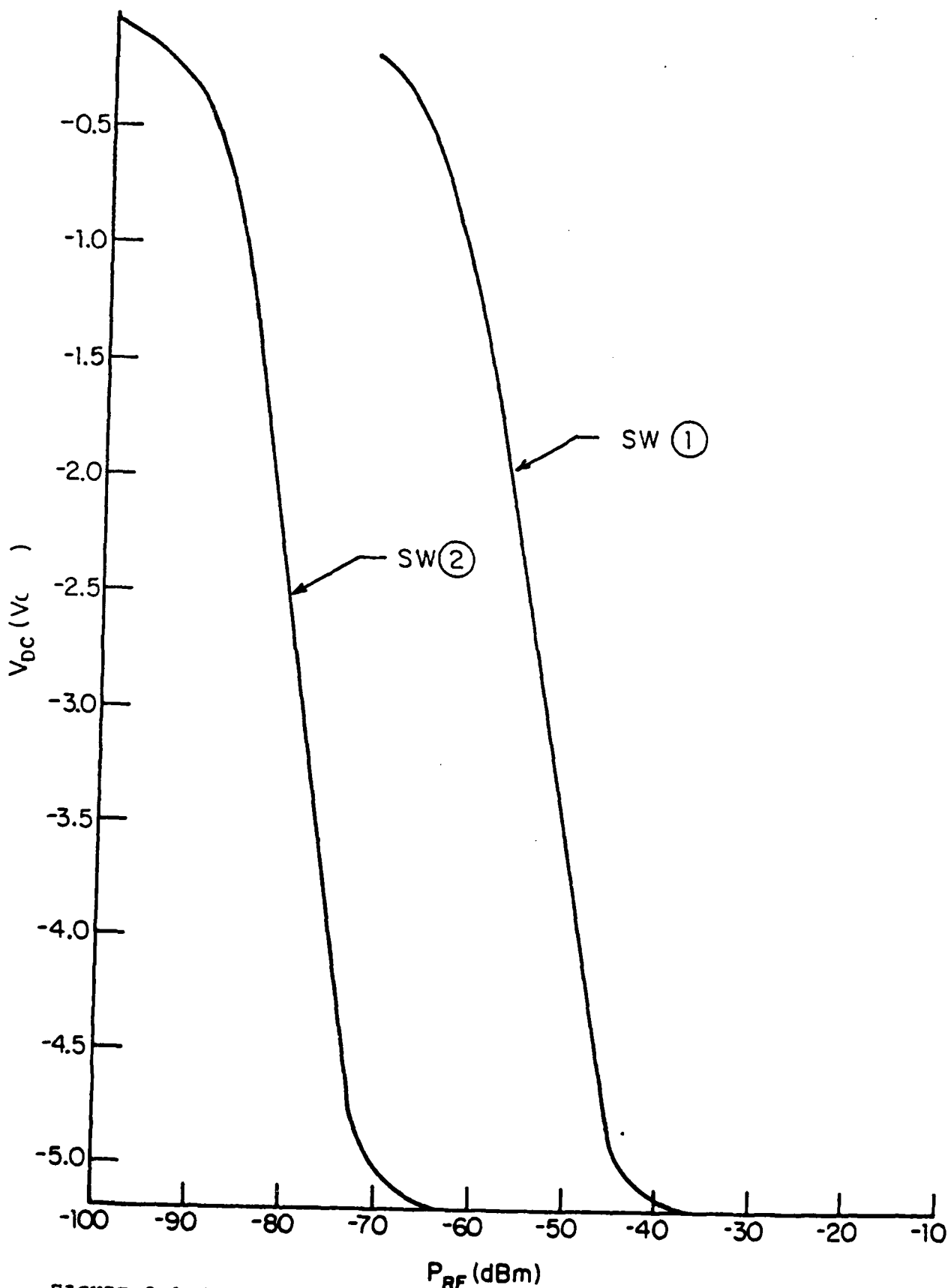
FIGURE 2.1-4   KENWOOD TR-8300 Receiver Front-End Plus Detector
                Input-Output Characteristics

2-8

2.1.2 Antenna Radiation Characteristics

The gain of an antenna is a basic property which has a
direct bearing in the path loss measurements. Gain is closely
associated with directivity, which in turn is dependent upon the
radiation patterns of an antenna.

The gain is usually defined as the ratio of the maximum
radiation intensity in a given direction to the maximum radiation
intensity produced in the same direction from a reference antenna
with the same input power. The reference antenna most commonly
used is the isotropic radiator (i.e., a hypothetical lossless
antenna which radiates uniformly in all directions).

For antennas that have no internal losses, the gain is the
same as the directivity. In general the gain of an antenna in
dB is given by

$$G = \eta + D \tag{2-1}$$

where η is the efficiency factor of the antenna in dB and is
equal to 0 if the antenna is lossless and D is the directivity
of the antenna in dB. However, while directivity can be computed
from either theoretical considerations or from measured radiation
patterns, the gain of an antenna is almost always determined by
a direct comparison measurement against a standard-gain antenna.
The gain of an antenna relative to the gain of the standard
antenna in dB may be expressed as

$$G = \gamma + G_o \ . \tag{2-2}$$

where G_o is the absolute gain of the standard antenna in dB (as defined by Eq. 2-1) and γ is the gain of the antenna in question in dB relative to the reference antenna. Thus, the absolute gain, G, of an antenna can be obtained from a direct measurement of γ and knowledge of G_o.

The gains of Eqs. (2-1) and (2-2) do not account for losses due to impedance mismatch between the radio and the antenna. Thus, it is convenient to define the effective or operational gain of an antenna system as

$$G_{eff} = G - M \hspace{4cm} (2-3)$$

where M is the mismatch loss in dB, G is the gain of the antenna as defined by Eq. (2-1) or (2-2), and G_{eff} is the effective gain of the antenna system in dB.

The gains of the antennas used in the three systems under consideration would ideally have to be determined experimentally. Furthermore, the measurement of the antenna gains would have to be made under conditions similar to those found while making the measurements. In particular, effects due to the proximity of the operator and other equipment would have to be included. Clearly, this is not a simple task and is beyond the scope of this work. Hence, we have used engineering judgment to estimate the gains of the various antennas from other available measurements.

The characteristics of the antenna systems that were used to make the measurements at 27 MHz, 49.8 MHz, and 446 MHz are summarized in Table 2.1-2. The gains of the whip antenna systems have been determined by estimating the efficiency of the system relative to a quarter-wave monopole antenna (G_o = 5.15 dB) using the measurements of Krupka [1968] as a guideline. The efficiency estimates, matching losses and gains of each antenna system, are summarized in Table 2.1-3. The 5-turn loop antenna system used at 27 MHz was designed and built (see Appendix II) by SIGNATRON while the 3-turn loop antenna used at 49.8 MHz was designed and built by Ohio State University for the

Table 2.1-2   VHF/UHF Antenna Systems Characteristics

	27 MHz		49.8 MHz		446 MHz
Function	Transmit & Receive	Receive	Transmit & Receive	Receive	Transmit & Receive
Type of Antenna	Telescopic Whip	Multiturn Loop	Tape Whip	Multiturn Loop	Quarter-Wave Whip
Polarization	Vertical	Vertical	Vertical	Vertical	Vertical
Length	5 Feet	10 Inches	3 Feet	8 Inches	6.5 Inches
Number of Turns		5		3	
Loop Diameter		5 Inches		5 Inches	
Matching Network	Yes	Yes	Yes	Yes	Yes
Extended Ground Plane	No	No	No	No	No

2-11

Table 2.1-3 Effective Antenna Gains

	27 MHz		49.8 MHz		446 MHz
Antenna Type	Telescopic Whip	5 Turn Loop	Tape Whip	3 Turn Loop	Quarter-Wave Whip
Electrical Length	.137 λ	.180λ	.152 λ	.199λ	.246 λ
Gain Relative to Quarter-Wave Monopole	-9. dB		-10. dB		-1. dB
Mismatch Losses	0.15 dB		0.15 dB		0.15 dB
Effective Antenna System Gain	-4. dB	-7.9dB+5.6dB	-5. dB	-5.2dB+3.dB	4. dB

U.S. Army Electronics Command (ECOM) at Ft. Monmouth under
contract DAAB07-74-C-0593 [Bohley, 1976]. The gains of these
loop antenna systems have been determined from a comparison
of the data taken with a receiving loop antenna and that
taken with a receiving whip antenna. The range in gains of
the loop antennas were due to variations in the tuning fre-
quency of the loop antenna caused by capacitive coupling
between the antenna, operator, and other equipment. The
frequency response of the 27 MHz and 49.8 MHz loop antenna
systems are shown in Figures 2.1-5 and 2.1-6, respectively.
Capacitive coupling between the loop antennas and nearby
objects tends to shift the tuning frequency, resulting
in additional tuning losses. A more thorough description
of the multiturn loop antenna and its design for the appli-
cation at hand is given in Appendix II.

2.2 Propagation Measurements: Choice of Locations

The propagation measurements made can be separated into
two types: path or transmission loss measurements and di-
versity (or correlation) measurements.

2.2.1 Path or Transmission Loss Measurement Sites

The transmission loss measurements were designed to in-
vestigate the following effects: (a) street-to-street propagation
losses using low elevation antennas; (b) street-to-building pene-
tration losses; (c) building-to-building transmission losses; and
(d) intrabuilding propagation losses.

The street-to-street propagation measurements between
low elevation antennas (5' high above local ground) were made
in two areas: Lexington Center and the business district of
Boston. Lexington Center is typical of a suburban town and
consists of two blocks of two and three story high brick
buildings, while the rest of the area consists of one and two

2-13
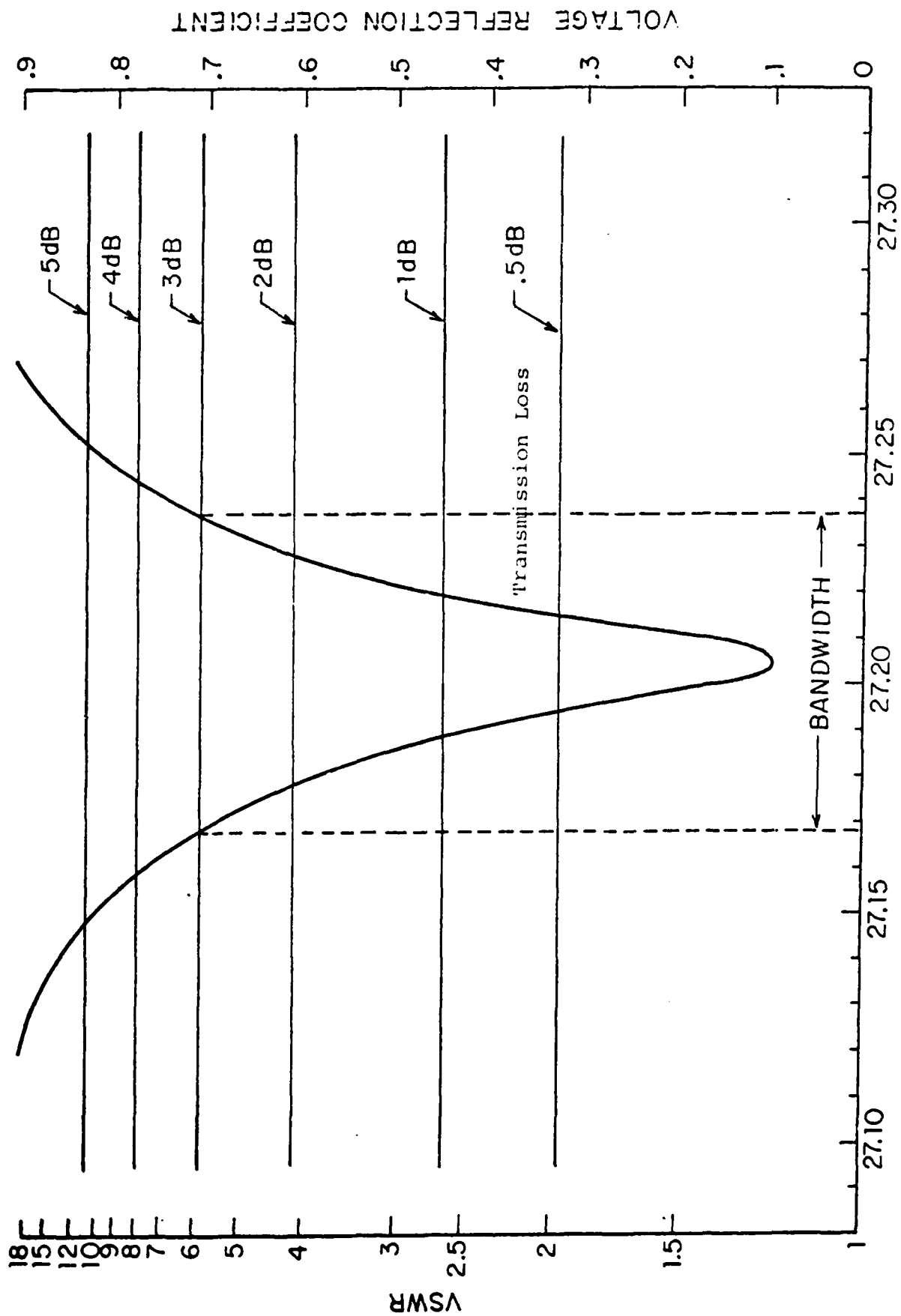
FIGURE 2.1-5 Frequency Response of Multiturn Loop Antenna Around 27.2 MHz
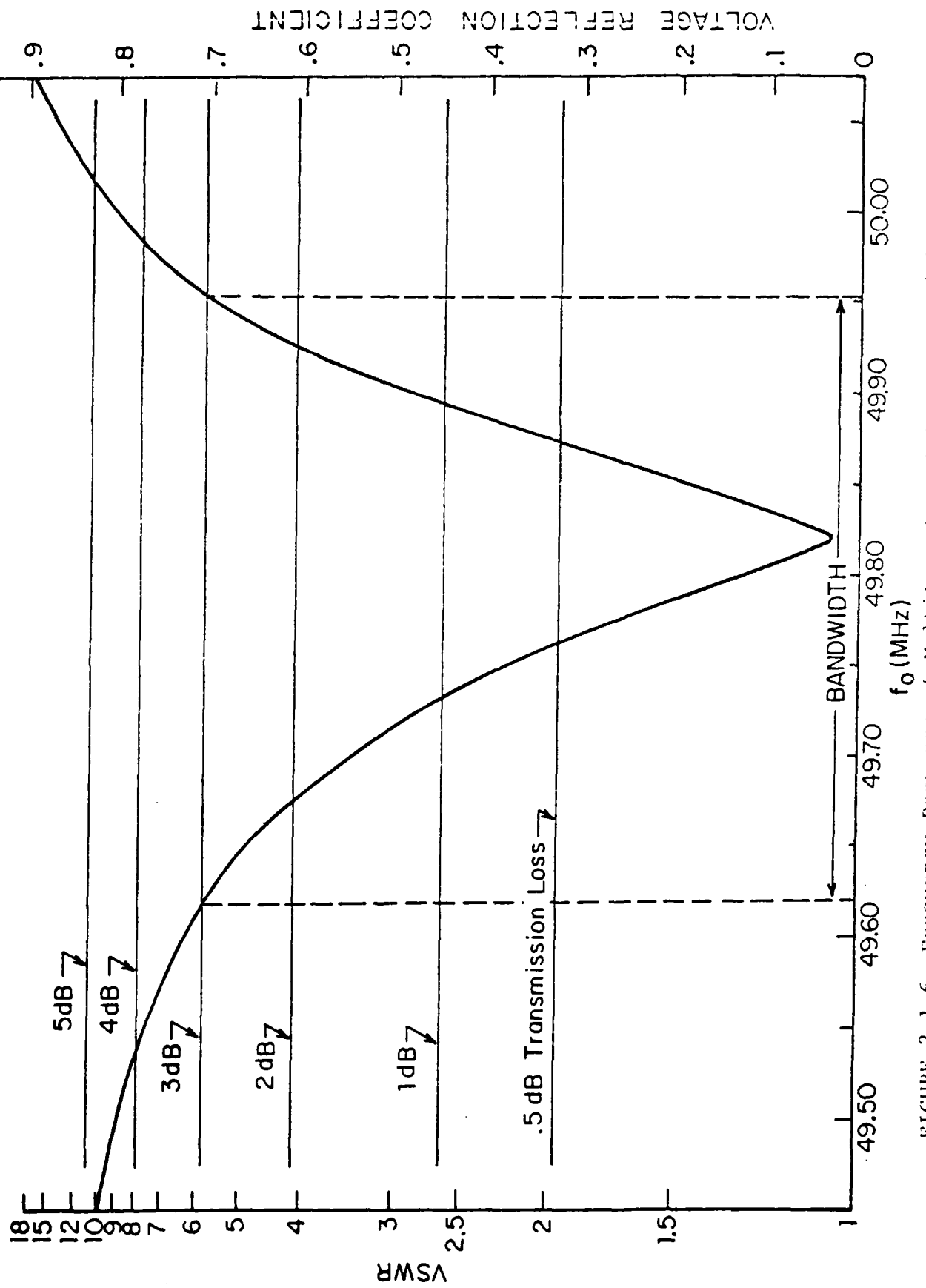
FIGURE 2.1-6 Frequency Response of Multiturn Loop Antenna Around 49.8 MHz
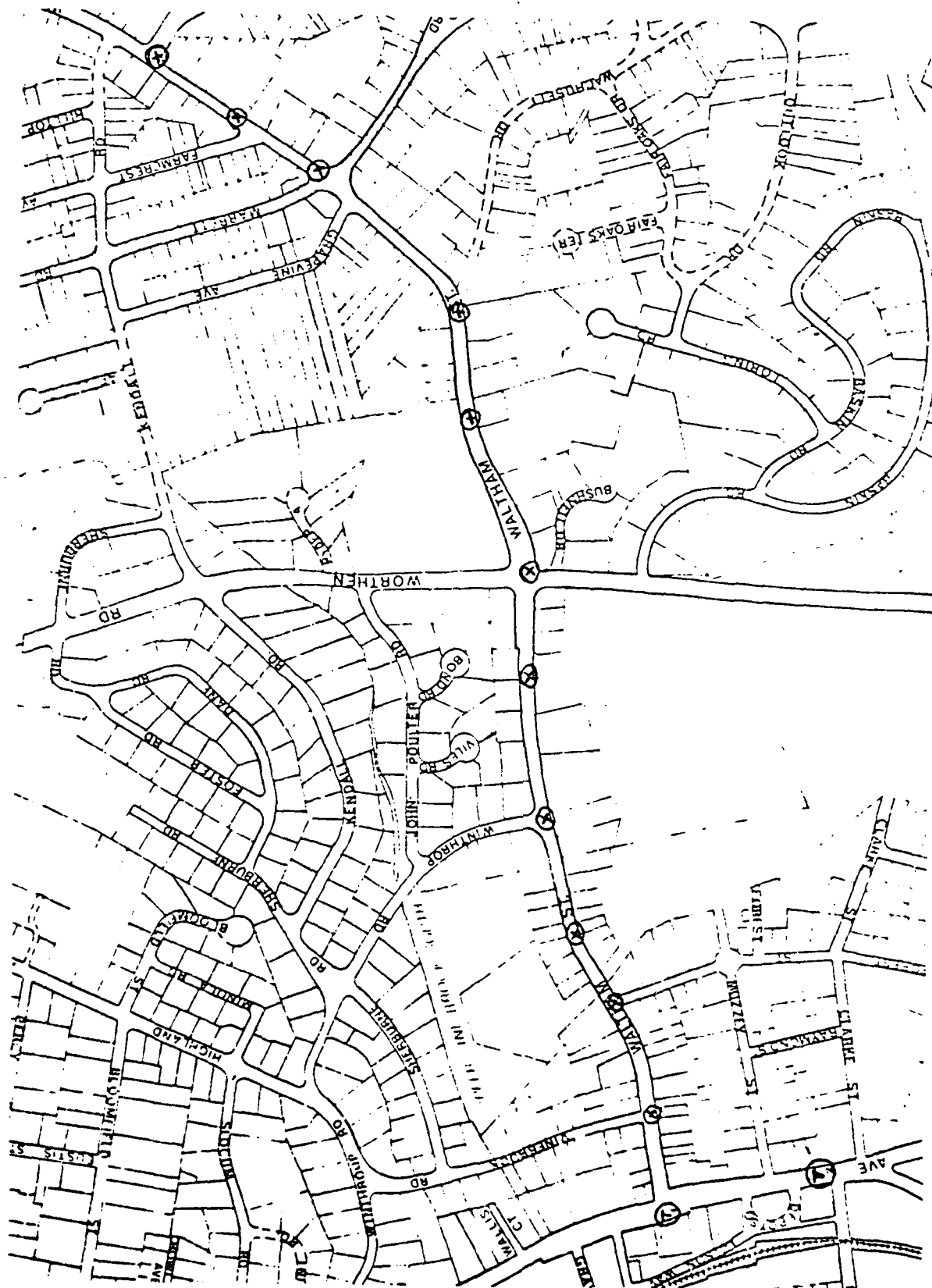
FIGURE 2.2-1 Street Map of Lexington Center
Showing Location of Test Sites

story high wood frame private homes flanked by trees. A
street map of Lexington Center is shown in Figure 2.2-1 indi-
cating the transmit locations, T_1 and T_2, and the various re-
ceive positions. As indicated in the map, two sets of measure-
ments were made: one set in which the transmit and various
receive locations were on the same street (Waltham Street),
and the other set in which the transmit location was on
Massachusetts Avenue while the various receive locations were
on Waltham Street. By making these two sets of measurements we
were able to determine the difference in path losses between
along-street and off-street transmitter-receiver orientation.

The business district of Boston is typical of a highly
built-up urban area. It consists of 5 to 30 story high re-
inforced concrete buildings spanning an area 8 city blocks long
by 8 city blocks wide. A street map of the area indicating the
transmit locations and various receive locations is shown in
Figure 2.2-2. Three sets of measurements were made in the
Boston business district: one in which the transmit and re-
ceive locations were on Congress Street; another in which the
transmit location was at the intersection of Cambridge Street
and New Sudbury Street and the receive locations were on Congress
Street; and a third set in which the transmit location was on
Summer Street and the receive locations were on various streets
near Summer Street. A detailed picture of the three transmit
locations and the various receive locations for the three
sets of measurements is presented in Figure 2.2-3. In par-
ticular, note that the third set of measurements was made
from two different transmit locations on Summer Street. Lo-
cation 3 was used for the measurements at 27 MHz and 446 MHz
while location 3a was used for the measurements at 49.8 MHz.
The Congress Street and Cambridge Street transmit locations
were in a fairly open, wide street area although the neigh-
boring buildings (Government Center) were high structures.
On the other hand, the Summer Street transmit location was on

Figure 2.2-2 Map of the Boston Business District Showing
Test Sites 1, 2, 3, and 3a

2-18

All receive locations on Congress St. (X's).

Transmit loc. 1 on Congress St. & New Sudbury St intersection

All receive locations on Congress St. (X's)

transmit loc. 2 on New Sudbury St and Cambridge St. intersection

transmit loc. 3a on Summer St. (49.8 MHz only)

transmit loc. 3 on Summer St. (27 MHz and 446 MHz)

Receive locations on various Streets (X's)
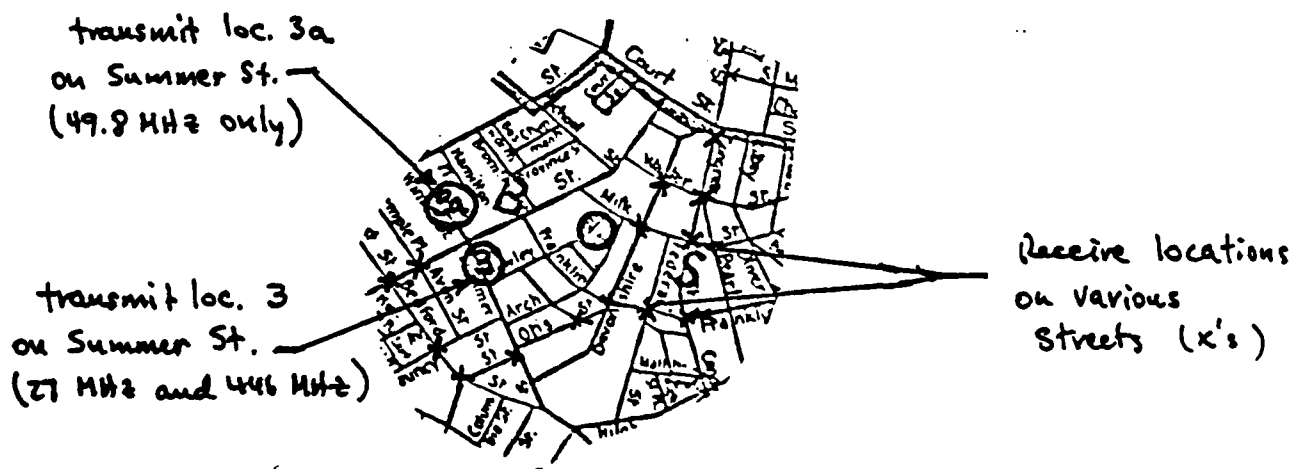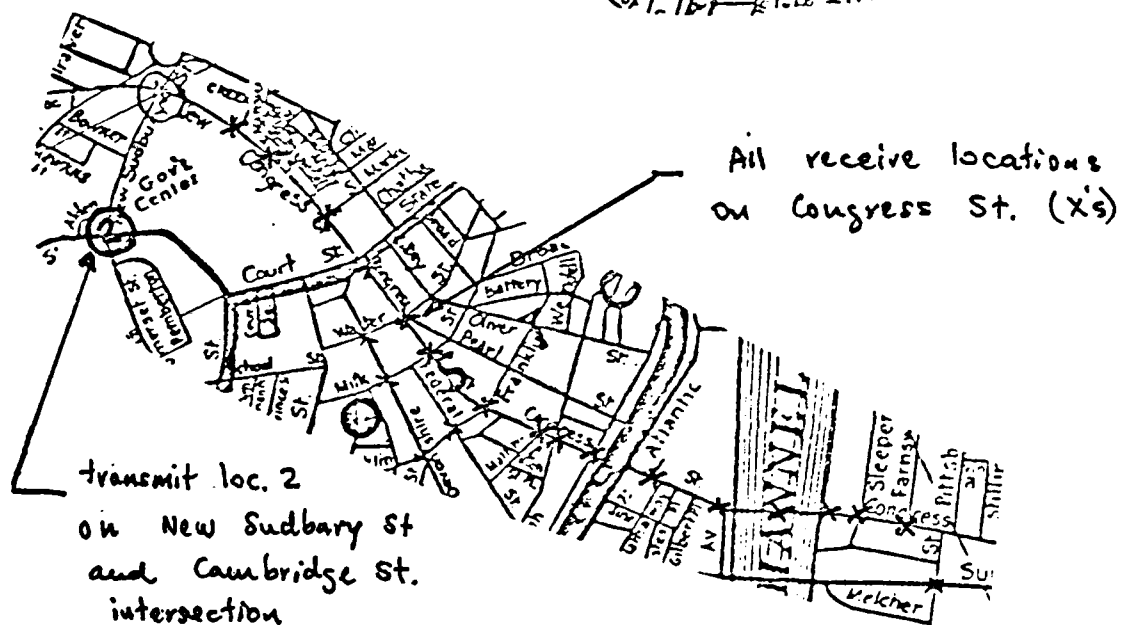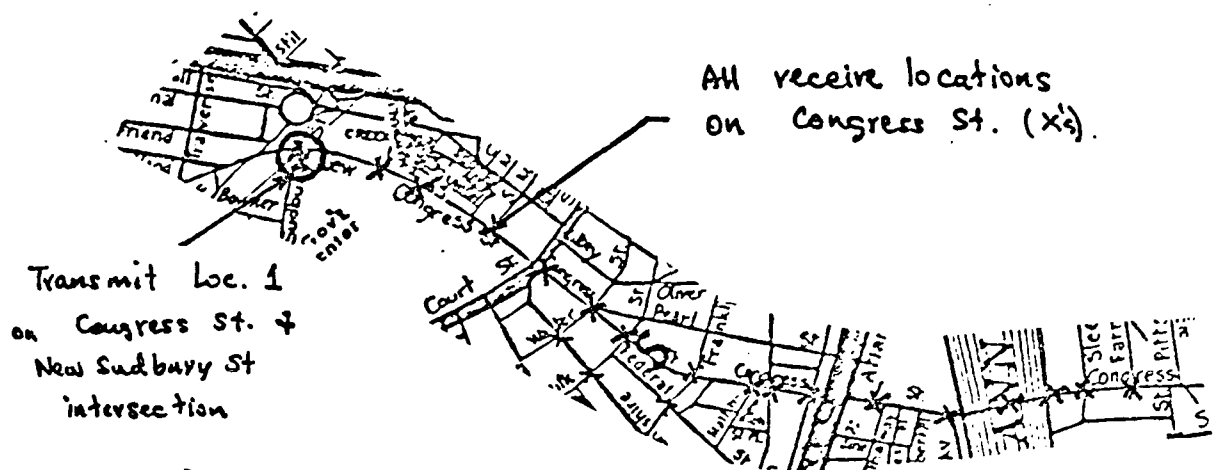
FIGURE 2.2-3   Description of the Three Urban Paths Used to Make the Street-to-Street Propagation Measurements

a narrow city street surrounded by high density high rises. From these sets of measurements, it was possible to reach some conclusions about street orientation and building proximity effects in urban areas.

The intrabuilding, building-to-building and street-to-building propagation measurements were made in two reinforced concrete office buildings located in the business district of Boston. The two buildings are adjacent to each other on the same side of the street (New Sudbury Street). One of the buildings is 5 stories high and has a garage-basement; the other building is a 24 story office high rise. Some of the street-to-building and intrabuilding measurements were repeated inside the one story SIGNATRON building located in Lexington, MA. The outside walls of this one story building are made of cinder block with brick veneer, while the interior consists of a wooden frame with gypsum walls.

The street-to-building propagation measurements were made along a floor as a function of distance from the transmitter and in various floors as a function of elevation. The measurements along a floor were made in the SIGNATRON cinder block building while the measurements as a function of elevation were made in the reinforced concrete office building.

The building-to-building propagation measurements were made between the two reinforced concrete office buildings on New Sudbury Street as a function of elevation. The receiver was placed at two different fixed positions on the third floor of the 5 story building (low-rise). The transmitter was placed near a window on each floor of the 24 story building (high-rise). A scaled (100 ft./in.) floor map of the two adjoining buildings is shown in Figure 2.2-4 indicating the relative positions of the transmit site (at every floor) and the two receive sites, R_1 and R_2 on the third floor.
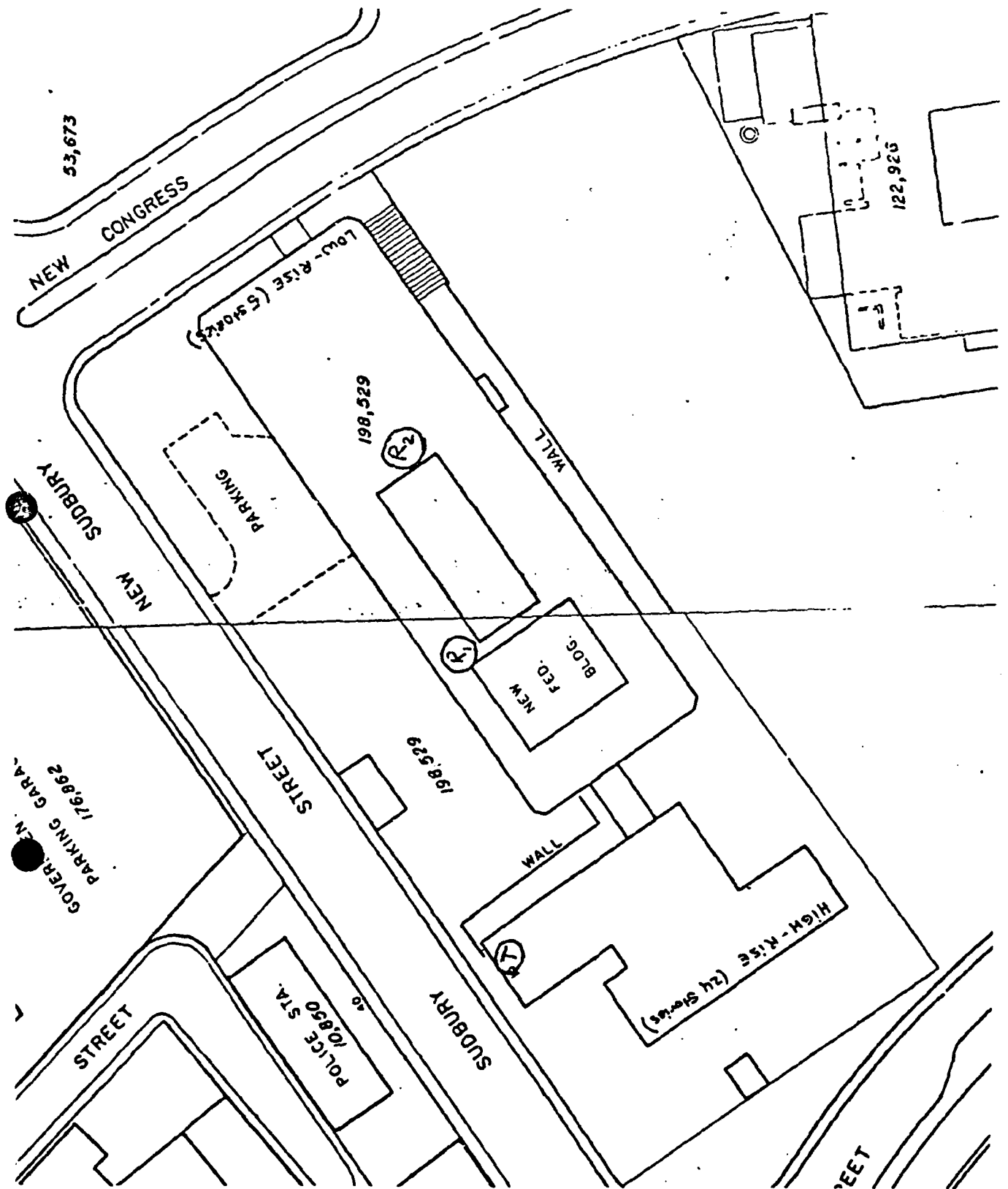
FIGURE 2.2-4   Floor Map of Two Adjoining Concrete Office Buildings

2-21

The intrabuilding propagation measurements gathered data for the following effects: (a) propagation losses along straight and winding corridors; (b) transmission losses between above-ground floors; (c) transmission losses between a basement and above-ground floors; and (d) transmission losses along elevator shafts and stairwells. All of these measurements were made in the concrete-wall building (low-rise). In addition, the propagation measurements along corridors were repeated in the suburban building with wooden frame and gypsum walls.

2.2.2 Diversity Measurements

In addition to the non-diversity measurements, data to determine whether MOBA diversity reception would be practical was gathered. The data obtained consisted of the received signal levels from diversity antennas relative to the normal receiver antenna. Two types of diversity reception were investigated: (a) field diversity at 27 MHz and 49.8 MHz; and (b) space diversity at 49.8 MHz and 446 MHz.

The field diversity measurements were made using two collocated vertically polarized antennas: one was a standard whip antenna which couples to the electric field component of the received signal, and the other was a multiturn loop antenna which couples to the magnetic field component. Since both antennas had equal polarizations but coupled to different components of the received electromagnetic field, we can obtain an estimate of the electric and magnetic field (de)-correlation after propagation in a built-up area from the ensemble correlation of the two antenna measurements.

The space diversity measurements at 49.8 MHz were made by correlating the measured received signal levels at locations 10 feet apart (.506 λ). Similarly, the space diversity measurements at 446 MHz were made by correlating the received signal levels at distances of 1.67 feet (.75 λ) and 3.3 feet (1.5 λ).

2.3   Street-to-Street Propagation Measurements

2.3.1   Urban Path Loss Measurements

The street-to-street propagation measurements made in Boston are shown in Figures 2.3-1 to 2.3-9. Figures 2.3-1 to 2.3-3 show the received signal level in dBm as a function of transmitter-to-receiver distance for the case in which the transmit and receive locations were on Congress Street. The 'circles' represent the data taken with a receive whip antenna while the 'exes' represent the data taken with a receive loop antenna. The solid line and the dashed line are 'the best fits' (median received signal levels) to the data taken with the whip and loop antennas, respectively. The standard deviations away from the median are shown in parenthesis in the legend. Figures 2.3-4 to 2.3-6 show the equivalent data for the case in which the transmit location was at Cambridge and New Sudbury Street and the receive locations were on Congress Street. The data for the case in which the transmit location was on Summer Street and the receive locations were on various different streets are shown in Figures 2.3-7 to 2.3-9.

From the slopes of the 'best fit' lines we can determine the distance dependence (and attenuation rate) of the received signal level. The assumed linear distance dependence of the received signal in dBm implies that the received signal level, P_r, varies as: $P_r \sim kd^{-n}$ where k is a proportionality constant (which depends on the transmitted power and antenna gains), d is the distance and n is the slope of the 'best fit line' divided by 10. We see from the urban data at 27 MHz that

$$@ \ 27 \ MHz \quad n= \begin{cases} 4.69 & \text{Along street path 1} \\ 4.0 & \text{NLOS path 2*} \\ 2.03 & \text{NLOS path 3*.} \end{cases}$$

Similarly, from the data at 49.8 MHz and 446 MHz, we have

---

*NLOS = not line-of-sight

FIGURE 2.3-1 Received Signal Level vs. Distance Along Urban Street
(Congress St., Boston, MA)

2-24

FIGURE 2.3-2 Received Signal Level vs. Distance Along Urban Street (Congress St., Boston, MA)

FIGURE 2.3-3   Received Signal Level vs. Distance Along Urban Street
(Congress St., Boston, MA)

DISTANCE (feet)

RECEIVED SIGNAL LEVEL (dBm)

f_o = 27 MHz

⊙   whip ($\pm$3.42 dB)

x   loop ($\pm$6.55 dB)
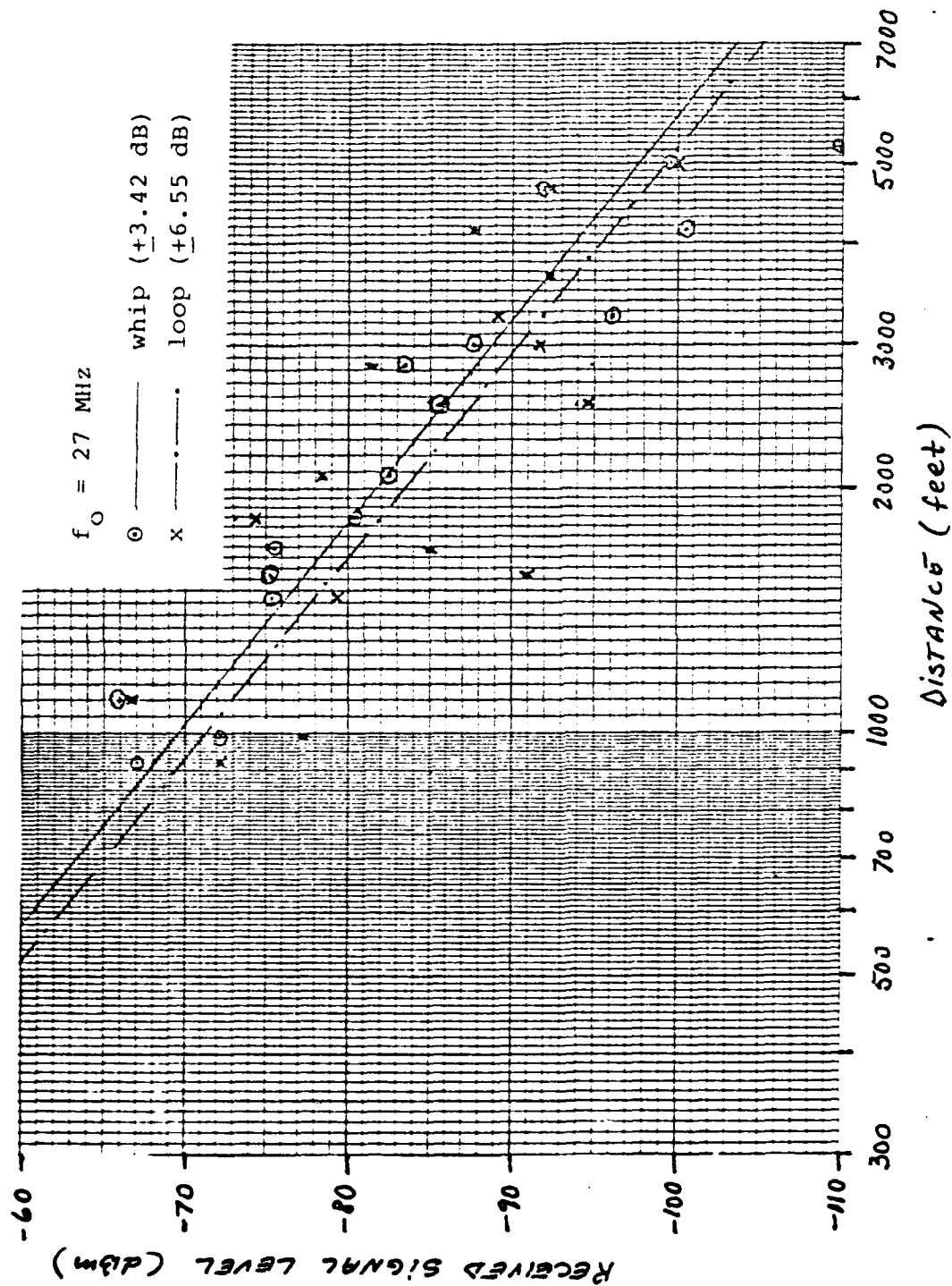
FIGURE 2.3-4   Received Signal Level vs. Distance for a Non-Line of Sight Urban Path (Transmitter at Cambridge and New Sudbury Sts., Boston, MA)
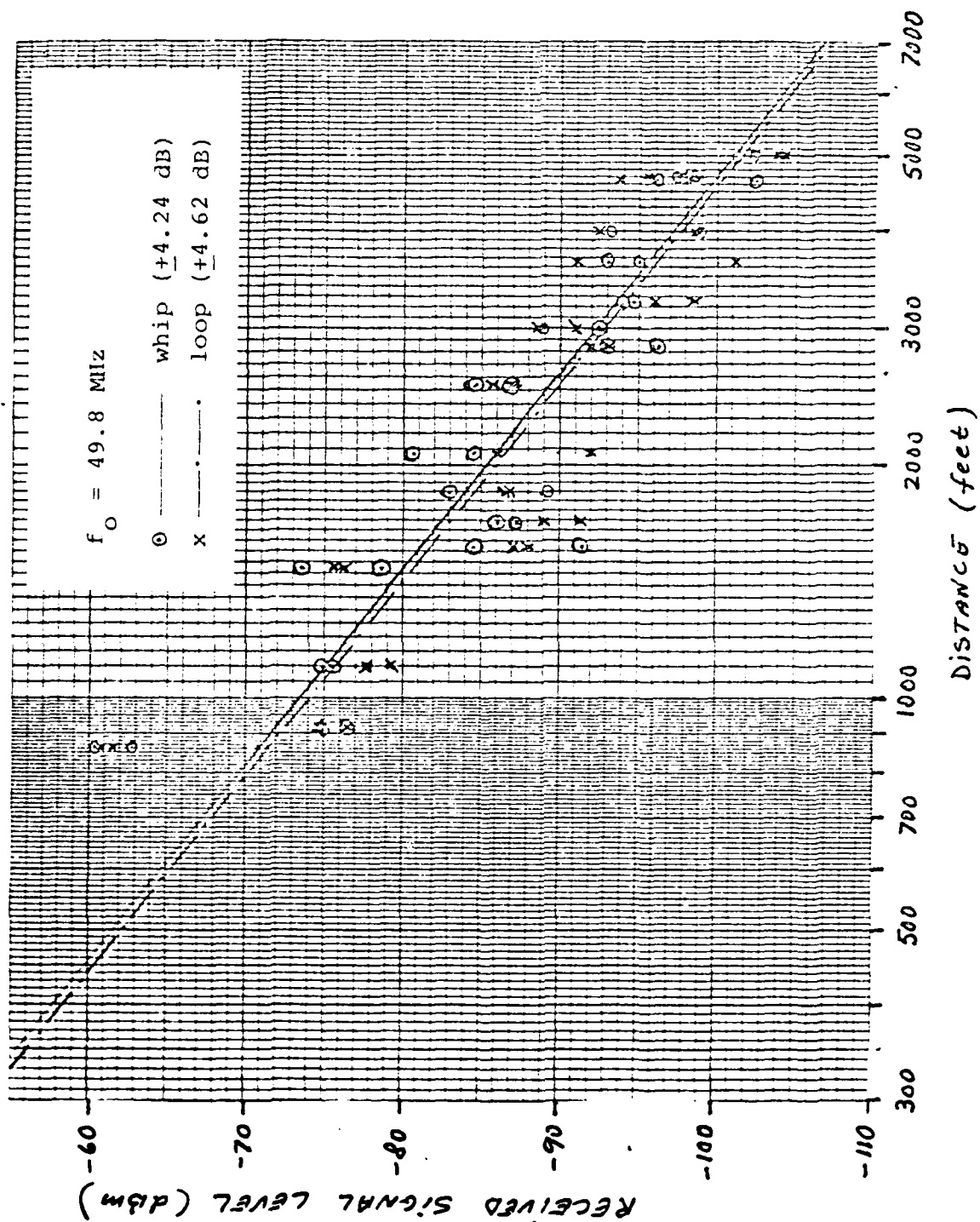
FIGURE 2.3-5 Received Signal Level vs. Distance for a Non-Line-of-Sight Urban Path (Transmitter at Cambridge and New Sudbury Sts., Boston, MA)
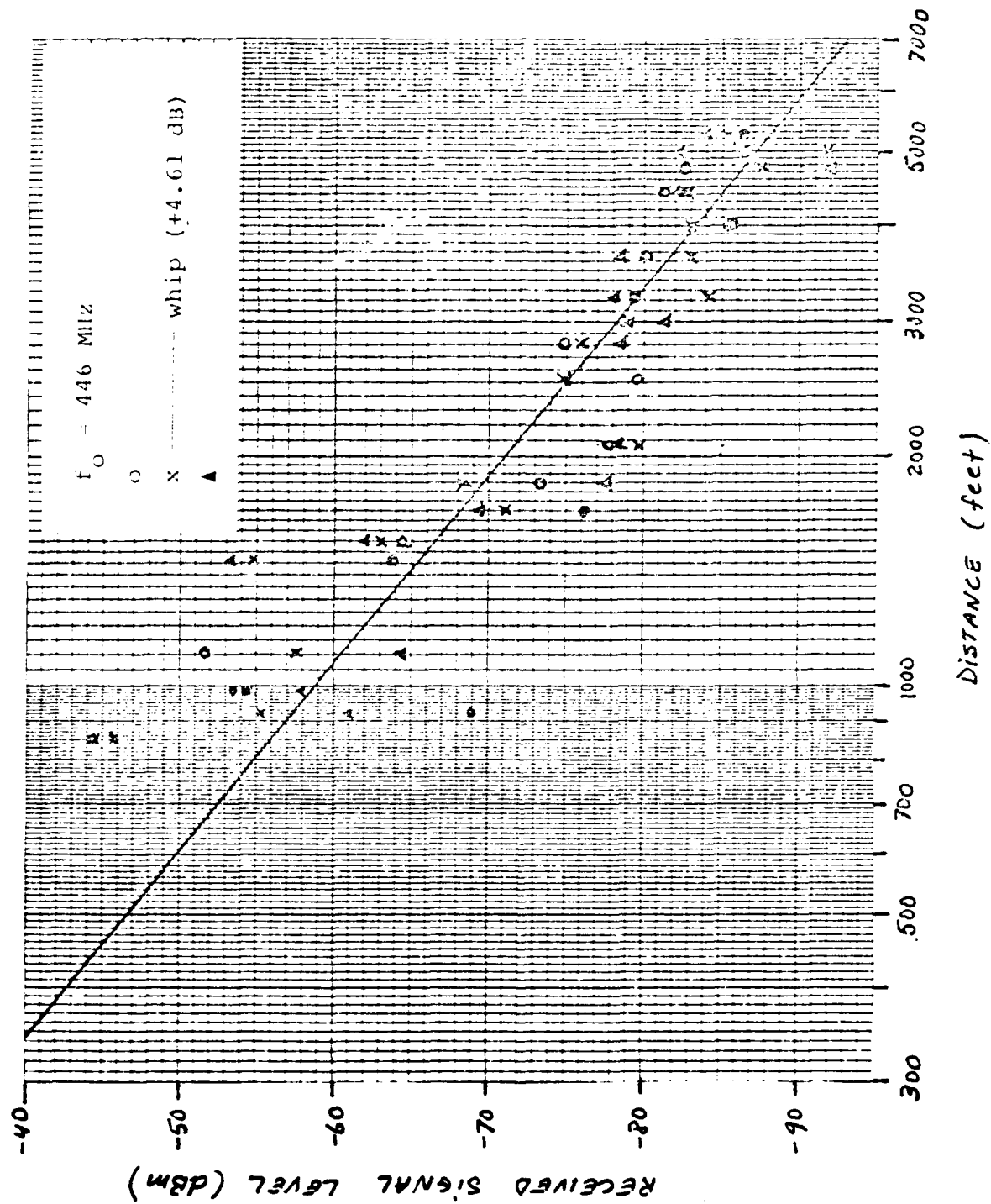
FIGURE 2.3-6   Received Signal Level vs. Distance for a Non-Line-of-
Sight Urban Path (Transmitter at Cambridge and New
Sudbury Sts., Boston, MA)
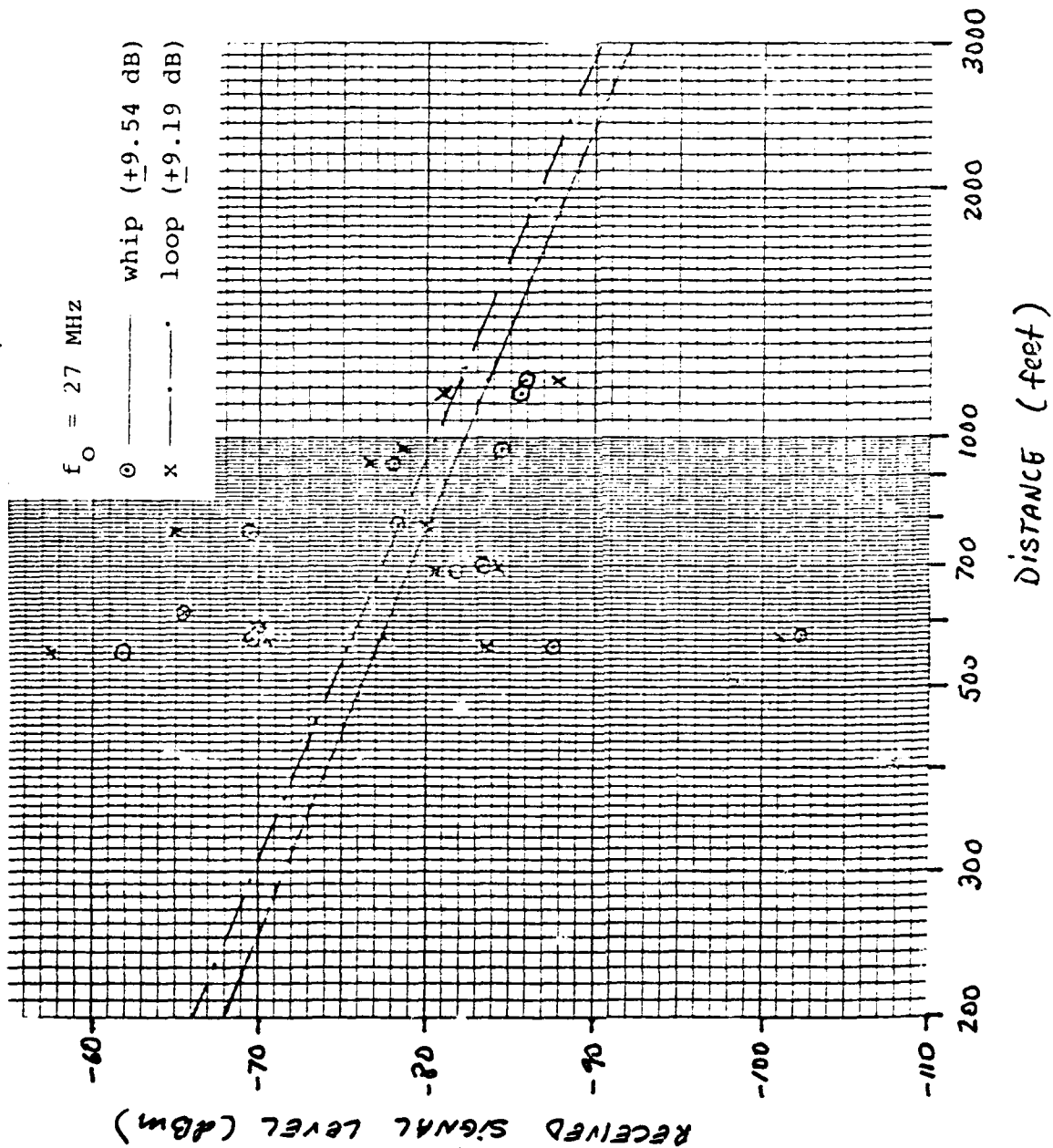
FIGURE 2.3-7 Received Signal Level vs. Distance for a Non-Line-of-Sight Urban Path (Transmitter on Summer St., Boston, M?.
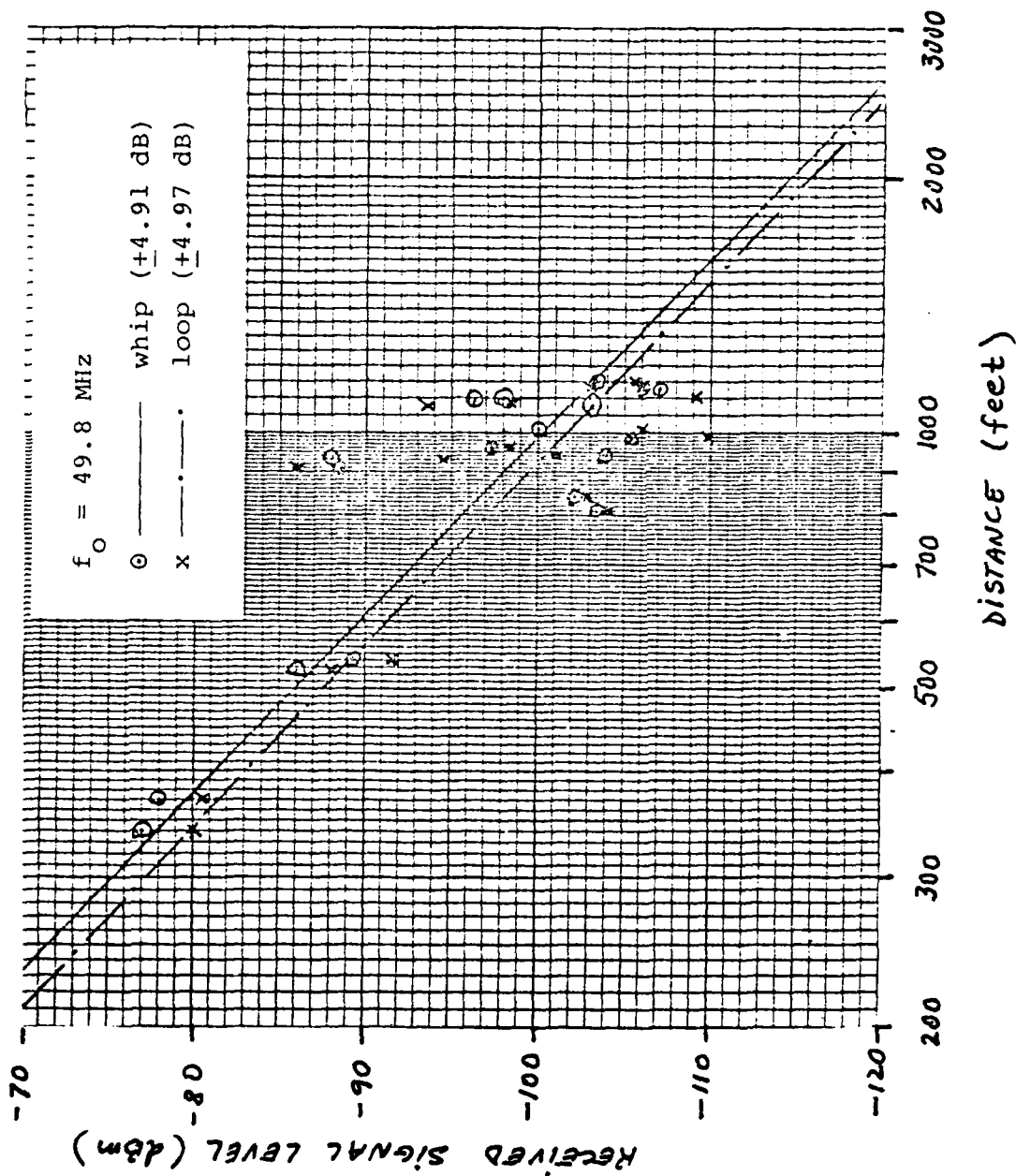
FIGURE 2.3-8 Received Signal Level vs. Distance for a Non-Line-of-Sight Urban Path (Transmitter on Summer St., Boston, MA)

FIGURE 2.3-9 Received Signal Level vs. Distance for a Non-Line-of-Sight Urban Path (Transmitter on Summer St., Boston, MA)

2-32
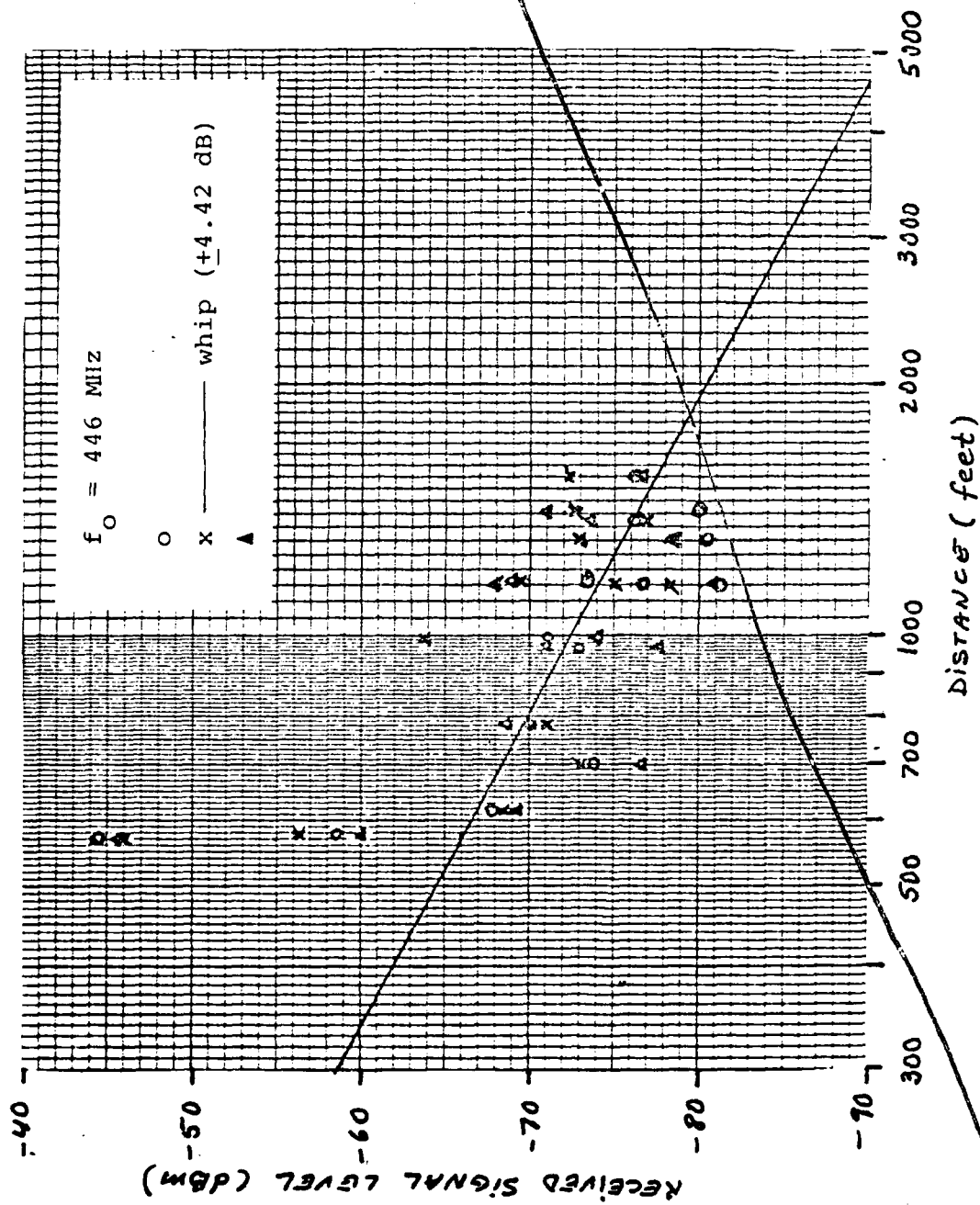
$$@ \text{ } 49.8 \text{ MHz} \quad n = \begin{cases} 4.5 & \text{Along street path 1} \\ 3.95 & \text{NLOS path 2*} \\ 4.67 & \text{NLOS path 3*} \end{cases}$$

$$@ \text{ } 446 \text{ MHz} \quad n = \begin{cases} 4.26 & \text{Along street path 1} \\ 4.08 & \text{NLOS path 2*} \\ 2.65 & \text{NLOS path 3*.} \end{cases}$$

Of the nine sets of measurements, seven exhibited approximately inverse fourth power law (n≃4.) distance dependence independent of the frequency. This implies that the propagation mechanism is similar to that of plane-earth propagation. Of the seven sets, six correspond to the cases in which the transmit site was either at the Congress Street - New Sudbury Street intersection (Figures 2.3-1 to 2.3-3) or Cambridge Street - New Sudbury Street intersection (Figures 2.3-4 to 2.3-6). Both of these locations are fairly open areas with no high structures within 50 feet to the front or side of the transmitter. The remaining set of measurements with near inverse fourth power law distance dependence is the set of measurements at 49.8 MHz from a transmit location on Summer Street (Figure 2.3-8), which is a narrow street with medium tall structures (3 to 6 stories high) on both sides of it. The two sets of measurements which exhibit approximately inverse square law (n≃2.) distance dependence were also made from a transmit location on Summer Street at 27 MHz (Figure 2.3-7) and 446 MHz (Figure 2.3-9). The difference between these two sets of measurements and the set of measurements at 49.8 MHz is that the latter were made with the transmitter on the sidewalk while the other two (27 MHz and 446 MHz) were made with the transmitter on the middle of the street.

The significance of the distance dependence versus transmitter location is interpreted as follows: typically, energy will propagate (in a built-up area) from transmitter

---

*NLOS = not line-of-sight

to receiver via diffraction over and around buildings and scattering and/or reflection from buildings. When the predominant mode of propagation is diffraction over buildings, the median received signal will exhibit near inverse square law distance dependence, if there is only just one predominant diffraction path. On the other hand, when energy propagates via reflection and diffraction around buildings (or there are many significant paths after diffraction over buildings) there tend to be more than one significant path, which, when adding out of phase, result in a near-inverse fourth power law distance dependence. Hence, we conclude that in the case of the 49.8 MHz measurements with the transmitter on the sidewalk, energy most likely propagated via reflection and diffration around buildings (guided street propagation). On the other hand, in the case of the 27 MHz and 446 MHz measurements with the transmitter on the middle of the street, energy propagated predominantly along a single path over the adjacent buildings. Furthermore, two of the data points at 27 MHz (Figure 2.3-7) were taken with the transmitter located on the sidewalk (rather than the middle of the street). The measured received signal level in this instance was 20 dB lower than the signal level measured with the transmitter on the middle of the street and 25 dB below the expected median. This measurement illustrates the gain one might expect when moving away from a building towards a more open area. Much of our data was, in fact, obtained with the receiver in the middle of the street because the received signal level was not measurable on the sidewalk close to the building.

Aside from the propagation law, we can also determine the maximum transmission range for 1-10 Watt transmissions at VHF and UHF from Figures 2.3-1 to 2.3-9. We see that when the transmitter is in a relatively open area (Figures 2.3-1 to 2.3-6), even though the receiver might not be, the maximum transmission range is 5,000 feet independent of the frequency.

On the other hand, when both transmitter and receiver are surrounded by high structures, the maximum range is 1,000 - 2,000 feet depending on how close the transmitter and receiver are to the nearby structures.

In conclusion, these measurements indicate that the urban attenuation rate between low elevation antennas is approximately 40 dB per decade (independent of frequency) whenever there are no obstacles higher than a few wavelengths within a few wavelengths of the transmit site and 20 dB per decade if the opposite is true. The diffraction loss associated with the 20 dB decade transmission may, however, be significant.

The frequency dependence of the net path loss of the urban propagation measurements cannot be determined until the antenna gains and transmitted power are subtracted out. Thus we postpone discussing them as well as the E-H field correlation until the next section.

2.3.2   Suburban Path Loss Measurements

The suburban street-to-street propagation measurements made in Lexington are shown in Figures 2.3-10 to 2.3-15. The received signal level in dBm as a function of distance for the case in which the transmit location was at the intersection of Massachusetts Avenue and Waltham Street is shown in Figures 2.3-10 to 2.3-12. Again, the circles represent the data obtained with a whip receive antenna while the "exes" represent the data obtained with a loop receive antenna. The solid and dashed lines are 'the best fits' to the data taken with the whip and loop antennas, respectively. The standard deviations of the data from their median levels (solid and dashed lines) are shown in the legend. Similarly, the equivalent data obtained when the transmit location was on Massachusetts Avenue and the various receive locations were on Waltham Street are shown in Figures 2.3-13 to 2.3-15.

2-35
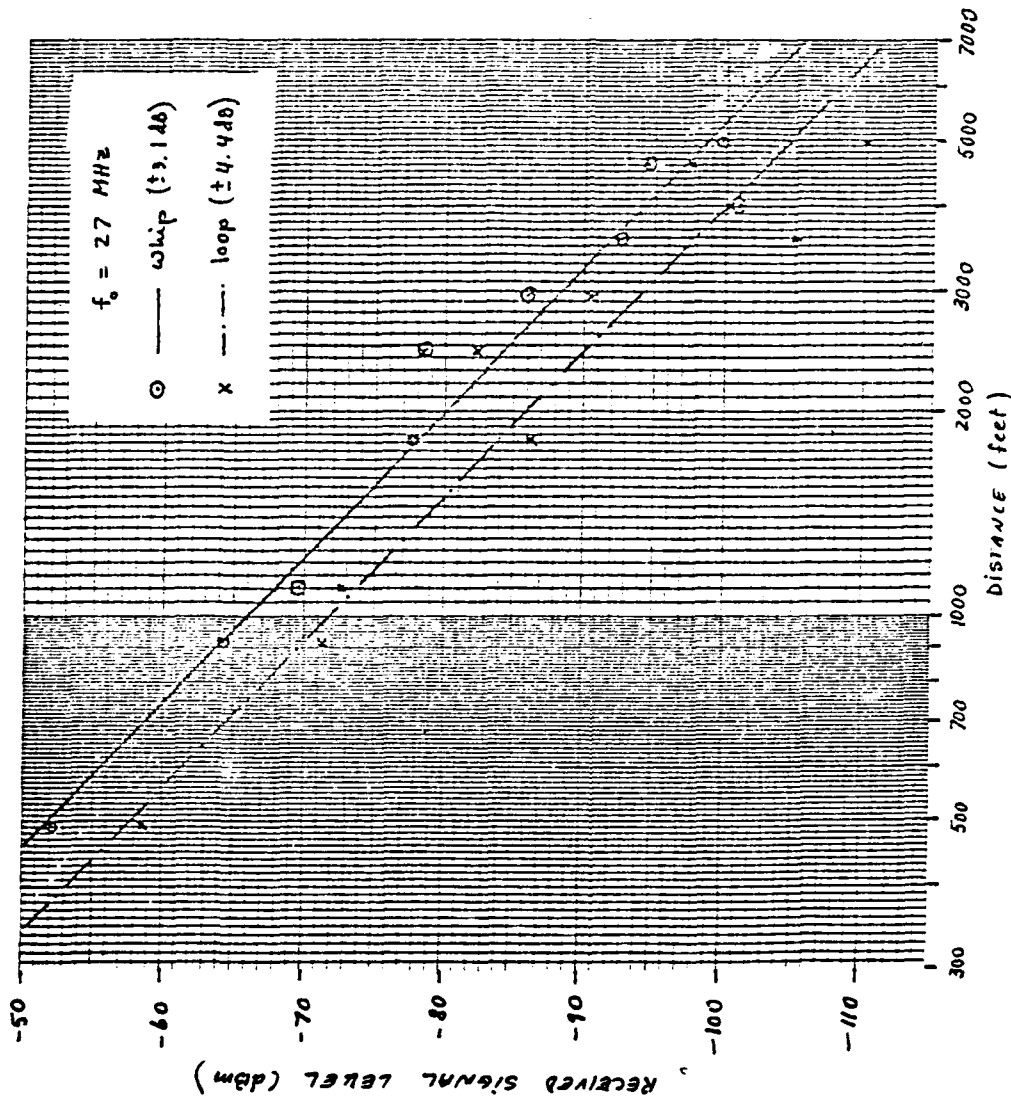
FIGURE 2.3-10 Received Signal Level vs. Distance Along
Suburban Street (Waltham St., Lexington,
MA)
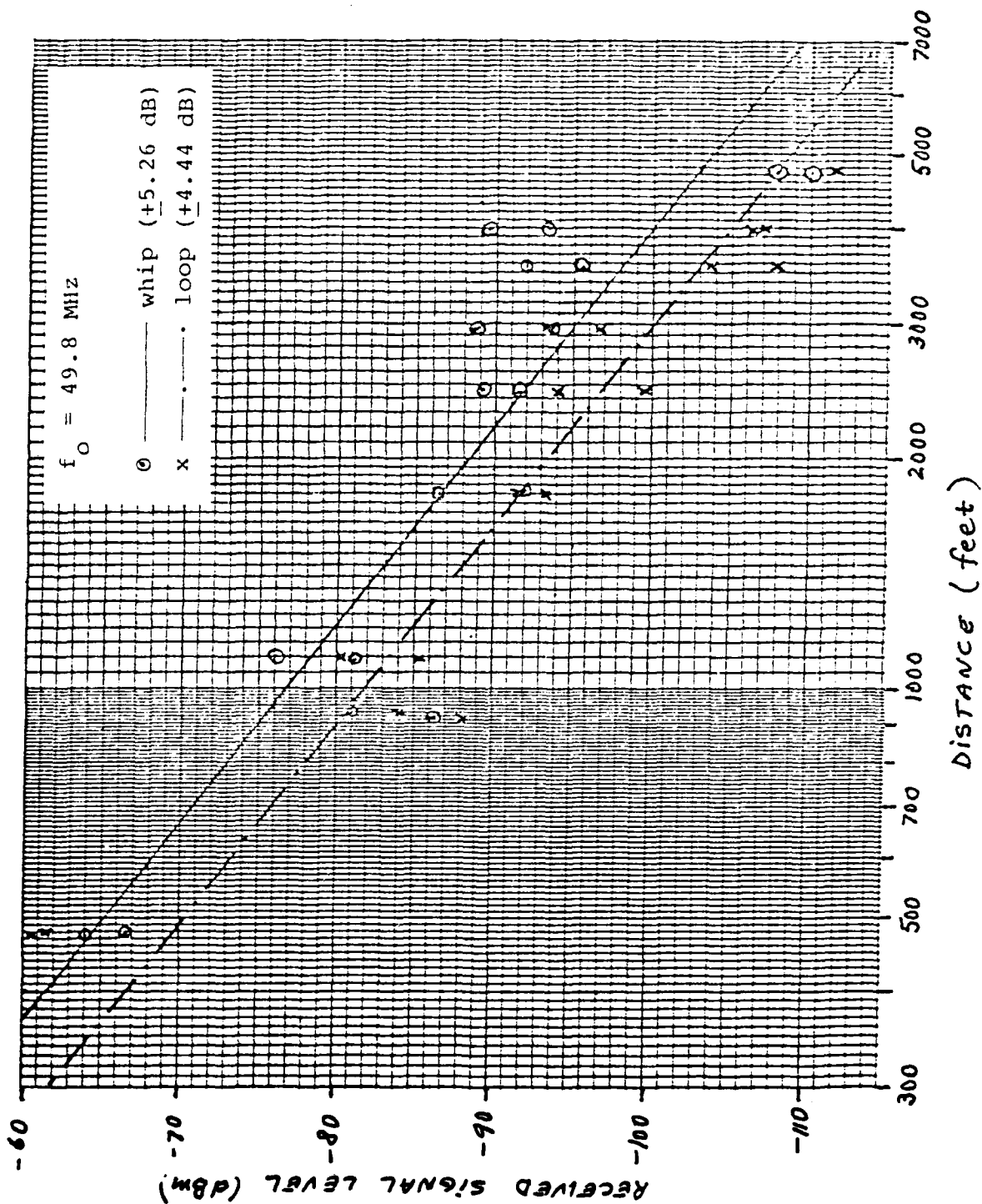
FIGURE 2.3-11 Received Signal Level vs. Distance Along Suburban
Street (Waltham St., Lexington, MA)
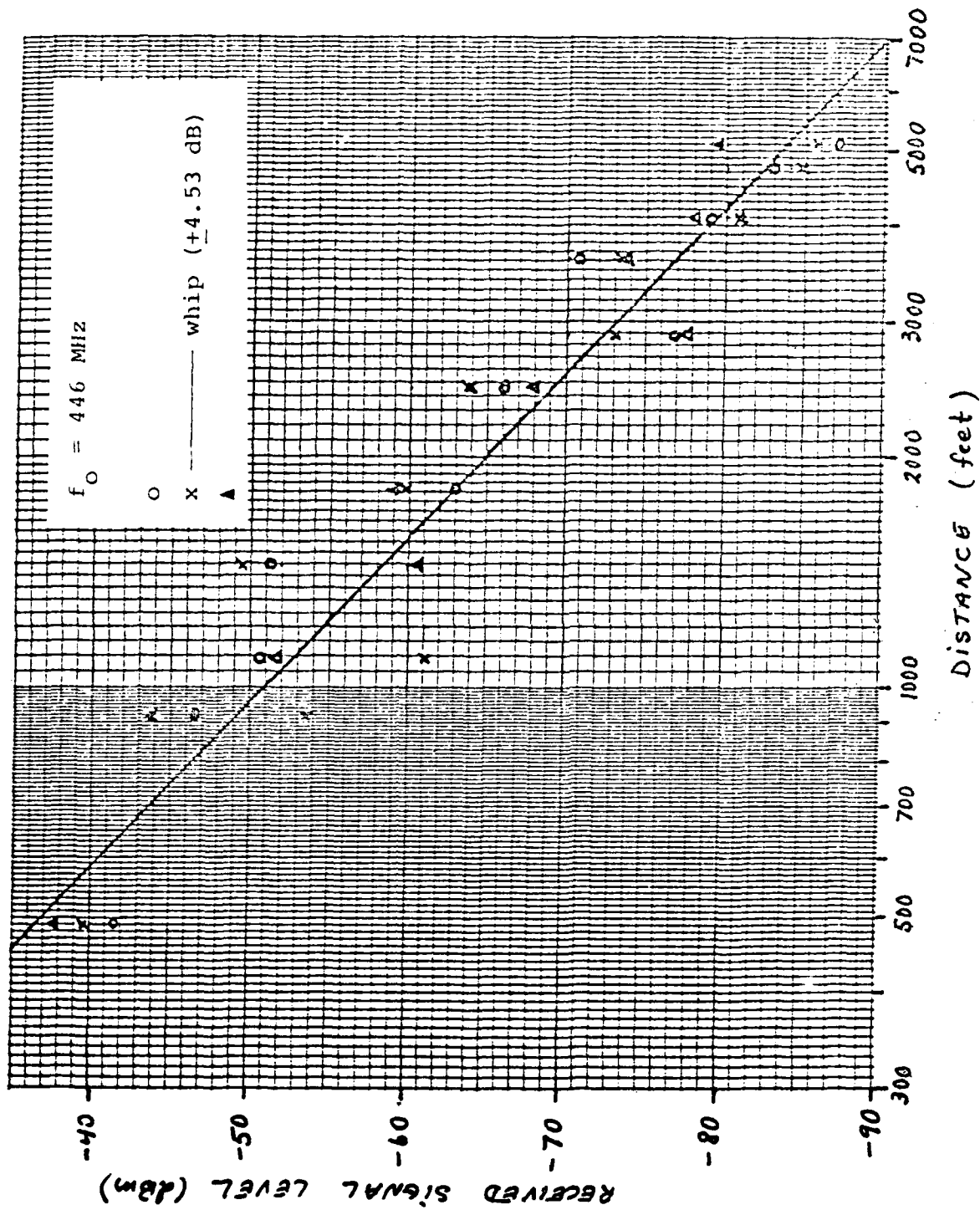
FIGURE 2.3-12   Received Signal Level vs. Distance Along
Suburban Street (Waltham St., Lexington, MA)
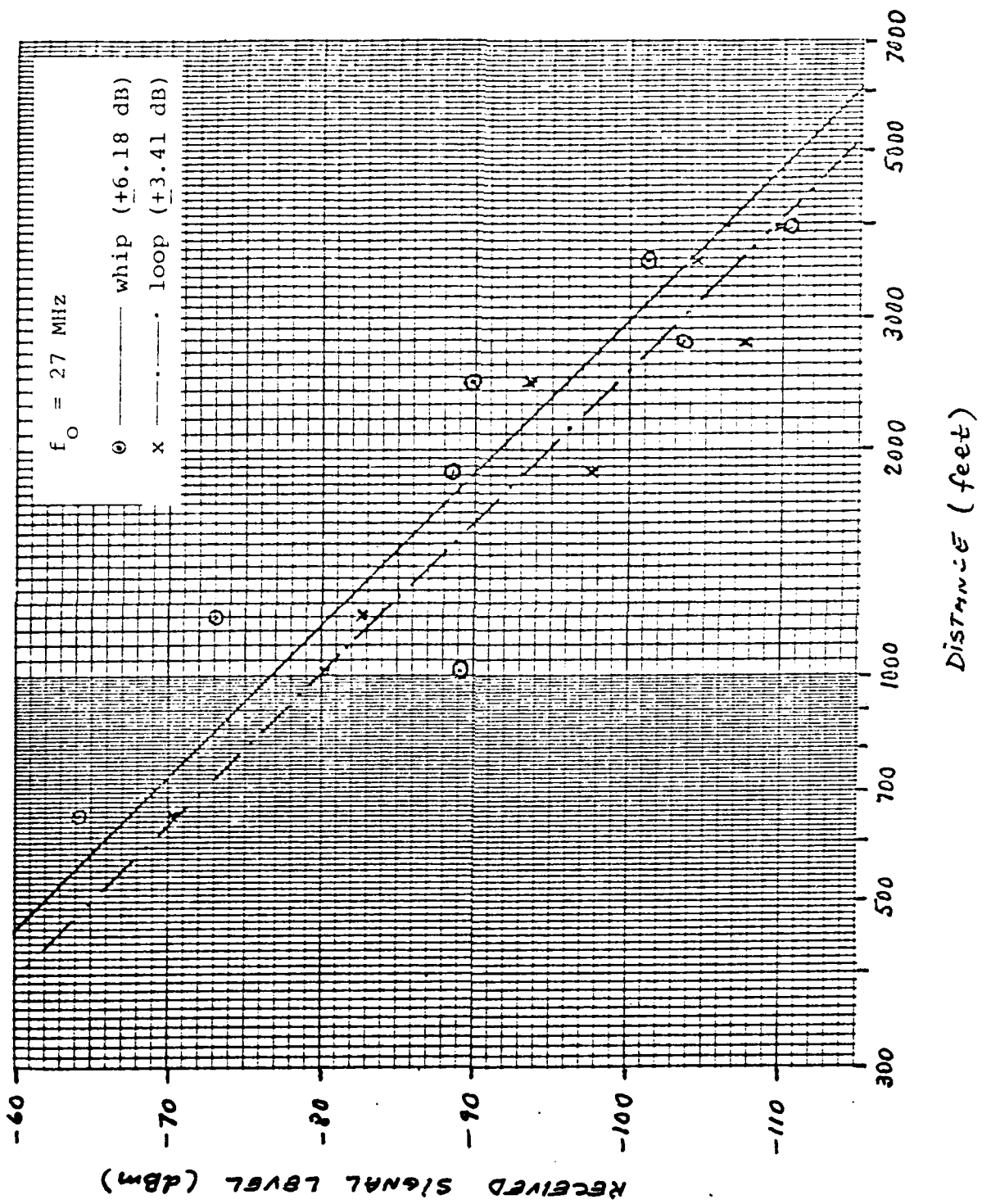
FIGURE 2.3-13 Received Signal Level vs. Distance for a Non-Line-of-Sight Suburban Path (Transmitter on Mass. Ave., Lexington, MA)
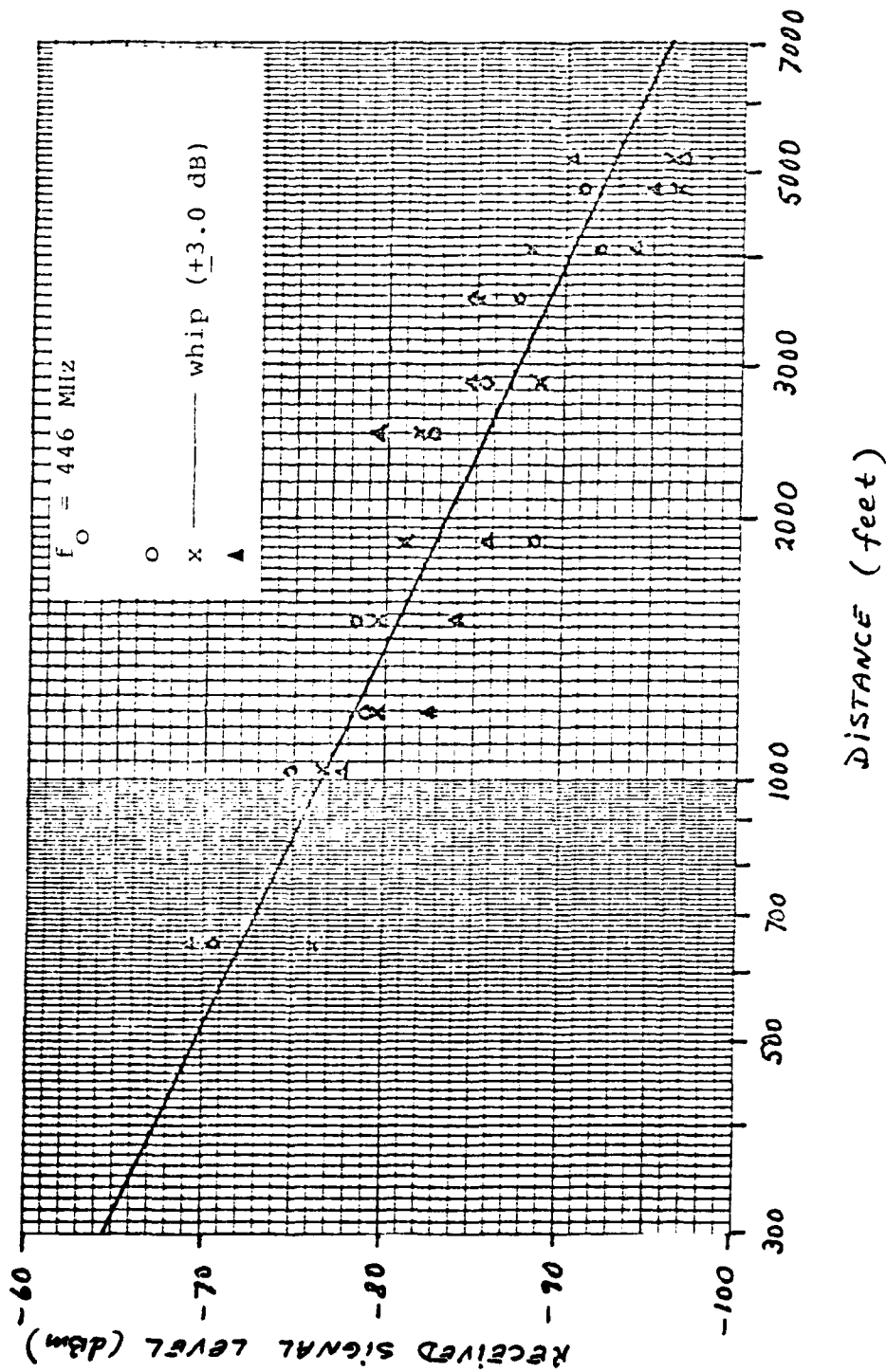
FIGURE 2.3-14 Received Signal Level vs. Distance for a Non-Line-of-Sight Suburban Path (Transmitter on Mass. Ave., Lexington, MA)
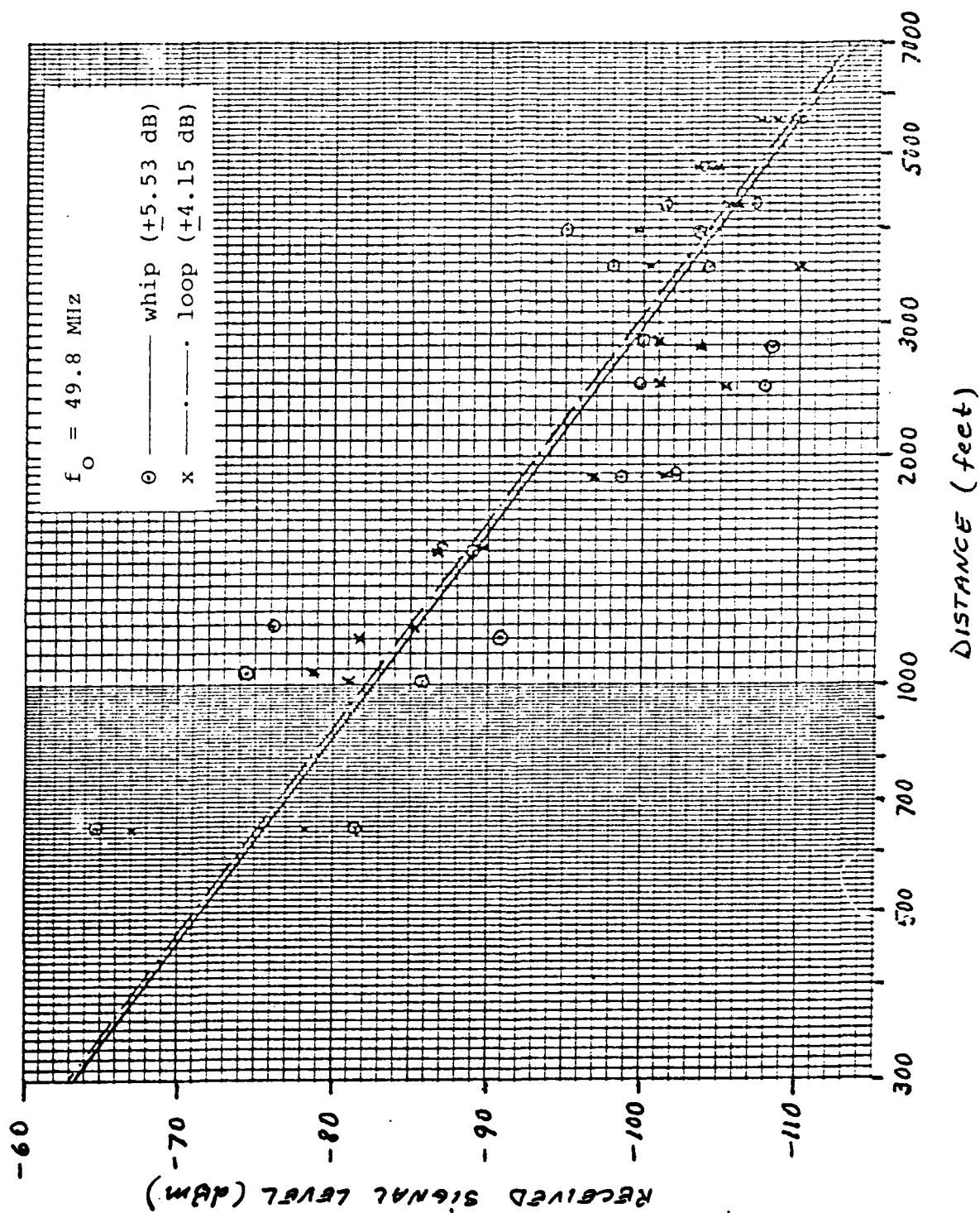
FIGURE 2.3-15 Received Signal Level vs. Distance for a Non-Line-of-Sight Suburban Path ("Transmitter on Mass. Ave., Lexington, MA)

2-41

The distance dependence (propagation law) of the sub-urban measuements can be determined from the slopes of the best fit lines to the data (median received signal levels). We see that if a $P_r \sim kd^{-n}$ type of distance dependence is assumed for the median received signal level, then we find from Figures 2.3-10 to 2.3-15 that

$$@ \ 27 \ MHz \quad n= \begin{cases} 4.68 & \text{Along street path} \\ 4.96 & \text{NLOS path} \end{cases}$$

$$@ \ 49.8 \ MHz \quad n= \begin{cases} 3.85 & \text{Along street path} \\ 3.58 & \text{NLOS path} \end{cases}$$

$$@ \ 446 \ MHz \quad n= \begin{cases} 4.66 & \text{Along street path} \\ 2.28 & \text{NLOS path.} \end{cases}$$

We conclude from the data that all but one of the sets of measurements exhibited near inverse fourth power law distance dependence which corresponds to a plane-earth type of propagation mechanism. The remaining set of measurements at 446 MHz exhibited a near inverse square law type of distance dependence which indicated that the probable propagation mechanism was a diffraction plus free-space type of propagation. This is not surprising since the transmitter was positioned on the sidewalk with a two story high brick building directly in front, along a straight line connecting the transmit and receive locations. At 27 MHz ($\lambda \approx 11m \approx 36$ ft) and 49.8 MHz ($\lambda \approx 6m \approx 19.2$ ft), the height of the building (30 ~ 40 ft) is in the order of the wavelength, λ, so that for all practical purposes the building does not represent an obstacle capable of diffracting the radiated signal. However at 446 MHz ($\lambda \approx 7m \approx 2.3$ ft) the building is many wavelengths high so that it does represent a diffracting obstacle.

We can then conclude that the suburban attenuation rate between low elevation antennas is also around 40 dB per decade when no obstacles larger than the wavelength are in the immediate vicinity of the transmit site and 20 dB per decade when the converse is true.

We can also see from Figures 2.3-10 to 2.3-15 that the range of the radios in a suburban area was 5,000 feet independent of the transmit location or frequency. This maximum range is similar to that measured in an urban area (Boston) with the transmitter located in an open (no obstacles within 50 feet) area.

The measurements of Figures 2.3-1 to 2.3-15 represent samples at isolated receiving sites and provide us with sufficient information to determine the average path loss as a function of distance for the various test frequencies. However, they do not give any information about the short scale distance dependence (distances in the order of a few wavelengths) of the received signal level. This type of information is important because it gives an indication of the changes in received signal level that one might expect by moving a few feet. Thus, in order to obtain this information, we repeated the suburban path loss measurements but this time we mounted the receive antenna on a car and recorded the received signal level on a portable Gould strip chart recorder. The transmit and receive radios were the AN/PRC-77 radios previously described equipped with 3 foot whip antennas. The recordings were made at two frequencies: 30 MHz and 49.8 MHz and are shown in Figures 2.3-16 and 2.3-17. Figure 2.3-16 shows the recorded received signal level as a function of distance for the case in which the transmitter and receiving mobile unit were both on Waltham Street while Figure 2.3-17 shows the same information for the case in which the transmit location was on Massachusetts Avenue and the mobile moved along Waltham Street. The actual distance was estimated by placing identifying marks on the recordings.

From these recordings, we can see that the received signal exhibits extreme variations in amplitude. Fade depths varying from a few dB to in excess of 20 dB below the mean sig-
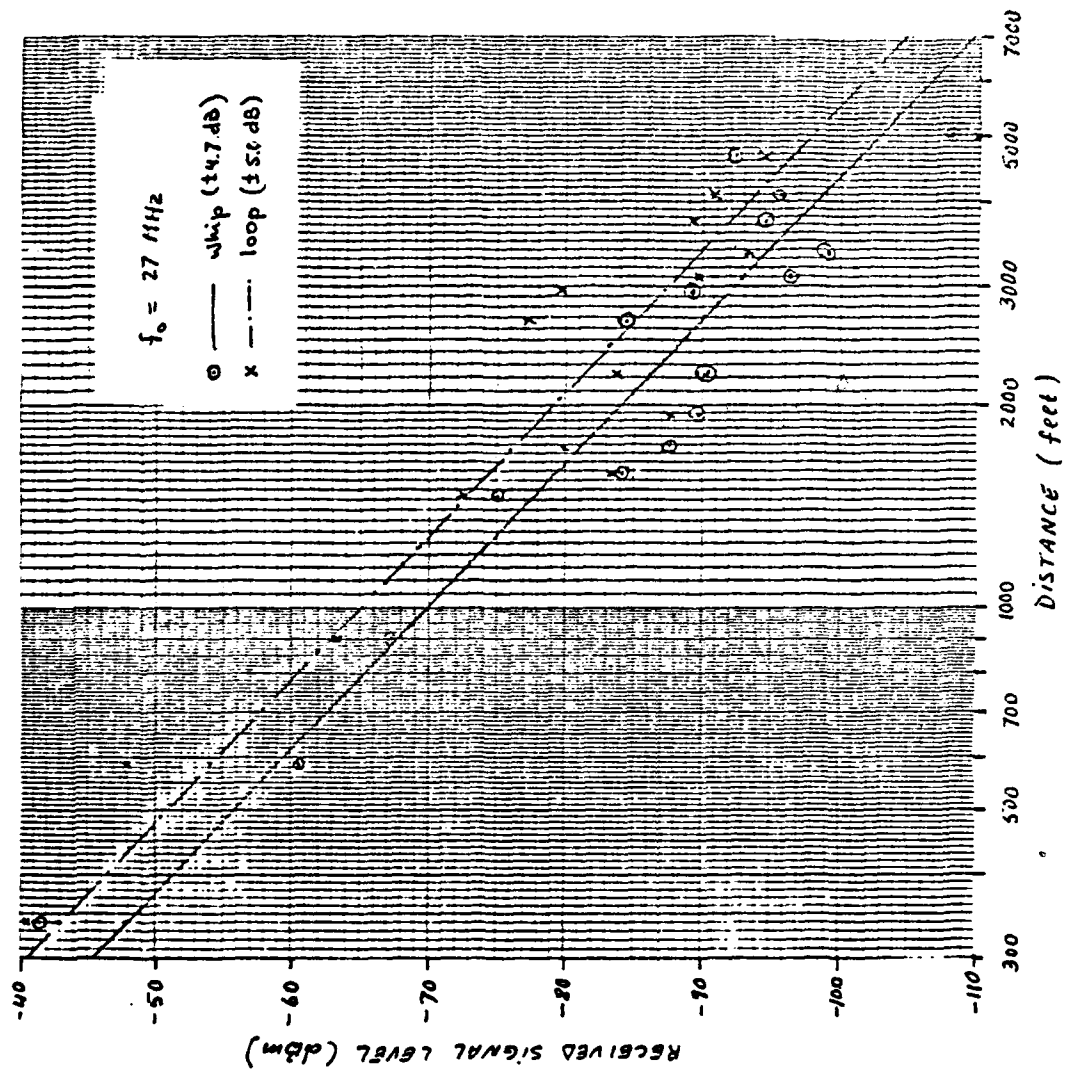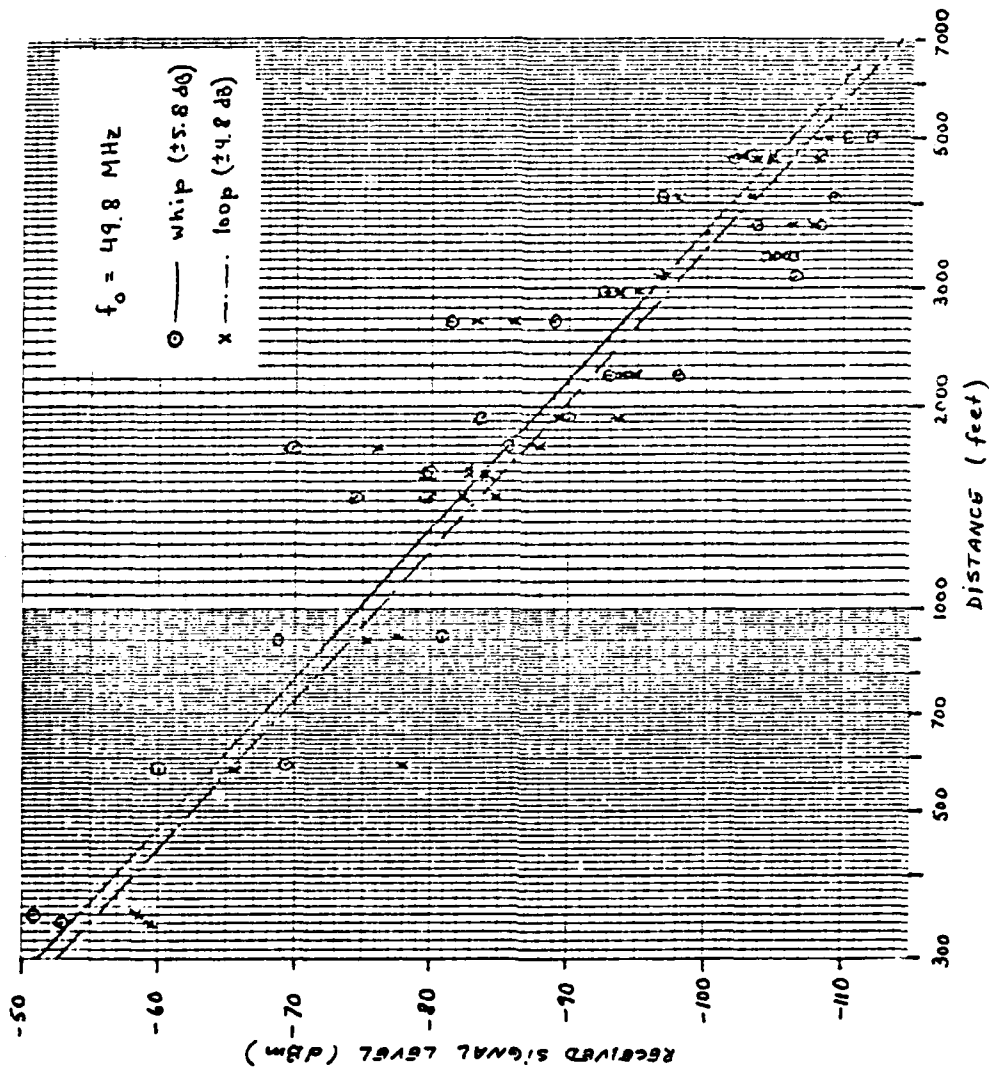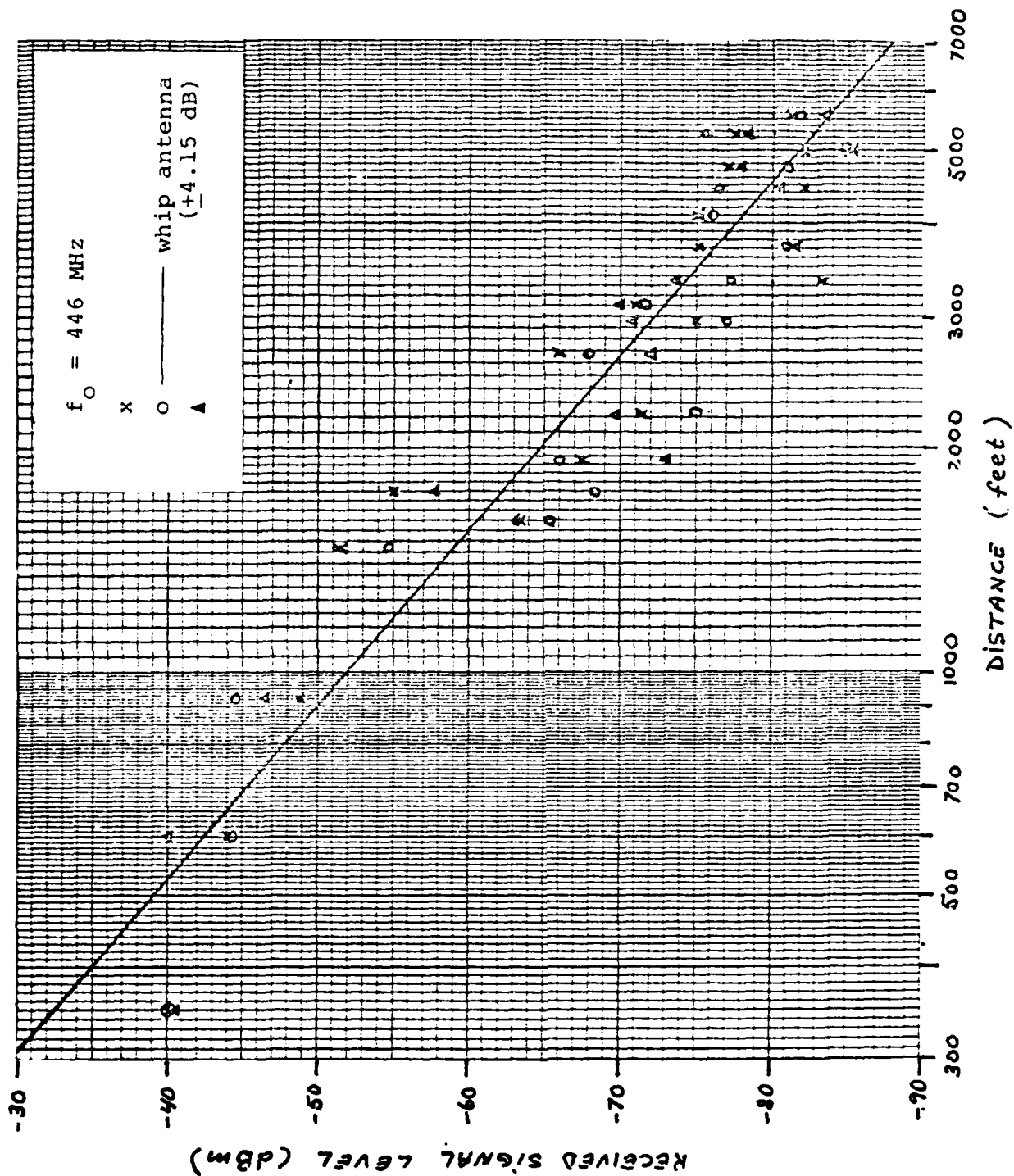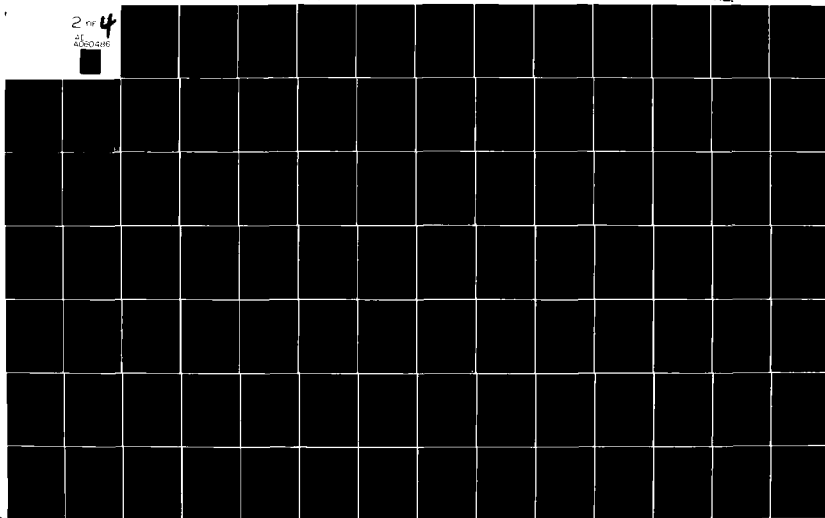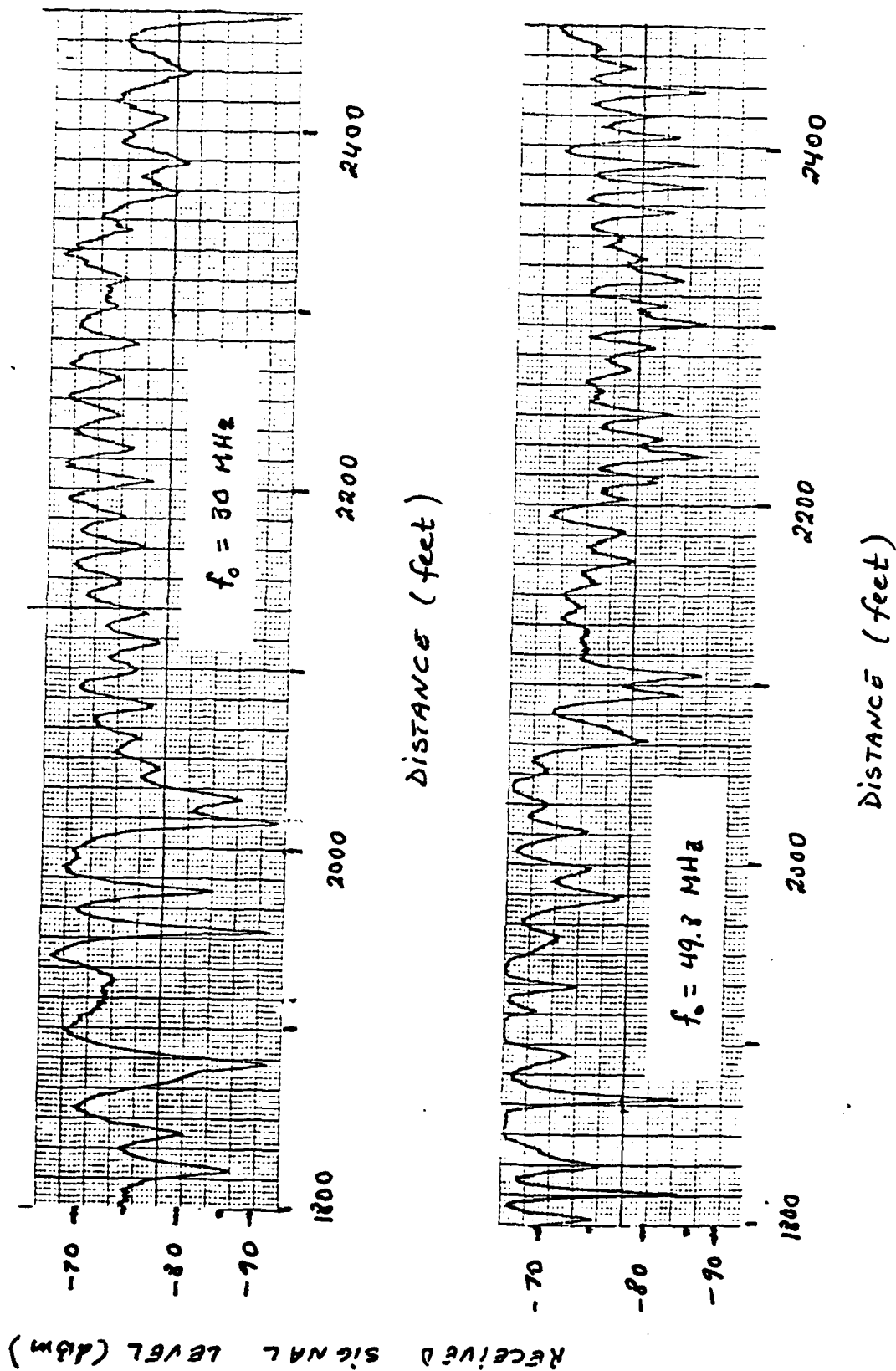
FIGURE 2.3-16   Received Signal Level vs. Distance Along Suburban
Street (Waltham St., Lexington, MA)
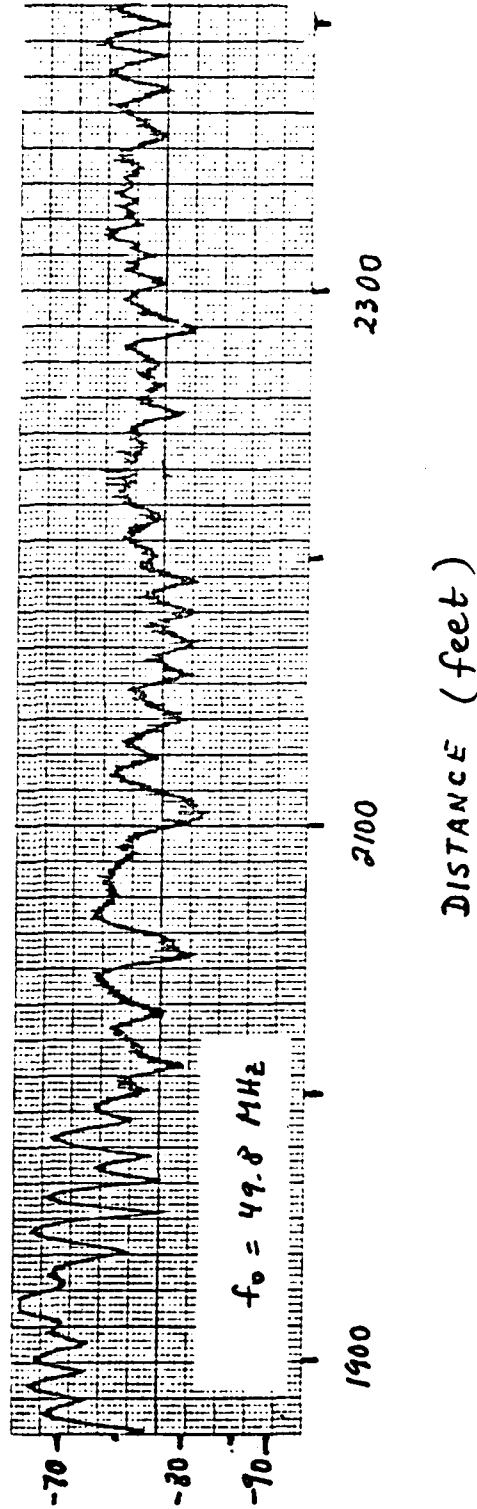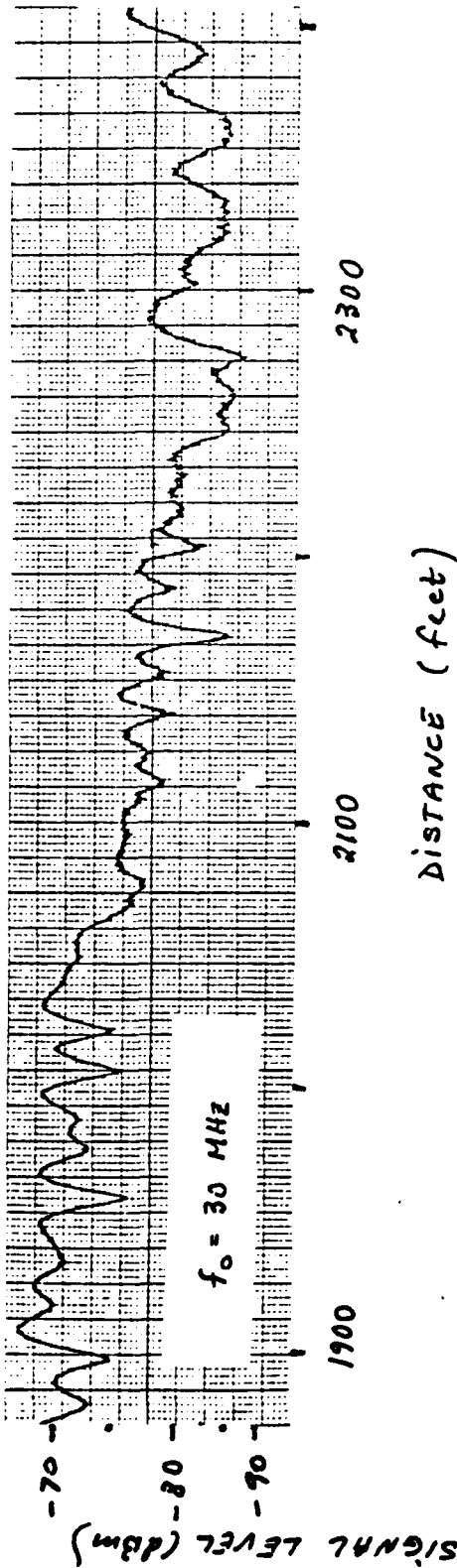
FIGURE 2.3-17 Received Signal Level vs. Distance Along Suburban Street when Transmit Site is on Different Street ((T) on Mass. Ave., (R) on Waltham St., Lexington, MA)

2-45

nal level are seen, with successive minima occurring approximately every wavelength of the carrier frequency ($\lambda \approx 33$ ft at 30 MHz, $\lambda \approx 20$ ft at 50 MHz). Fading is observed even when both transmitter and receiver are located on the same street (Figure 2.3-16) and the fade depths are actually seen to be greater in this case than in the case of no clear line-of-sight path between transmitter and receiver (Figure 2.3-17). This is not as surprising as it may seem because the greatest fades are observed when two equal strength signals (at the same frequency) combine out of phase to form a null (minimum). This is more likely to occur when both transmitter and receiver are on the same street. From these observations, we then conclude that changes in received signal levels as high as 20 dB may be achieved by moving to a location of a half-wavelength (20 feet at 50 MHz) away.

If we compare the mean received signal level observed from the strip chart recordings (Figure 2.3-16) at a distance of 2,200 feet from the transmitter, we can see that the mean received signal level is about 10 dB stronger than that obtained from the isolated point measurements of Figures 2.3-10 and 2.3-11. This difference is probably due to the higher gain (+5 dB) of a car mounted whip antenna (monopole) than that of a whip antenna placed in close proximity to a human operator (-4 to -5 dB).

2.4 Street-to-Building Propagation Measurements

The street-to-building measurements can be grouped into two categories: received signal level measurements as a function of receiver height (floor level) relative to the transmitter and received signal level measurements as a function of distance (inside the building) from a fixed transmitter.

The measurements of received signal level as a function of receiver height (floor level) are shown in Figures 2.4-1 to 2.4-3. The transmitter was located outside the building a few
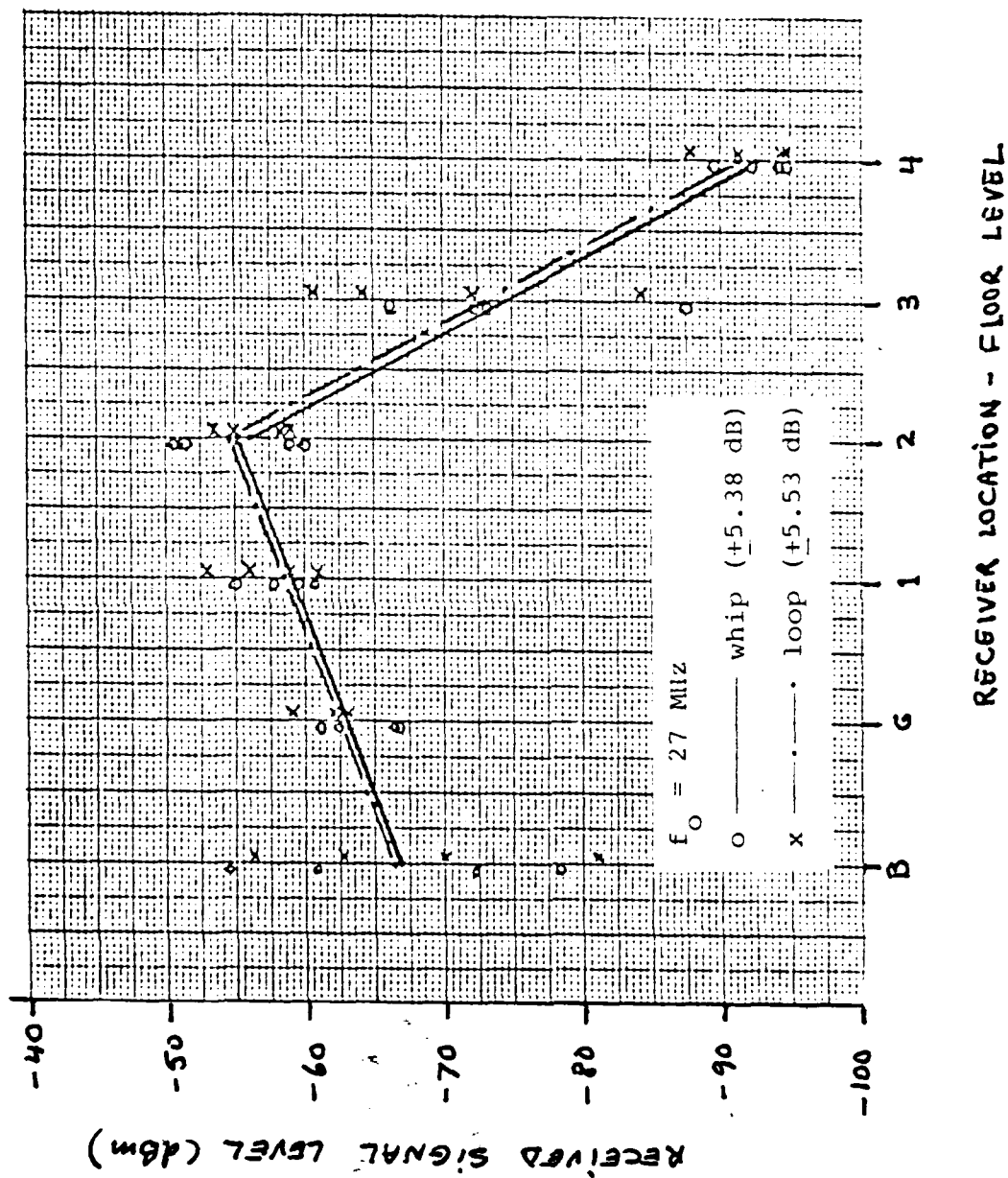
FIGURE 2.4-1   Received Signal Level vs. Floor Level in Street-to-
Building Transmission
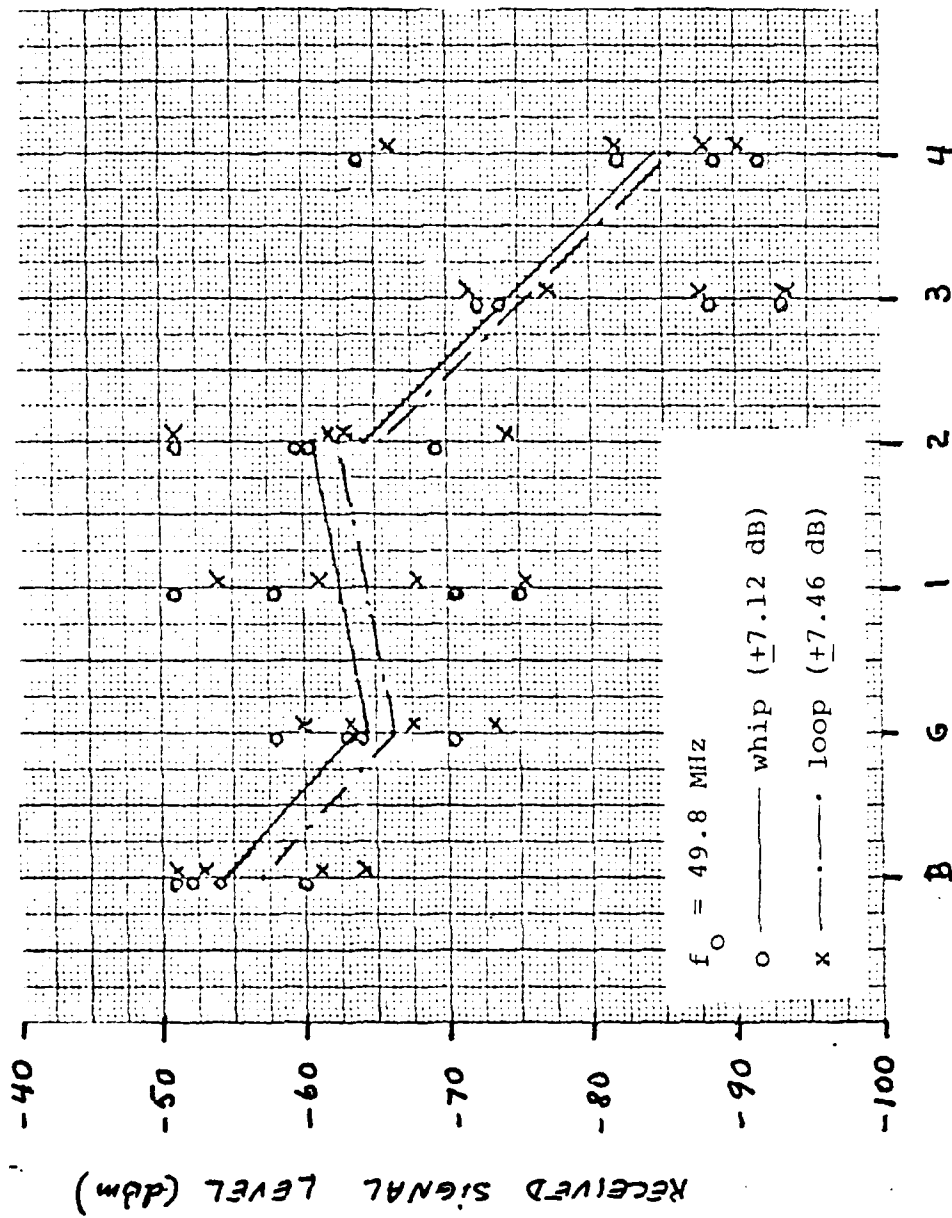
FIGURE 2.4-2   Received Signal Level vs. Floor Level in Street-to-
Building Transmission
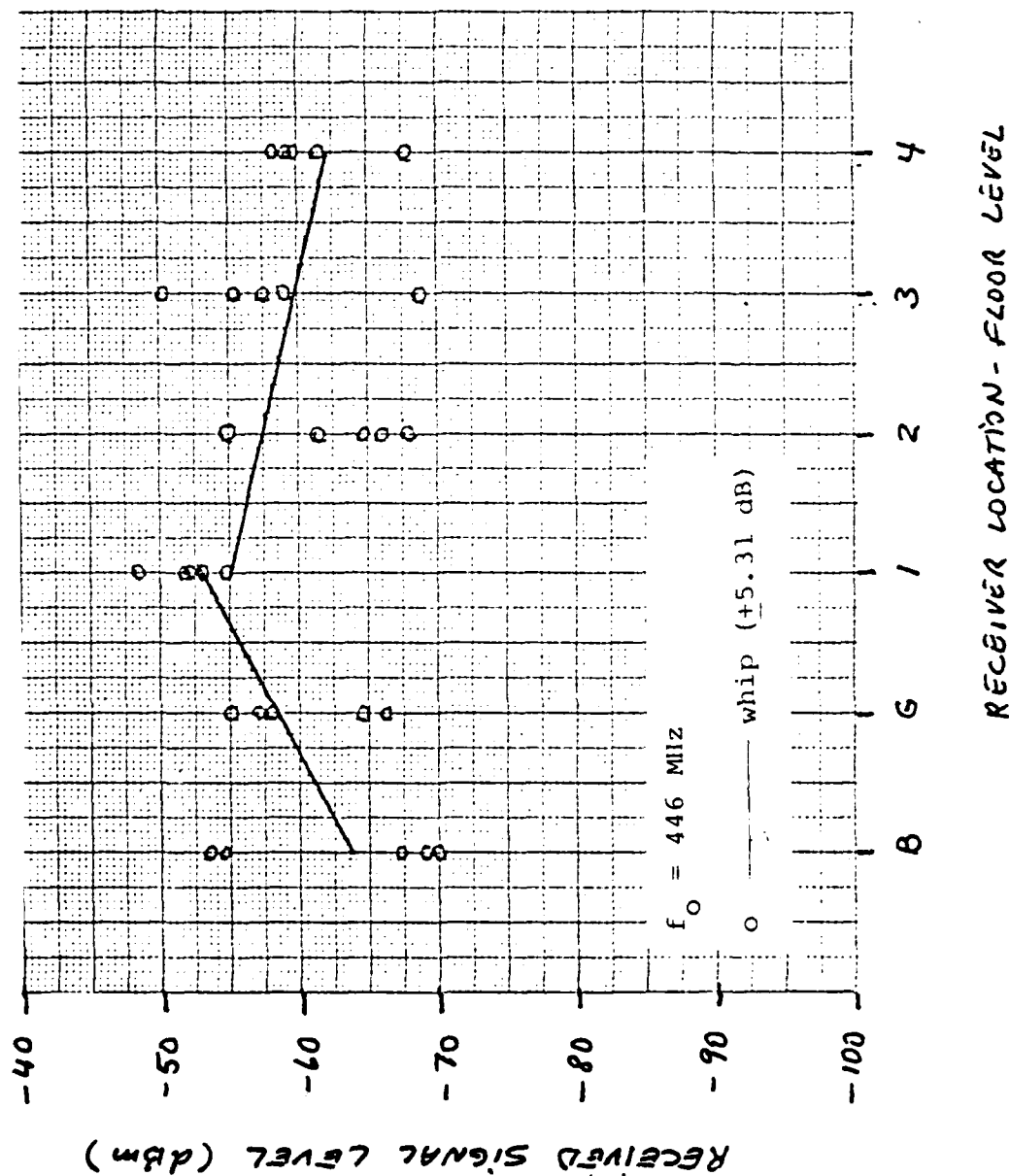
FIGURE 2.4-3 Received Signal Level vs. Floor Level in Street-to-Building Transmission

feet away from the building. The received signal level was measured on different floors inside the building, including a basement garage (B), the ground floor (G), and four additional floors above ground. Piece-wise best fit curves to the data measured with the whip (solid line) and loop (dashed line) antennas are also shown in the figures, along with the standard deviation of the data from the best fit curves (shown in the legend). The piece-wise best fit to the data assumes an exponential dependence of received power with height, i.e., $P_r \sim ke^{-\alpha h}$, where h is the receiver height relative to the transmitter in floor units. This type of dependence was found to be more appropriate than a power dependence, i.e., $P_r \sim k'h^{-n}$ since the standard deviation of the data was smaller in the former case. From these measurements we can see that there is no height gain effect but rather the received signal level decreases as the receiver height is increased. This is somewhat misleading though because the higher the receiver is, the longer the path the signal has to travel. Thus, in order to determine if a height gain effect is observed, we must subtract the effects of propagation path length (i.e., the free-space path loss). We postpone this discussion, though, to Section 3.

The measurements of received signal inside the building as a function of distance from the transmitter are shown in Figures 2.4-4 to 2.4-6. The transmitter and receiver were both located at the same level (ground level) during these measurements. In the case of the measurements at 49.8 MHz and 446 MHz, the transmit site was 156 feet and 140 feet away from the building, respectively. The reason for placing the transmitter at such a distance was so that the received signal level everywhere within the building could be within the dynamic range of the receive system. The receive system for the measurements at 27 MHz had a greater dynamic range, though, so that the transmit site was only one foot away from the building.
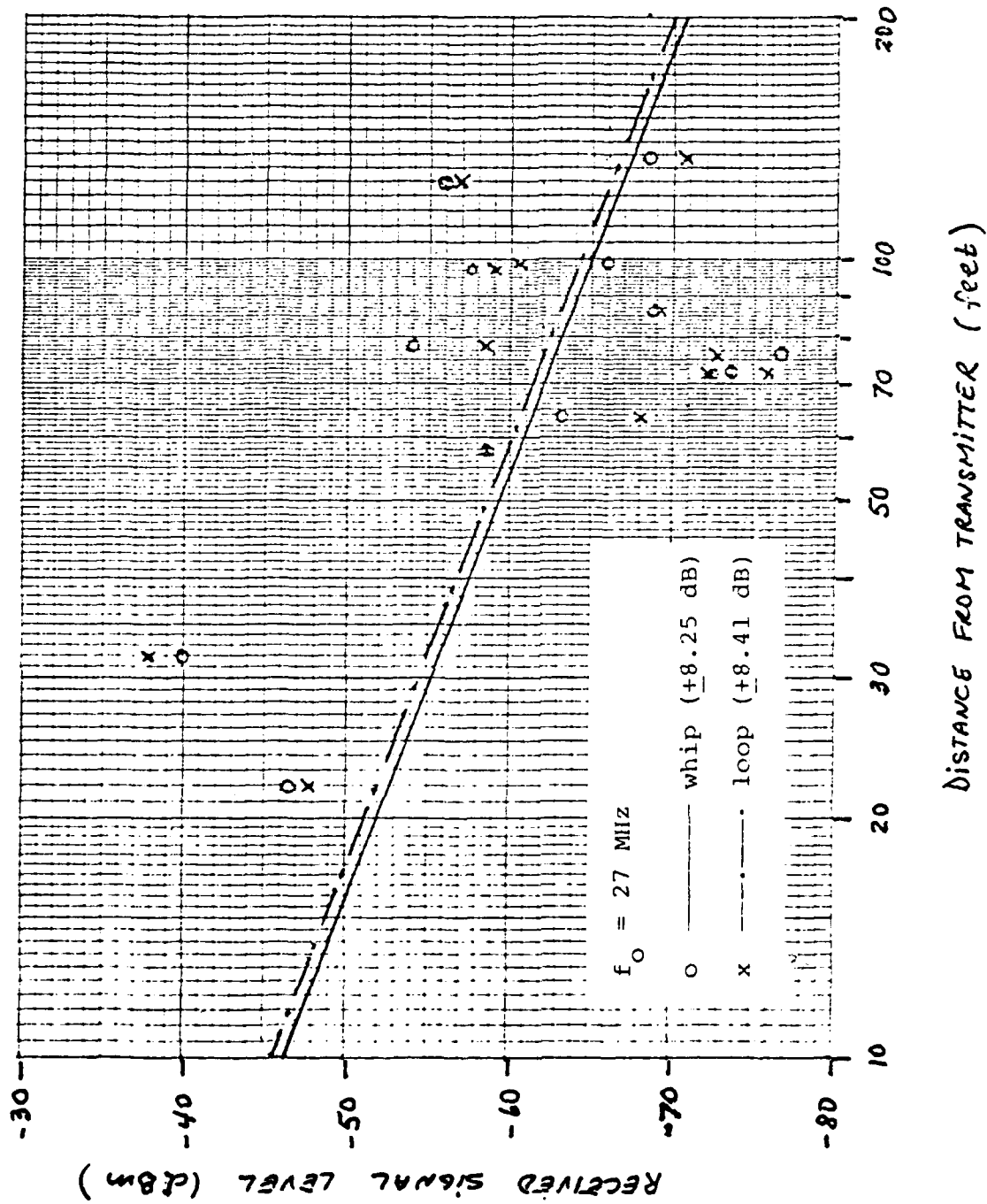
FIGURE 2.4-4   Received Signal Level vs. Distance from Transmitter in Street-to-Building Transmission

2-51
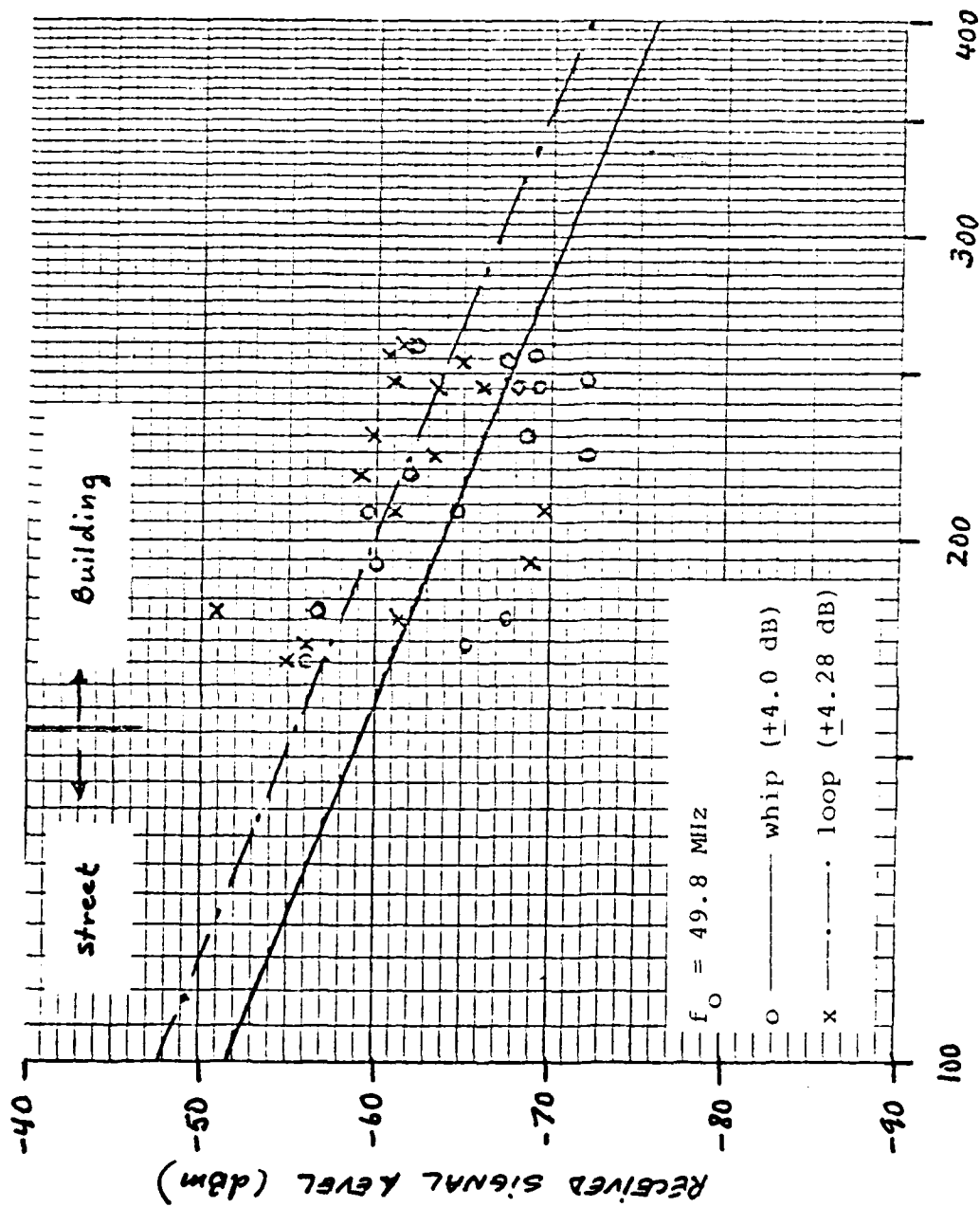
FIGURE 2.4-5 Received Signal level vs. Distance from Transmitter in Street-to-Building Transmission
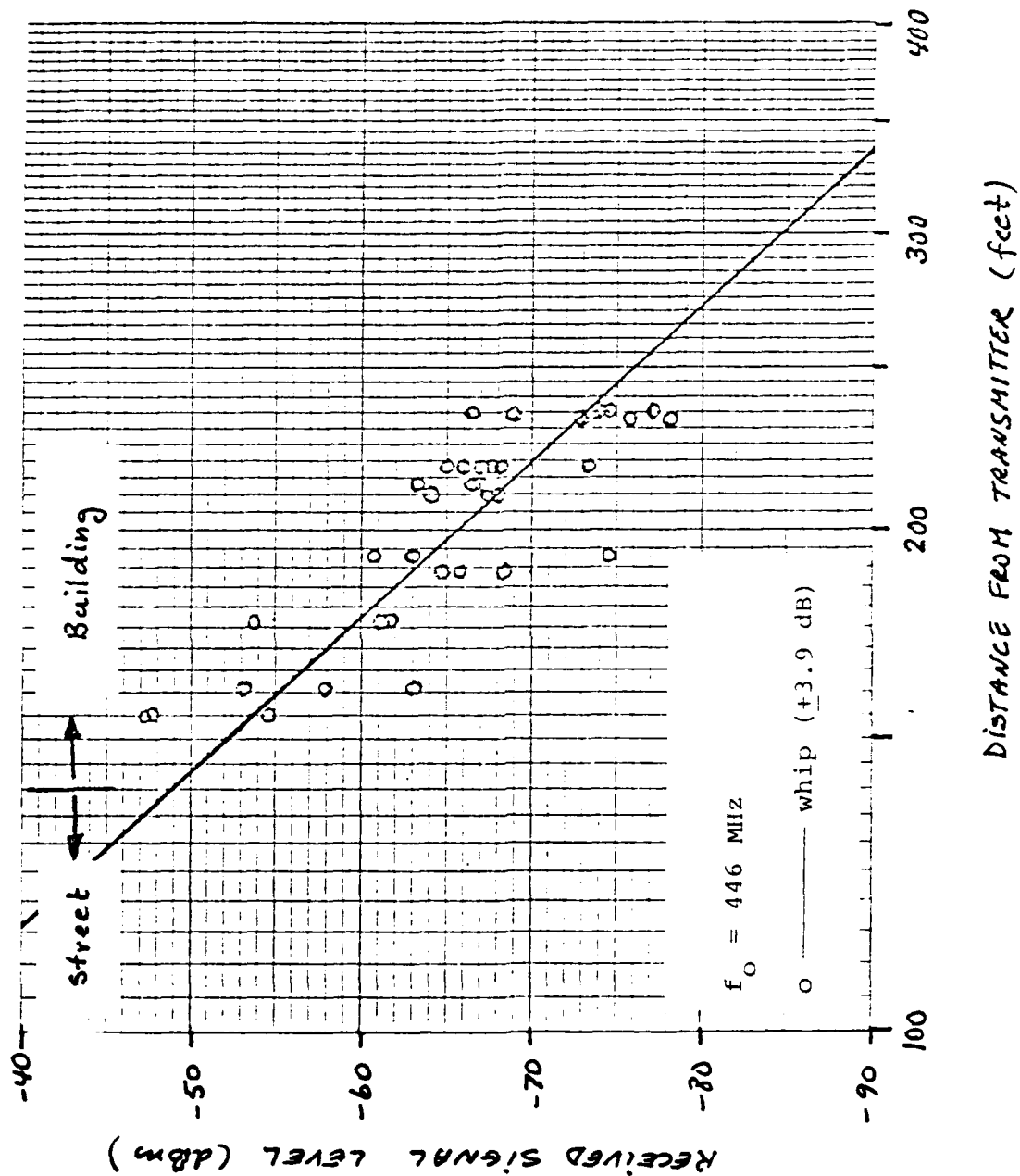
FIGURE 2.4-6 Received Signal Level vs. Distance from Transmitter for Street-to-Building Transmission

2-53

A 'best-fit' curve to the data is also shown in Figures 2.4-4 to 2.4-6, with the standard deviation indicated in the legend. The best fit curves assume a power law type of distance dependence, i.e., $P_r \sim kd^{-n}$ where d is the distance from transmitter to receiver and n is the power law dependence. This type of distance dependence was found to have a lower standard deviation than an exponential type of distance dependence (i.e., $P_r \sim ke^{-\alpha d}$) at all three frequencies. The power law dependence for the three measurement frequencies are:

$$n = \begin{cases} 1.89 & @ \; 27 \text{ MHz} \\ 4.03 & @ \; 49.8 \text{ MHz} \\ 10.6 & @ \; 446 \text{ MHz}. \end{cases}$$

Thus, we can see that at 27 MHz, the received signal exhibited near inverse square law distance dependence while at 49.8 MHz it exhibited near inverse fourth power law dependence. The reason for this difference may be explained as follows. The fourth power law dependence at 49.8 MHz indicates that the received signal was composed of two or more signals which travelled along different ray paths. One was possibly a direct ray which penetrated the various walls inside the building and the other was a ground reflected ray (prior to incidence upon the outside wall of the building) which also penetrated the various walls and interfered with the other ray to form an inverse fourth power law distance dependence typical to plane earth type of propagation. The presence of a direct and a ground reflected ray was made possible by the fact that the distance of the transmit site from the outside wall of the building was more than half the total distance from transmitter to receiver (a ground reflection occurs approximately half way between transmitter and receiver if both are at roughly the same height above the

ground). This was not the case for the 27 MHz measurements so that only a direct ray was present in the latter measurements resulting in an inverse square law distance dependence. Both of these measurements also indicate that the cumulative effect of the walls inside the building (gypsum walls) was minimal compared to the attenuation due to partial reflection from and transmission through the outside wall (cinder block and brick veneer). On the other hand, the measurements at 446 MHz exhibit an inverse tenth power law distance dependence. This indicates that the walls inside the building introduced additional losses comparable to those due to the outside wall. Since the farther away the receive site inside the building was the more walls the signal had to penetrate, then the received signal had to exhibit a more pronounced distance dependence. The reason why the gypsum walls are lossier at higher frequencies is that their thickness (5 in. ≃ 12.7 cm) is in the order of the wavelength at 446 MHz ($\lambda \simeq 70$ cm) but are negligibly thin at 27 MHz ($\lambda \simeq 11$ m) and 49.8 MHz ($\lambda \simeq 6$ m). In conclusion, these measurements indicate that the received signal level in street-to-building transmission increases the farther the receive site (or transmit) is inside the building. The attenuation rate is frequency dependent.

In addition to the isolated point measurements, strip chart recordings of the received signal level at 30 MHz, 49.8 MHz, and 446 MHz were also made inside the building along a corridor and inside an office with no windows. The transmit site was approximately 40 feet away from the building and the office and corridor were approximately 40 to 50 feet further away. These measurements are shown in Figure 2.4-7 as a function of the approximate distance covered along the corridor and inside the office. The received signal is seen to fade in a manner similar to signals recorded outdoors which indicates the presence of multipath. The distance between nulls (fades) is in the order of
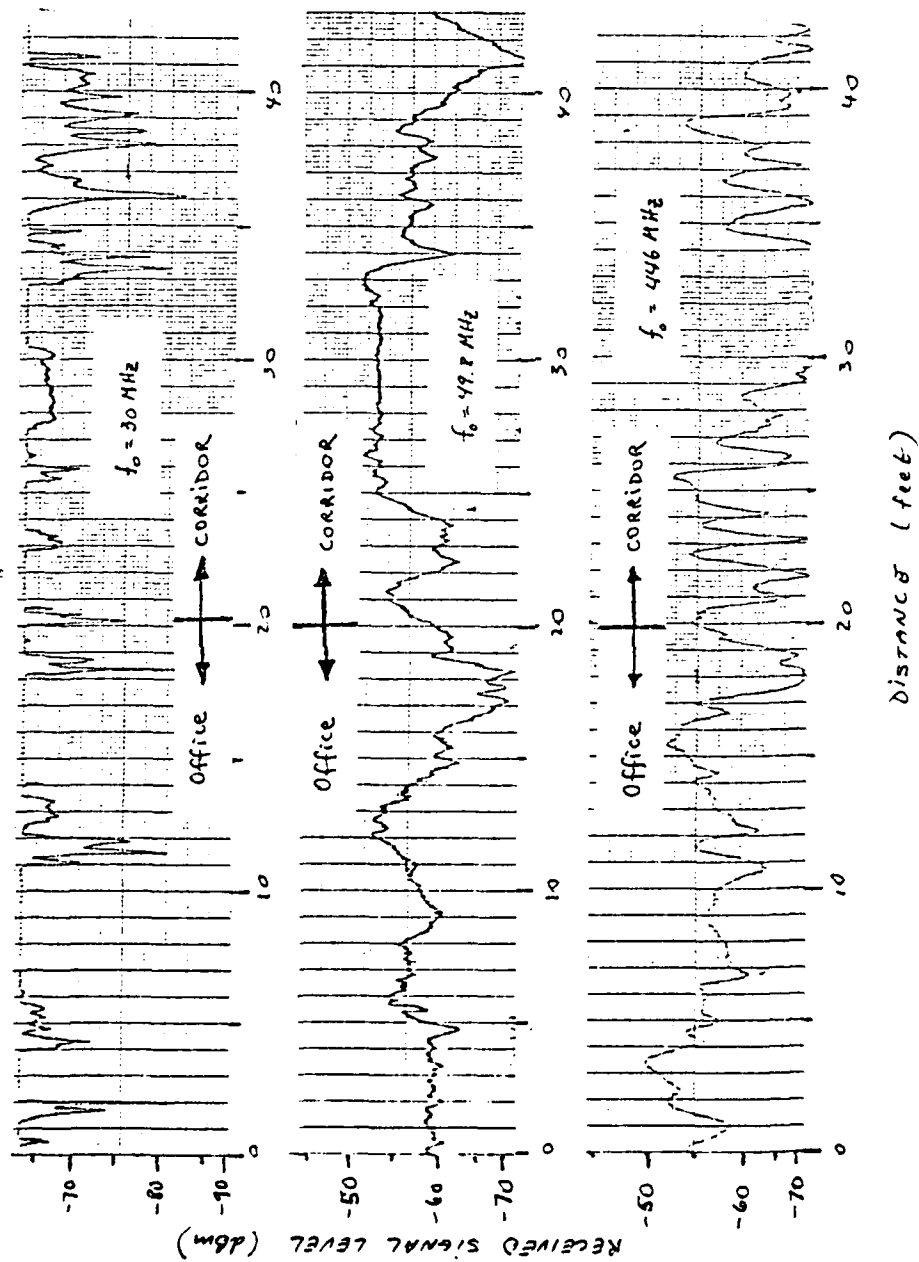
FIGURE 2.4-7   Received Signal Level Inside Building from a
Transmitter Located Approximately 80 Feet Away

a wavelength and the depth of the fades is as great as 20 dB. This indicates that the difference in received signal levels between two locations a few feet apart inside a building can be as great as 20 dB.

2.5 Building-to-Building Propagation Measurements

The measurements of received signal level for transmissions between two adjacent concrete buildings are shown in Figures 2.5-1 to 2.5-6. The measurements of Figures 2.5-1 to 2.5-3 correspond to a situation in which the receive site was located on the third floor of a 5 story building, in an ample lobby at the end of the building closest to the adjacent high-rise building as shown in Figure 2.1-9 (R_1). The transmit site in the high-rise building was varied from floor to floor but was always at the same horizontal position relative to the receive site (as indicated by T in Figure 2.1-9). The data is shown in Figures 2.5-1 to 2.5-3 as a function of the difference in floor levels between the transmit and receive sites. In addition, best fit curves to the data are shown where the height dependence was assumed to be of the form $P_r \sim kh^{-n}$ where h is the relative height in floor units and n is the power law dependence. This type of best fit was found to have a lower standard deviation (and thus deemed more appropriate) than an exponential type of best fit (i.e., $P_r \sim k'e^{-\alpha h}$). The median values of the data (best fit) is seen to exhibit little height dependence with the received signal level having a higher value at lower values of relative height (especially at 446 MHz). This height dependence is misleading though as the path lengths for the smaller height differentials are shorter. Thus in order to determine the 'true' height dependence we must subtract the path length dependence (free-space loss). This type of analysis is deferred to Section 3.

The same type of measurements for a second receive site (R_2 in Figure 2.1-9) located in another lobby on the third floor at the end farthest away from the high rise are shown in

2-57
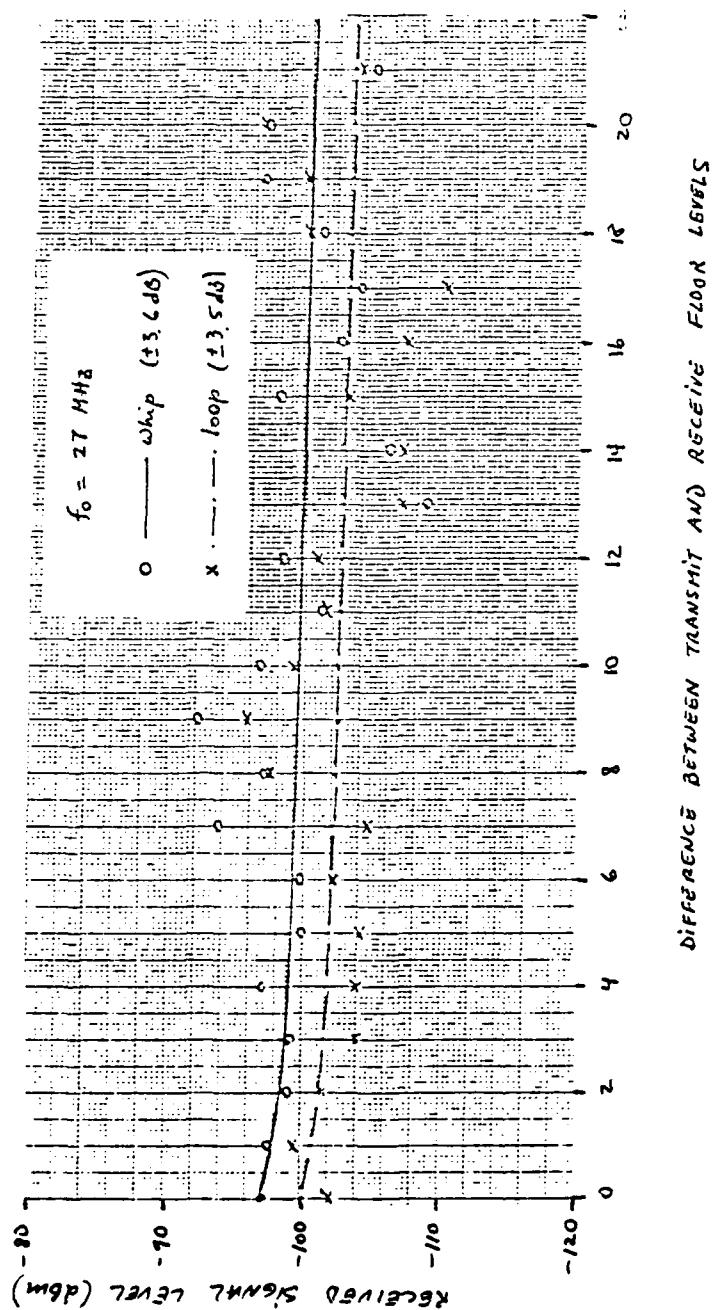
FIGURE 2.5-1 Received Signal Level as a Function of Transmitter
Height Relative to Receive Site Floor Level in
Building-to-Building Transmission (Receive Site
in Front of Building).
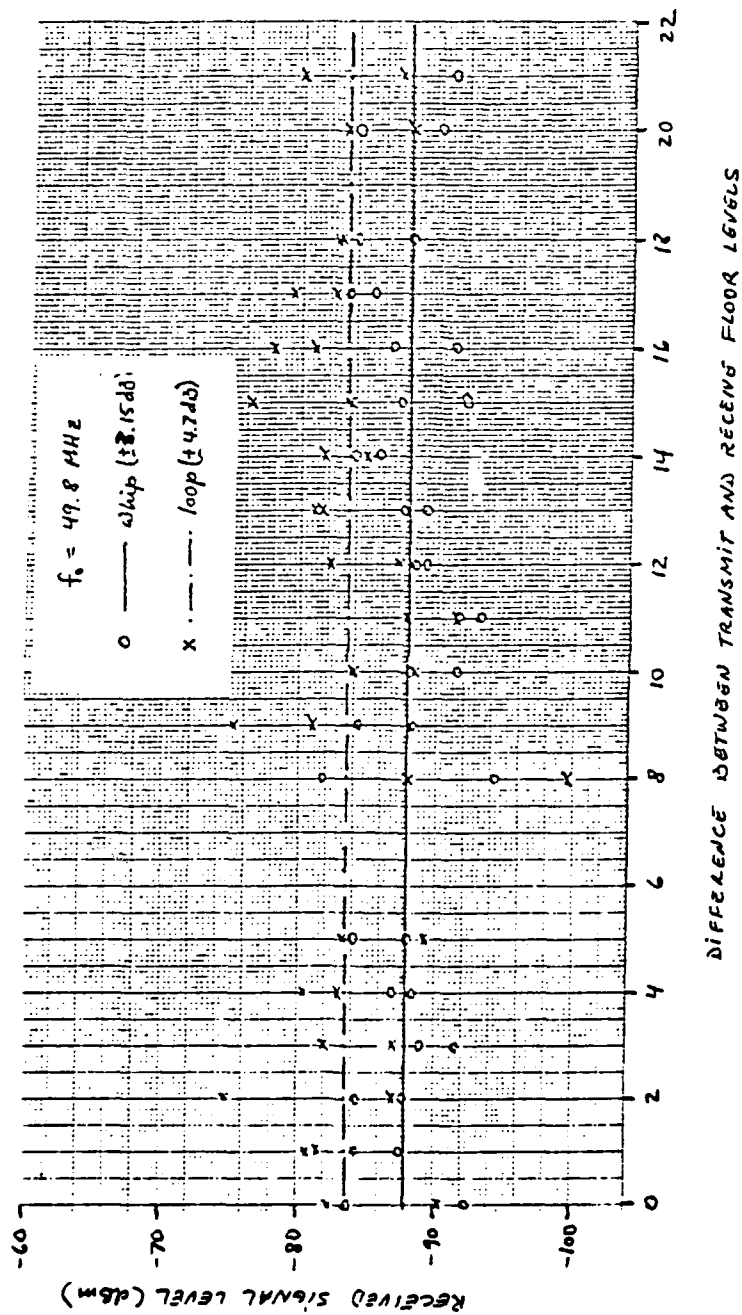
FIGURE 2.5-2 Received Signal Level as a Function of Transmitter
Height Relative to Receive Site Floor Level in
Building-to-Building Transmission (Receive Site
in Front of Building)
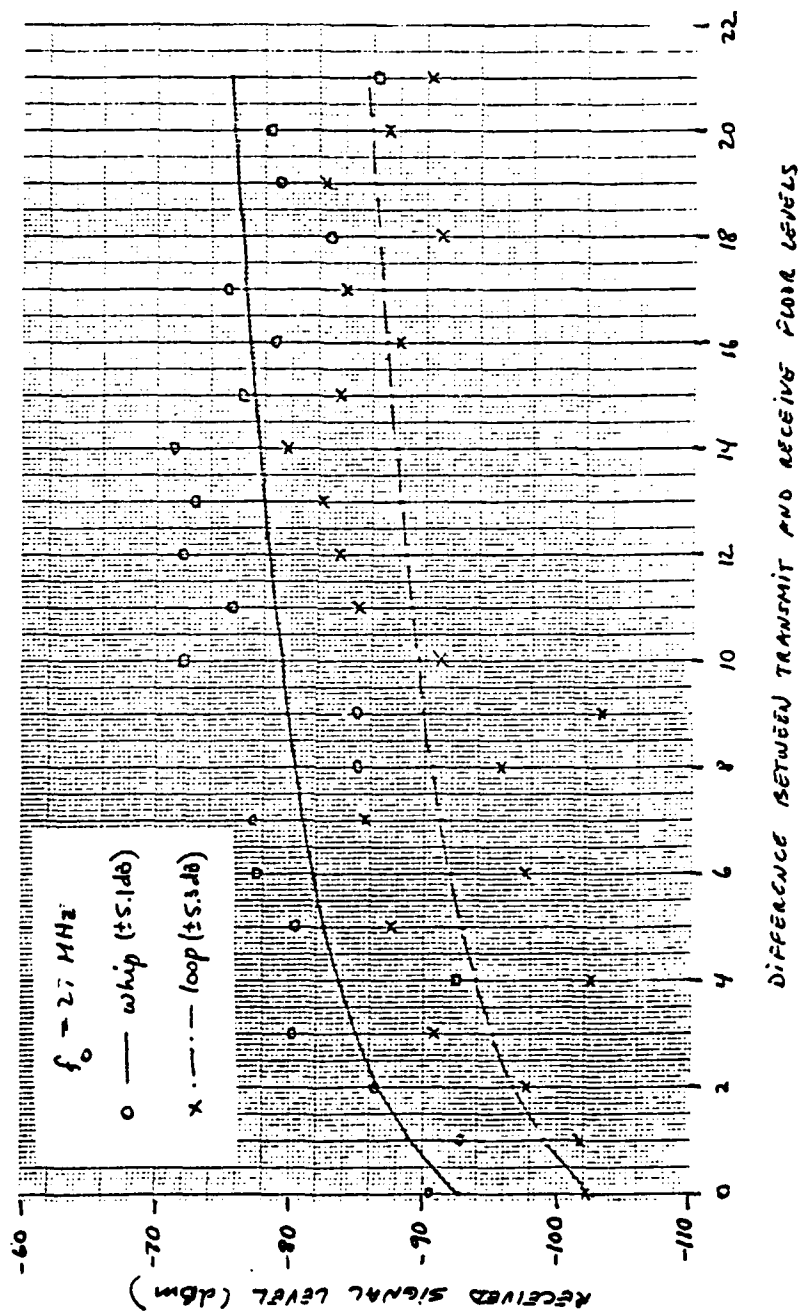
FIGURE 2.5-4 Received Signal Level as a Function of Transmitter Height Relative to Receive Site Floor Level for Building-to-Building Transmission (Receive Site in Rear of Building)
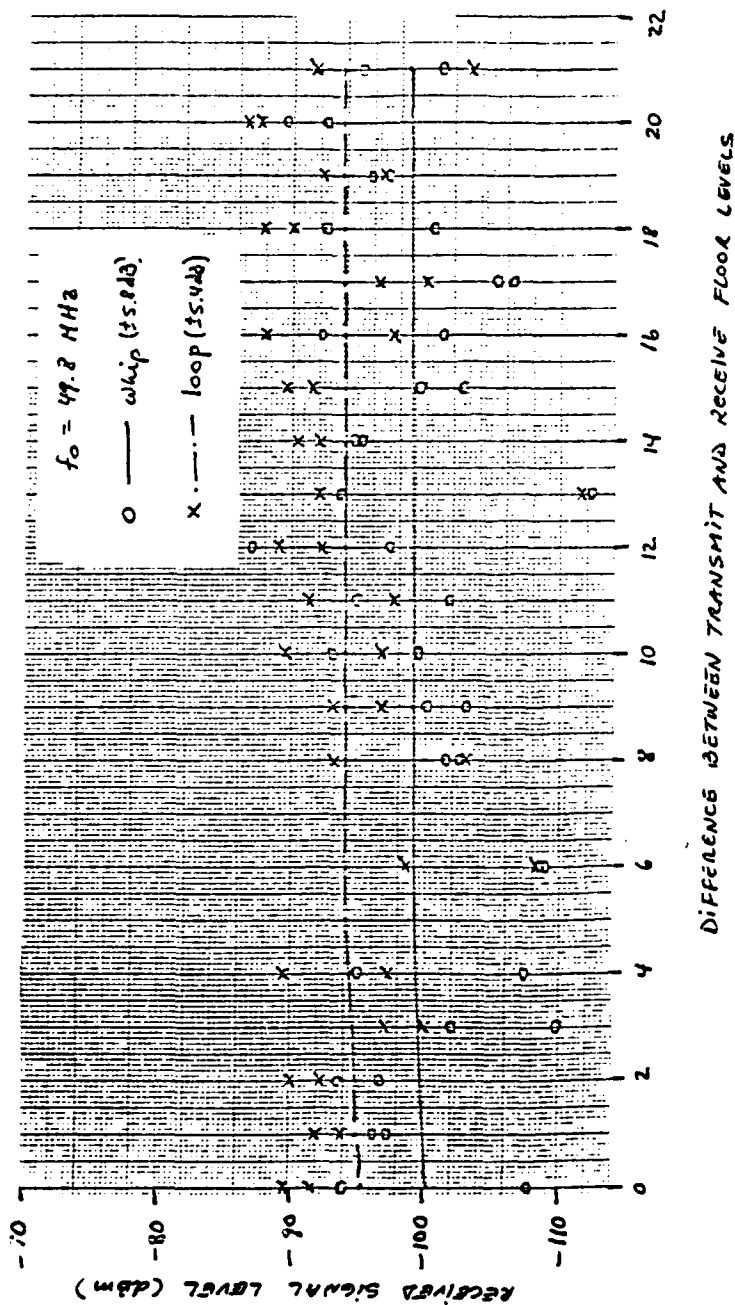
FIGURE 2.5-5   RECEIVED SIGNAL LEVEL AS A FUNCTION OF TRANSMITTER
HEIGHT RELATIVE TO RECEIVE SITE FLOOR LEVEL IN
BUILDING-TO-BUILDING TRANSMISSION (RECEIVE SITE
IN REAR OF BUILDING)
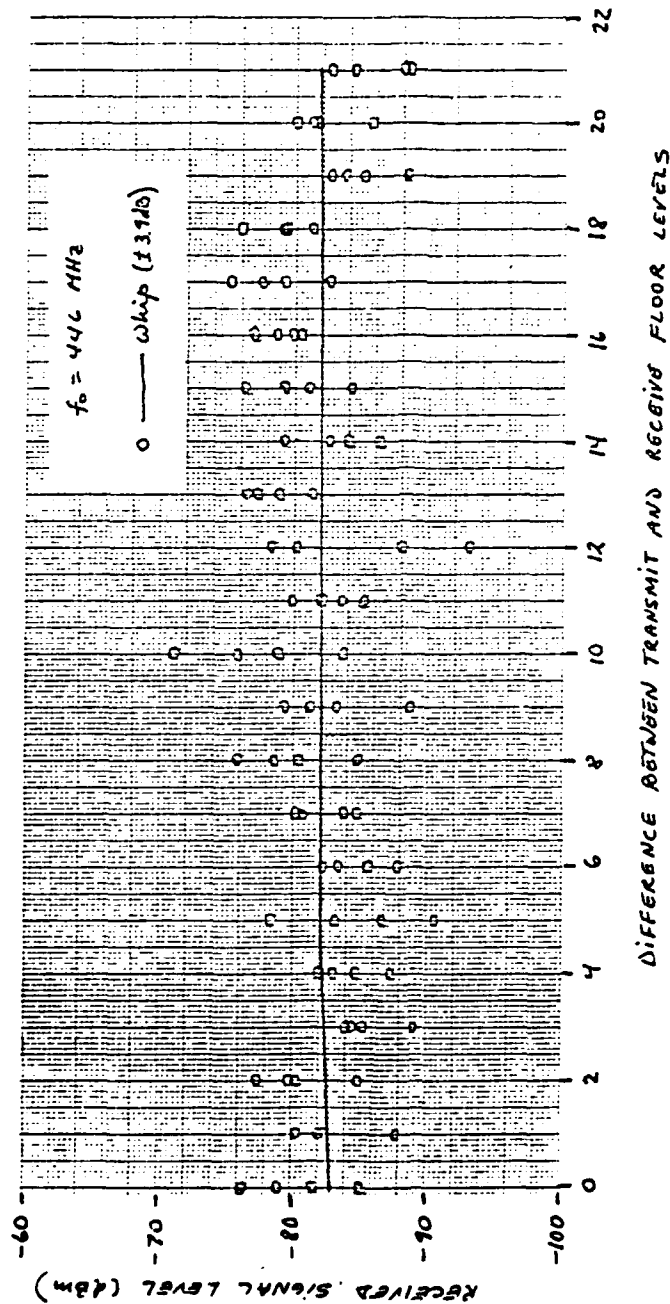
FIGURE 2.5-6   Received Signal Level as a Function of Transmitter Height Relative to Receive Site Floor Level in Building-to-Building Transmission (Receive Site in Rear of Building)

Figures 2.5-4 to 2.5-6. The 'best fit' curve to the data
exhibits almost no height dependence again except for the
measurements at 27 MHz. In this case, the median received sig-
nal levels for the smaller values of height differential are
seen to be lower indicating some sort of height gain as the
transmitter height is increased. This effect is not observed
though in the measurements at 49.8 MHz and 446 MHz. Further-
more, the median received signal levels in site R_2 are lower
than those in site R_1 at 49.8 MHz and 446 MHz as one might
expect but are considerably higher at 27 MHz (by about 10-20 dB).
A possible reason for this discrepancy is as follows. The receive
site R_1 at 49.8 MHz and 446 MHz was actually 20 feet closer to a
window than the receive site R_1 at 27 MHz. The proximity to the
window (which does not face the high-rise but rather the other way
though) and the fact that 20 feet is in the order of a half-
wavelength (i.e., received site could have been in a shadow
region) at 27 MHz might account for the rather low received
signal levels measured at 27 MHz. Thus we conclude that building-
to-building transmission losses exhibit little height dependence
and the attenuation is strictly determined by the type of building
structure.

2.6   Intrabuilding Propagation Measurements

The intrabuilding measurements can be grouped into four
categories: 1) transmission along straight and winding corridors;
2) transmission between above-ground floors; 3) transmission
between a garage basement and above-ground floors; and 4) trans-
mission along elevator shafts and stairwells.

2.6.1   Propagation Measurements Along Corridors

The measurements of received signal levels for trans-
mission along various types of corridors are shown in Figures
2.6-1 to 2.6-4. Best fit curves to the measurements are also
shown along with the standard deviation (in dB's) of the data
from the best fit curves (median levels). The measurements of
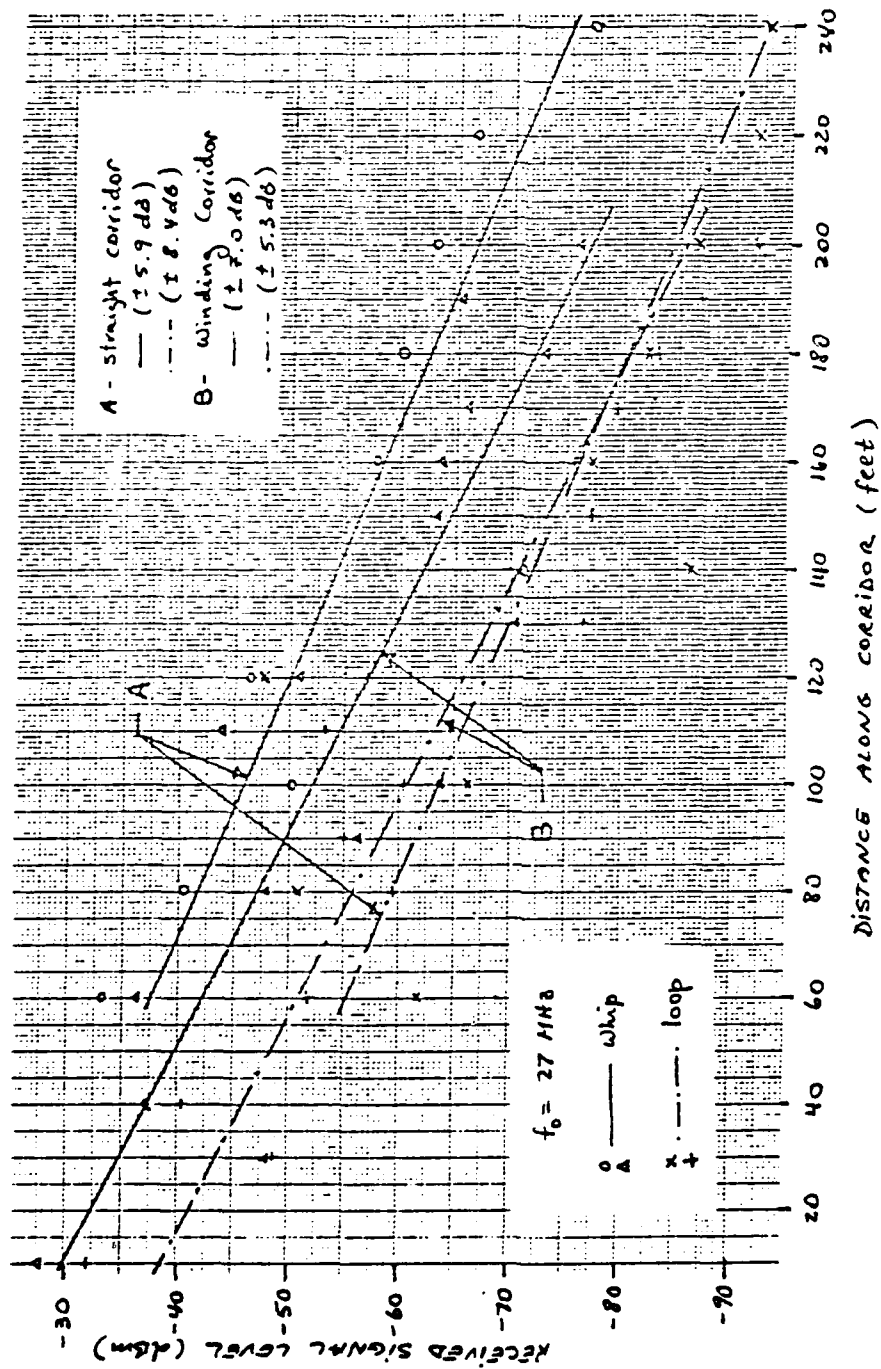
FIGURE 2.6-1 Received Signal Level vs. Distance Covered Along
Corridor in Intrabuilding Transmission
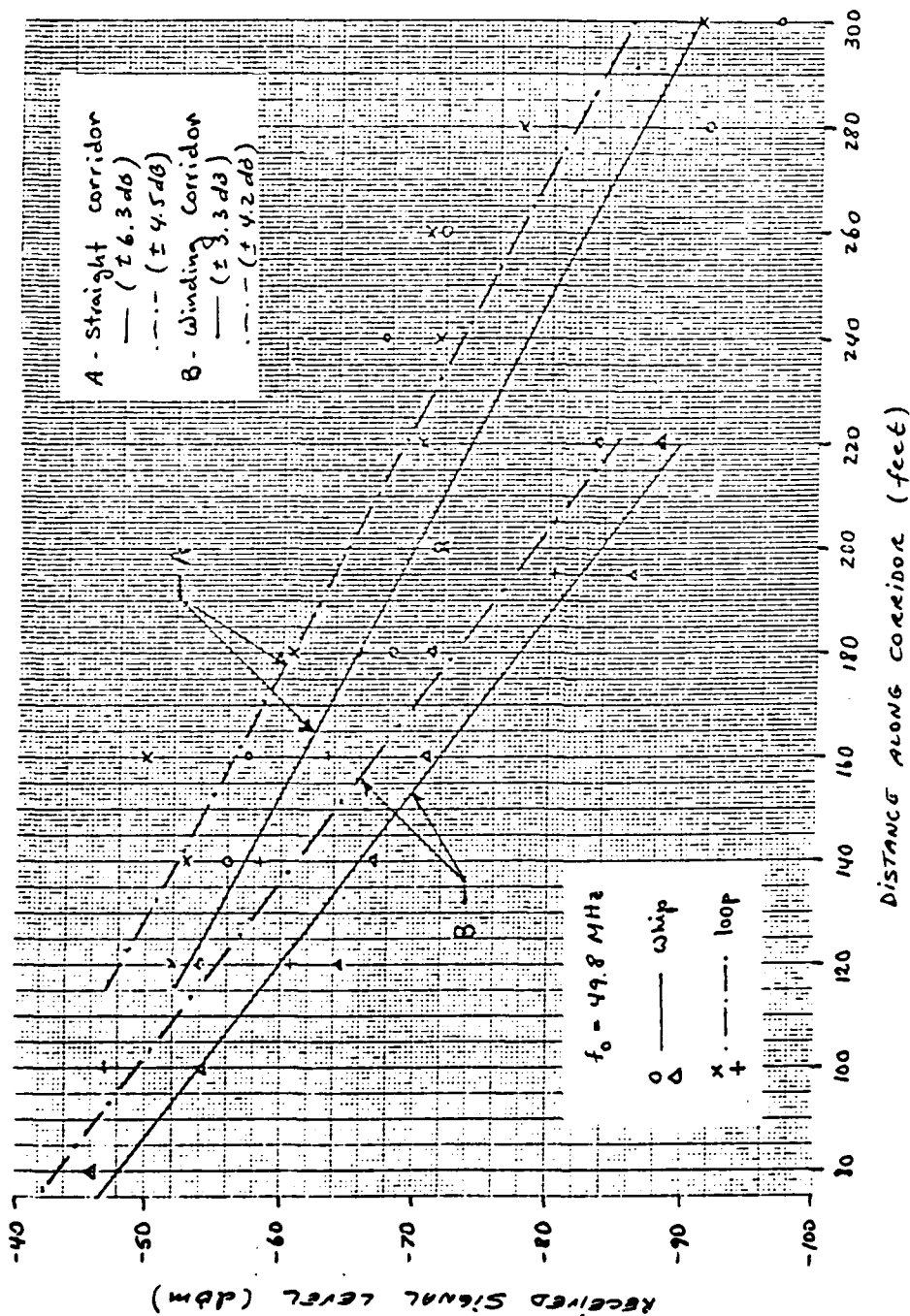
FIGURE 2.6-2 Received Signal Level vs. Distance Covered Along
Corridor in Intrabuilding Transmission
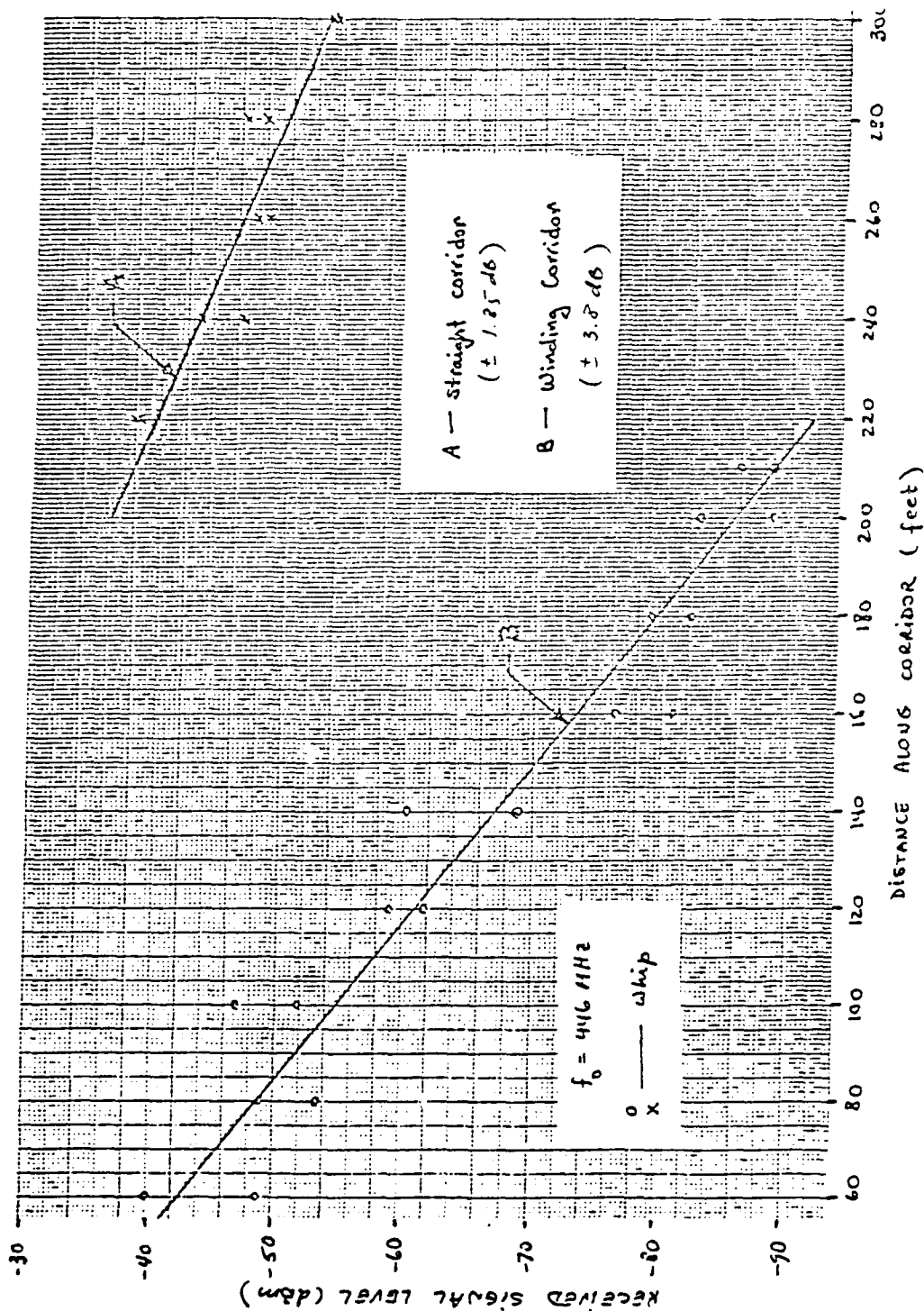
FIGURE 2.6-3 Received Signal Level vs. Distance Covered Along
Corridor in Intrabuilding Transmission
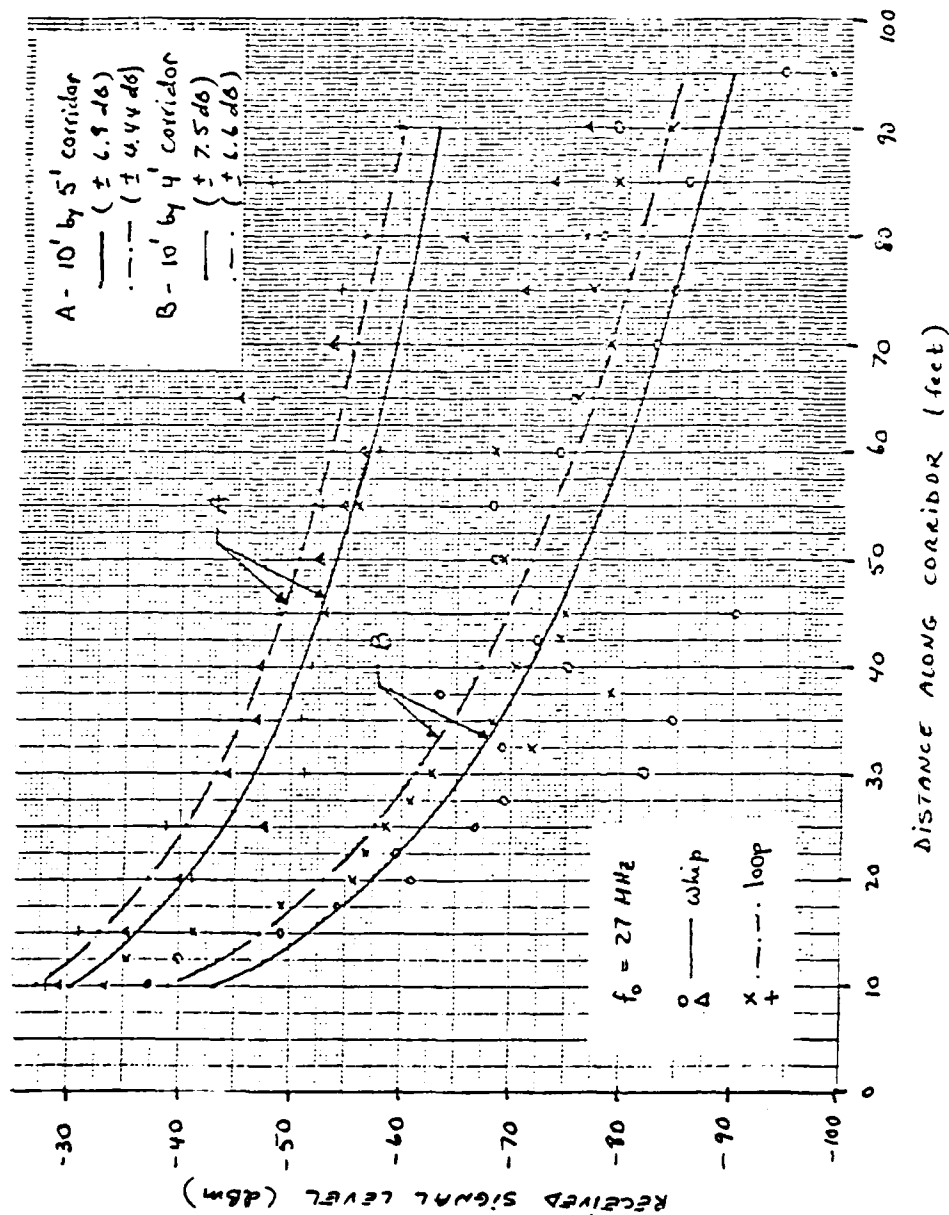
FIGURE 2.6-4   Received Signal Level vs. Distance Covered Along
Corridor in Intrabuilding Transmission

Figures 2.6-1 to 2.6-3 were made in t.   orridors whose width
was approximately 8 feet and the heigh   of the ceiling was approx-
imately 12 feet. The walls along the corridor were made of cinder
block covered with plaster. One of the corridors (A) was straight
with a total length of approximately 300 feet and with a few
doors (4-5) along its length. The second corridor (B) was a
winding one of approximate length of 220 feet. The 'line of
sight' section of this corridor was approximately 30 feet long,
and the additional straight sections measured approximately
110 feet, 40 feet, and 40 feet, respectively.

The distance dependence of the median levels of the
measured data at 27 MHz, 49.8 MHz, and 446 MHz for the two
corridors is exponential, i.e., $P_r \sim ke^{-\alpha d}$ where d is the distance
covered along the corridor. This type of distance dependence
was found to have a smaller standard deviation than a power law
distance dependence. The exponential type of distance dependence
is both characteristic and indicative of a waveguide type of pro-
pagation. Furthermore, the attenuation rates in dB per 100 ft
(slope = 4.3 α) at the three frequencies for the two corridors
are:

$$@ \ 27 \ \text{MHz} \qquad 4.3 \ \alpha = \begin{cases} 20.8 \ \text{dB/100 ft, A} \\ 24.8 \ \text{dB/100 ft, B} \end{cases}$$

$$@ \ 49.8 \ \text{MHz} \qquad 4.3 \ \alpha = \begin{cases} 20.8 \ \text{dB/100 ft, A} \\ 29.4 \ \text{dB/100 ft, B} \end{cases}$$

$$@ \ 446 \ \text{MHz} \qquad 4.3 \ \alpha = \begin{cases} 16.3 \ \text{dB/100 ft, A} \\ 30.8 \ \text{dB/100 ft, B.} \end{cases}$$

Thus we can see that the attenuation rate (slope of the best fit
curves) is somewhat dependent on the frequency and geometry. For
the straight corridor it is in the order of 20 dB per 100 ft at
lower VHF (30-80 MHz) and 16 dB per 100 ft at UHF (44.6 MHz). The
reason for the higher attenuation rate at VHF is possibly the fact
cross-sectional dimensions are in the order of a half-wavelength
in the low VHF frequency range but much greater than the wave-

length in the UHF range. The attenuation rate for the winding corridor is a few dB greater and varies from 25 dB/100 ft at 27 MHz to 30 dB/100 ft at 446 MHz. The higher attenuation rate is due to losses at each turn in the corridor. The excess loss rate due to the turns increases with frequency from 4 dB/100 ft at 27 MHz to 8.6 dB/100 ft at 49.8 MHz and to 14.5 dB/100 ft at 446 MHz. This is not surprising since the same phenomena is observed in waveguide and tunnel propagation.

In addition to the dimensions of the corridor, the material composition of the walls plays an important role in determining the total attenuation (and possibly the attenuation rate). This may be seen by comparing the median received signal levels in a corridor with cinder block wall and steel girded ceilings (Figure 2.6-1) with similar measurements made at 27 MHz in two corridors (straight) where the walls were made up of gypsum and the ceiling was suspended tile (Figure 2.6-4), We can see that at a distance of 60 feet the median received signal level in a corridor with gypsum walls is between 20 and 40 dB lower than the received signal level at an equal distance in a corridor with cinder block walls. This is probably due to the lower conductivity of gypsum compared to cinder block which results in much higher losses at each wall reflection. From Figure 2.6-4 we can also see that the best fit curves to the data exhibit a power law distance dependence rather than exponential. However, at distances greater than 40 feet, the best fit curve is very nearly a straight line so that at distances greater than 40 feet, the median received signal level is exponentially decaying while at distances less than 40 feet (about one wavelength at 27 MHz), it is better approximated by a power law type of dependence.

In conclusion, intrabuilding propagation along corridors exhibits a waveguide type of propagation behavior whose attenuation rate is dependent on the dimensions and material composition of the walls and which decreases with frequency for straight corridors. The excess attenuation rate due to turns in the corridors increases with frequency, though.

2.6.2 Transmission Measurements Between Above-Ground Floors

Measurements of received signal level for transmission between various floors in a high rise building are shown in Figures 2.6-5 to 2.6-7 as a function of the number of floors between the transmit and receive locations. The measurements show a general trend towards a decrease in the strength of the received signal as the number of floors that the signal must penetrate increases. The best fit curves to the average received signal levels are also shown in these figures. The curves exhibit a power law dependence on the number of floors penetrated by the signal, i.e., $P_r \sim kh^{-n}$, where h is an integer denoting the number of floors penetrated by the signal. This type of dependence was found to have a lower standard deviation than an exponential dependence on the number of floors penetrated.

From the best fit curves we can see that the attenuation rates in dB per decade (10 n) at the three frequencies are:

$$10 \; n \; = \; \begin{cases} 51.3 \text{ dB/decade} & \text{at 27 MHz} \\ 25.5 \text{ dB/decade} & \text{at 49.8 MHz} \\ 30.2 \text{ dB/decade} & \text{at 446 MHz.} \end{cases}$$

Thus we see that the attenuation rate first decreases with fre-~uency and then it increases. This may be explained as follows: at 27 MHz the distance between floors (~15 ft) is in the order of a half-wavelength ($\lambda \sim 36$ ft at 27 MHz) which results in high attenuation due to destructive interference set up by reflections at each ceiling. As the frequency increases the wavelength becomes small compared with the distance between floors so that the reflections at each ceiling are not totally out of phase as in the half-wavelength case resulting in a much lower attenuation rate. As the frequency increases further, the ceiling thickness (1 ~ 2 ft) becomes comparable to the wavelength ($\lambda \sim 2.3$ ft at 446 MHz) resulting in additional reflections which further attenuate the signal. Thus at frequencies in the UHF
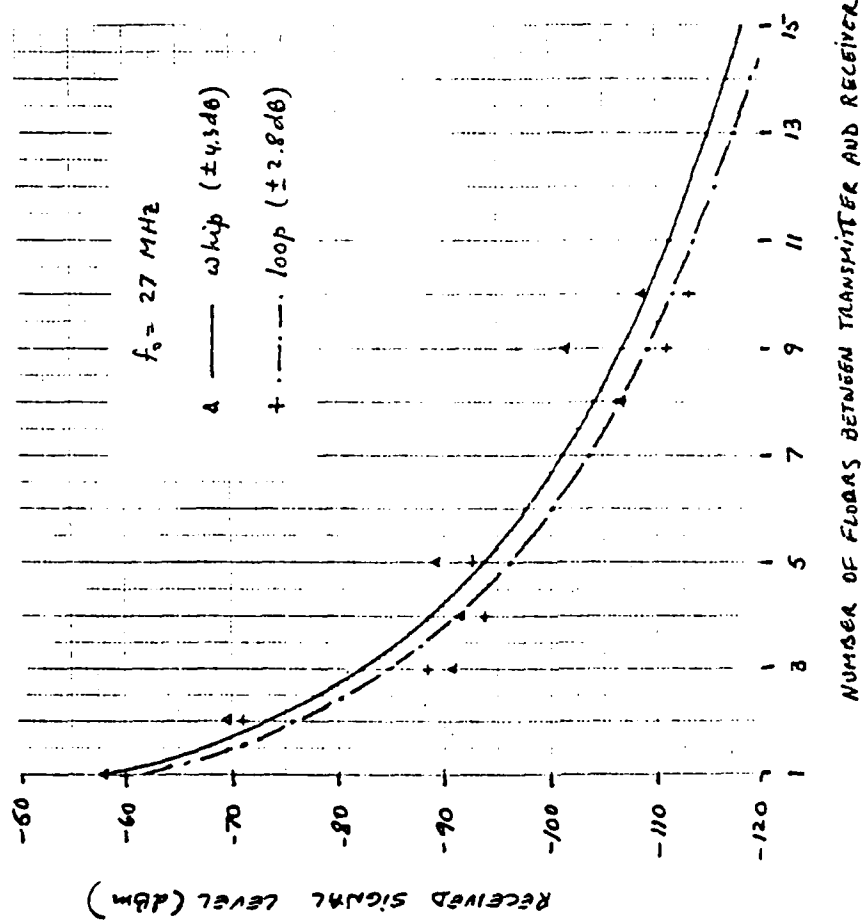
FIGURE 2.6-5   Received Signal Level in Floor to Floor Transmission
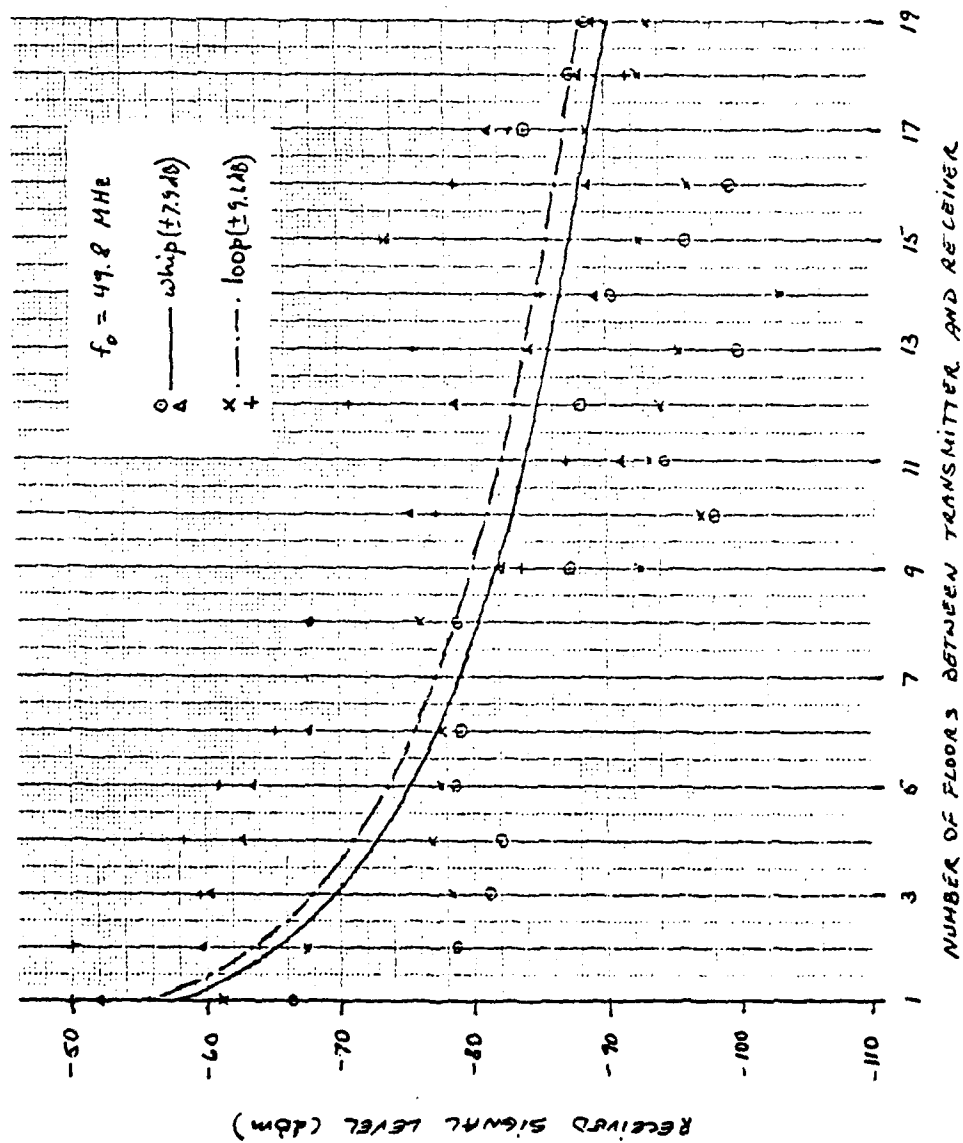
FIGURE 2.6-6   Received Signal Level in Floor to Floor Transmission
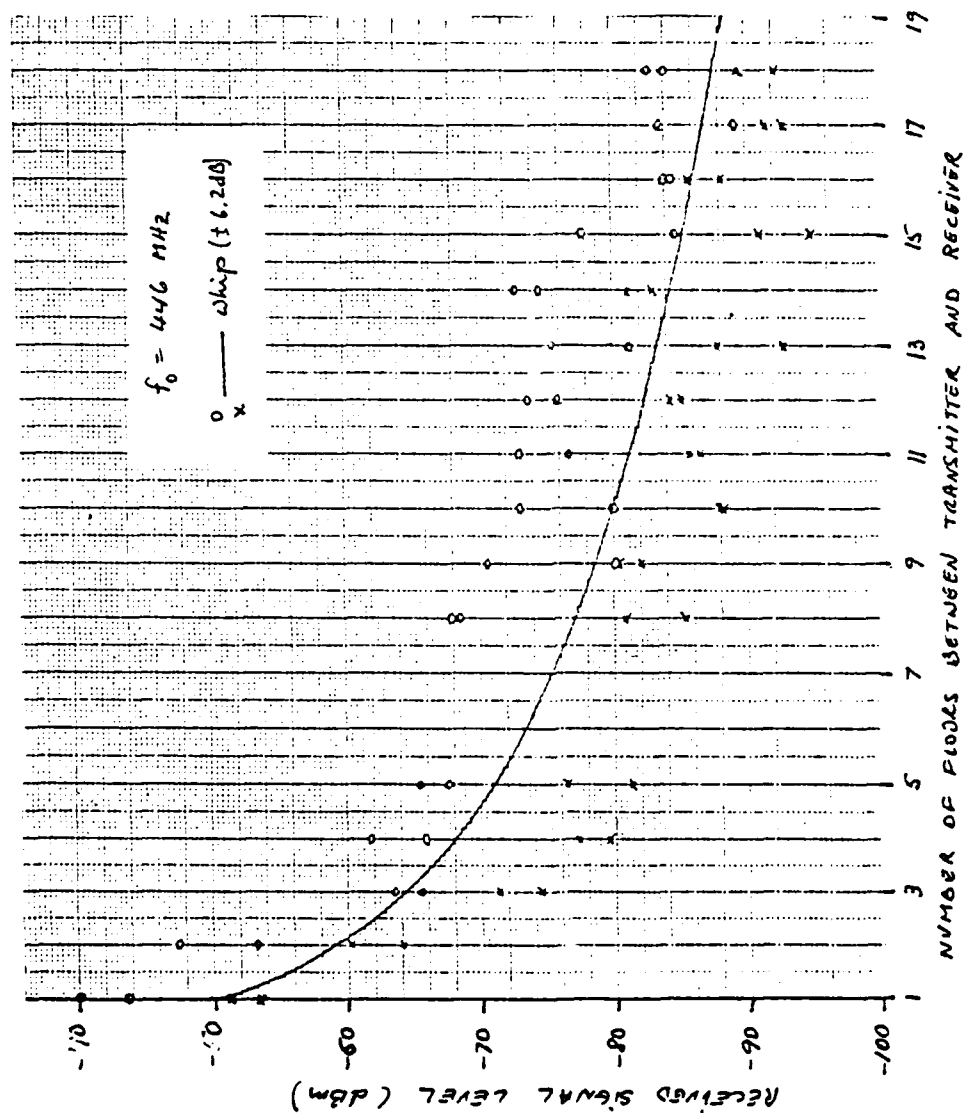
FIGURE 2.6-7 Received Signal Level in Floor to Floor Transmission

2-74

range the attenuation rate begins to increase with frequency.

Some of the attenuation is due to the path length itself while the rest is due to the presence of the building structure. We defer discussing the net loss due to the floor penetration to Section 3.

2.6.3 Transmission Measurements Between Above-Ground Floors and Basement

Measurements of received signal level for transmissions between various floors and the garage basement of a five story concrete building are shown in Figures 2.6-8 to 2.6-10 as a function of the number of floors between the transmit and receive sites. In addition, best fit curves are shown. These curves indicate that the median received signal level decreases as a power of the number of floors penetrated by the signal (i.e., $P_r \sim kh^{-n}$ where h is the number of floors and n is the power) in the VHF range and exponentially (i.e., $P_r \sim k'e^{-\alpha h}$) in the UHF range.

The attenuation rates in dB/decade (10 n) for the VHF frequencies are:

$$10\ n = \begin{cases} 56 \text{ dB/decade} & \text{at 27 MHz} \\ 44.5 \text{ dB/decade} & \text{at 49.9 MHz} \end{cases}$$

These attenuation rates are somewhat larger than the attenuation rates obtained from the transmission measurements between above-ground floors. However, they are consistent in that the attenuation rate decreases with frequency in the VHF range.

The exponential dependence of the median received signal level at 446 MHz is not necessarily inconsistent with the dependence obtained from measurements of received signal level at the same frequency in the transmissions between above ground floors. The reason is that a power law dependence approaches an exponential dependence as the power law (n) increases and the incremental distance (values of h) decreases. Thus, if it had been possible to obtain measurements of transmissions

2-75
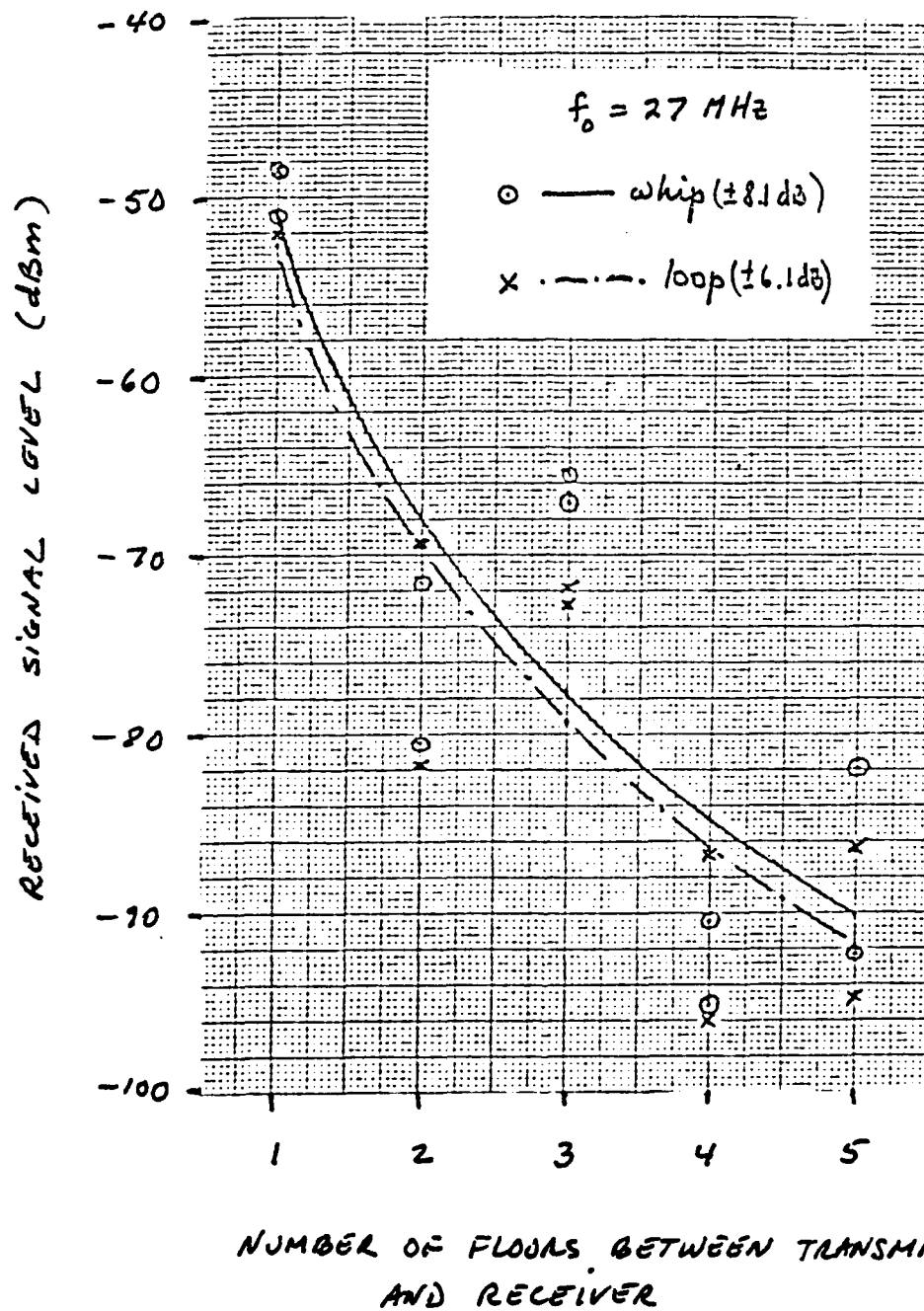
FIGURE 2.6-8   Received Signal Level in Above-Ground-Floor to
                Basement Transmission

2-76
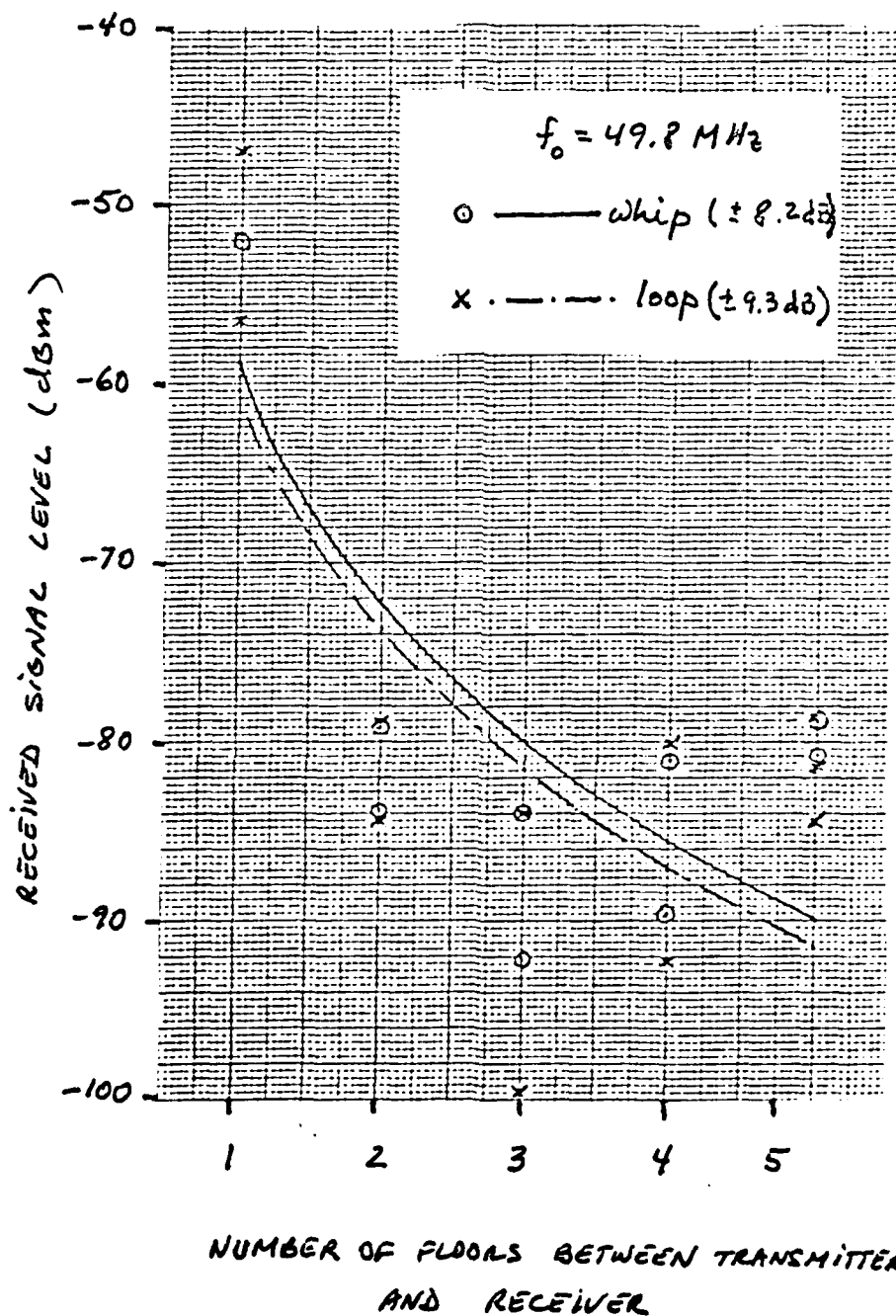
FIGURE 2.6-9   Received Signal Level in Above-Ground-Floor to Basement Transmission

2-77
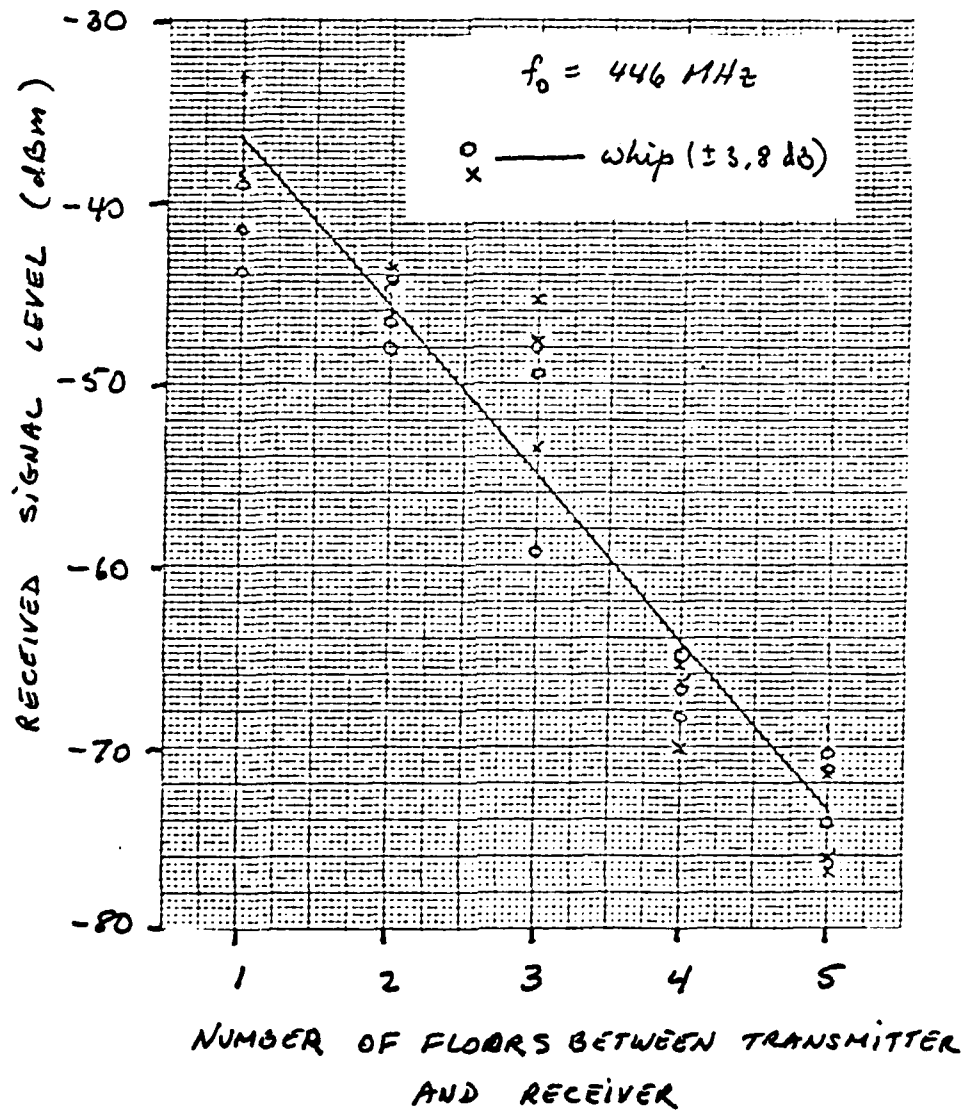
FIGURE 2.6-10   Received Signal Level in Above-Ground-Floor to
Basement Transmission

to the basement through a greater number of floors, it is conceivable that a power law dependence rather than an exponential dependence at 446 MHz would have been more appropriate. As it is, a sub-optimum (greater standard deviation) power law best fit to the measurements of Figure 2.6-10 yields an attenuation rate of 50 dB/decade at 446 MHz which is consistent with the trends exhibited by the transmission between above-ground floors. The actual attenuation rate at 446 MHz (for the optimum exponential dependence) is 9.19 dB/floor (i.e., 4.3 α = 9.19).

A comparison of the attenuation rates for transmissions between above ground floors and for transmissions from above ground floors to a basement (or vice versa) indicates that the latter have a 20 dB/decade higher attenuation rate at 49.8 MHz and 446 MHz. The increase in attenuation rate at 27 MHz is 5 dB/decade. The reason for a lower increase in attenuation rate at 27 MHz is probably due to the fact that the basement ceiling was about 30 feet high which is in the order of the wavelength (rather than the half-wavelength height for the above ground floors) so that one would expect an attenuation rate in the same order as that for 49.8 MHz since the room dimensions are greater than a half-wavelength in both cases.

2.6.4   Transmission Measurements Inside a Stairwell and
         Along Elevator Shafts

Measurements of received signal level inside a stairwell and along the elevator shafts of a 24 story high rise building are shown in Figures 2.6-11 to 2.6-14 as a function of the number of floors between the transmit and receive sites. The dimensions of the stairwell were about 8 feet by 16 feet while those of the elevator shafts were approximately 6 feet by 6 feet. In the case of the transmissions in a stairwell, both transmitter and receiver were located in the stairwell. However, in the case of the transmissions along the elevator shafts (there were 3 of them), both transmitter and receiver were located in front of the elevator shaft doors, about 3 to 5 feet
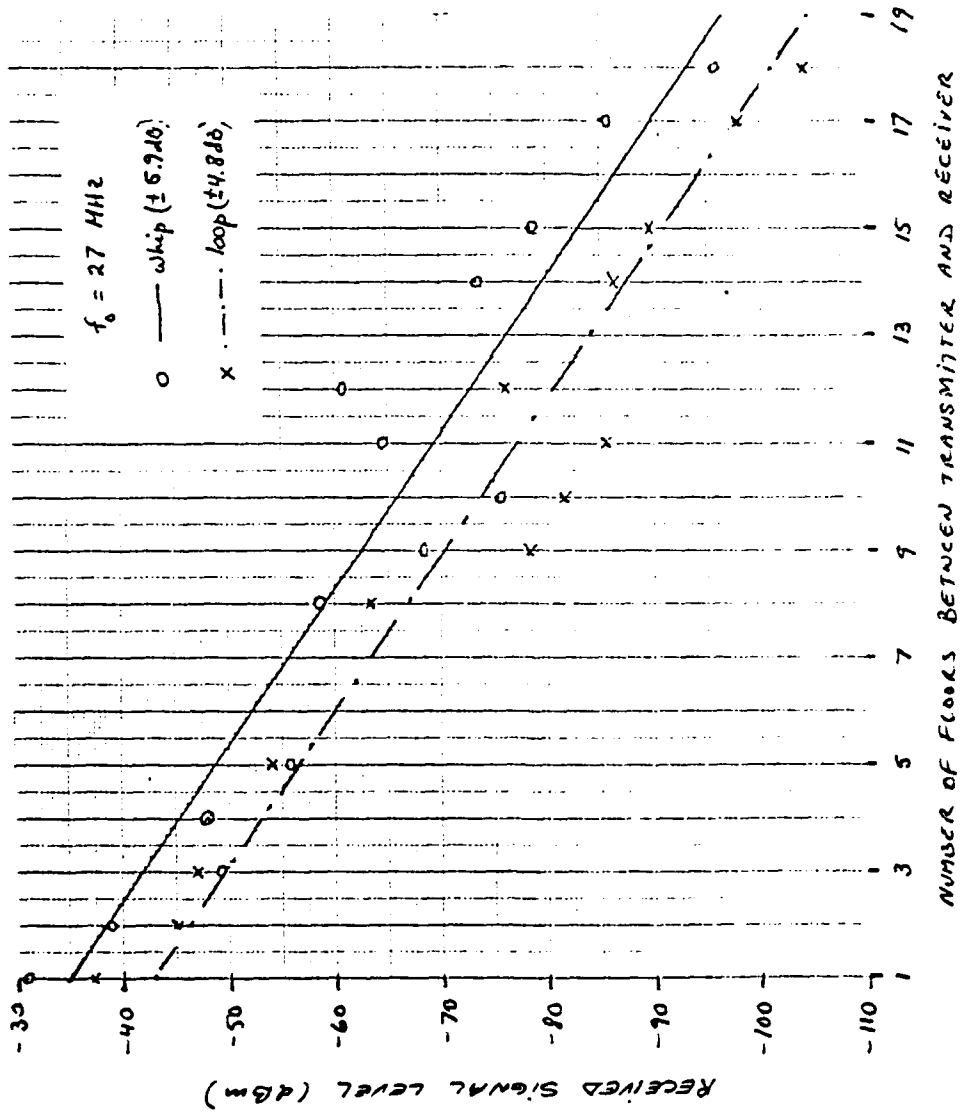
FIGURE 2.6-11 Received Signal Level for Transmissions Along Elevator Shafts
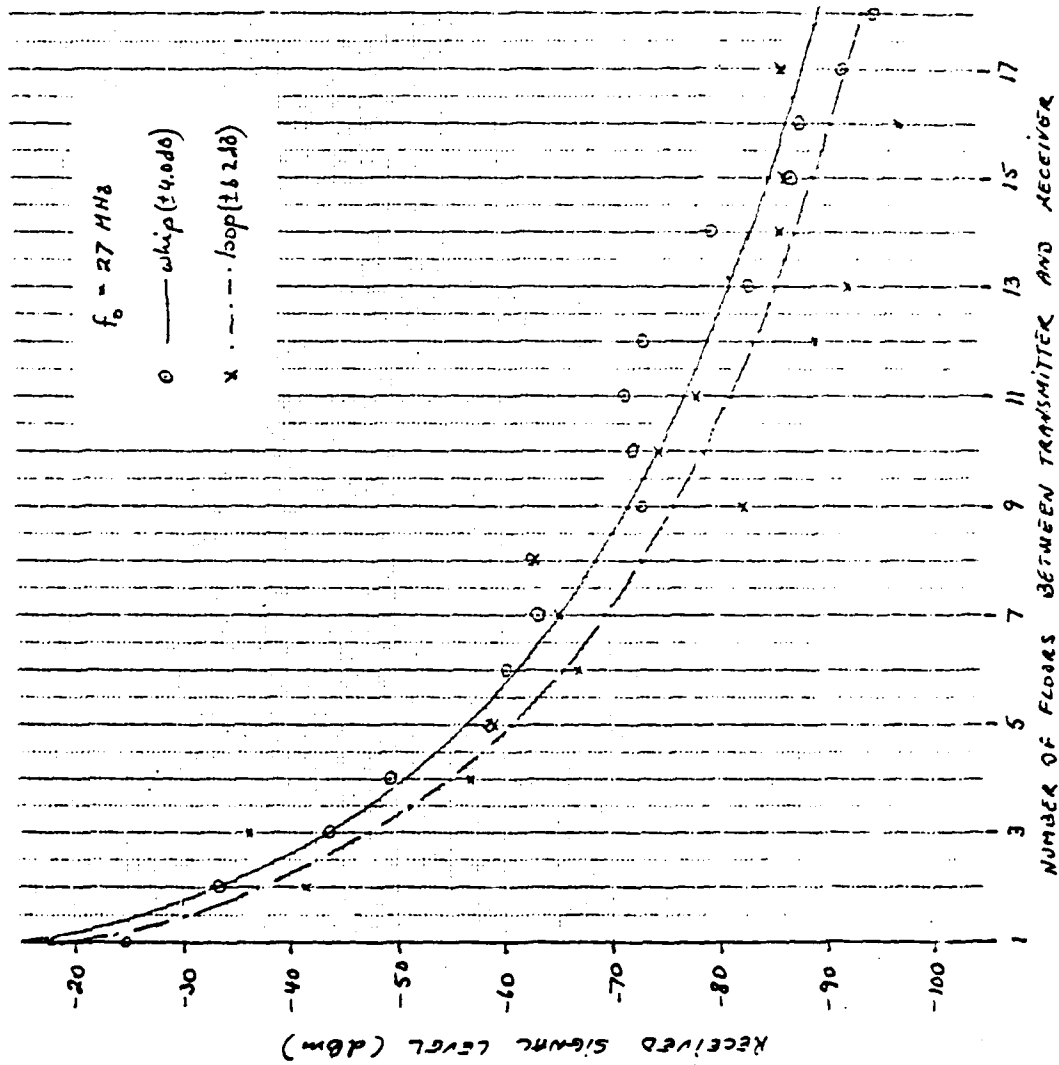
FIGURE 2.6-12 Received Signal Level for Transmissions Along
Elevator Shafts
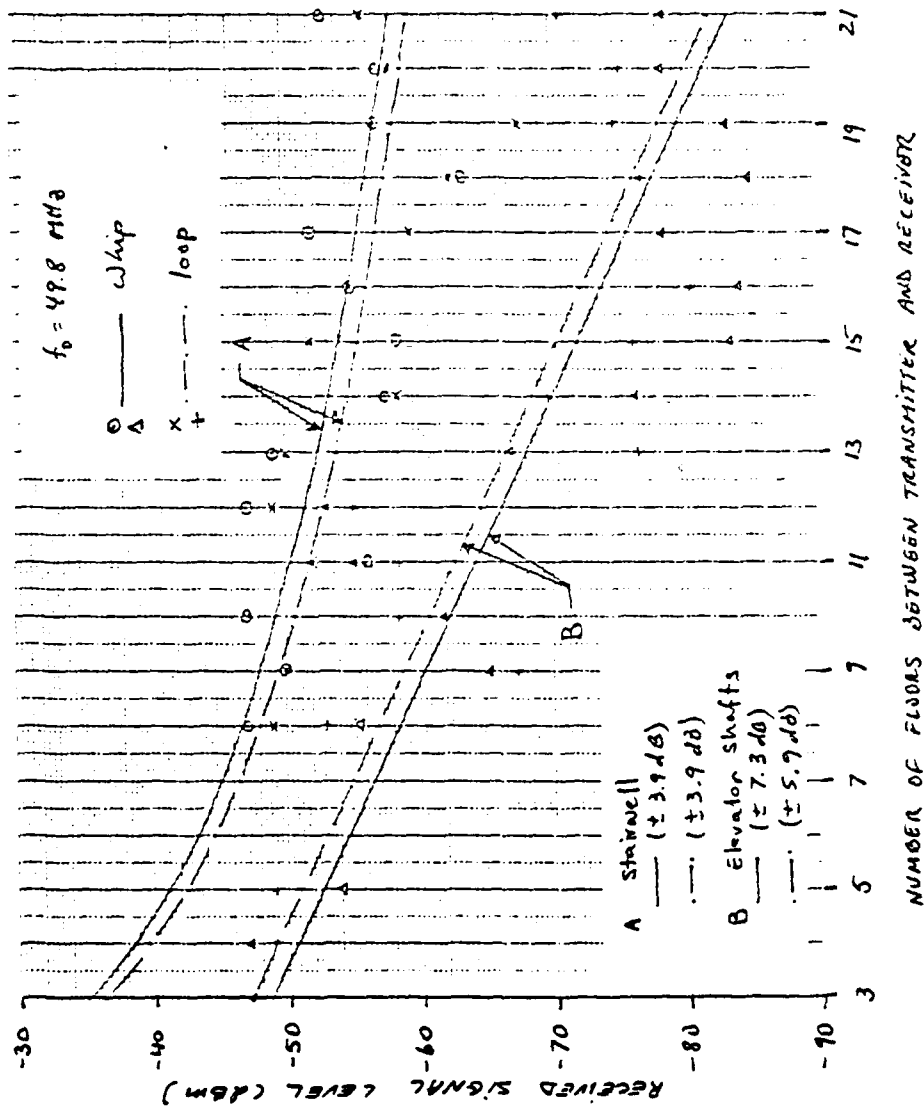
FIGURE 2.6-13 Received Signal Level for Transmissions in Stairwells and Along Elevator Shafts
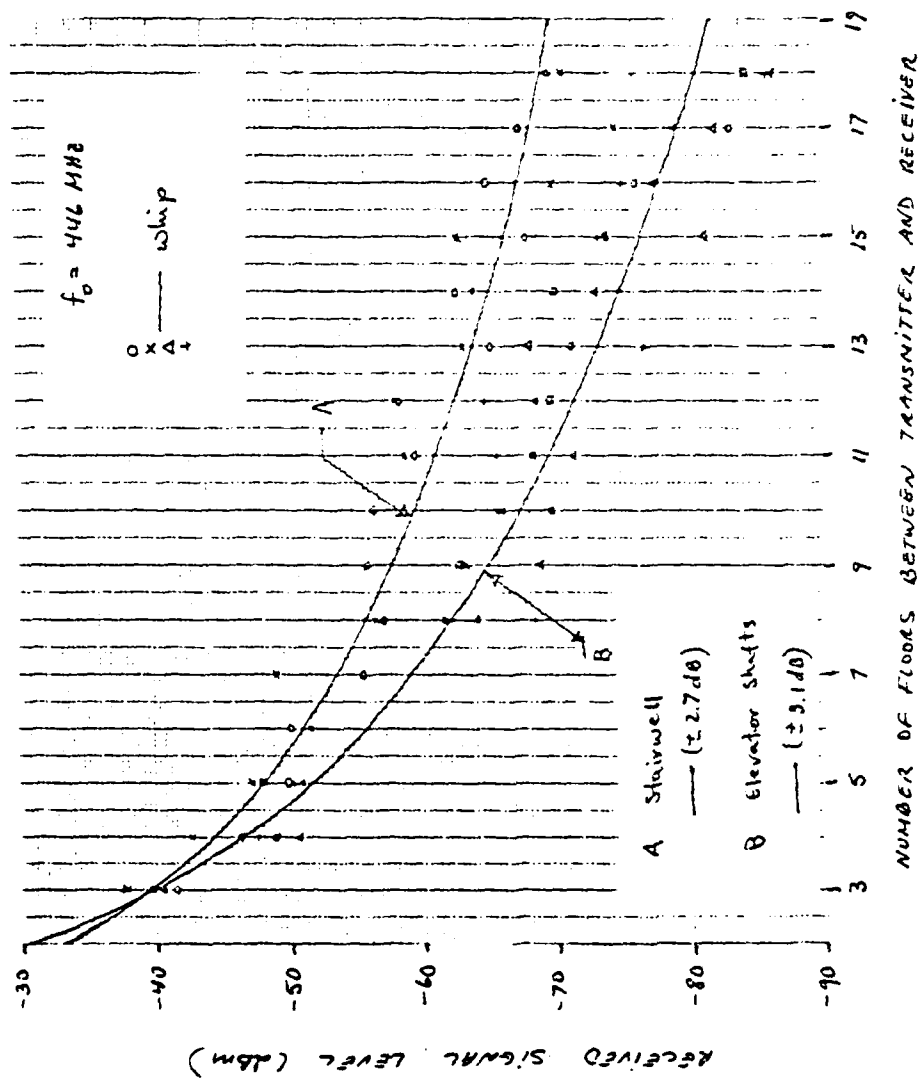
FIGURE 2.6-14 Received Signal Level for Transmissions
in Stairwells and Along Elevator Shafts

away. In some instances the measurements might have been made with the elevator box cars blocking all three shafts while in some other instances one or more of the elevator box cars may have been above the transmitter and receiver, allowing a clear path.

In order to determine the dependence of the received signal level on the length of the stairwell and the elevator shafts, best fit curves with their respective standard deviations are also shown in Figures 2.6-11 to 2.6-14. In the case of the measurements inside the stairwell, the median of the received signal (best fit curve) exhibits a power law distance dependence at all three frequencies (each floor was approximately 15 feet high), i.e., $P_r \sim kh^{-n}$ where h is the distance expressed in terms of the floor height units and n is the power law dependence. The attenuation rates in dB/decade (10 n) are:

$$10\ n = \begin{cases} 60 \text{ dB/decade} & \text{at 27 MHz} \\ 27.5 \text{ dB/decade} & \text{at 49.8 MHz} \\ 38 \text{ dB/decade} & \text{at 446 MHz.} \end{cases}$$

It can be seen that the attenuation rate exhibits the same frequency dependence as in the floor-to-floor transmissions, i.e., it decreases with frequency until the wavelength becomes comparable with the thickness of the staircase steps in which case it increases with frequency. Although the total attenuation is lower in the stairwell transmission than in the floor-to-floor transmissions (at least initially when there are only a few floors between transmitter and receiver), the fact that the attenuation rates are higher indicates that eventually as the distance (number of floors) becomes large enough, the attenuation will be higher in a stairwell. This is probably due to the fact that the stairwell dimensions (cross-section) are smaller than the room dimensions in the floor-to-floor transmissions.

In the case of the measurements along elevator shafts, the median of the received signal (best fit curves) exhibited an exponential distance dependence, i.e., $P_r \sim k'e^{-\alpha h}$ where h is

the distance in floor height units for the transmissions at 27 MHz and 49.8 MHz, and a power law dependence for the transmissions at 446 MHz. The reason for the difference in distance dependence between the VHF and UHF transmissions is probably due to the fact that at 50 MHz and below the dimensions of the elevator shafts are smaller than a half-wavelength resulting in a wave-guide type of propagation at frequencies below cut-off, while at UHF the dimensions of the elevator shaft are much greater than the wavelength resulting in a much lower attenuation rate. The attenuation rates at VHF in dB/floor (4.3 α) are:

$$4.3 \; \alpha = \begin{cases} 3.4 \text{ dB/floor} & \text{at 27 MHz} \\ 4.3 \text{ dB/floor} & \text{at 49.8 MHz} \end{cases}$$

while the attenuation rate at 446 MHz is 52.6 dB/decade (i.e., 10 n = 52.6). If we express the attenuation rate at 446 MHz in dB/floor it would be approximately equal to 2.61 dB/floor which is lower than at the two VHF frequencies.

It should be noted though that although the attenuation rates for the transmissions inside stairwells and along elevator shafts are higher than in floor-to-floor transmissions, the total attenuations measured for distances up to 20 floors high are lowest inside stairwells and highest for floor-to-floor trans-missions. The reason is that at shorter distances (transmissions through a few floors) there are fewer obstacles inside a stair-well or elevator shaft than in a floor-to-floor transmission (which must penetrate through the ceiling) resulting in a lower attenuation. However, as the distance (number of floors) increases, the stairwell, elevator shaft, and room dimensions begin to play a more important role resulting in higher attenu-ation rates for those transmission media where the dimensions are in the order or smaller than the wavelength. This effect does not become crucial though until the transmission distance exceeds 20 floors.

2.7　Summary

Summarizing the results presented in this section, propagation measurements were made at 27 MHz, 49.8 MHZ, and 446 MHz. The data consists of measurements of received signal level obtained with two co-located vertically polarized receive antenna systems: one a whip receive antenna (at 27 MHz, 49.8 MHz, and 446 MHz) and the other a loop antenna system (at 27 MHz and 49.8 MHz). The whip antenna couples to the electric field component of the received signal while the loop antenna couples to the magentic field component of the received signal. Estimates of the field decorrelation can thus be obtained from the ensemble correlation of the data collected with the two receive antenna systems.

The measurements can be grouped into four types of propagation measurements: street-to-street propagation measurements between low elevation antennas; street-to-building transmission measurements; building-to-building transmission measurements; and intrabuilding propagation measurements.

The street-to-street propagation measurements were made in two areas: a highly built-up area (urban) and a medium built-up area (suburban). A summary of the 'best fit' to the data taken along the three urban and two suburban paths is given in Table 2.7-1. In addition, the measurements in the urban and suburban areas exhibited the following trends:

- Both urban and suburban propagation exhibit around 40 dB/decade attenuation rate (inverse fourth power law type of propagation) when there are no large (relative to the wavelength) diffracting obstacles within a few wavelengths of the fixed station (be it transmitter or receiver). A building is considered to be a diffracting obstacle if it is more than a few wavelengths high. At lower VHF this means a building higher than 40 feet (3 stories) while at UHF it means a building higher than 4 ~ 6 ft (1 story).

TABLE 2.7-1

Best Fit Characteristics of Urban and Suburban Street-to-Street Propagation Data as a Function of Transmitter-Receiver Separation, d

PATH	27 MHz			49.8 MHz			446 MHz		
	TYPE OF BEST FIT P_r	EXPONENT n=	RATE OF ATTEN. dB/decade	TYPE OF BEST FIT P_r	EXPONENT n=	RATE OF ATTEN. dB/decade	TYPE OF BEST FIT P_r	EXPONENT n=	RATE OF ATTEN. dB/decade
Along Street Urban Path	d^{-n}	4.69	46.9	d^{-n}	4.5	45	d^{-n}	4.26	42.6
NLOS Urban Path 2	d^{-n}	4.0	40	d^{-n}	3.95	39.5	d^{-n}	4.08	40.8
NLOS Urban Path 3	d^{-n}	2.03	20.3	n^{-n}	4.67	46.7	d^{-n}	2.65	26.5
Along Street Suburban Path	d^{-n}	4.68	46.8	d^{-n}	3.85	38.5	d^{-n}	4.66	46.6
NLOS Suburban Path	d^{-n}	4.96	49.6	d^{-n}	3.58	35.8	d^{-n}	2.28	22.8

- When a diffracting obstacle is within a few wavelengths of the fixed station, the attenuation rate is around 20 dB/decade (inverse square law type of propagation).

- The measured maximum ranges that can be attained in built-up areas with a 2 watt transmitter are:

  1) Five thousand feet at frequencies from 27 MHz to 446 MHz in both urban and suburban areas when either transmitter or receiver or both are not surrounded by tall structures.

  2) When both transmitter and receiver are located among high buildings, the observed ranges were: 5,000 feet at 27 MHz if either or both the transmitter and receiver are located in the middle of the street and 500 feet to 1,000 feet if both are located on the sidewalk (i.e., close to a building); 900 to 1,000 feet at 49.8 MHz when both transmitter and receiver are located on the sidewalk next to a building; and 3,000 feet at 446 MHz when either transmitter or receiver are located in the middle of the street. No useful data were obtained for the case in which both transmitter and receiver were both on the sidewalk.

- At distances within the range of the transmitter, signal level variations (fades) as large as 20 dB were observed to occur periodically at distances in the order of the wavelength (that is 33 feet at 27 MHz, 20 feet at 50 MHz, and 2.3 feet at 446 MHz).

The street-to-building transmission measurements were made as a function of receiver height inside the building and as a function of distance (inside the building) from the transmitter. A summary of the characteristics of the 'best fit' curves to the data taken along a floor is given in Table 2.7-2. In addition, the measurements exhibited the following trends:

- No height gain was observed in the data taken in various floors of the building.
- The attenuation rate (as a function of the distance inside the building) is frequency dependent and varies according to the type of structure. Gypsum walls are not lossy at VHF but are considerably lossy at UHF. In the UHF frequency range the attenuation rate is around 100 dB/decade. Reinforced concrete walls are considerably lossier than gypsum walls.

The building-to-building transmission measurements were made between two adjacent reinforced concrete office type buildings as a function of location inside the building (horizontal and vertical). The following observations were made:

- Reception was only possible when either the transmitter or receiver was located near a window.
- No reception was possible when either transmitter or receiver was located in the basement.
- There was no height gain for the cases in which reception was possible.

The intrabuilding propagation measurements can be grouped into four categories: transmission along straight and right-angle corridors; transmission between above-ground floors; transmission between a basement and above-ground floors; and

TABLE 2.7-2

Best Fit Characteristics of Street-to-Building Propagation Data
As a Function of Distance Along a Floor, d

	TYPE OF BEST FIT	EXPONENT	RATE OF ATTENUATION
27 MHz	$P_r \sim d^{-n}$	$n = 1.89$	18.9 dB/decade
27 MHz	$P_r \sim d^{-n}$	$n = 4.03$	40.3 dB/decade
27 MHz	$P_r \sim d^{-n}$	$n = 10.6$	106.0 dB/decade

transmission along stairwells and elevator shafts. A summary
of the characteristics of the 'best fit' curves to the data is
presented in Table 2.7-3. In addition, the measurements ex-
hibited the following trends:

- Waveguide type of propagation was observed along
  corridors. The attenuation rate decreases with
  frequency in straight corridors and increases
  with frequency in corridors at right angles.

- The measurements for transmissions between above
  ground floors, basement to above ground floors,
  and along stairwells exhibited a power law type
  of distance dependence (i.e., an inverse de-
  pendence on the number of floors penetrated
  through). The attenuation rates (power law)
  decreased with frequency in all three cases
  until the wavelength became comparable to the
  thickness of the ceilings where an increase
  in the attenuation rate with frequency was
  observed.

- The measurements for transmissions along ele-
  vator shafts exhibit a waveguide type of
  attenuation at the VHF frequencies and a power
  law distance dependence at UHF. This is probably
  due to the fact that elevator shaft dimensions
  were smaller compared to the wavelength at VHF
  but much larger at UHF.

- The total attenuation and the attenuation rates
  were higher in the above ground floor to base-
  ment transmissions than in the transmissions
  between above ground floors.

- The attenuation for transmissions along stair-
  wells and elevator shafts was lower than the
  transmissions between above ground floors.

TABLE 2.-3

Best Fit Characteristics of Intrabuilding Propagation Data as a Function of Distance (Along a Corridor), d, or Number of Floors Between Transmitter and Receiver, h

TYPE OF TRANS-MISSION	27 MHz			49.8 MHz			446 MHz		
	TYPE OF BEST FIT $\tilde{P}_r$	EXPONENT	RATE OF ATTEN.	TYPE OF BEST FIT $\tilde{P}_r$	EXPONENT	RATE OF ATTEN.	TYPE OF BEST FIT $\tilde{P}_r$	EXPONENT	RATE OF ATTEN.
Along Straight Corridor	$e^{-\alpha d}$	$\alpha=.048$ nepers/ft	20.8 dB/100 ft	$e^{-\alpha d}$	$\alpha=.048$ nepers/ft	20.8 dB/100 ft	$e^{-\alpha d}$	$\alpha=.038$ nepers/ft	16.3 dB/100 ft
Along a Winding Corridor	$e^{-\alpha d}$	$\alpha=.058$ nepers/ft	24.8 dB/100 ft	$e^{-\alpha d}$	$\alpha=.068$ nepers/ft	29.4 dB/100 ft	$e^{-\alpha d}$	$\alpha=.072$ nepers/ft	30.8 dB/100 ft
Between Above Ground Floors	h^{-n}	$n=5.13$	51.3 dB/decade	h^{-n}	$n=2.55$	25.5 dB/decade	h^{-n}	$n=3.02$	30.2 dB/decade
Between Above Gnd. Flrs. & Basmnt.	h^{-n}	$n=5.6$	56 dB/decade	h^{-n}	$n=4.45$	44.5 dB/decade	h^{-n}	$n=5.0$	50 dB/decade
Inside a Stairwell	h^{-n}	$n=6.0$	60 dB/decade	h^{-n}	$n=2.75$	27.5 dB/decade	h^{-n}	$n=3.8$	38 dB/decade
Along Elevator Shafts	$e^{-\alpha h}$	$\alpha=.79$ nepers/ft	3.4 dB/floor	$e^{-\alpha h}$	$\alpha=1.0$ nepers/floor	4.3 dB/floor	h^{-n}	$n=5.26$	52.6 dB/decade

However, the converse was true for the
attenuation rates. This implies that for
transmissions through a few floors, the
attenuation is mainly determined by the
obstacles (i.e., walls, ceilings, staircase)
but as the number of floors (distance) in-
creases, the dimensions of the stairwell,
elevator shaft, and room begin to play an
important role in determining the attenuation
rate.

The conclusions based on the measured data presented
in this section are qualitative. Before we can give a quanti-
tative description and comparison of the various effects tested
for, we have to take into account the differences in trans-
mitted power and antenna gain at the three frequencies. This
type of analysis as well as a correlation analysis of the data
is performed in the next section.

REFERENCES FOR SECTION 2

Bohley, P., (1976), "Development of the Multiturn Loop Antenna
    at VHF for Vehicular Applications", ECOM Report 74-
    0593-F

Krupka, Z., (1968), "The Effect of the Human Body on Radiation
  * Properties of Small-Sized Communication Systems", IEEE
    Trans. Antennas and Prop., V AP-16, No. 2, March 1968,
    pp. 154-163

SECTION 3
VHF AND UHF DATA ANALYSIS

3.0 Introduction

In this section presents an analysis of the data
described in Section 2. An estimate is given for the
average path or transmission loss of each of the propa-
gation paths previously described is obtained from the set of
measurements. In addition, we also obtain an estimate of the
correlation between the data taken with colocated whip and loop
antennas at 27 MHz and 49.8 MHz (E-H field correlation) as well
as an estimate of the correlation between measurements taken
at fixed distances (spatial correlation) at 49.8 MHz and 446 MHz.

The average path or transmission loss is a measure of the
average attenuation introduced by the environment (propagation
medium) independent of the transmitting and receiving apparatus.
As such, in the most general case, it varies with frequency,
transmitter-receiver separation, and the heights of the transmit
and receive locations. Thus, the purpose of the path loss
analysis is to determine the dependence of the data on these
three factors. The average path loss is obtained from the
following relationship between transmitted power, P_t, average
received power, $\hat{P}_r$, and transmit and receive antenna gains,
G_t and G_r respectively:

$$\hat{P}_r = P_t + G_t + G_r - L \qquad (3.0\text{-}1)$$

where all quantities are in dB and L is the average path loss.
By defining the path loss in this manner, we have removed all
the effects of the hardware (equipment) on the measured data,
P_r. Note however, that the measured received signal, P_r, is not

3-1

actually equal to the average value but it rather fluctuates
randomly about it. The fluctuations are due to the fading nature
of the transmission medium, the fading being due to the existence
of multiple propagation paths (multipath) between a transmitter
and receiver. The average signal level is thus defined as the
minimum mean-squared error linear fit to a set of measurements
in dB. Thus, if p_r is the instantaneous received signal in Watts,
then the received signal in dB is given by

$$P_r = 10 \log p_r = \hat{P}_r + \Delta P_r \qquad (3.0-2)$$

where $\hat{P}_r$ is the average of the received signal level in dB and
ΔP_r is the zero mean fluctuation (in dB) of the received signal
about the average. The average value in Watts, or mean received
signal level, is related to the dB average through

$$\bar{p}_r = E\{\exp[(\hat{P}_r + \Delta P_r)/4.34]\} \qquad (3.0-3)$$

where $E\{\cdot\}$ denotes ensemble averaging over the fluctuations ΔP_r.
If the fluctuations (in dB) are Gaussian distributed with a
standard deviation σ, then the mean received signal level in Watts
is given by

$$\bar{p}_r = \exp[(2\hat{P}_r + \sigma^2)/8.68].$$

However, since many of the measurements in a given set were made
at different transmitter and receiver locations, we expect the
average received signal level $\hat{P}_r$, to exhibit a distance and/or
height dependence. Thus it is important to remove the distance
and/or height dependance of the data before performing any averag-
ing of a set of data in order to determine the average path loss.

The field and spatial correlation coefficients of the data
are a measure of the decrease in the input signal-to-noise
ratio that a communications system employing field or spatial

diversity will require. By this we can mean that a receiving system employing two antennas, a whip and a colocated loop antenna or two whip antennas separated by at least a half-wavelength, will require a lower signal-to-noise ratio to achieve the same level of performance as a system employing a single receiving antenna. The improvement is determined by the correlation between the signals received with the two diversity antennas, defined as

$$r = \frac{E\{X_1 X_2\} - E\{X_1\} E\{X_2\}}{\left[E\{X_1^2 - \overline{X}_1^2\} E \{X_2^2 - \overline{X}_2^2\} \right]^{1/2}}$$
(3.0-4)

where X_1 and X_2 are the instantaneous signal (amplitudes and phase) and $E\{\cdot\}$ denotes ensemble averaging over the fluctuations of X_1 and X_2. If the two signals are uncorrelated $r = 0$. On the other hand if X_1 and X_2 are perfectly correlated, i.e. they fluctuate identically, then $r = \pm 1$. Thus, the range of values of r is

$$-1 \leq r \leq 1$$
(3.0-5)

Hence this section will be concerned with obtaining estimates of the average path loss L and the field and spatial correlation coefficients, r_{eh} and r_s respectively. Section 3.1 is concerned with the path or transmission loss analysis of the data while section 3.2 deals with the correlation analysis of the data. Finally in Section 3.3 we make use of the results of the path loss analysis to extend the existing data base.

3.1   Path or Transmission Loss Analysis

In this section we obtain an estimate of the average path loss for each of the sets of measurements described in Section 2. The average path loss is in general dependent on the distance from transmitter to receiver and/or the relative height between the

transmit and receive locations. Thus part of the analysis of the
data is to determine the distance and/or height dependence. Further-
more, from physical considerations, the distance and/or height
dependence of the data is assumed to be well behaved (i.e. deter-
ministic), with any deviations of the data from the expected value
being due to multipath fading and terrain variations (including
building density, number of walls penetrated, etc.). The path
loss is thus related to (by Eq. 3.0-1) the average value of the
measured data (in dB), averaged over the fluctuations about a
deterministic distance and/or height dependent value (the least-
mean-squared error fit). We may thus express this mathematically
by writing the average of the received signal level data at the
·ith location as

$$\hat{p}_i = Kf(X_i) \qquad\qquad (3.1-1)$$

where $\hat{p}_i$ is the average of the received signal (in Watts) at a
distance or height X_i relative to the emitter, K is a proportionality
constant which depends on the transmitted power and antenna gains,
and $f(\cdot)$ is a function which describes the type of distance or
height dependence exhibited by the data. If the data exhibits a
power law type of distance or height dependence, then

$$f(X) = X^{-n} \qquad\qquad (3.1-2)$$

where n is the power law dependence. On the other hand, if the
data exhibits an exponential type of distance or height dependence,
then

$$f(X) = e^{-\lambda X} \qquad\qquad (3.1-3)$$

where λ is the rate of decay.

Since the distance dependence is assumed to be deterministic,
the actual received signal data, p_i (as opposed to its average
value $\hat{p}_i$) should exhibit the same distance dependence. However, the

proportionality constant is random and varies from data point to data point (i.e. $p_i = K_i f(X_i)$). The problem of obtaining the average path loss is then reduced to finding the values of the constants K and n or α that yield the smallest standard deviation between the measured data $\{p_i\}$ and $\{Kf(X_i)\}$.

Since the actual gathered data is in dBm, it is convenient to rewrite (3.1-1) as

$$\hat{P}_i = I - SY_i \qquad\qquad (3.1\text{-}4)$$

where $\hat{P}_i = 10 \log_{10} \hat{p}_i$,

$\quad I = 10 \log_{10} K$,

$$S = \begin{cases} 10n & \text{if power law dependence} \\ 10\alpha\log_{10}e & \text{if exponential dependence} \end{cases}$$

and

$$Y_i = \begin{cases} \log_{10} X_i & \text{if power law dependence} \\ X_i & \text{if exponential dependence.} \end{cases}$$

The average path loss is then determined by finding the I and S which minimize the distance (standard deviation) between the data in dBm $\{P_i\}$ and $\{I-SY_i\}$.

The values of I and S which minimize the mean-squared distance between the measured data $\{P_i\}$ and the best estimate $\{P_i = I-SY_i\}$ or average path loss are [Papoulis, 1965].

$$S = \frac{-\dfrac{1}{N}\sum_{i=1}^{N} P_i Y_i + \left[\dfrac{1}{N}\sum_{i=1}^{N} P_i\right]\left[\dfrac{1}{N}\sum_{i=1}^{N} Y_i\right]}{\dfrac{1}{N}\sum_{i=1}^{N} Y_i^2 - \left[\dfrac{1}{N}\sum_{i=1}^{N} Y_i\right]^2} \qquad (3.1\text{-}5)$$

$$I = \frac{1}{N} \sum_{i=1}^{N} (P_i + SY_i) \qquad (3.1-6)$$

where N is the number of data points. The standard deviation
(or spread) of the data is defined as:

$$\sigma = \sqrt{\frac{1}{N} \sum_{i=1}^{N} (P_i - \hat{P}_i)^2}. \qquad (3.1-7)$$

The expressions for the slope, S, and intercept, I, are
valid as long as all the measurements in a given set are made with
the same receiving antenna. However, the measurements at 27 MHz
and 49.8 MHz were made with two types of receiving antennas: a
whip and a loop. From physical considerations, we expect the two
sets of measurements made with the two antennas to exhibit the
same distance dependence. However, since the gains of the two
antennas were not necessarily equal, then the intercept of the
two sets of data must be different. In this case, we express the
estimates of the data collected with the two antennas as:

$$\hat{P}_i(e) = I_e - Y_i$$

$$\qquad (3.1-8)$$

$$\hat{P}_i(h) = I_h - Y_i$$

where e and h denote the data obtained with the whip antenna and
loop antenna, respectively. The values of S, I_e, and I_h which
minimize the mean-squared distance between the measured data,
$\{P_i(e)\}$ and $\{P_i(h)\}$, and the values $\{I_e - SY_i\}$ and $\{I_h - SY_i\}$,
are given by

$$S = -\frac{1}{2} \frac{\frac{1}{N} \sum_{i=1}^{N} \{P_i(e) + P_i(h)\} Y_i - \left[\frac{1}{N} \sum_{i=1}^{N} \{P_i(e) + P_i(h)\}\right] \left[\frac{1}{N} \sum_{i=1}^{N} Y_i\right]}{\frac{1}{N} \sum_{i=1}^{N} Y_i^2 - (\frac{1}{N} \sum_{i=1}^{N} Y_i)^2} \qquad (3.1-9)$$

3-6

$$I_e = \frac{1}{N} \sum_{i=1}^{N} \{P_i(e) + SY_i\} \qquad (3.1\text{-}10)$$

$$I_h = \frac{1}{N} \sum_{i=1}^{N} \{P_i(h) + SY_i\} \qquad (3.1\text{-}11)$$

where N is the number of data points collected with each of the antennas.

The standard deviation of the data obtained with each of the antennas is given by:

$$\sigma_e = \sqrt{\frac{1}{N} \sum_{i=1}^{N} \{P_i(e) - \hat{P}_i(e)\}^2}$$

$$(3.1\text{-}12)$$

$$\sigma_h = \sqrt{\frac{1}{N} \sum_{i=1}^{N} \{P_i(h) - \hat{P}_i(h)\}^2}.$$

The best fit curves presented in Section 2 along with the data points were obtained using Eqs. (3.1-8) to (3.1-11) for the measurements at 27 MHz and 49.8 MHz; and Eqs. (3.1-4) to (3.1-6) for the measurements at 446 MHz. The standard deviations shown in the legends of the figures were computed using Eqs. (3.1-12) and (3.1-7) respectively.

Once the average of the received signal is obtained, we determine the average path or transmission loss in dB from Eq. (3.0-1), i.e.,

$$L_i = P_t + G_t + G_r - \hat{P}_i \qquad (3.1\text{-}13)$$

3-7

The levels of transmitted power in Watts (1 Watt =
30 dBm) for the measurement systems at 27 MHz, 49.8 MHz,
and 446 MHz are given in Table 2.1-1. The gains of the
respective antenna systems are discussed in Section 2.1-2
and estimates of the effective gains are given in Table 2.1-3.
Since the gains of the antennas could only be estimated, the
variance (square of the standard deviation) of the actual (as
opposed to average) path loss is equal to the sum of the
variance of the received signal plus the variance (uncertainty)
of the estimates of the antenna gains.

A complete analysis of the data involves determining the
frequency and distance and/or height dependence of the path loss
for the street-to-street, street-to-building, building-to-
building, and intrabuilding propagation measurements. In
addition, in the analysis of the street-to-street propagation
data we also discuss the effects of urban vs. suburban environ-
ment. Included in this discussion are the effects of building
height as well as the proximity of the transmit (or receive)
location to the buildings. However, this latter discussion is
more of a qualitative (with some quantitative values given)
nature as there is not enough data to do a statistical analysis.
The analysis of the street-to-building and building-to-building
propagation measurements includes a limited discussion of the
effects of the type of structure in addition to position (dis-
tance and floor level) within the building. Finally, the
analysis of transmission loss for the intrabuilding propagation
measurements includes a discussion of the effects of room
dimensions.

In the remainder of Section 3.1, we present the results
of the average path loss analysis for the street-to-street,
street-to-building, building-to-building, and intrabuilding
propagation measurements. The spread of the data about the
average path loss curves given in tne following sections is shown
in the legend of the corresponding figure presented in Section 2.

3.1.1 Average Path Loss in Street-to-Street Propagation

3.1.1.1 Urban Average Path Loss

The results of the path loss analysis for the urban street-to-street propagation measurements described in Section 2.3.1 are shown in Figs. 3.1.1-1 to 3.1.1-3. The solid curves of Fig. 3.1.1-1 represent the average path loss at the three frequencies for the case in which the transmit and receive locations were both on Congress Street. Similar curves for the case in which the transmit location was at the intersection of Cambridge Street and New Sudbury Street and the various receive locations were along Congress Street are shown in Fig. 3.1.1-2. The curves of Fig. 3.1.1-3 represent the average path loss at the three test frequencies for the case in which the transmit location was on Summer Street and the various receive locations were on different streets in the immediate area on both sides of Summer Street. The path loss curves were calculated from Eqs. (3.1-8) and (3.1-13).

The dashed lines denoted by L_p represent the path loss that can be expected for transmissions between two vertically polarized antennas placed 1.5 meters (~5 ft) above a perfectly conducting plane ground (i.e., plane-earth path loss):

$$L_p = -20 \log_{10} \left(\frac{h_1 h_2}{d^2} \right) \qquad (3.1.1-1)$$

where h_1 and h_2 are the antenna heights and d is the distance between the two antennas. Thus, it is seen that in all three cases, the path loss exceeds the plane-earth path loss, L_p. The amount by which the plane earth path loss is exceeded depends on the frequency and varies from path to path. Furthermore, the path loss curves (solid lines) of Figs. 3.1.1-1 and 3.1.1-2 are closely parallel to the plane-earth path loss (dashed line). This would seem to suggest that the path loss in dB between low elevation antennas may be expressed as the sum of a term purely

3-9

Y-axis: MEDIAN PATH LOSS (dB) — 70, 80, 90, 100, 110, 120, 130, 140

X-axis: DISTANCE (meters) — 100, 200, 300, 500, 700, 1000, 2000

Curve labels: 27 MHz, 79.8 MHz, 446 MHz, L$_p$
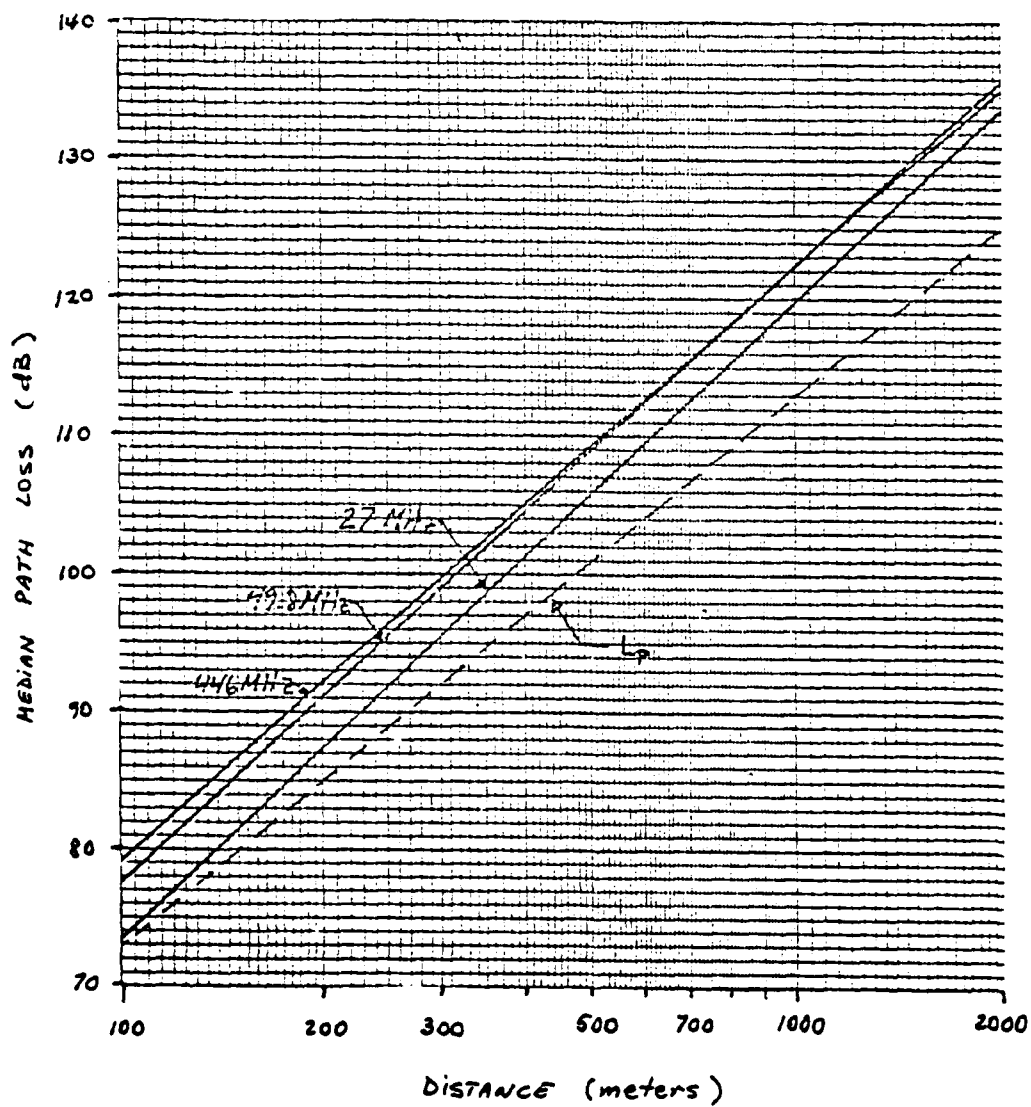
FIGURE 3.1.1-1   Median Path Loss Along Urban Street
(Congress St., Boston, MA)

3-10
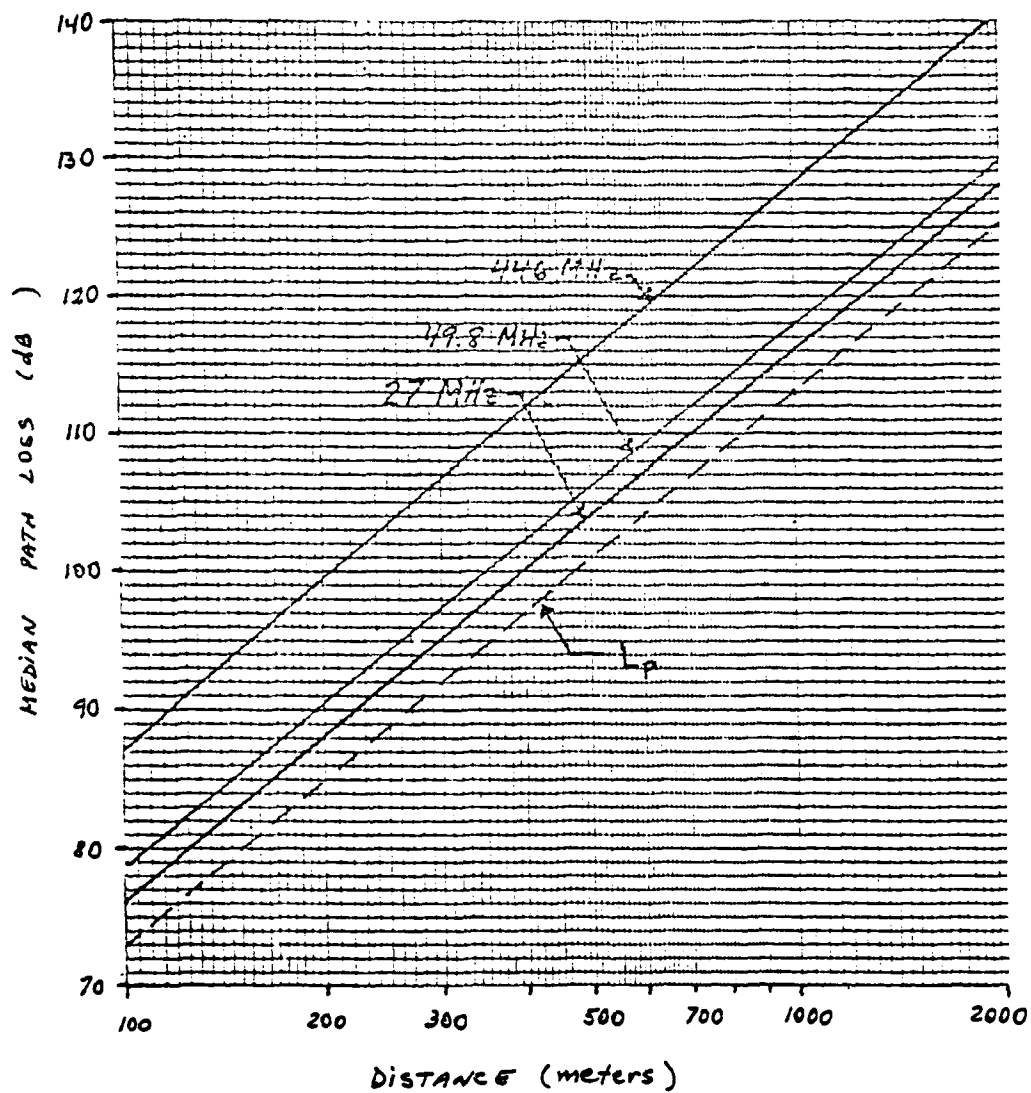
FIGURE 3.1.1-2 Median Path Loss Along a Non-Line-of-Sight
Urban Path (Transmitter at Cambridge St.
and New Sudbury St., Boston, MA)
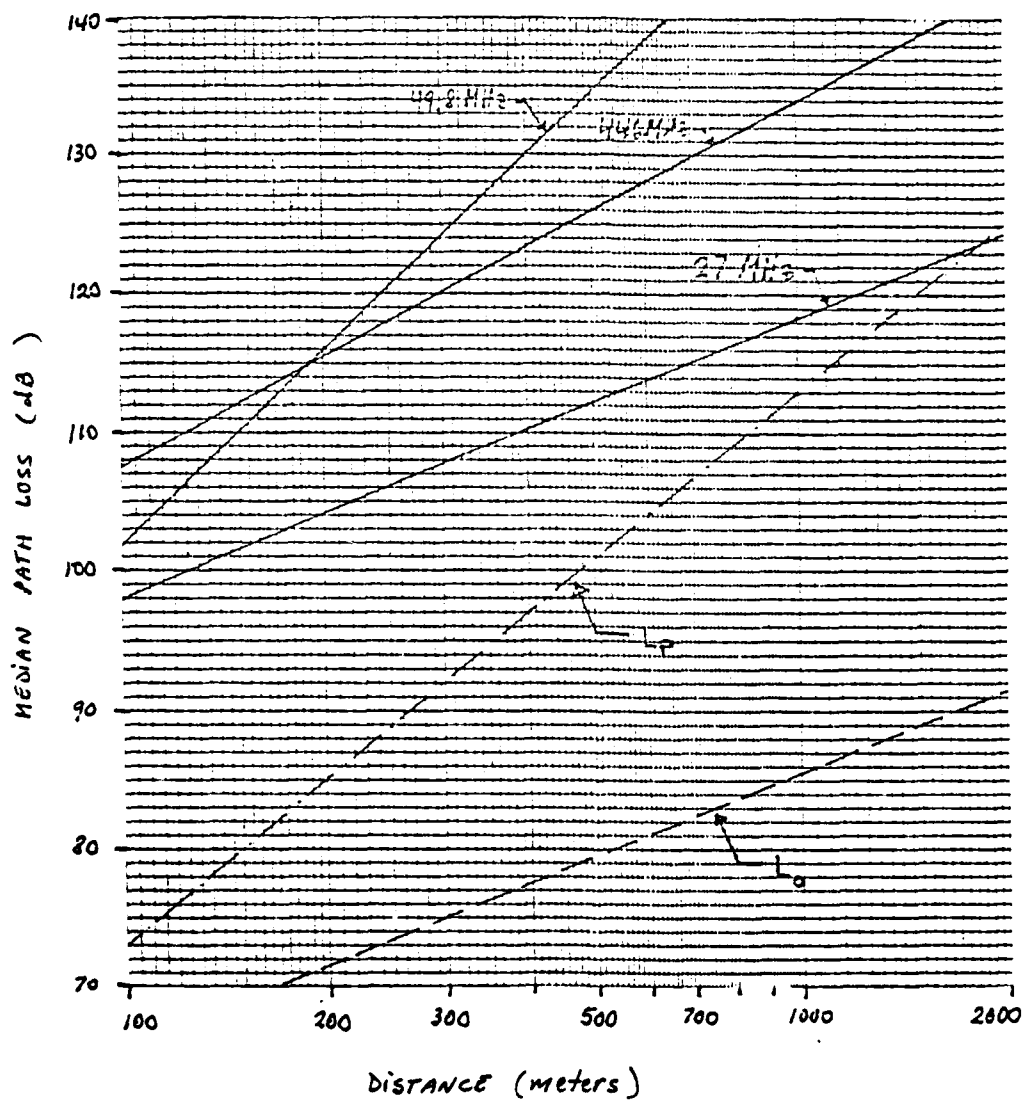
FIGURE 3.1.1-3   Median Path Loss Along a Non-Line-of-Sight
                 Urban Path (Transmitter on Summer St.,
                 Boston, MA)

3-12

dependent on the distance and antenna heights but independent of frequency, plus a term dependent on the frequency and nearby environment (i.e., building height and density as well as street orientation) but independent of the distance. However, this is not always the case as the curves of Fig. 3.1.1-3 show that the path loss at 49.8 MHz is nearly parallel to the plane-earth path loss, L_p, but the path losses at 27 MHz and 446 MHz are more nearly parallel to the free-space path loss defined as:

$$L_o = -20 \log_{10} \left(\frac{\lambda}{4\pi d}\right) \qquad (3.1.1-2)$$

where λ is the wavelength at the operating frequency and d is the distance. The free space loss is thus frequency dependent, so that the dashed line denoted by L_o in Fig. 3.1.1-3 represents the free-space loss at 446 MHz. Aside from the frequency dependence, the free-space path loss increases with distance at a rate of 20 dB per decade whereas the plane-earth path loss increases with distance at a rate of 40 dB per decade.

Hence, analysis of the urban measurements indicates that the path loss in dB may be represented in some instances as a plane-earth loss plus an excess loss due to environmental clutter or as a free-space loss plus some other excess loss in some other cases. In order to understand when one type of distance dependence or the other applies, it is helpful to consider a simplified model of the propagation medium which may not be accurate in terms of predicting the actual path loss but which gives a qualitative description of the mechanisms involved in determining the distance dependence.

The urban propagation problem involves, in general, one or more obstructions between the transmitting and receiving antennas. When two or more obstructions are involved, graphical integration of the obstacles into a single obstacle as shown in Fig. 3.1.1-4(a) yields a shadow loss which is within a few dB of the actual loss computed when the various obstacles are considered [Bullington, 1977]. Thus, with no loss in generality
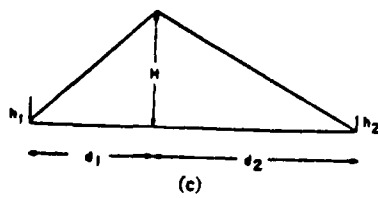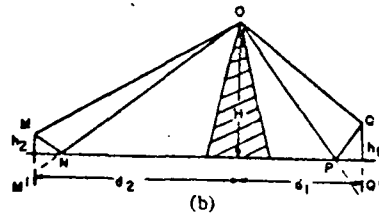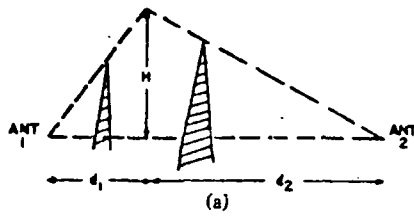
FIGURE 3.1.1-4   Ideal Profiles Used in Developing Theory
of Diffraction over Buildings and Other
Structures

we assume that the urban propagation problem can be represented qualitatively by a single knife-edge diffration problem.

Furthermore, when the transmitting and receiving antennas are not at ground level but rather at some height h_1 and h_2, respectively, it is necessary to include the effects of waves reflected from the ground. This results in four paths, namely, MOQ, MOQ', M'OQ, and M'OQ' shown in Fig. 3.1.1-4(b) for a single obstruction. Each of these paths is similar in form to the single path illustrated by Figure 3.1.1-4(a). The sum of the field intensities over these four paths, considering both magnitude and phase, is given by the following equation:

$$\left|\frac{E}{E_o}\right| = S_1 \left| 1 - \frac{S_2}{S_1}e^{-j(\Delta+b)} - \frac{S_3}{S_1}e^{-j(\Delta+c)} + \frac{S_4}{S_1}e^{-j(b+c)} \right| \quad (3.1.1-3)$$

where,

E	is the received field intensity,
E_o	is the free-space field intensity,
S_1	is the magnitude of the shadow loss over path MOQ,
S_2	is the magnitude of the shadow loss over path MOQ',
S_3	is the magnitude of the shadow loss over path M'OQ,
S_4	is the magnitude of the shadow loss over path M'OQ',
$\Delta =$	$4\pi h_1 h_2/\lambda (d_1+d_2)$ radians
b	is approximately equal to $4\pi h_2 H/\lambda d_2$ rad,
c	is approximately equal to $4\pi h_1 H/\lambda d_1$ rad.

This equation assumes that the reflection coefficient is -1. This means that the ground reflections are assumed to be at near grazing angles. The equation fails when either antenna height approaches zero. The angles b and c are phase angles associated with the diffraction phenomena and the approximate values given above assume that H is greater than h_1, or h_2. This assumption permits the shadow losses to be averaged so that $S_1=S_2=S_3=S_4=S$. After several algebraic manipulations (3.1.1-3) can be put into the form,

$$\left|\frac{E}{E_o}\right| = 4S\left|\sin\frac{\Delta}{2}\cos\frac{b+c}{2} + j\left(\sin^2\frac{b+c}{4} - \sin^2\frac{b-c}{4}\right)e^{-j\Delta/2}\right| \quad (3.1.1\text{-}4)$$

where S is the average shadow loss for the four paths. This means that the shadow triangle should be drawn midway between the location of the actual antenna and the image antenna as shown in Fig. 3.1.1-4(c). When the antenna heights are small compared to d_1 and d_2, the angles $(b+c)/4$ and $(b-c)/4$ are small and

$$\left|\frac{E}{E_o}\right| \simeq 4S\left|\sin\frac{\Delta}{2}\cos\frac{b+c}{2}\right|. \quad (3.1.1\text{-}5)$$

The ratio of received power to transmitted power may be expressed in terms of Eq. (3.1.1-5) as:

$$\frac{P_r}{P_t} \simeq \left|\frac{E}{E_o}\right|^2 \frac{|E_o|^2}{P_t} \quad (3.1.1\text{-}6)$$

$$= \left(\frac{\lambda}{4\pi x}\right)^2 \left(\frac{4\lambda d_1 d_2}{\pi^2 H^2 d}\right)\left|\sin\frac{4\pi h_1 h_2}{\lambda d}\cos\frac{4\pi H}{\lambda}\left(\frac{h_2}{d_2} + \frac{h_1}{d_1}\right)\right|^2$$

where the first term is the free-space loss, the second is the shadow loss and where $d = d_1 + d_2$. When the antenna heights are much smaller than the distance, the sin ($\cdot$) term can be replaced by its argument since the angle $4\pi h_1 h_2/\lambda d$ becomes very small and

$$\frac{P_r}{P_t} \simeq \left(\frac{\lambda}{4\pi x}\right)^2 \left(\frac{4\lambda d_1 d_2}{\pi^2 H^2 d}\right)\left(\frac{4\pi h_1 h_2}{\lambda d}\right)^2 \cos^2\frac{4\pi H}{\lambda}\left[\frac{h_2}{d_2} + \frac{h_1}{d_1}\right]$$

$$(3.1.1\text{-}7)$$

$$= \frac{4\lambda d_1 d_2}{\pi^2 H^2 d}\left(\frac{h_1 h_2}{d^2}\right)^2 \cos^2\left[\frac{4\pi H}{\lambda}\left(\frac{h_2}{d_2} + \frac{h_1}{d_1}\right)\right]$$

Let us assume, for simplicity, that the two antenna
heights are nearly equal, i.e., $h_1 \approx h_2 = h$. Then, (3.1.1-7)
takes on two different limiting distance dependences when
$d_1 \approx d_2$ and when $d_1 \gg d_2$. First consider the case in which
the obstruction is about halfway between transmitter and re-
ceiver, i.e., $d_1 \approx d_2 = d/2$. In this case, (3.1.1-7) becomes:

$$\frac{p_r}{p_t} \approx \left(\frac{h_1 h_2}{\pi H}\right)^2 \frac{\lambda}{d^3} \tag{3.1.1-8}$$

which indicates that the path loss in this case increases with
distance at a rate of 30 dB per decade. At the other extreme,
when $d_1 \gg d_2$, $d_1 \approx d$, and (3.1.1-7) becomes

$$\frac{p_r}{p_t} \approx \frac{4\lambda d_2}{\pi^2 H^2} \left(\frac{h_1 h_2}{d^2}\right)^2 \cos^2 \frac{4\pi H h_2}{\lambda d_2} \tag{3.1.1-9}$$

which shows that the path loss increases with distance at a rate
equal to the plane-earth path loss rate, 40 dB per decade.

This simplistic model illustrates how variations in dis-
tance dependence from inverse cubic to inverse fourth power law
can be explained in terms of multiple diffraction paths and the
distance from the terminals to the diffraction point.

When the reflection coefficient is much less
than 1 (not perfectly conducting ground and nongrazing reflection
angle), $S_2 \ll S_1$, $S_3 \ll S_1$, and $S_4 \ll 1$, so that most of the
received energy propagates along path MOQ. In this case, the
ratio of received to transmitted power is given by

$$\frac{p_r}{p_t} \approx \frac{\lambda d_1 d_2}{4\pi^2 H^2 d} \left(\frac{\lambda}{4\pi d}\right)^2 \tag{3.1.1-10}$$

where the first term is the shadow loss S_1 and the second term
is the free-space loss. When the obstruction is halfway between

transmitter and receiver, $d_1 \simeq d_2 \simeq d/2$ and

$$\frac{p_r}{p_t} \simeq \left(\frac{1}{8\pi^2 H} \right)^2 \frac{\lambda^3}{d} \qquad (3.1.1\text{-}11)$$

which indicates an inverse distance dependence for the path loss. On the other hand, when $d_1 \simeq d \gg d_2$, (3.1.1-10) becomes

$$\frac{p_r}{p_t} \simeq \left(\frac{1}{8\pi^2 H} \right)^2 \frac{\lambda^3 d_2}{d^2} \qquad (3.1.1\text{-}12)$$

which exhibits an inverse squared distance dependence. These two results illustrate how variations in distance dependence from inverse distance to inverse squared distance dependence may be explained in terms of a single diffraction path and the distance from transmitter and receiver to the diffraction point.

We can now use these qualitative results to understand the differences in distance dependence between the average path loss curves of Figures 3.1.1-1, 3.1.1-2, and 3.1.1-3. The results of Figures 3.1.1-1 and 3.1.1-2 indicate the presence of two or more equal strength diffraction paths with the effective diffraction point being located near the transmit or receive location. The same conclusion may be reached about the path loss curve at 49.8 MHz in Fig. 3.1.1-3. However, the excess loss above the plane-earth loss (due to diffraction effects) is much larger owing to the taller structures found in the area of these measurements. On the other hand, the path loss curves at 27 MHz and 446 MHz in Fig. 3.1.1-3 seem to indicate the presence of a diffraction path which is stronger than the other possible paths with the diffraction point being close to the transmit or receive location. The reason for the difference in the distance behavior between the path loss at 49.8 MHz and the path losses at 27 MHz and 446 MHz in Fig. 3.1.1-3 is that the transmit locations were not actually the same at all frequencies for this situation. As pointed out in Section 2, the measurements at 27 MHz and

446 MHz were made with the transmitter located in the middle of the street while the measurements at 49.8 MHz were made with the transmitter located on the sidewalk. By moving to the middle of the street, it is possible that one of the multiple diffraction paths is much less attenuated than the others resulting in a slower rate of attenuation with distance.

Another characteristic that can be observed from Figs. 3.1.1-1, 3.1.1-2, and 3.1.1-3 is that for a given transmitter/receiver location, the path loss increases with frequency. This effect may also be explained by the simple model described earlier. From Eqs. (3.1.1-7) and (3.1.1-10) we can see that the smaller the wavelength (higher frequency), the lower the received power. Equation (3.1.1-7) also shows that when the distance dependence varies between inverse third and fourth power laws, the path loss increases linearly with frequency. Thus, from the model, the difference in path loss at 27 MHz and 446 MHz should be in the order of 12.2 dB while the difference in path loss between 49.8 MHz and 446 MHz is around 9.5 dB. This type of distance dependence and frequency dependence is exhibited by the non-line-of-sight (diffraction) path curves of Fig. 3.1.1-2. Equation (3.1.1-10) shows that when the distance dependence varies between inverse distance and inverse squared power law the path loss increases with the cube of the frequency. However, it is difficult to assess from these two equations what the frequency dependence would be when the distance dependence varies between inverse squared and inverse third power law. The 27 MHz and 446 MHz curves of Fig. 3.1.1-3 exhibit distance dependence in this range and the difference in path loss is in the order of 16 dB. This is, as one might expect, somewhat in excess of that predicted by linear frequency dependence and somewhat less than that predicted by cubic frequency dependence.

Finally the curves of Fig. 3.1.1-1 did not exhibit the frequency dependence predicted by Eq. (3.1.1-7). However, the differences in path loss between 49.8 MHz and 446 MHz are very small for this case, which would indicate that there was little

3-19

diffraction loss (and therefore no frequency dependence)
along this path. This is not surprising, since both trans-
mitter and receiver were located on the same street.

3.1.1.2 Suburban Average Path Loss

The results of the path loss analysis for the suburban
street-to-street propagation measurements described in Section
2.3.1 are shown in Figures 3.1.1-5 and 3.1.1-6. The solid lines
represent the average path loss at the three test frequencies as
calculated from Eqs. (3.1-13) and (3.1-8). The dashed line de-
noted L_p in the plane-earth path loss (see Eq. 3.1.1-1) while
the dashed line denoted L_o is the free-space loss (Eq. 3.1.1-2)
at 446 MHz. The curves of Fig. 3.1.1-5 represent the path
loss for the case in which the transmit and receive locations
were both on the same street (Waltham Street, Lexington) while
the curves of Fig. 3.1.1-6 represent the path loss for the
case in which the transmit location was on Massachusetts Ave.
and the various receive locations were on Waltham Street.

The suburban path loss curves at 27 MHz and 49.8 MHz are
nearly parallel to the plane-earth loss in both cases, i.e., they
exhibit an approximate path loss rate with distance of 40 dB per
decade. In addition, the excess path loss is seen to increase
with frequency. The path loss at 446 MHz exhibits a loss rate
near 40 dB per decade for the case in which the transmitter and
receiver were located on the same street (Fig. 3.1.1-5) and a
loss rate just over 20 dB per decade for the non-line-of-sight
case (Fig. 3.1.1-6). Qualitatively the suburban path loss curves
are similar to the urban path loss curves. The reason the path
loss rate at 446 MHz differs from that at 49.8 MHz and 27 MHz is
that a two story ($\simeq$ 10-12 m) building situated in the proximity
of the transmitter was high enough to cause large shadow losses
in all but one of the four possible diffraction paths at 446 MHz
as illustrated in Fig. 3.1.1-4(b) resulting in a near inverse
square distance dependence. However since the wavelengths at
27 MHz (11 m) and 49.8 MHz ($\sim$6 m) were of the same order of mag-
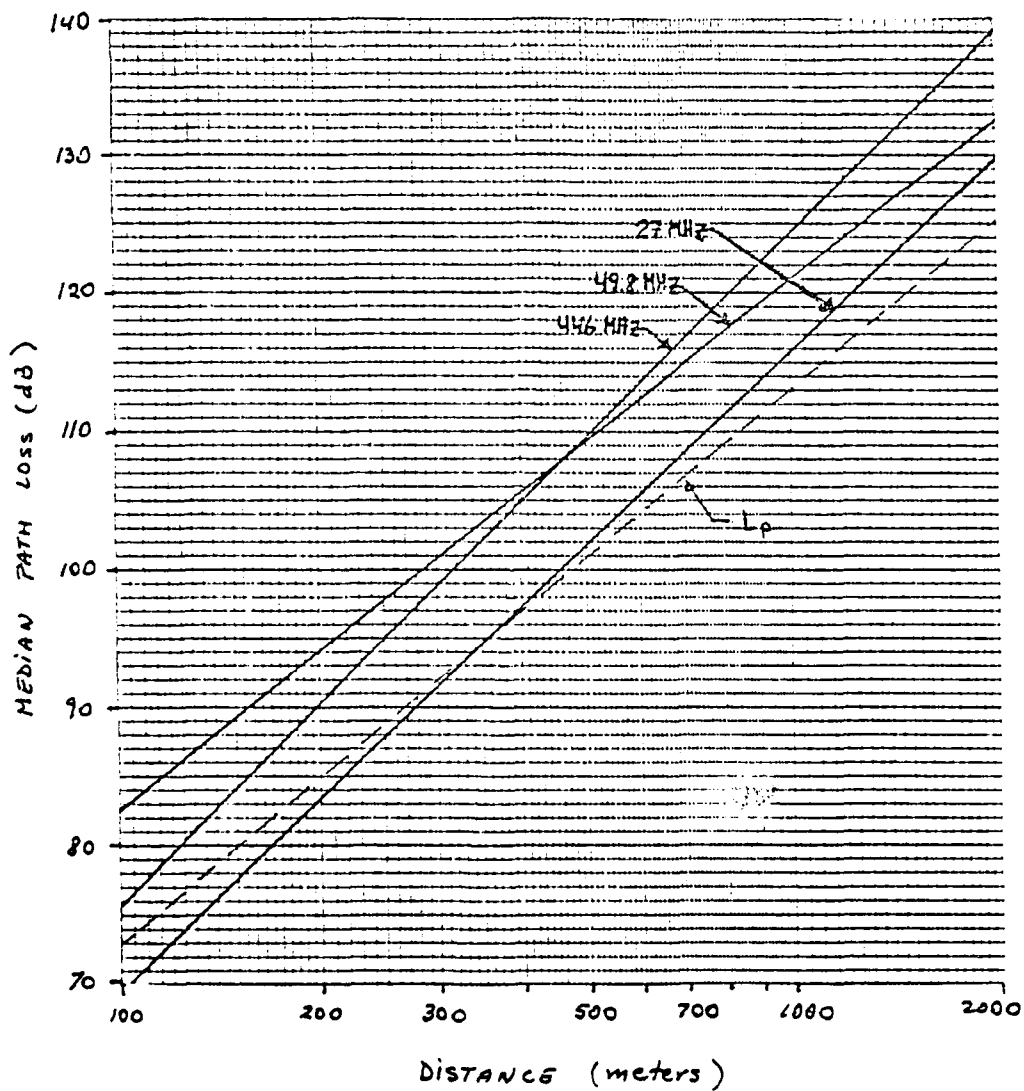
FIGURE 3.1.1-5   Median Path Loss Along a Suburban Street
(Waltham St., Lexington, MA)

3-21
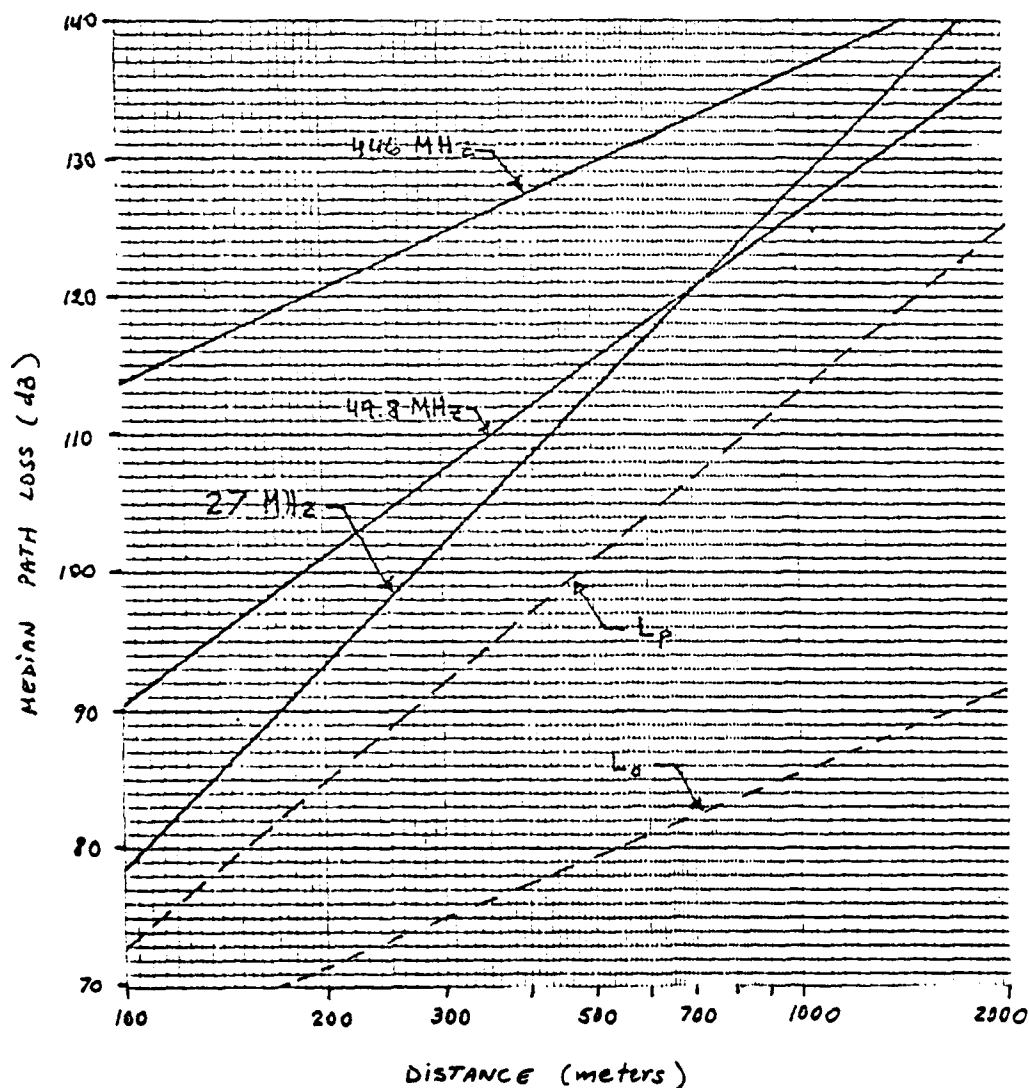
FIGURE 3.1.1-6   Median Path Loss for a Non-Line-of-Sight Suburban
Path (Transmit Location on Mass. Ave. and Receive
Location on Waltham St., Lexington, MA)

3-22

nitude as the building height, the shadow losses were sufficiently small on two or more of the four diffraction paths to result in an inverse fourth power distance dependence.

The difference in path loss at 27 MHz and 49.8 MHz is around 5 dB (at d = 1000 m) for the line-of-sight path and 4 dB (at d = 400 m) for the non-line-of-sight path. Both these values are slightly higher than the 3.7 dB predicted by Eq. (3.1.1-7). The path loss at 446 MHz is, however, 6 to 7 dB lower than that predicted by the same equation. The differences are not considered to be sufficiently different to imply a propagation mechanism other than that described by the simple model presented earlier.

Aside from these differences, the path losses in a suburban area appear to be in the same order (if not slightly higher) as the path losses in an urban area in all cases, other than the urban measurements at 49.8 MHz. In that case the transmit location was in the midst of high buildings, and the urban path losses far exceed (by about 20-30 dB) the losses in the other urban and suburban paths.

Comparing the path losses at 49.8 MHz at a distance of 500 meters, we see that

$$L \simeq \begin{cases} 104\text{-}106 \text{ dB}, & \text{urban paths that are surrounded by high buildings} \\ 135 \text{ dB} \quad , & \text{urban path amidst high buildings (transmit location on sidewalk)} \\ 109\text{-}113 \text{ dB}, & \text{suburban paths with low buildings and trees.} \end{cases}$$

These relative values are considered to be representative at lower VHF, i.e., 30-80 MHz. The reason the suburban path losses are higher than the losses for urban paths not surrounded by high buildings might be due to the presence of trees and the hilly nature of the suburban terrain.

A similar comparison of path losses at 446 MHz at a distance of 500 meters results in

$$L \approx \begin{cases} 109\text{-}116 \text{ dB,} & \text{urban paths not surrounded by high} \\ & \text{buildings} \\ 126 \text{ dB} \quad, & \text{urban path amidst high buildings} \\ & \text{(transmit location in middle of} \\ & \text{the street)} \\ 110 \text{ dB} \quad, & \text{suburban path (no immediate buildings)} \\ 129 \text{ dB} \quad, & \text{suburban path (buildings immediately} \\ & \text{in front).} \end{cases}$$

Thus, we see that at UHF even a two story suburban building tends to have the same effect as high buildings in an urban area. However, the lower increase in path loss in urban areas at UHF due to the presence of high buildings is more a result of the fact that the transmitter was in the middle of the street rather than on the sidewalk. Hence, if the transmitter had been in the middle of the street at 49.8 MHz also, the path loss might have been around 116 dB rather than 135 dB. The 20 dB difference is a measure of the improvement in signal-to-noise ratio one might expect by moving from a transmit (or receive) location close to a building to a more open area like the middle of the street. At UHF, this increase might be more in the order of 30 dB since shadow (diffraction) losses increase linearly with the frequency.

The distance and frequency dependence obtained from this analysis as well as the effects of the environment such as urban vs. suburban area, building height, proximity to building, and street orientation are used in Section 3.3 to extend the current data base in the literature.

3.1.2 Average Transmission Loss in Street-to-Building Propagation

Transmission loss curves obtained from Eqs. (3.1-13) and (3.1-8) are shown in Figs. 3.1.2-1 and 3.1.2-2 for the street-to-building propagation measurements. The solid curves represent

3-24
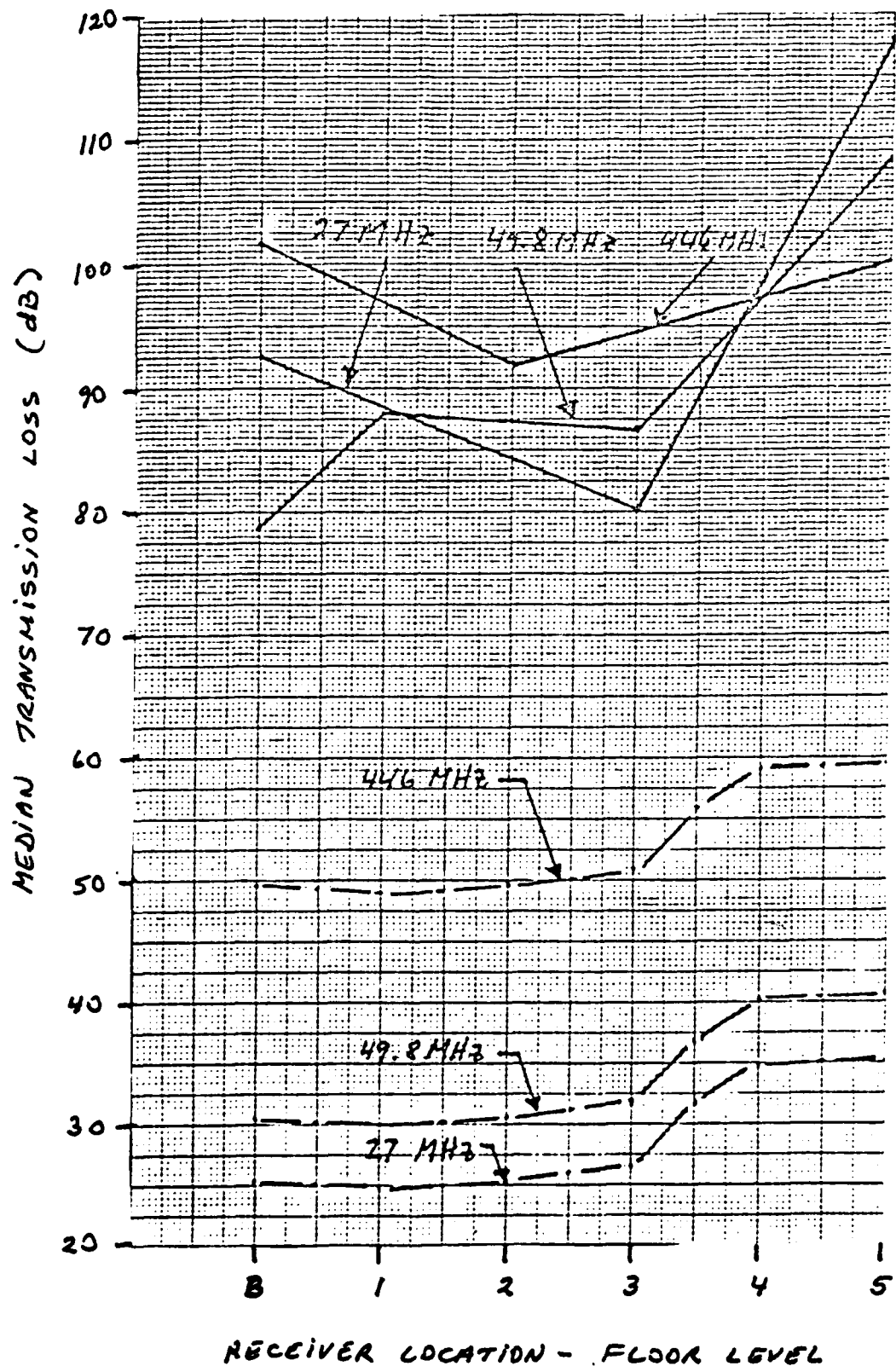
FIGURE 3.1.2-1 Median Transmission Loss as a Function of Height Inside Building in Street-to-Building Transmission
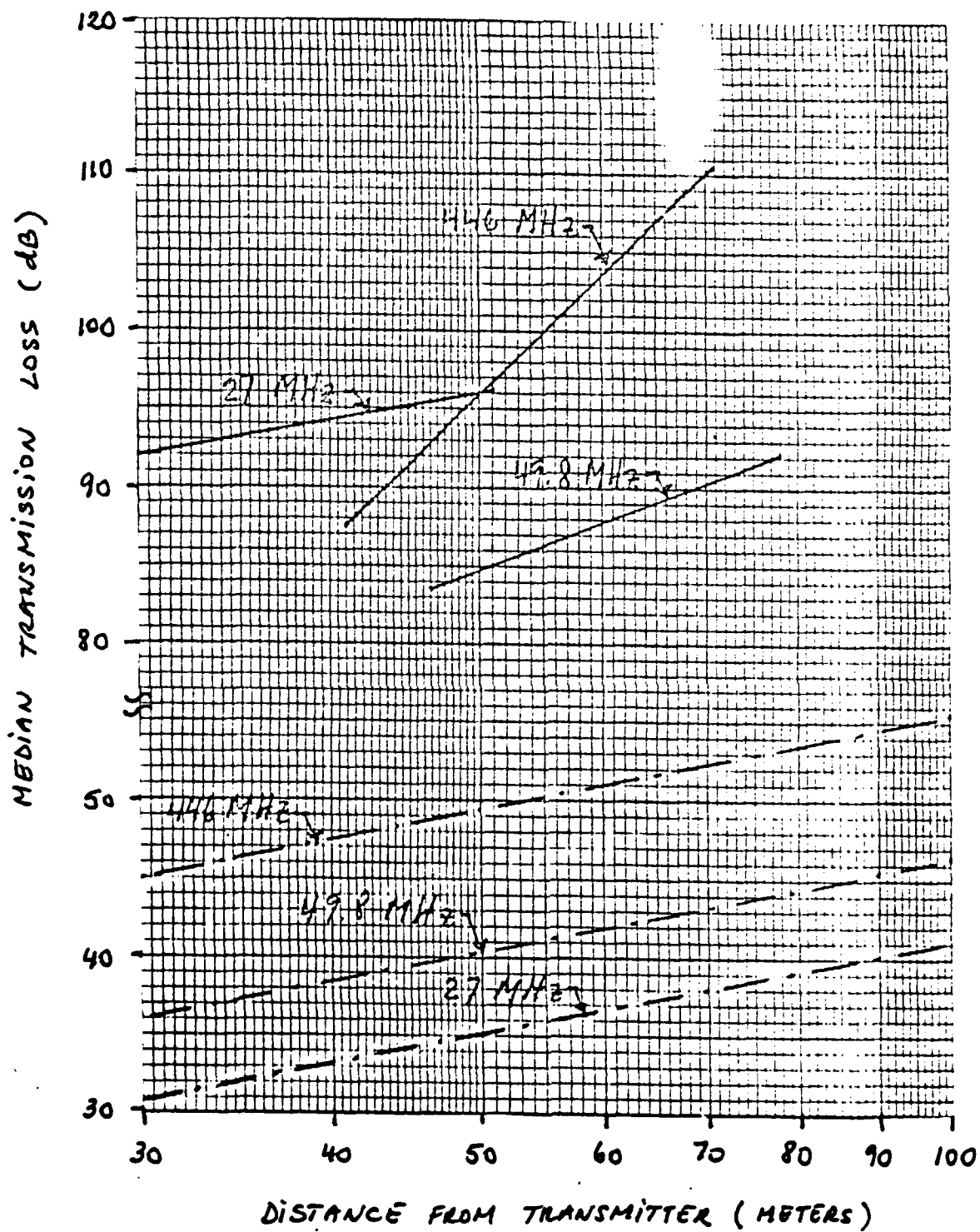
FIGURE 3.1.2-2   Median Transmission vs. Distance Inside
Building in Street-to-Building Transmission

3-26

the average transmission loss at the three test frequencies while the dashed lines represent the free-space loss, i.e., the power loss that would be incurred between a transmitter and a receiver located in free space with no obstacles in between. The difference between the average transmission loss and the free-space loss is defined as the building penetration loss, L_B. The average transmission loss as a function of receiver height (floor location) is shown in Fig. 3.1.2-1. The average transmission loss as a function of distance, i.e., location within a floor in the building, is shown in Fig. 3.1.2-2. It should be noted that these two types of measurements were made in two different buildings so that differences in the penetration losses are attributable to difference in the structural composition of the two buildings. The transmission loss measurements as a function of floor level were made in a reinforced concrete office building. The measurements of transmission loss as a function of position within a floor (measured in terms of distance from the transmitter) were made in a building whose outside walls were made of brick veneer cinder block, and whose inside consisted of a wooden frame with gypsum walls.

From Fig. 3.1.2-1 we see that the building penetration loss for a street-to-basement transmission is

$$
L_B = \begin{cases} 67.5 \text{ dB} & \text{at} & 27 \text{ MHz} \\ 58. \text{ dB} & \text{at} & 49.8 \text{ MHz} \\ 52. \text{ dB} & \text{at} & 446 \text{ MHz}. \end{cases} \tag{3.1.2-1}
$$

Thus, the 'basement' penetration loss is seen to decrease with frequency although the total average path loss (which includes the free-space loss) increases with frequency at frequencies above 50 MHz. This is due to the increase of the free-space loss with frequency.

Similarly the penetration losses to various other floors are also seen to decrease with frequency. However, no height gain is observed but rather the penetration losses varied randomly from

one floor to another. These variations are probably due to differences in the number of windows or the number of walls between transmitter and receiver from one floor to another. The range of values of the building penetration losses above the free-space losses are:

$$L_B = \begin{cases} 54 - 80 \text{ dB} & \text{at 27 MHz} \\ 54 - 68 \text{ dB} & \text{at 49.8 MHz} \\ 38 - 48 \text{ dB} & \text{at 446 MHz.} \end{cases} \qquad (3.1.2-2)$$

These numbers indicate that the variance of the median of the penetration loss, a well as the penetration loss itself, decrease with frequency.

The curves of Fig. 3.1.2-2 indicate the rate at which the penetration loss increases with distance within the building. The range of values of the penetration loss at various locations within the ground floor of a wooden frame building are:

$$L_B = \begin{cases} 61 \text{ dB} & \text{at 27 MHz} \\ 44 - 48 \text{ dB} & \text{at 49.8 MHz} \\ 40 - 58 \text{ dB} & \text{at 446 MHz} \end{cases} \qquad (3.1.2-3)$$

where the smallest value (at each frequency) corresponds to the penetration loss in that part of the building closest to the transmit site and the largest value in the penetration loss in that part of the building farthest from the transmit site.

From Eq. (3.1.2-3) we see that the penetration loss in that part of the building closest to the transmit site decreases with frequency. These values represent the loss due to absorption by the outer wall of the building (cinder block) and are fairly close to the penetration losses measured in the reinforced concrete building (Eq. 3.1.2-2). The values of the penetration losses in that part of the building farthest from the transmit site represent the loss due to absorption by the outer wall of the building as well as the inside walls. At 27 MHz, the penetration

loss is nearly identical everywhere in the building (61 dB) so that the inside walls (which are made out of gypsum) are not lossy at this frequency. At 49.8 MHz and 446 MHz the penetration losses are 4 dB and 18 dB greater at the farthest end of the building than at the end closest to the transmit site. This indicates that at these frequencies the inside walls are somewhat lossy. The losses due to the cinder block walls may be determined from the difference in the slopes of the average transmission loss (solid lines) and the slopes of the free space loss (dashed lines). At 27 MHz, the two slopes are equal so that there are no additional losses due to the inside walls. At 49.8 MHz, the losses due to the inside walls increase at 20 dB/decade as we move farther away from the transmit site. Hence, if the penetration losses one meter inside the building are a certain amount, the penetration losses 10 meters away from the outside wall closest to the transmit site are 20 dB greater. Note that since the free space losses increase at 20 dB/decade also, the total average transmission loss 10 meters away from the outside wall is 40 dB greater than at one meter from the outside wall. At 446 MHz, the penetration losses due to the inside walls increase at a much faster rate (86 dB/decade), the reason being that at this frequency the thickness of the walls (12.7 cm) is in the order of the wavelength ($\lambda \approx 70$ cm at 446 MHz). The total average transmission loss inside a building (including free space losses) at 446 MHz increases at a rate of 106 dB/decade as we move away from the transmit site, which explains the greater increase in the penetration losses at 446 MHz as indicated by Eq. (3.1.2-3). The variability, or equivalently the increase of the penetration losses along a floor, may also explain some of the variability of the penetration losses measured in different floors (Eq. (3.1.2-2)) since these measurements were made at random locations within each floor.

As a final comment, a penetration loss of 40 dB implies that when a communications link is set up such that one end of the link is inside a building, the maximum transmitter-receiver range for

which the signal-to-noise ratio is acceptable will be one order of
magnitude less than if both ends of the link were set up outside
the building.

3.1.3 Average Transmission Loss in Building-to-Building Propagation

The average transmission loss for the building-to-building
propagation measurements are shown in Figs. 3.1.3-1 and 3.1.3-2
as a function of the transmit site relative to the receive floor
level. The solid lines represent the average transmission losses
at the three test frequencies, while the dashed lines represent
the free-space losses at equivalent distances. The difference
between the average transmission loss and the free-space loss at
each frequency represents the building-to-building penetration
loss which is a measure of the losses introduced by the two
structures. The curves of Fig. 3.1.3-1 correspond to the average
transmission (and penetration) losses for a receive site R_1
located in a lobby at the end of the building closest to the
transmit site (see Fig. 2.3-3). The curves of Fig. 3.1.3-2
give the equivalent information for a receive site R_2 located
in a lobby in that part of the building farthest away from the
transmit site (refer to Fig. 2.3-3).

The average transmission (and penetration) losses exhibit
little height dependence in all cases except for the average
transmission loss at 27 MHz in the receive site R_2. In this
case, the height gain has a power law dependence so that the
transmission loss decreases at a rate of 12.8 dB/decade as the
height of the transmit site increases. The average transmission
losses at 49.8 MHz and 446 MHz in the same receive site (R_2) do
not exhibit any height dependence at all.

By comparing the penetration losses at the two receive
sites, we can get an estimate of the variations of the average
penetration loss within a building. Thus, the range of values
of the average penetration loss in receive site R_1 are:
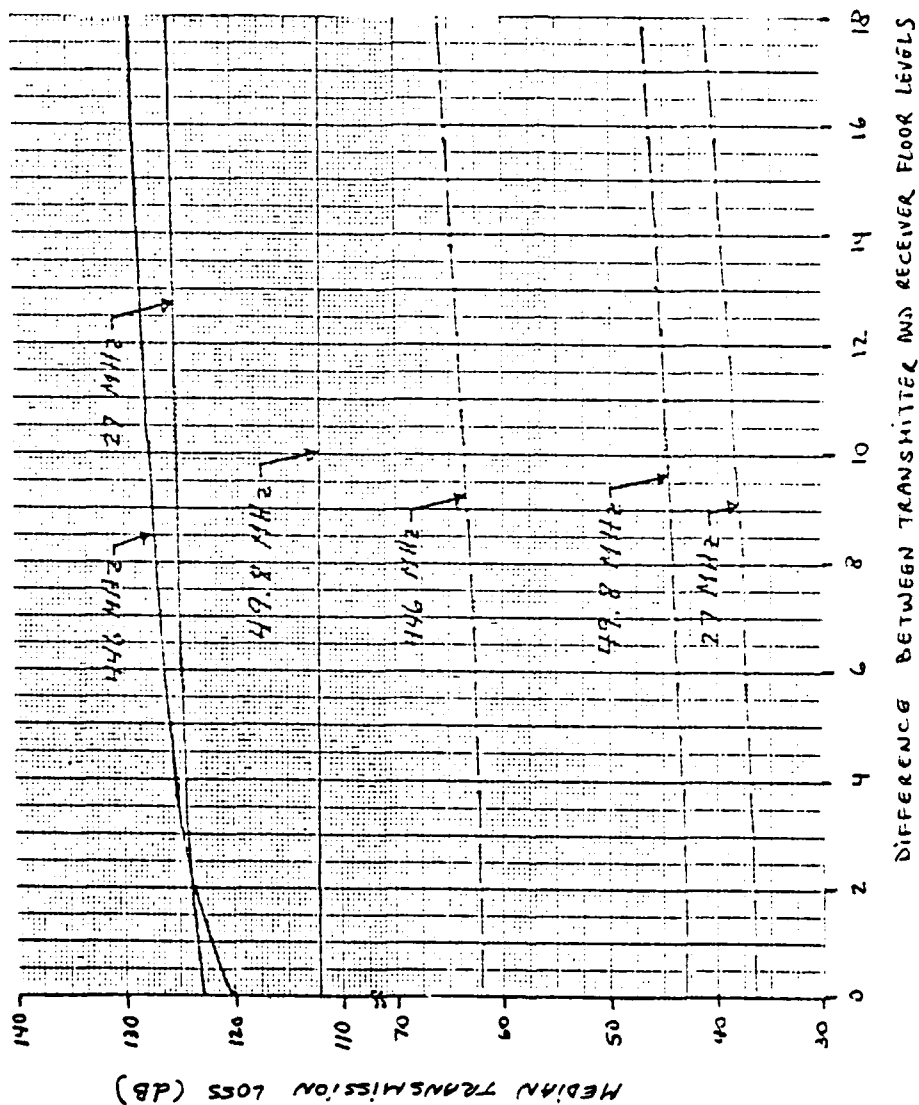
FIGURE 3.1.3-1 Median Transmission Loss as a Function of
Transmit Site Relative to the Receive Floor
Level (Receive Site in Front Part of Building)
in Building-to-Building Transmission
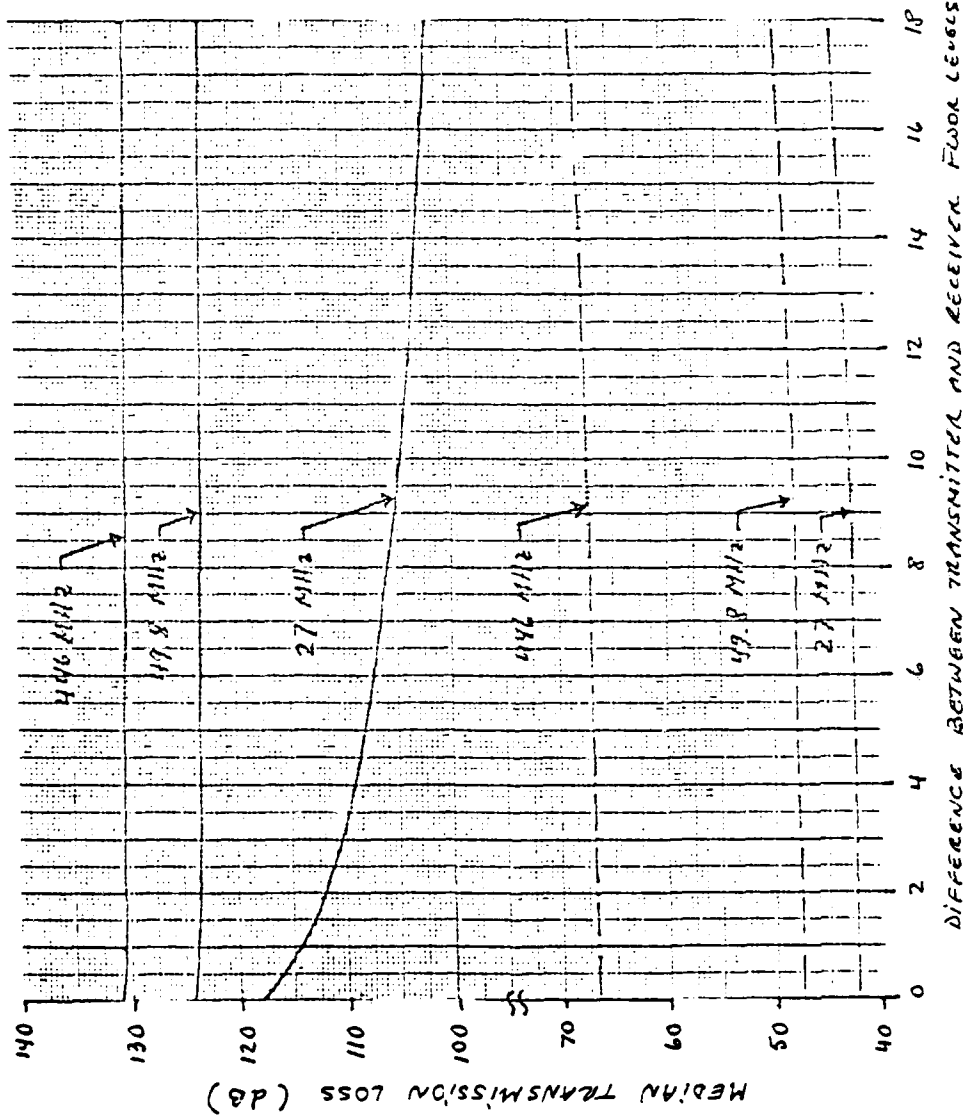
FIGURE 3.1.3-2 Median Transmission Loss as a Function of Transmit Site Relative to the Receiver Floor Level (Receive Site in Rear of Building) in Building-to-Building Transmission

$$@R_1 \quad L_{BB} = \begin{cases} 84 - 86 \text{ dB} & \text{at } 27 \text{ MHz} \\ 65 - 69 \text{ dB} & \text{at } 49.8 \text{ MHz} \\ 58 - 63 \text{ dB} & \text{at } 446 \text{ MHz} \end{cases} \quad (3.1.3\text{-}1)$$

while the range of values in receive site R_2 are:

$$@R_2 \quad L_{BB} = \begin{cases} 57.5 - 75.5 \text{ dB} & \text{at } 27 \text{ MHz} \\ 73 - 77 \quad \text{ dB} & \text{at } 49.8 \text{ MHz} \\ 61 - 64.5 \quad \text{dB} & \text{at } 446 \text{ MHz.} \end{cases} \quad (3.1.3\text{-}2)$$

We can see from these values that the penetration losses in site R_2 are higher than those in site R_1 at 49.8 MHz and 446 MHz. This is not surprising since receive site R_2 was further away from the transmit site so that the additional losses account for the effects of the interior of the building. However, the penetration losses at 27 MHz are lower in receive site R_2. In addition, we can also see from Eq. (3.1.3-1) that the penetration losses decreased with frequency in site R_1. This trend is consistent with that obtained from the street-to-building propagation measurements. The losses in receive site R_2 are lower at 27 MHz and higher at 49.8 MHz.

Finally, if we compare the building-to-building penetration loss with the street-to-building penetration loss we can determine the effects of the additional building. Thus, if we subtract the penetration losses of Eq. (3.1.2-2) from those of Eq. (3.1.3-1), we get,

$$L_{BB} - L_B = \begin{cases} 4 - 32 \text{ dB} & \text{at } 27 \text{ MHz} \\ 1 - 15 \text{ dB} & \text{at } 49.8 \text{ MHz} \\ 10 - 25 \text{ dB} & \text{at } 446 \text{ MHz.} \end{cases} \quad (3.1.3\text{-}3)$$

Thus, we see that the losses due to penetration of the additional building are not as large as the losses due to a single building. This small increase reflects the fact that the transmit site in the high rise building was near a window since it was not possible to make contact with the receive site from a location further

inside the high rise. Thus, we conclude that the penetration
losses per building are in the order of those obtained from the
street-to-building measurements (Eq. 3.1.2-2)
(or transmit) site is well inside the building. However, when
the receive (or transmit) site is near or at a window facing the
transmit (or receive) location, the penetration losses per building
are more closely given by those of Eq. (3.1.3-3).

3.1.4 Average Transmission Loss in Intrabuilding Propagation

The types of intrabuilding measurements made can be
divided into four groups: a) transmission along corridors;
b) transmission between above ground floors; c) transmission
between a basement and above ground floors; and d) transmission
in stairwells and along elevator shafts. Hence, we will con-
sider the average transmission loss for each of these cases
separately.

3.1.4.1 Average Transmission Loss Along Corridors

Transmission loss curves for the intrabuilding
measurements in various corridors are shown in Figs. 3.1.4-1,
3.1.4-2, and 3.1.4-3 as a function of distance along the
corridors. The curves of Figs. 3.1.4-1 and 3.1.4-2 represent
the transmission loss at the three test frequencies in a straight
and a winding corridor in an office building with concrete walls.
The curves of Fig. 3.1.4-3 represent, on the other hand, the
transmission loss at 27 MHz in four different corridors: A
and B correspond to the transmission loss in two corridors
with gypsum walls while C and D correspond to the transmission
loss in a winding and a straight corridor with cinder block
walls, respectively.

The curves of Figs. 3.1.4-1 and 3.1.4-2 show that the
transmission loss in dB increases linearly with distance. This
indicates that the distance dependence of the average transmission
loss is exponential (as defined in Eq. 3.1-3) which is charac-
teristic of a lossy waveguide type of propagation mechanism.
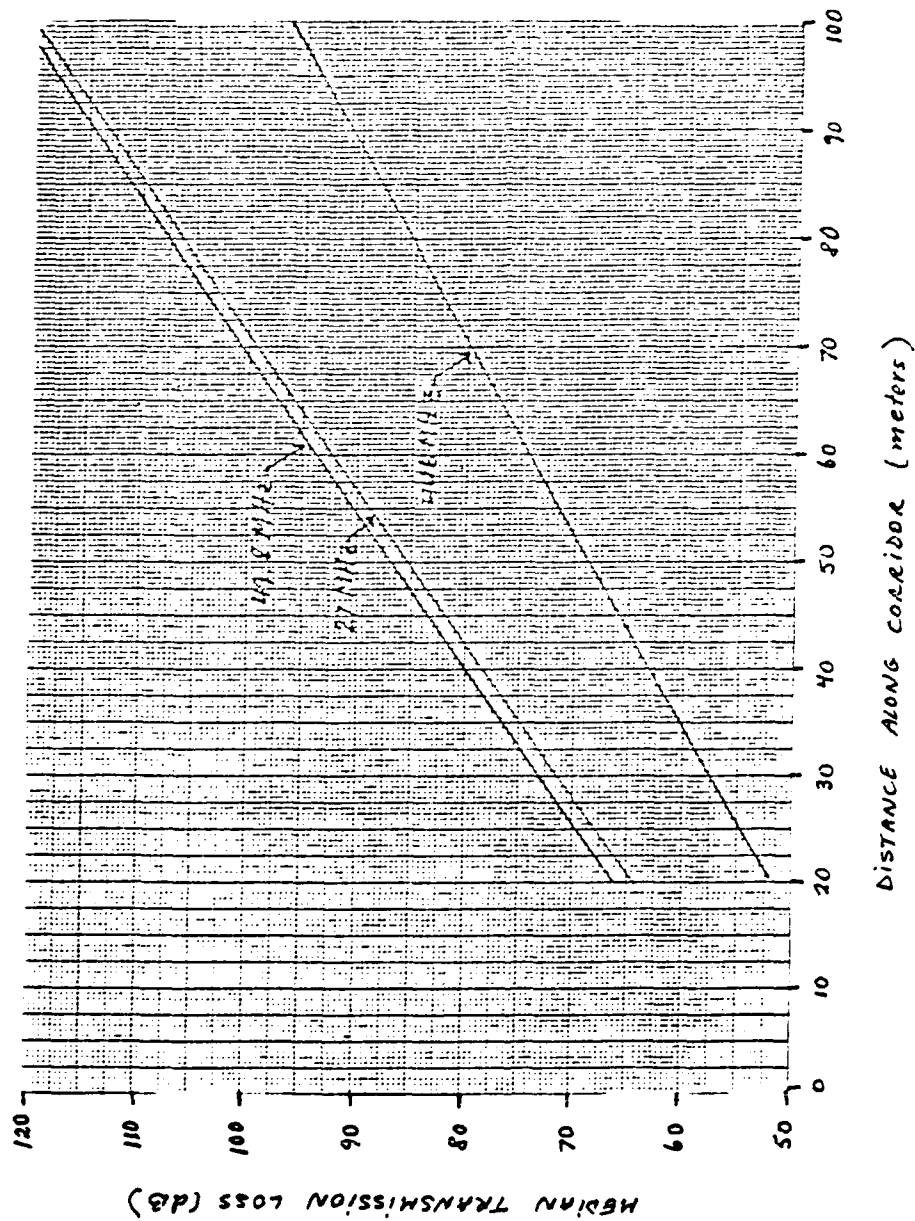
FIGURE 3.1.4-1   Median Transmission Loss Along a Straight Corridor
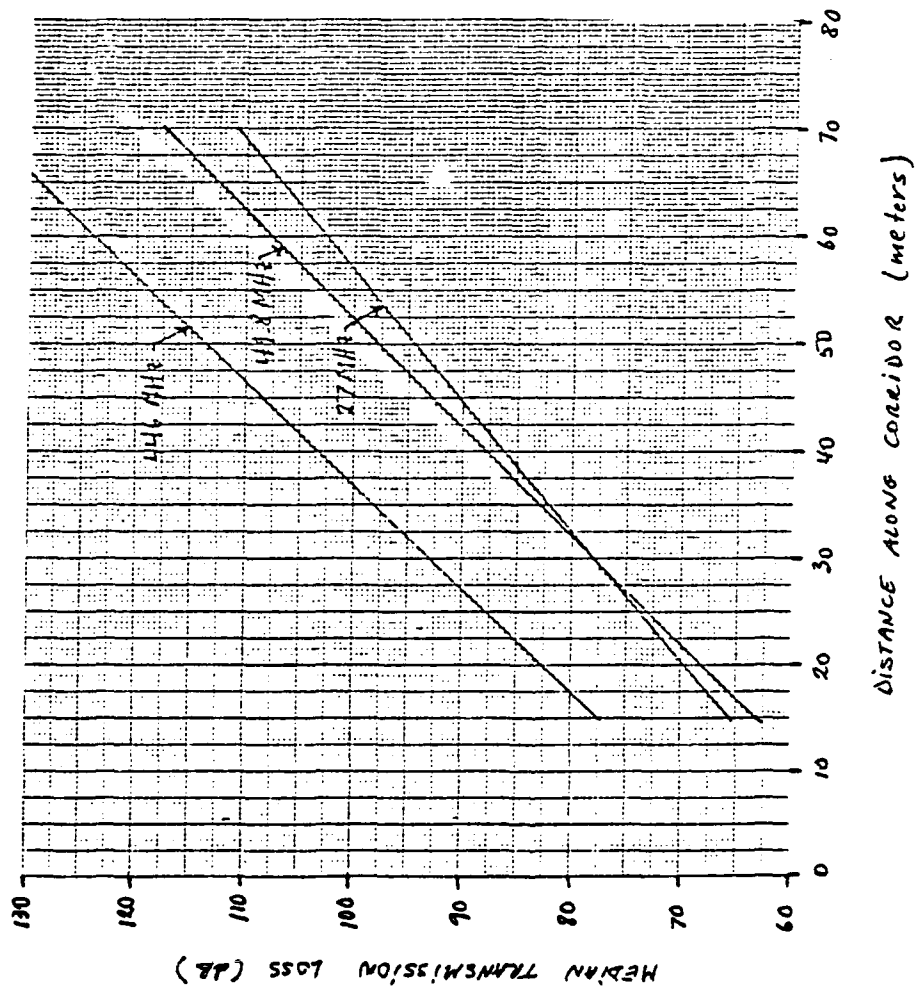
FIGURE 3.1.4-2   Median Transmission Loss Along a Winding Corridor
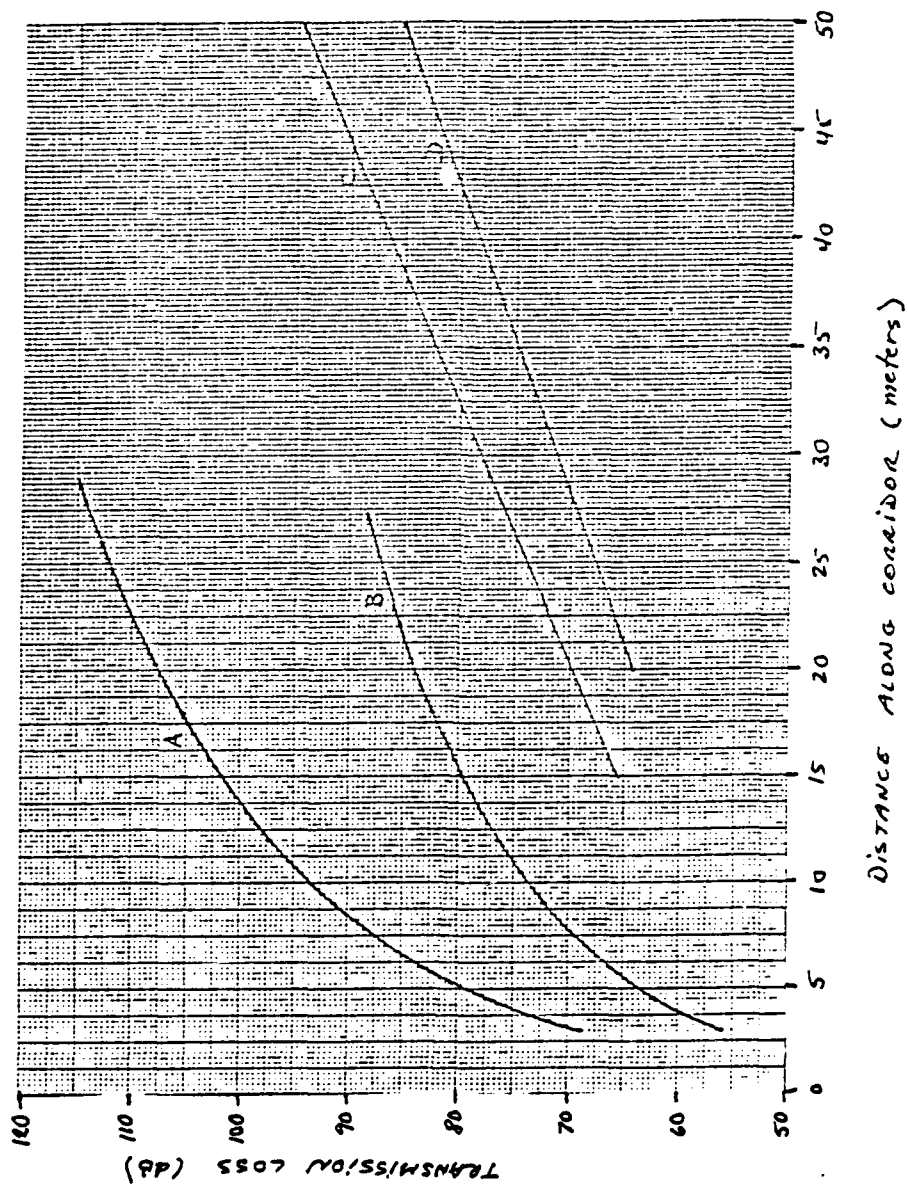
FIGURE 3.1.4-3 Median Transmission Loss Along Various Corridors
at 27 MHz

The losses are due to the finite conductivity of the walls of the 'waveguide' (i.e., corridor). The slope of the curves is defined as the loss rate and is seen to be nearly equal for the three test frequencies but varies from one corridor to another. This suggests that the loss rate is determined by the geometry of the corridor. In addition, the transmission loss varies from one frequency to another which indicates that the loss is also dependent on the material composition of the walls.

Since the average transmission loss varies linearly with distance along the corridor, it can be written as

$$L(x) = L_o + SX \qquad (3.1.4-1)$$

where S is the transmission loss rate which varies from one corridor to another and from one frequency to another. From Figs. 3.1.4-1 we see that for the straight corridor

$$S = \begin{cases} 6.9 \text{ dB/10 meters} & \text{at 27 MHz} \\ 6.9 \text{ dB/10 meters} & \text{at 49.8 MHz} \\ 5.4 \text{ dB/10 meters} & \text{at 446 MHz} \end{cases} \qquad (3.1.4-2)$$

and,

$$L_o = \begin{cases} 50.7 \text{ dB} & \text{at 27 MHz} \\ 52.5 \text{ dB} & \text{at 49.8 MHz} \\ 41.0 \text{ dB} & \text{at 446 MHz} \end{cases} \qquad (3.1.4-3)$$

which shows that both the transmission loss and loss rate are higher at VHF (27 and 49.8 MHz) than at UHF (446 MHz). This is most likely due to the fact that the dimensions of the corridor (~ 2m by 3m) are in the order of a half-wavelength at the VHF frequencies ($\lambda \simeq 11$ m at 27 MHz) but greater than the wavelength at the UHF frequencies. Similarly, from Fig. 3.1.4-2 we see that for the winding corridor,

$$S = \begin{cases} 8.3 \text{ dB/10 meters} & \text{at 27 MHz} \\ 9.8 \text{ dB/10 meters} & \text{at 49.8 MHz} \\ 10.2 \text{ dB/10 meters} & \text{at 446 MHz} \end{cases} \quad (3.1.4-4)$$

and

$$L_o = \begin{cases} 50.7 \text{ dB} & \text{at 27 MHz} \\ 52.5 \text{ dB} & \text{at 49.8 MHz} \\ 41.0 \text{ dB} & \text{at 446 MHz} \end{cases} \quad (3.1.4-5)$$

which shows that the loss rate is greater for a winding corridor than a straight one as expected. Furthermore, if we compare the average transmission losses at a distance of 20 meters we can determine the losses due to a single turn (at approximately 10 meters) in a corridor. Thus, if L_W and L_S are the losses at a distance of 20 meters in the winding and the straight corridors, then,

$$L_W - L_S = \begin{cases} 5.6 \text{ dB} & \text{at 27 MHz} \\ 1.8 \text{ dB} & \text{at 49.8 MHz} \\ 30.7 \text{ dB} & \text{at 446 MHz} \end{cases} \quad (3.1.4-6)$$

which shows that the increase in the losses due to a bend in the corridor is particularly significant at UHF (446 MHz) and is in the order of 30 dB compared to 2 to 5 dB at lower VHF (30-50 MHz).

The effects of the material composition of the walls can be determined from Fig. 3.1.4-3 which shows the average transmission loss at 27 MHz for two corridors with gypsum walls (A and B) and two corridors with cinder block walls covered with plaster (C and D). We see that at a distance of 20 meters, the transmission losses of the four corridors are:

$$L = \begin{cases} 108 \text{ dB} & \text{Corridor A} \\ 84 \text{ dB} & \text{Corridor B} \\ 70 \text{ dB} & \text{Corridor C} \\ 64 \text{ dB} & \text{Corridor D} \end{cases} \quad (3.1.4.7)$$

where corridors B and D are straight and corridors A and C have at least one bend (the dimensions are given in Section 2.6.1 and

3-39

are approximately of the same order). Thus, we can see that the losses are much greater in the corridor with gypsum walls due to the lower conductivity (hence, easier to penetrate) of this material. The loss rate (slope) is nearly equal for the four corridors at distances greater than the wavelength.

3.1.4.2 Average Transmission Loss Between Above Ground Floors

Transmission loss curves for the transmission measurements between above ground floors are shown in Figure 3.1.4-4 as a function of the number of floors between the transmit and receive locations. The average transmission loss in dB is seen to increase linearly with the log of the distance (number of floors) which indicates that the received signal is inversely proportional to a power of the number of floors transmitted through. The power is determined by the slope of the transmission loss curves. Thus we can write the average transmission loss in dB as

$$L = L_o + S \log_{10} N \qquad (3.1.4-8)$$

where N is the number of floors transmitted through, L_o is the loss due to transmission through one floor and S is the transmission loss rate in dB/decade. From Fig. 3.1.4-4, we see that

$$L_o = \begin{cases} 83 \text{ dB} & \text{at 27 and 49.8 MHz} \\ 88 \text{ dB} & \text{at 446 MHz} \end{cases} \qquad (3.1.4-9)$$

and,

$$S = \begin{cases} 51.3 \text{ dB/decade} & \text{at 27 MHz} \\ 25.5 \text{ dB/decade} & \text{at 49.8 MHz} \\ 30.2 \text{ dB/decade} & \text{at 446 MHz} \end{cases} \qquad (3.1.4-10)$$

where a decade is a ten-fold increase in the number of floors transmitted through. These values indicate that the losses due to transmission through one floor are 5 dB greater at UHF than VHF. However, as the number of floors increase, the transmission
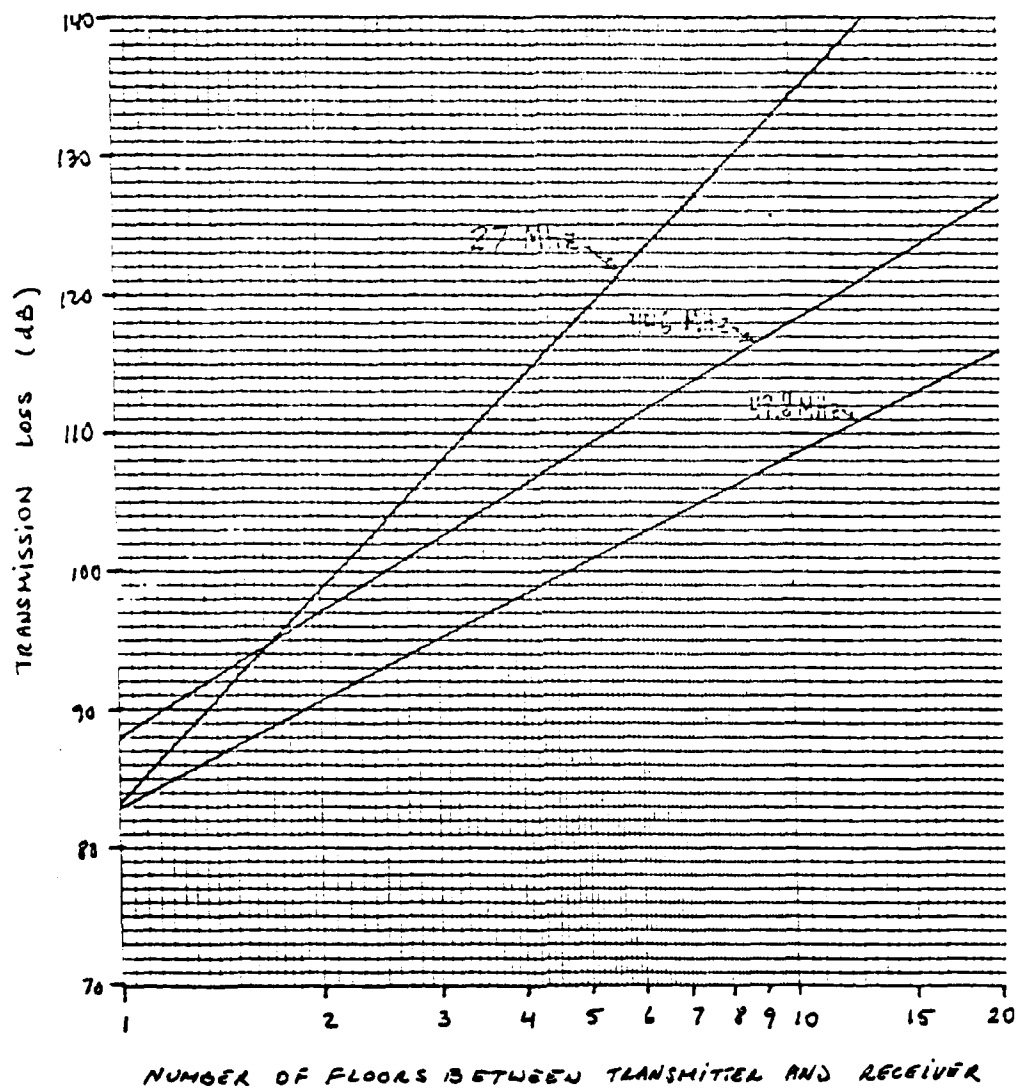
FIGURE 3.1.4-4   Median Transmission Loss for Transmission
                 Between Above Ground Floors

loss increases more rapidly at 27 MHz. This is probably due to
the fact that the distance between floors (height of the ceiling
~ 5 meters) is in the order of a half-wavelength at 27 MHz
($\lambda \simeq 11$ meters). As the frequency increases, the distance
between floors becomes greater than a half-wavelength resulting
in smaller losses at each ceiling (and hence a lower loss rate).
However, as the frequency increases further, the wavelength be-
comes in the order of the thickness of the ceiling (~1-2 feet)
resulting in additional losses at every ceiling and an increase
in the loss rate. It is probably for this reason that the loss
rate at 446 MHz is greater than at 49.8 MHz.

3.1.4.3 Average Transmission Loss Between Above Ground Floors and Basement

Transmission loss curves for the transmission
measurements between above ground floors and the basement are
shown in Fig. 3.1.4-5 as a function of the number of floors
between the transmit and receive locations. As in the previous
case, the transmission loss in dB increases linearly with the
log of the distance (number of floors) between the transmit and
receive locations. Thus we may also express the average trans-
mission loss in dB as in Eq. (3.1.4-8). From Figure 3.1.4-5, we
see that

$$L_o = \begin{cases} 77 \text{ dB} & \text{at } 27 \text{ MHz} \\ 83 \text{ dB} & \text{at } 49.8 \text{ MHz} \\ 82 \text{ dB} & \text{at } 446 \text{ MHz} \end{cases} \qquad (3.1.4\text{-}11)$$

and,

$$S = \begin{cases} 56 \text{ dB/decade} & \text{at } 27 \text{ MHz} \\ 44.5 \text{ dB/decade} & \text{at } 49.8 \text{ MHz} \\ 50 \text{ dB/decade} & \text{at } 446 \text{ MHz} \end{cases} \qquad (3.1.4\text{-}12)$$

from which we can see that the average transmission loss from the
first floor to the basement (L_o) is slightly lower than the
transmission loss through one above ground floor (Eq. 3.1.4-9).

3-42
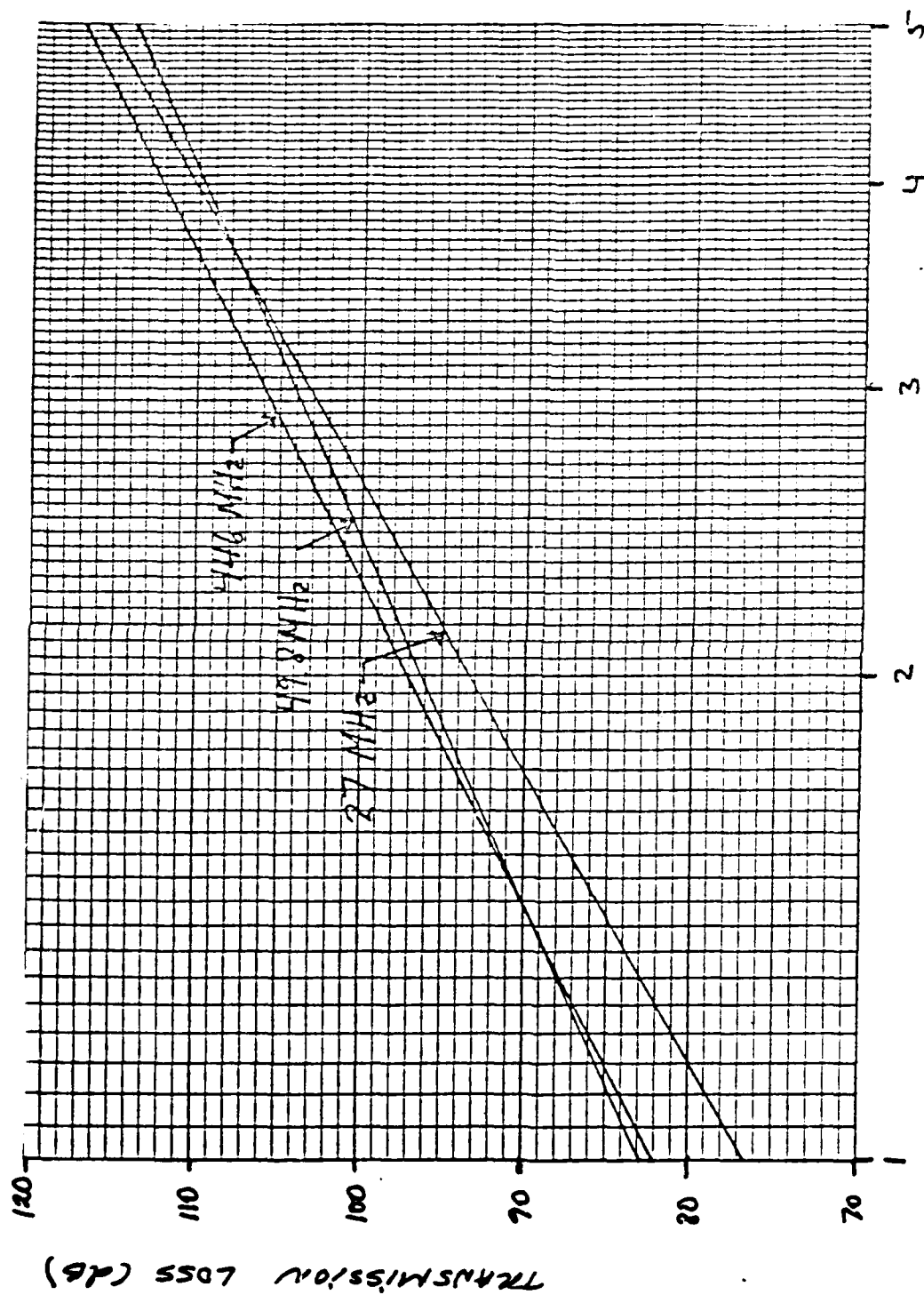
FIGURE 3.1.4-5   Average Transmission Loss for Transmission Between Above-Ground Floors and Basement

This could be attributed to the fact that the basement has a much higher ceiling than the above ground floors. On the other hand, the loss rate (S) is higher for above ground floor-to-basement transmission than for transmission between above ground floors. The increase in loss rate for above ground floor-to-basement transmission with respect to the loss rate for transmission between above ground floors is

$$\Delta S = \begin{cases} 4.7 \text{ dB/decade} & \text{at } 27 \text{ MHz} \\ 19 \text{ dB/decade} & \text{at } 49.8 \text{ MHz} \\ 19.8 \text{ dB/decade} & \text{at } 446 \text{ MHz} \end{cases} \qquad (3.1.4\text{-}13)$$

which shows that the increase in loss rate is particularly significant at the higher frequencies although the actual loss rate is still higher at 27 MHz for reasons previously indicated.

3.1.4.4 <u>Average Transmission Loss in Stairwells and Near</u>
          <u>Elevator Shafts</u>

Transmission loss curves for the transmission measurements in a stairwell and near elevator shafts are shown in Figs. 3.1.4-6 and 3.1.4-7, respectively, as a function of the number of floors between the transmit and receive locations. The average transmission loss in dB in a stairwell is seen to vary linearly with distance (number of floors) at all three frequencies. This implies that the loss can be expressed as in the previous two situations by means of Eq. (3.1.4-8). From Fig. 3.1.4-6 we see that in a stairwell,

$$L_0 = \begin{cases} 40 \text{ dB} & \text{at } 27 \text{ MHz} \\ 45.6 \text{ dB} & \text{at } 49.8 \text{ MHz} \\ 59.4 \text{ dB} & \text{at } 446 \text{ MHz} \end{cases} \qquad (3.1.4\text{-}14)$$

and,

$$S = \begin{cases} 60 \text{ dB/decade} & \text{at } 27 \text{ MHz} \\ 27.5 \text{ dB/decade} & \text{at } 49.8 \text{ MHz} \\ 38 \text{ dB/decade} & \text{at } 446 \text{ MHz.} \end{cases} \qquad (3.1.4\text{-}15)$$

3-44
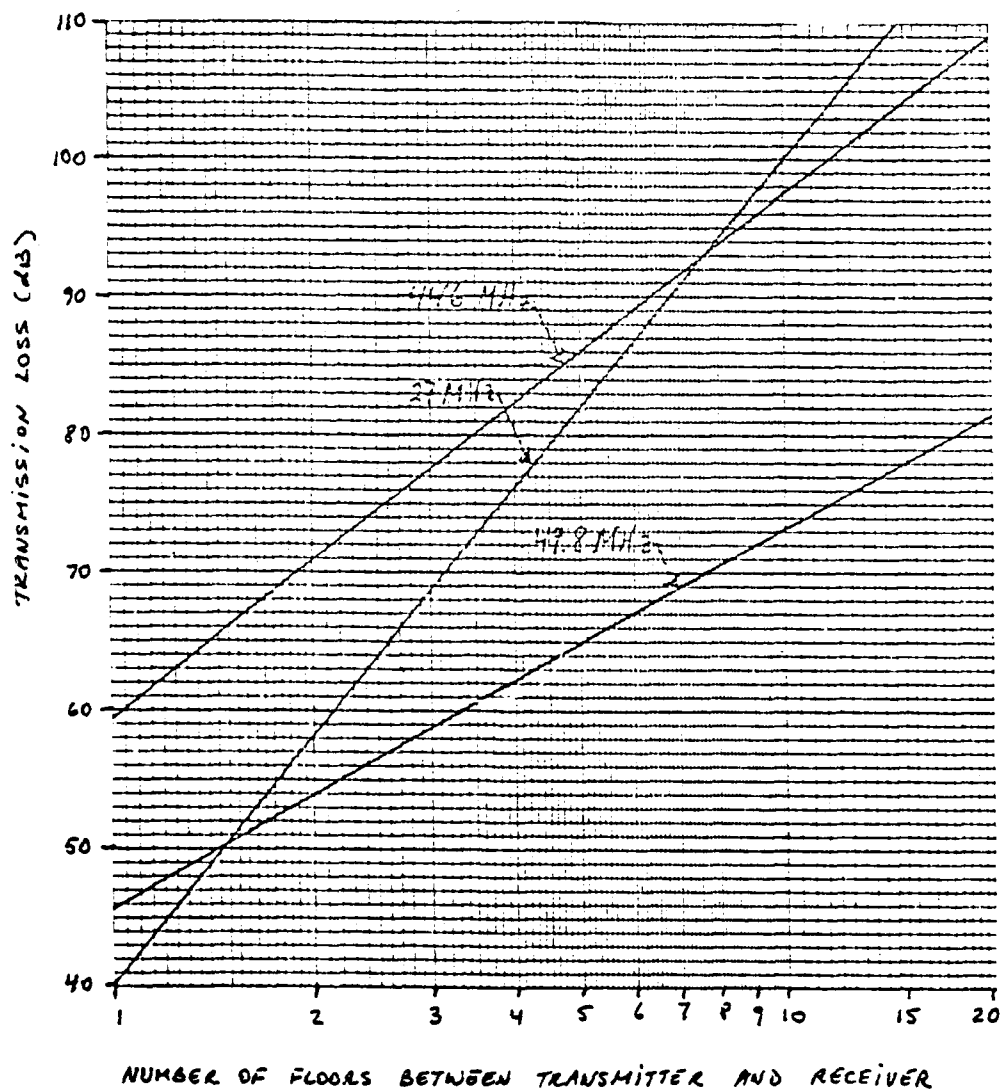
FIGURE 3.1.4-6 Median Transmission Loss for Transmission
in a Stairwell
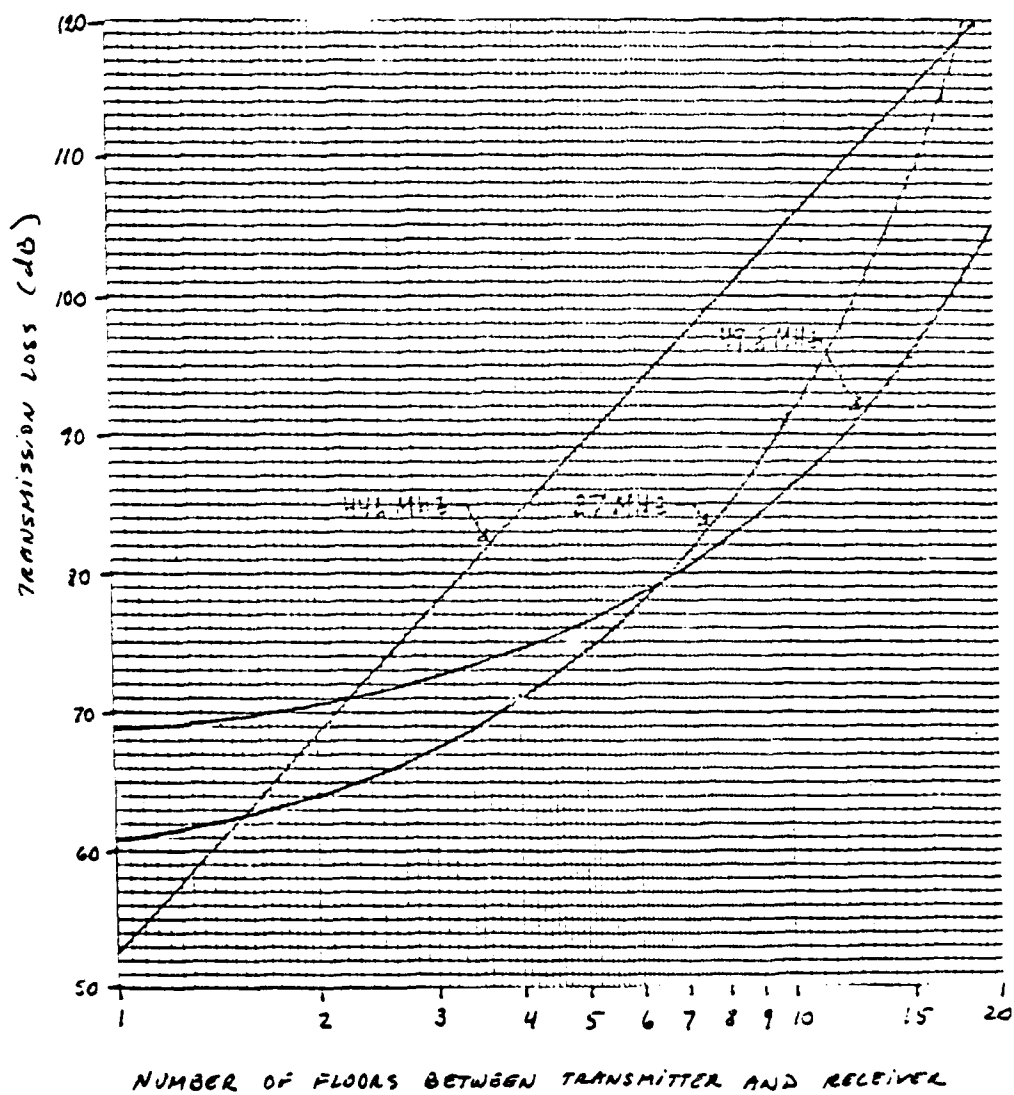
FIGURE 3.1.4-7   Median Transmission Loss for Transmissions
Near Elevator Shafts

AD-A080 486   SIGNATRON INC LEXINGTON MASS   F/G 17/2.1
                COMMUNICATIONS DATA BASE ANALYSIS FOR MILITARY OPERATIONS IN A --ETC(U)
                AUG 79 L EHRMAN, A MALAGA, F ZIOLKOWSKI   DAAG29-77-C-0020
UNCLASSIFIED   A-223-F   ARO-15068.1-A-EL   NL

3··4
AD
A080486
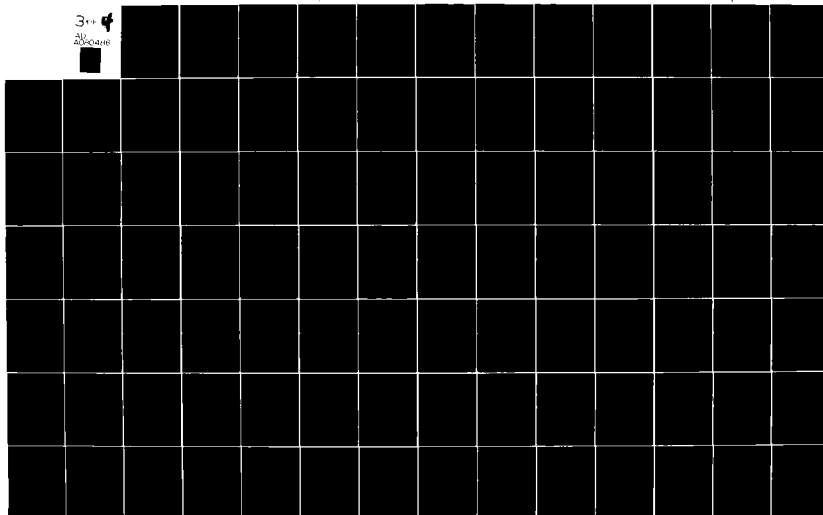
Thus, the loss due to transmission through one floor (L_o) is much
lower when both transmitter and receiver are in a stairwell (by
a factor of a half at VHF and two thirds at UHF). However, the
loss rate (S) in a stairwell is higher than when both trans-
mitter and receiver are inside the building away from the stair-
well. The reason for the higher loss rate in a stairwell
especially at 27 MHz is that the cross-sectional dimensions of
the stairwell are smaller than the length and width of the
floors. The increase in the loss rate in a stairwell with
respect to the loss rate in the floor-to-floor transmissions
is

$$\Delta S = \begin{cases} 8.7 \text{ dB} & \text{at 27 MHz} \\ 2 \text{ dB} & \text{at 49.8 MHz} \\ 8.2 \text{ dB} & \text{at 446 MHz.} \end{cases} \qquad (3.1.4\text{-}16)$$

It should be noted, however, that the losses in a stairwell are
still far less than the losses in the floor-to-floor trans-
missions and do not become comparable until the transmission
distance is well in excess of 50 floors.

The transmission loss (in dB) at VHF when both trans-
mitter and receiver are located near elevator shafts is seen to
vary linearly with the number of floors separating the trans-
mitter and receiver (or exponentially with the log N) while at
UHF it varies with the log of the distance. The reason for this
fundamental difference in the distance dependence is that at VHF
the dimensions of the elevator shaft are much smaller than the
wavelength so that the elevator shaft acts as an undersized
waveguide. Thus, the propagating signal decays exponentially
(linearly in dB). At UHF, however, the dimensions of the
elevator shaft are greater than the wavelength so that the
elevator shaft affects the signal in the same manner as a stair-
well.

The transmission loss at 446 MHz may again be represented by Eq. (3.1.4-8) with

$$L_o = 52. \text{ dB}$$
$$S = 52.6 \text{ dB/decade} \tag{3.1.4-17}$$

which shows that the loss at 446 MHz due to transmission through one floor (L_o) is smaller near elevator shafts than in a stairwell and much smaller than when there are no elevator shafts or stairwells. However, the loss rate is much greater owing to the smaller dimensions of the elevator shafts.

At VHF, the transmission loss near elevator shafts may be expressed as,

$$L = L_S + SN \tag{3.1.4-18}$$

where S is the loss rate in dB/floor, N is the number of floors, and $L_S + S = L_o$ is the transmission loss through one floor. From Fig. 3.1.4-7, we see that

$$L_o = \begin{cases} 61 \text{ dB} & \text{at 27 MHz} \\ 69 \text{ dB} & \text{at 49.8 MHz} \end{cases} \tag{3.1.4-18}$$

and

$$S = \begin{cases} 3.4 \text{ dB/floor} & \text{at 27 MHz} \\ 4.3 \text{ dB/floor} & \text{at 49.8 MHz} \end{cases} \tag{3.1.4-19}$$

which shows that both the loss rate and loss due to transmission through one floor increase with frequency.

Although the loss rate near elevator shafts is greater than the floor-to-floor transmission loss rate (Eq. 3.1.4-10), the average transmission loss near elevator shafts is, up to transmissions through 20 floors, still well below both the transmission loss between above ground floors and above ground floors to basement.

3.2   Correlation Analysis

In this section, we obtain estimates of the correlation between the data obtained with diversity antennas. The types of diversity reception investigated were field diversity at 27 MHz and 49.8 MHz and space diversity at 49.8 MHz and 446 MHz. The correlation coefficient for a narrow band Gaussian process (which is the model of the received signal in an urban or suburban environment) is a complex number of magnitude $|r|$ and phase Θ. The measured data were the received power, a real number. Thus, we can only determine the real correlation coefficient, ρ, between the envelopes (or amplitudes) of the two received signals. However, ρ is approximately equal to the square of the correlation between the two complex signals (amplitude and phase) defined as r in the introduction [e.g., Jakes, 1974]. The exact and $\rho \approx r^2$ approximations are plotted in Figure 3.2-1.

The envelope correlation, ρ, of two random variables, x and y, is similar to that defined in Eq. (3.0-4) where x and y now represent only the amplitude of the two received signals. When a sufficiently large number of samples of each random variable is available, the ensemble averaging may be replaced by an average over the set of samples $\{x_i\}$ and $\{y_i\}$. Thus, if we define

$$\text{cov}(x,y) = \frac{1}{N} \sum_{i=1}^{N} x_i y_i - \left(\frac{1}{N} \sum x_i \right)\left(\frac{1}{N} \sum y_i \right) \qquad (3.2\text{-}1)$$

$$\text{var}(x) = \frac{1}{N} \sum_{i=1}^{N} x_i^2 - \left(\frac{1}{N} \sum_{i=1}^{N} x_i \right)^2 \qquad (3.2\text{-}2)$$

$$\text{var}(y) = \frac{1}{N} \sum_{i=1}^{N} y_i^2 - \left(\frac{1}{N} \sum_{i=1}^{N} y_i \right)^2 \qquad (3.2\text{-}3)$$
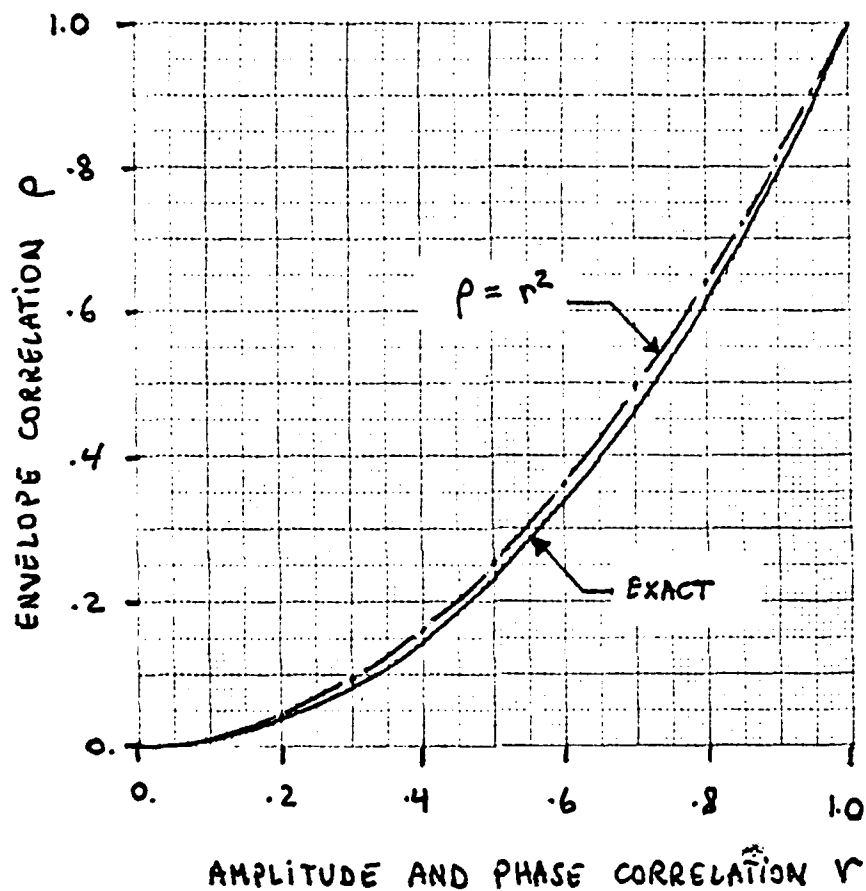
FIGURE 3.2-1   Exact and Approximate Relationship Between the
Envelope Correlation c and the Complex (Amplitude
and Phase) Correlation r of Two Rayleigh Fading
Signals

then an estimate of the envelope correlation coefficient, ρ, of the two random variables is given by

$$\rho = \frac{\text{cov } (x,y)}{\left(\text{var}(x) \cdot \text{var}(y)\right)^{1/2}} \simeq r^2 \qquad (3.2.4)$$

where r is the amplitude and phase correlation coefficient. The accuracy of the estimate improves as the number of samples in the set, N, increases.

The definition of the (envelope) correlation coefficient by Eq. (3.2-4) is used in this section to determine the field and space (envelope) correlation for each of the sets (paths) of measurements described in Section 2. Since many of the sets of data were obtained in the same propagation environment (e.g., urban, suburban, street-to-building, etc.) but with different transmit and receive locations, we define the average correlation coefficient for a particular propagation environment as a weighted sum of the correlation coefficients for each particular path (set of measurements). Thus,

$$\bar{\rho} = \sum_{k=1}^{M} w_k \rho_k \qquad (3.2-5)$$

where M is the number of paths (runs) tested in each environment, the ρ_k are the correlation coefficients for each path, and the w_k are the weights. Since each set of measurements is independent from the other, the weights should depend on the number of points in each data set and the variance of each data set only. Thus, each weighting factor is given by

$$w_k = \frac{n_k \left[\text{var}_k (x) \cdot \text{var}_k (y)\right]^{1/2}}{\left[\sum_{k=1}^{M} n_k \cdot \text{var}_k (x)\right]^{1/2} \left[\sum_{k=1}^{M} n_k \text{var}_k (y)\right]^{1/2}}$$

$$(3.2-6)$$

3-51

where n_k is the number of data points in the k'th set. Note that when the variances of all the data sets (paths) are equal, the weights become

$$w_k = \frac{n_k}{\sum\limits_{k=1}^{M} n_k} = \frac{n_k}{N} . \qquad (3.2-7)$$

Furthermore, if the covariances of all data sets are also equal, (i.e., $\rho_k = \rho$ for all k), then the average value of the correlation coefficient is equal to that of each path as might be expected.

   In the remainder of this section we present values of the correlation coefficients (in tabulated form) for each data set in a given propagation environment, as well as an average correlation coefficient for the combined paths in that environment.

   Furthermore, since many of the data points in each data set were taken at different transmitter-receiver separations, it was necessary to compensate for distance effects by defining the correlation coefficient in terms of the normalized data. The normalization was effected by assuming each data pair to be of the form

$$p_i(e,d) = e_i^2 f(d_i)$$
$$\qquad (3.2-8)$$
$$p_i(h,d) = h_i^2 g(d_i)$$

where the $\{p_i(e,d)\}$ and $\{p_i(h,d)\}$ are the measured received signal levels (in Watts or milliwatts) with the whip and loop antennas, respectively, for the field diversity case at a distance d_i from the emitter. The functions $f(\cdot)$ and $g(\cdot)$ describe the distance dependence of the data obtained with each diversity antenna. The sets $\{e_i\}$ and $\{h_i\}$ represent the normalized values of the envelope of the received signal. Thus

3-52

in the field diversity case the correlation coefficient is defined as the correlation between sets $\{e_i\}$ and $\{h_i\}$, i.e.,

$$\rho_{eh} = \frac{\text{cov } (e,h)}{\left[\text{var}(e) \cdot \text{var}(h)\right]^{1/2}} = \frac{\text{cov } (e,h)}{\sigma_e \sigma_h} \; . \qquad (3.2-9)$$

A similar definition applies to the space diversity case.

In order to determine the effect of the normalization on the correlation coefficient, we considered various types of distance dependence. The most general case considered (Case I) was one in which the distance dependence of the data obtained with each diversity antenna was determined independently (Eq. (3.1-5) and (3.1-6)) so that $f(\cdot) \neq g(\cdot)$. However, from physical considerations we would expect the distance dependence of two diversity antenna outputs to be identical (Case II) so that $f(\cdot)=g(\cdot)$, (Eq. (3.1-9), (3.1-10), and (3.1-11)). Finally, in the case of the street-to-street propagation other types of known distance dependence such as inverse fourth power law or inverse square law were investigated (Case III) where appropriate. The actual distance dependence for each case is indicated in the tables.

The tables of correlation coefficients for the field diversity measurements at 27 MHz and 49.8 MHz are presented in Section 3.2.1. Similar tables for the space diversity measurements at 49.8 MHz and 446 MHz are given in Section 3.2.2. The implications of the correlation of the data on power and signal-to-noise ratio gains which may be realized by using diversity reception in a MOBA environment are discussed in Section 3.2.3.

3.2.1 Field Correlation

Values of the field correlation coefficients at 27 MHz and 49.8 MHz for the street-to-street, street-to-building, building-to-building, and intrabuilding propagation measurements are given in Tables 3.2-1, 3.2-2, 3.2-3, and 3.2-4, respectively.

From Table 3.2-1 we see that the field correlation coefficient in a suburban area (Lexington) varies from .52 to .74 at 27 MHz and from .07 to .54 at 49.8 MHz depending on the propagation path. Weighted average values for the field correlation coefficient in Lexington are .58 at 27 MHz and .26 at 49.8 MHz.

Similarly, we can also see from Table 3.2-1 that field correlation coefficients in an urban area (Boston) range from .14 to .90 at 27 MHz and from .61 to .86 at 49.8 MHz depending on the propagation path. The weighted average values are .76 at 27 MHz and .73 at 49.8 MHz. These values are greater than the suburban average values which is somewhat surprising. Finally, if we combine the urban and suburban data we obtain a weighted average correlation coefficient of .74 at 27 MHz and .61 at 49.8 MHz.

The field correlation coefficients in a street-to-building propagation environment (Table 3.2-2) can be seen to vary from .37 to .79 at 27 MHz and from .63 to .90 at 49.8 MHz in a concrete wall building, and are around .87 at 27 MHz and .32 at 49.8 MHz in a cinder-block building. Weighted average values for the reinforced concrete building are .56 at 27 MHz and .89 at 49.8 MHz. Weighted average values for the two types of buildings are .79 at 27 MHz and .87 at 49.8 MHz. The values of the correlation coefficients for the street-to-building propagation measurements are seen to be larger than for the street-to-street propagation measurements which indicates that fewer reflections occur in the street-to-building environment. This is not surprising since the propagation paths are much shorter.

TABLE 3.2-1

Field Correlation in Urban and Suburban
Street-to-Street Propagation

FREQUENCY			27 MHz				49.8 MHz			
k	PATH	CASE	$\ell_{en} k$	$\ell_e k$	$\ell_{en} k$	N_k	$\ell_{en} k$	$\ell_e k$	$\ell_n k$	N_k
1	Along Urban Street Boston	I II III	.4846 .4804 .5700	.6745 .6770 .8678	.6859 .6851 .9079	15	.5662 .7922 .8060	1.109 1.130 1.203	.9002 .9062 .7991	14
2	NLOS Urban Path Boston	I II III	.9001 .8987 .8988	1.492 1.506 1.512	2.100 2.098 2.096	14	.6199 .6160 .6259	.9114 .9009 .9031	.789 1.168 1.118	15
3	NLOS Urban Path Boston	I II III	.2099 .1486 .1486	.4069 .4045 .4045	.8317 .8388 .8388	16	.3852 .8467 .3429	.8885 .6009 .5891	.7743 .6986 .6774	14
4	Along Suburban Street Lexington	I II III	.7362 .7414 .7414	.3962 .4310 .4311	.6809 .6957 .6957	10	.4610 .0719 .0813	.6046 .7641 .8160	.5061 .6999 .6014	15
5	NLOS Suburban Path Lexington	I II III	.5218 .5203 .5812	.7318 .7339 .9603	.4490 .4531 .4999	8	.4734 .4453 .5459	.8545 .8050 .8221	.5038 .5419 .4959	24
	COMBINED PATHS		ℓ_{eh}	ℓ_e	ℓ_h	N	ℓ_{eh}	ℓ_e	ℓ_h	N
1 to 3	Boston	I II III	.7736 .7648 .7582	.9454 .9574 1.0100	1.3345 1.3327 1.3544	45	.7701 .7344 .7370	.8739 .8864 .9191	.8054 .8030 .8063	96
4 to 5	Lexington	I II III	.5668 .5820 .5779	.5703 .5853 .7163	.6074 .6070 .6552	18	.4626 .2651 .3173	.7576 .7997 .8195	.5049 .6039 .5580	40
1 to 5	Lexington & Boston	I II III	.7504 .7431 .7273	.8552 .8675 .9357	1.1668 1.1542 1.1825	63	.7000 .6173 .6361	.8339 .8603 .9976	.7058 .7087 .7041	128

Case I: $\rho(e,d) = e^2 d^{-n}$ Case II: $\rho(e,d) = e^2 d^{-k}$ Case III: $\rho(e,d) = e^2 d^{-4}$

$\rho(h,d) = h^2 d^{-m}$, $\rho(h,d) = h^2 d^{-k}$, $\rho(h,d) = h^2 d^{-4}$

3-55

TABLE 3.2-2

Field Correlation in Street to Building Propagation

FREQUENCY		27 MHz				49.8 MHz			
PATH	CASE	ρ_{ch}	$\rho_c(k)$	$\rho_b(k)$	n_k	$\rho_{ch}(k)$	$\rho_c(k)$	$\rho_b(k)$	N_k
Reinforced Concrete Building (various floor levels)	I	.7902	.9270	.6857	16	.6556	.4836	.6706	8
	II	.7904	.9169	.6936		.6451	.4790	.6689	
Reinforced Concrete Building (various floor levels)	I	.4930	.6206	1.065	12	.8815	1.1031	1.138	12
	II	.3701	.6122	1.067		.8834	1.105	1.134	
Reinforced Concrete Building (various floor levels)	I	.8977	1.865	1.942	14	.8880	3.248	2.603	12
	II	.8796	1.783	2.048		.9063	3.045	2.716	
Cinder Block Building (various locations on 1st floor)	I					.4266	.5008	.5186	16
	II					.5295	.5115	.4967	
COMBINED PATHS		ρ_{ch}	ρ_c	ρ_b	n_k	ρ_{ch}	ρ_c	ρ_b	N_k
Reinforced Concrete Buildings	I	.966	.8100	.8888	22	.8760	2.113	1.772	2
	II	.5624	.8073	.8734	28	.8963	1.751	1.417	12
Reinforced Concrete and Cinder Block Buildings	I	.8048	1.264	1.327	42	.8570	.998	1.833	48
	II	.7909	1.222	1.381		.8773	1.658	1.524	

Case I: $\rho(c,d) = c^2 d^{-n}$, $\rho(b,d) = b^2 d^{-m}$

Case II: $\rho(c,d) = c^2 d^{-k}$, $\rho(b,d) = b^2 d^{-k}$

TABLE 3.2-3

Field Correlation in Building-to-Building Propagation

FREQUENCY		27 MHz				49.8 MHz			
PATH	CASE	$\rho_{eh}(k)$	$\sigma_e(k)$	$\sigma_h(k)$	N_k	$\rho_{eh}(k)$	$\sigma_e(k)$	$\sigma_h(k)$	N_k
Receiver in Near End	I	.6714	.4605	.4537	22	.1248	.3834	.5660	19
	II	.6426	.4523	.4716		.1215	.3859	.5616	
Receiver in Far End	I	.6386	.6151	.6139	22	.6866	.7813	.5744	20
	II	.6263	.6051	.6364		.6895	.7879	.5646	
COMBINED PATHS		ρ_{eh}	σ_e	σ_h	N	ρ_{eh}	σ_e	σ_h	N
Composite	I	.6503	.5433	.5398	44	.4840	.6202	.5703	39
	II	.6322	.5342	.5544		.4832	.6252	.5631	

Case I: $p(e,d) = e^2 d^{-n}$ or $p(e,d) = e^2 \exp(-\alpha d)$

$p(h,d) = h^2 d^{-m}$ or $p(h,d) = h^2 \exp(-\beta h)$

Case II: $p(e,d) = e^2 d^{-k}$ or $p(e,d) = e^2 \exp(-\alpha d)$

$p(h,d) = h^2 d^{-k}$ or $p(h,d) = h^2 \exp(-\alpha d)$

TABLE 3.2-4

Field Correlation in Intrabuilding Propagation

FREQUENCY		27 MHz				49.8 MHz			
PATH	CASE	$\rho_{ch}(k)$	$\sigma_e(k)$	$\sigma_h(k)$	N_A	$\rho_{ch}(k)$	$\sigma_e(k)$	$\sigma_h(k)$	N_A
Straight Corridor	I	.3035	.4950	.2762	11	.4866	1.166	.6058	10
	II	.2665	.4805	.2917	16	.5137	1.113	.6134	8
Winding Corridor	I	.6395	.9215	.7766		.6840	.4789	.5985	
	II	.5010	.9306	.8448		.6840	.4789	.5985	
Straight Corridor	I	.5655	.8825	1.551	25				
L-Shaped Corridor	II	.5834	.8958	1.484					
	I	-.0287	1.266	.6106	17				
	II	.0338	1.093	.7446					
Between Above-Ground Floors	I	.5822	.5018	.3566	8	.6471	1.232	1.822	40
	II	.5006	.5119	.3799		.6821	1.213	1.770	
Upper Floor to Basement	I	.8422	1.367	.7547	10	.7368	1.174	1.408	10
	II	.8100	1.392	.7448		.6750	1.207	1.465	
Near Elevator Shafts	I	.5509	.8547	.4518	14	.8506	1.582	.8350	17
	II	.2808	.9469	.5275		.8601	1.476	.8881	
In Stairwell	I	.3098	.4637	.8887	18	.4611	.4311	.4321	14
	II	.2242	.4941	.9328		.4276	.4523	.4172	
COMBINED PATHS		ρ_{ch}	σ_e	σ_h	N	$\rho_{ch}(k)$	$\sigma_e(k)$	$\sigma_h(k)$	N
In Corridors	I	.3842	.9555	1.0562	69	.4974	.9247	.6026	18
	II	.3881	.9070	1.0553		.5218	.8877	.6068	
Floor-to-Floor	I	.5144	.8343	.6897	50	.6407	1.2154	1.4362	81
	II	.4158	.8760	.7247		.6689	1.1826	1.4169	
Floor to Floor and Corridors	I	.4186	.9066	.9201	119	.6242	1.1679	1.1243	99
	II	.1921	.8944	.9108		.6526	1.1349	1.1075	

CASE I: (Same as Table 2.3-3)

CASE II: (Same as Table 2.3-3)

3-58

From Table 3.2-3, we can see that the field correlation coefficient for the building-to-building propagation measurements ranges from .62 to .67 at 27 MHz and from .12 to .68 at 49.8 MHz depending on the path. Weighted average values of the field correlation are around .63 at 27 MHz and .48 at 49.8 MHz. These values indicate a stronger decorrelation of the electric and magnetic field components than in the previous two types of measurements.

The field correlation coefficients for the intrabuilding measurements are given in Table 3.2-4. We see that in the case of the measurements made along corridors, it varies from -.02 to .63 at 27 MHz and from .48 to .68 at 49.8 MHz. In the case of the measurements between above ground floors, it varies from .50 to .58 at 27 MHz and from .64 to .68 at 49.8 MHz. In the case of the measurements between above ground floors, it varies from .50 to .58 at 27 MHz and from .64 to .68 at 49.8 MHz. Similarly, for the measurements between above ground floors and the basement, it varies from .83 to .84 at 27 MHz and from .67 to .73 at 49.8 MHz while in a stairway, it varies from .22 to .30 at 27 MHz and from .42 to .46 at 49.8 MHz. Weighted average values of all these coefficients are .39 at 27 MHz and .65 at 49.8 MHz which indicate that there is significant field decorrelation inside buildings on the average.

In conclusion, the average field diversity coefficient in the various MOBA environments ranges from .4 to .8 at both 27 MHz and 49.8 MHz.

3.2.2   Spatial Correlation

Values of the spatial correlation coefficient (at varying distances) at 49.8 MHz and 446 MHz are given in Tables 3.2-5 to 3.2-11 for the various types of propagation measurements described in Section 2.

Values of the correlation coefficient at 49.8 MHz for two antennas 3 meters apart in the street-to-street propagation

TABLE 3.2-5

Spatial Correlation at 49.8 MHz in Street-to-Street Propagation

PATH	CASE	CORRELATION DISTANCE	WHIP ANTENNA:		E-FIELD		LOOP ANTENNA:		H-FIELD	
			$\rho(k)$	$\sigma_1(k)$	$\sigma_2(k)$	N_k	$\rho(k)$	$\sigma_1(k)$	$\sigma_2(k)$	N_k
Along Urban Street (Boston)	I	3m	.1070	.9274	1.267	17	.4749	.7933	.8227	17
	II		.1050	.8870	1.327		.5270	.8524	.8207	
	III		.1454	.8941	1.439		.4652	.7833	.8272	
NLOS Urban Path (Boston)	I	3m	.4667	.5954	.5944	17	.7400	.6915	.7381	17
	II		.4881	.6161	.6031		.7231	.6669	.7266	
	III		.4720	.6004	.5964		.7129	.6530	.7210	
NLOS Urban Path (Boston)	I	15m	.6844	.7736	.9290	9	.4839	1.288	.8001	9
	II		.6874	.7639	.9194		.4865	1.301	.8175	
	III		.7066	.7443	.8996		.4792	1.253	.7590	
Along Suburban Street (Lex.)	I	3m	.5301	.7253	.4968	9	.5432	.4634	.5719	9
	II		.6551	.9297	.6084		.7196	.6962	.7413	
	III		.6794	.9929	.6492		.6794	.6183	.6792	
NLOS Suburban Path (Lex.)	I	3m	-.0263	1.064	.4109	12	.1713	.4581	.5662	12
	II		-.0028	1.010	.4330		.1545	.4322	.6517	
	III		.1310	.9707	.5204		.2438	.4971	.5168	
COMBINED PATHS	CASE	CORRELATION DISTANCE	ρ	σ_1	σ_2	N	ρ	σ_1	σ_2	N_k
Boston	I	3m	.1886	.7793	.9896	14	.5912	.7441	.7815	14
	II		.1917	.7637	1.0307		.6061	.7653	.7751	
	III		.2123	.7615	1.1015		.5693	.7211	.7759	
Lexington	I	3m	.1792	.9340	.4497	21	.3327	.4604	.5686	21
	II		.3169	.9764	.5155		.4746	.5608	.6915	
	III		.3972	.9803	.5791		.1815	.5523	.5919	
Lexington & Boston	I	3m	.1706	.8417	.8262	55	.5338	.6508	.7079	55
	II		.2093	.8512	.8707		.5660	.6944	.7443	
	III		.2458	.8517	.9370		.5466	.6618	.7113	

Table 3.2-5

Spatial Correlation at 49.8 MHz in Street-to-Street Propagation (Con't)

PATH	CASE	CORRELATION DISTANCE	WHIP ANTENNA:		E-FIELD		LOOP ANTENNA:		H-FIELD	
			p	σ_1	σ_2	N	p	σ_1	σ_2	N_k
Boston (E + H)	I	3m	.3601	.7619	.8917	68				
	II		.3672	.7645	.9199					
	III		.3514	.7416	.9527					
Lexington (E + H)	I	3m	.2151	.7363	.5126	42				
	II		.3538	.7962	.6099					
	III		.4117	.7956	.5855					
Lexington and Boston (E + H)	I	3m	.3149	.7522	.7693	110				
	II		.3557	.7768	.8100					
	III		.3574	.7627	.8118					

CASES I, II, and III: (Same as Table 2.3-1)

TABLE 3.2-6

Spatial Correlation at 446 MHz in Street-to-Street Propagation

CORRELATION DISTANCE		$r_{12} = 50$ cm				$r_{23} = 50$ cm				$r_{13} = 100$ cm			
PATH	CASE	$\rho_{12}(k)$	$\sigma_1(k)$	$\sigma_2(k)$	N_k	$\rho_{23}(k)$	$\sigma_2(k)$	$\sigma_3(k)$	N_k	$\rho_{13}(k)$	$\sigma_1(k)$	$\sigma_3(k)$	N_k
k													
1 Along Urban Street (Boston)	I	.4157	.5782	.4923	18	.5172	.4923	.4928	18	.6931	.5782	.4928	18
	II	.4112	.6036	.5073		.5419	.5073	.5430		.7106	.6036	.5430	
2 NLOS Urban Path (Boston)	I	.7415	.7651	.4834	13	.5086	.4834	.5799	13	.2932	.7651	.5799	13
	II	.7902	.8703	.6034		.4585	.6034	.5905		.4074	.8703	.5905	
3 NLOS Urban Path (Boston)	I	.2726	.6033	.6594	18	.7158	.6594	.8480	18	.1150	.6033	.8480	18
	II	.2852	.6182	.6785		.7418	.6785	.8603		.1146	.6182	.8603	
4 Along Suburban Street (Lexington)	I	.6432	.6742	.5406	11	.1239	.5406	.4908	11	-.0933	.6742	.4908	11
	II	.6237	.7488	.6189		.1065	.6189	.5879		-.0537	.7488	.5879	
5 NLOS Suburban Path (Lexington)	I	.1674	.3531	.2815	11	.3897	.2815	.4738	11	.2891	.3531	.4738	11
	II	.1878	.3357	.3242		.4278	.3242	.4730		.2347	.3357	.4730	

COMBINED PATHS	CASE	ρ	σ_1	σ_2	N					ρ	σ_1	σ_3	N_k
1 Boston	I	.5100	.6011	.6138	98					.3014	.6417	.6651	49
	II	.5485	.6463	.6453						.3449	.6893	.6875	
2 Lexington	I	.2561	.4878	.4577	44					.0337	.5382	.4824	22
	II	.4391	.5389	.5142						.0220	.5803	.5336	
3 Lexington & Boston	I	.4555	.5684	.5700	142					.2436	.6115	.6144	71
	II	.5233	.6150	.6077						.2715	.6575	.6437	

Case I: $p(e,d) \sim e^2 d^{-n}$

Case II: $p(e,d) \sim e^2 d^{-4}$ or $p(e,d) \sim e^2 d^{-2}$

TABLE 3.2-7

Spatial Correlation at 446 MHz in Street-to-Building Propagation

CORRELATION DISTANCE	$r_{12} = 50$ cm				$r_{23} = 50$ cm				$r_{13} = 100$ cm			
COMMENTS	ρ_{12}	σ_1	σ_2	N	ρ_{23}	σ_2	σ_3	N	ρ_{13}	σ_1	σ_3	N
CINDER BLOCK BUILDING	.5402	.4909	.5523	12	-.1314	.5523	.3364	12	-.0157	.4909	.3364	12
LINEAR COMBINATION OF $W_1\rho_{12}+W_2\rho_{23}$	.2554	.5225	.4573	24								

$$p(e,d) = e^2 d^{-n}$$

TABLE 3.2-8

Spatial Correlation at 49.8 MHz in Building-to-Building Propagation

TRANSMITTER AND RECEIVER LOCATIONS	CASE	CORRELATION DISTANCE	WHIP ANTENNA: E-FIELD				LOOP ANTENNA: H-FIELD			
			$\rho(k)$	$\sigma_1(k)$	$\sigma_2(k)$	N_k	$\rho(k)$	$\sigma_1(k)$	$\sigma_2(k)$	N_k
(T)(R) NEAR WINDOW IN FRONT OF BUILDING	I II	4.5 m	-.0384 -.0491	.4022 .4057	.3316 .3328	19	.2403 .2522	.6279 .6183	.3903 .3954	19
(T)(R) NEAR WINDOW IN REAR OF BUILDING	I II	4.5 m	.1607 .1789	.5986 .6118	.8847 .8903	20	.1386 .1387	.6328 .6195	.5047 .4986	20
AVERAGE CORRELATIONS			ρ	σ_1	σ_2	N	ρ	σ_1	σ_2	N
AVERAGE CORRELATION OVER BOTH LOCATIONS	I II	4.5 m	.1191 .1320	.5124 .5217	.6745 .6786	39	.2949 .2996	.6304 .6189	.4528 .4513	39
AVERAGE CORRELATIONS			ρ	σ_1	σ_2	N				
AVERAGE CORRELATION OVER TWO ANTENNAS WHEN (R) IS IN FRONT	I II	4.5 m	.1409 .1440	.5273 .5229	.3625 .3654	39				
AVERAGE CORRELATION OVER TWO ANTENNAS WHEN (R) IS IN REAR	I II	4.5 m	.2179 .2274	.6159 .6157	.7202 .7215	40				
AVERAGE CORRELATION OVER TWO ANTENNAS AND BOTH LOCATIONS	I II	4.5 m	.1900 .1977	.5744 .5724	.5745 .5762	78				

Case I: $\rho(e,d) = e^2 d^{-n}$
$\rho(h,d) = h^2 d^{-m}$

Case II: $\rho(e,d) = e^2 d^{-k}$
$\rho(h,d) = h^2 d^{-k}$

TABLE 3.2-9

Spatial Correlation at 446 MHz in Building-to-Building Propagation

LOCATIONS		CORRELATION DISTANCE r_{ij} = 50 cm					CORRELATION DISTANCE r_{ij} = 350 cm			
		ρ_{ij}	σ_i	σ_j	N_{ij}		ρ_{ij}	σ_i	σ_j	N_{ij}
TRANSMITTER NEAR WINDOW	i=1 j=2	-.0251	.3774	.3126	20	i=1 j=3	.1196	.3774	.5849	20
	i=3 j=4	.6203	.5849	.6973	20	i=1 j=4	-.1677	.3774	.6973	20
RECEIVER IN FRONT END OF BUILDING						i=2 j=3	.2344	.3126	.5849	20
						i=2 j=4	.2102	.3126	.6973	20
TRANSMITTER NEAR WINDOW	i=1 j=2	.2980	.6573	.3436	22	i=1 j=3	.3824	.6573	.5398	22
	i=3 j=4	.1598	.5398	.3631	22	i=1 j=4	.2090	.6573	.3631	22
RECEIVER IN REAR END OF BUILDING						i=2 j=3	.7178	.3436	.5398	22
						i=2 j=4	.0159	.3436	.3631	22
AVERAGE CORRELATIONS		ρ	σ_1	σ_2	N		ρ	σ_1	σ_2	N
R IN FRONT END OF BUILDING		.4700	.4922	.5403	40		.3793	.3465	.6436	30
R IN REAR END OF BUILDING		.2267	.6017	.3535	44		.3322	.5248	.4600	36
COMPOSITE		.3395	.5523	.4522	84		.2024	.4488	.3550	166

$$p(e,d) = e^2 d^{-n}$$

TABLE 3.2-10

Spatial Correlation at 49.8 MHz in Interbuilding Propagation

TRANSMITTER AND RECEIVER LOCATIONS	CASE	CORRELATION DISTANCE	WHIP ANTENNA: E FIELD				LOOP ANTENNA: H-FIELD			
			$\rho(k)$	$\sigma_1(k)$	$\sigma_2(k)$	N_k	$\rho(k)$	$\sigma_1(k)$	$\sigma_2(k)$	N_k
FLOOR TO FLOOR TRANSMISSION	I	4.5 m	.1067	.4233	1.273	20	.4240	.3215	1.974	20
	II		.1327	.4599	1.249		.4118	.3105	1.877	
UPPER FLOOR TO BASEMENT TRANSMISSION	I	4.5 m	.7311	1.419	1.477	5	.6616	.8807	.5458	5
	II		.7252	1.333	1.514		.6799	.8751	.5269	
AVERAGE CORRELATIONS			ρ	σ_1	σ_2		ρ	σ_1	σ_2	
UPPER FLOOR TO BASEMENT & FLOOR-TO-FLOOR TRANS.	I	4.5 m	.3586	.7009	1.336	25	.3203	.4877	1.7824	25
	II		.3738	.7243	1.306		.3131	.4799	1.6953	
AVERAGE CORRELATIONS			ρ	σ_1	σ_2	N				
AVERAGE CORRELATION OVER BOTH ANTENNAS FOR FLOOR-TO-FLOOR	I	4.5 m	.2611	.7759	1.660	40				
	II		.2528	.8924	1.594					
AVERAGE CORRELATION OVER BOTH ANTENNAS FOR UPPER FLOOR-TO-BASEMENT	I	4.5 m	.6977	1.121	1.111	10				
	II		.6952	1.127	1.133					
AVERAGE CORRELATION OVER BOTH ANTENNAS FOR BOTH CASES	I	4.5 m	.3220	.6018	1.566	50				
	II		.3272	.6144	1.513					

CASE I: $\rho(e,d) = e^2 d^{-n}$
$\rho(h,d) = h^2 d^m$

CASE II: $\rho(e,d) = e^2 d^{-k}$
$\rho(h,d) = h^2 d^{-k}$

TABLE 3.2-11
Spatial Correlation at 446 MHz in Intrabuilding Propagation

LOCATION	CORRELATION DISTANCE r_{ij} = 50 cm				CORRELATION DISTANCE r_{ij} = 100 cm			
	ρ_{ij}	σ_i	σ_j	N_{ij}	ρ_{ij}	σ_i	σ_j	N_{ij}
STRAIGHT CORRIDOR	.5734	.2495	.2140	5				
WINDING CORRIDOR	.1009	.2723	.7698	9				
BETWEEN ABOVE-GROUND FLOORS	.3217 .6893	.6754 .2669	.9552 .2687	16				
UPPER FLOOR TO BASEMENT	.3662 .7182	.2280 .9408	.9408 .6422	5	.5534 -.1920	.2210 -.6429	.6422 .1576	5
NEAR ELEVATOR SHAFTS	.1669 .4059	.4419 .3321	.3321 .3337	14	.2962	.4419	.3337	14
IN STAIRWELL	-.1959	.3809	.2609	16				
AVERAGE CORRELATIONS	ρ	σ_1	σ_2	N	ρ	σ_1	σ_2	N
IN CORRIDORS	.1472	.2644	.6303	14				
FLOOR-TO-FLOOR	.3213	.4787	.5544	86	.2093	.4588	.3950	24
FLOOR-TO-FLOOR & CORRIDORS	.2984	.4548	.5657	100				

environment are given in Table 3.2-5. The spatial correlation coefficient at this distance is seen to vary from .00 to .71 in a suburban area (Lexington) and from .10 to .74 in an urban area (Boston). Average values of the correlation coefficient in Lexington and Boston are .35 and .36, respectively while the average value for all locations is .35.

Similar values for the spatial correlation coefficient at 446 MHz for two antennas separated by distances of 50 cm and 100 cm are given in Table 3.2-6. At distances of 50 cm, they are seen to range from .12 to .64 in a suburban area (Lexington) and from .27 to .79 in an urban area (Boston). Average values in Lexington and Boston are .43 and .54 respectively while the average value for all locations is .52. At distances of 100 cm, the spatial correlation coefficient ranges from .00 to .28 in Lexington and from .11 to .71 in Boston. Average values in Lexington and Boston are .02 and .34 respectively while the average value for all locations is .27.

Values for the spatial correlation at 446 MHz in the case of street-to-building propagation and for antennas 50 cm and 100 cm apart are given in Table 3.2-7. The spatial correlation at distances of 50 cm is seen to vary from -.13 to .54 with an average value of .25. At a correlation distance of 100 cm, the correlation coefficient is -.01 which indicates complete decorrelation. Street-to-building spatial correlation measurements at 49.8 MHz were not made.

Table 3.2-8 gives values of the spatial correlation at 49.8 MHz of two receiving antennas located 4.5 meters apart for the case of building-to-building propagation. The correlation coefficient is seen to vary from -.04 to .33 with an average value of .19 for all locations and types of receiving antennas. Similarly, Table 3.2-9 gives values of the spatial correlation at 446 MHz for diversity antennas located 50 cm and 350 cm apart for the case of building-to-building transmission. At distances of 50 cm, the correlation coefficient is seen to range from -.02 to .62 with an average value for all locations

of .33, while at distances of 350 cm, it varies from -.16 to .38 with an average value of .20 for all locations.

Spatial correlation values at 49.8 MHz for diversity antennas located 4.5 m apart are given in Table 3.2-10 for the intrabuilding measurements. These values range from .10 to .41 for the transmissions between above ground floors with an average value of .25. For the basement-to-above ground transmissions, it ranges from .66 to .73 with an average value of .69. The average value for all intrabuilding transmissions is .32. The corresponding correlation values at 446 MHz for diversity antennas 50 cm and 100 cm apart are given in Table 3.2-11. At a correlation distance of 50 cm, these values range from .32 to .68 for transmissions between above-ground floors; from .36 to .71 for transmissions from a basement to above-ground floors; from .16 to .40 for transmissions near elevator shafts; and from .10 to .57 in corridors. The average value for all these measure-ments is .29. Similarly, at correlation distances of 100 cm, the correlation coefficient for measurements between above-ground floors range from -.19 to .55 with an average value of .20.

In conclusion, the average spatial correlation coefficient at 446 MHz for diversity antennas 50 cm apart ranges from .25 to .5 for the various MOBA environments, and from .00 to .30 for diversity antennas 100 cm apart. Similar correlation values at 49.8 MHz are obtained at correlation distances of 3 and 4.5 meters. The implications of the correlation values determined in this section are discussed in the remainder of Section 3.2.

3.2.3 Diversity Gain vs. Correlation

Having determined the correlation between the outputs of radio receivers employing field (VHF) and spatial (VHF/UHF) dual diversity, we now discuss the gains that may be realized by using such a system. The improvement (gain) may be explained in terms of the minimum average signal-to-noise ratio required to achieve a certain level of performance. For a fixed trans-mitted power, the average signal-to-noise ratio at the receiver decreases with transmitter-receiver separation so that the

a local (short term) mean signal level, S_o. These amplitude fluctuations have been shown to be closely approximated by the Rayleigh distribution [Clarke, 1968 and Gans 1972]. Furthermore, examination of the strip-chart recordings also shows that the local mean signal level, S_o, varies at a slower rate over larger distances and hence longer periods. These large area variations in the mean have been found to be lognormally distributed about a 'global' mean, also known as the median signal level, $\tilde{S}_o$ [Longley, 1976 and Okumura, 1968]. We have used this statistical description of the signal amplitude, $\sqrt{2S}$, and its mean level, S_o, to derive the probability that the output of a dual selection diversity receiver is below threshold (see Appendix III), i.e., $P(S<S_T)$, as a function of the threshold level normalized to the median signal level in a single diversity branch, $S_T/\tilde{S}_o$, and for various values of the correlation, r, between the signals in the two diversity branches. Note that the ratio $\tilde{S}_o/S_T$ is the median (or global average) signal-to-noise ratio in each diversity branch. In deriving these results it was assumed that the median signal-to-noise ratio in the two diversity branches is the same. This is a reasonable assumption in an environment dominated by ambient noise even if the two antenna gains are not equal.

Plots of the probability that the received signal be below threshold for various correlation values are shown in Figures 3.2-2 and 3.2.3. The curves of Figure 3.2-2 correspond to the case in which the local mean signal level in each branch is constant, i.e., $S_o=\tilde{S}_o$ (pure Rayleigh fading), while the curves of Figure 3.2-3 are for the case in which the local mean signal level in each branch varies according to the lognormal distribution with a standard deviation $\sigma = 8$ dB (typical of MOBA environments). A correlation value of $r = 1$ corresponds to the case of perfect correlation or no diversity reception.

If we define the desired level of performance as $P(S<S_T) \leq 10^{-2}$, then we can see from Figure 3.2-2 that for pure Rayleigh fading, the minimum median signal-to-noise ratio,
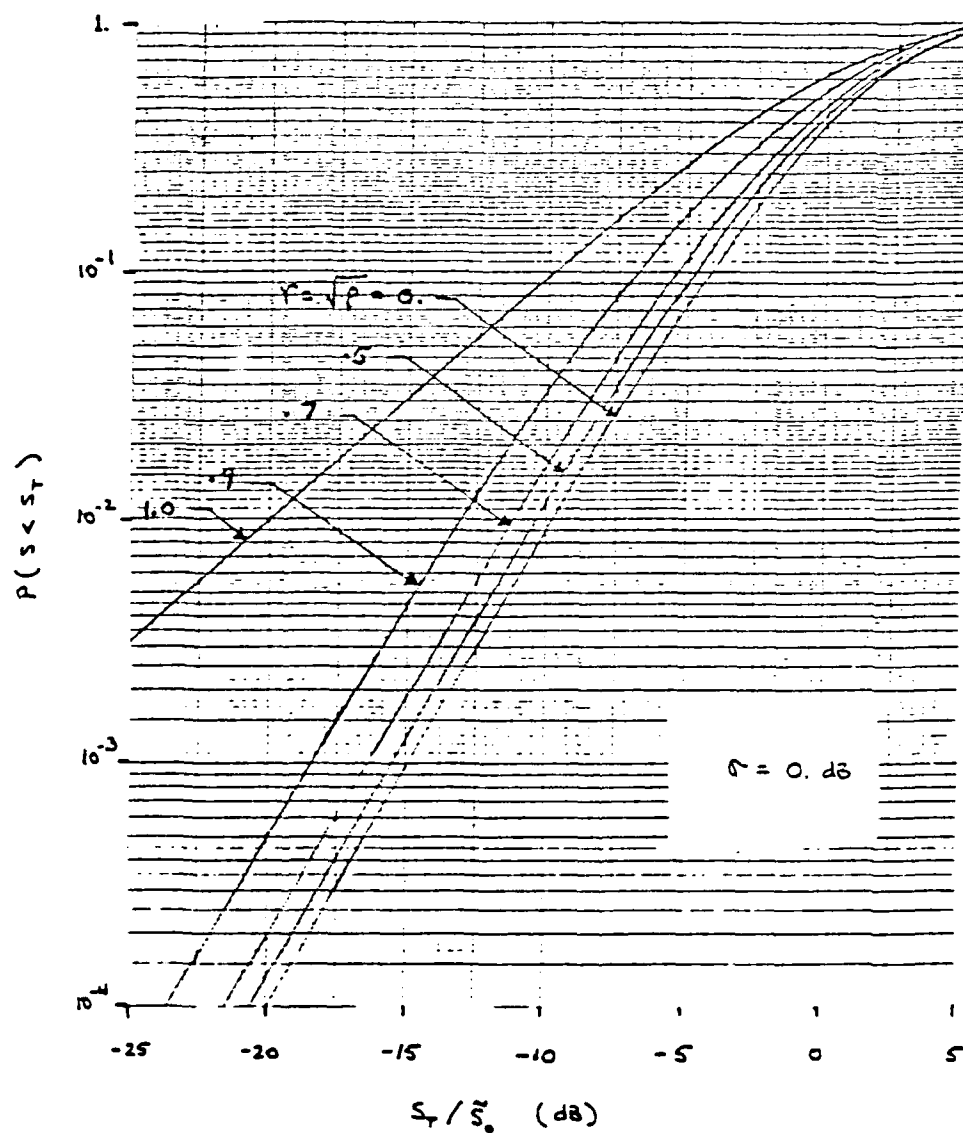
FIGURE 3.2-2   Probability that Received Signal Level is Below
the Threshold Level, S_T, for Correlated Dual
Selection Diversity in Pure Rayleigh Fading

3-72
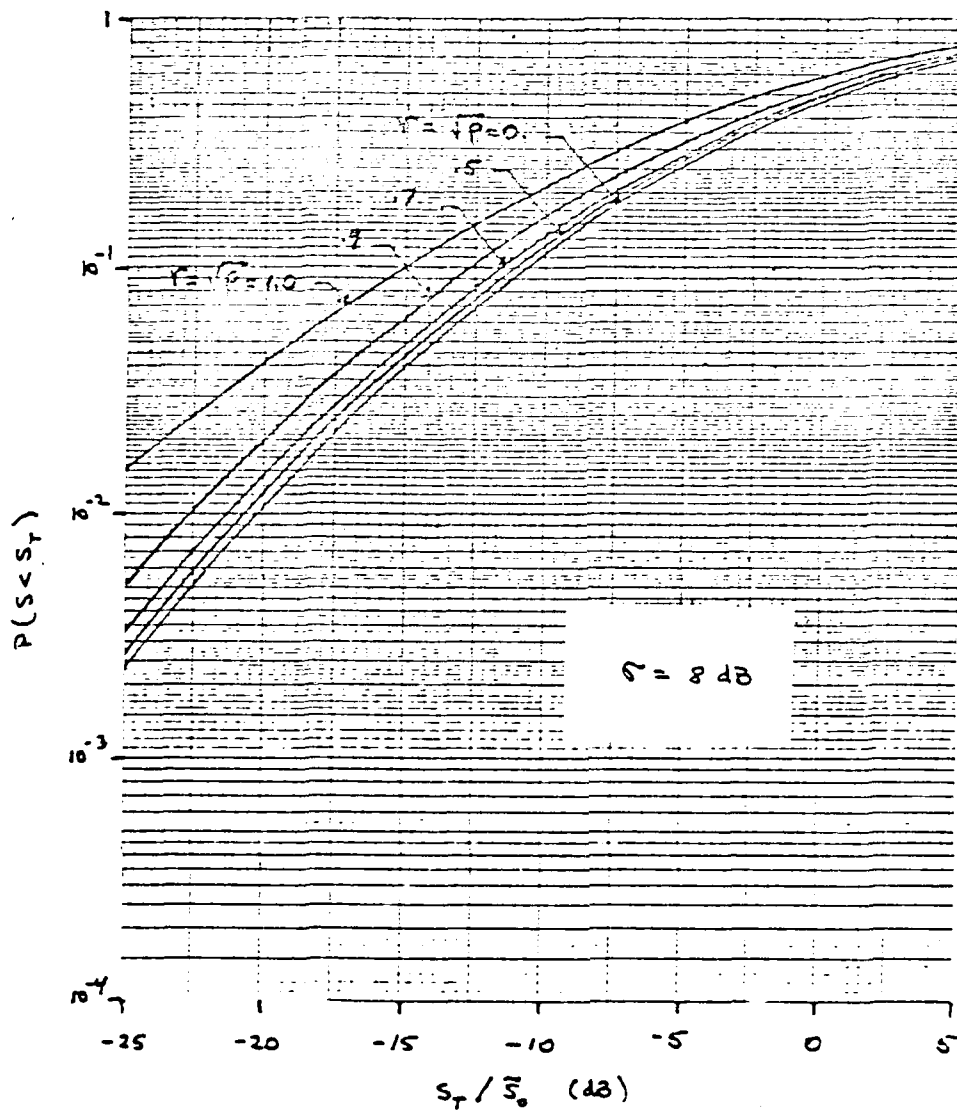
FIGURE 3.2-3   Probability that Received Signal Level is Below
the Threshold Level, S_T, for Correlated Dual Selection
Diversity in Rayleigh-Lognormal Fading

$\tilde{S}_o/S_T$, required when no diversity is used (r=1) is 20 dB. A system using dual selection diversity will require 10.2 dB lower median signal-to-noise ratio (i.e., $\tilde{S}_o/S_T$ = 9.8 dB), if the two branches are uncorrelated (r=0) and 8.8 dB lower signal-to-noise ratio (i.e., $\tilde{S}_o/S_T$ = 11.2 dB) if the correlation between the branches is .7. This implies that if the path loss increases with distance at a rate of 40 dB/decade, then the range of a system employing dual selection diversity will increase by a factor of 1.8 if the two branches are uncorrelated and by a factor of 1.66 if the correlation between the branches is .7. If the path loss increases at a rate of 20 dB/decade, the range will increase by a factor of 3.2 (r=0) and 2.75 (r=.7) respectively. The increase in range due to the diversity gain is shown in Fig. 3.2-4 as a function of the rate of increase of the path loss and for various correlation values.

When the mean signal level varies randomly (σ = 8 dB) the required median signal-to-noise ratios for a performance level of $P(S<S_T) \leq 10^{-2}$ are 27 dB (r=1), 21.2 (r=.7), and 20.2 (r=0) for the no diversity, correlated diversity, and uncorrelated diversity receivers, respectively. The increase in the range is in the order of 1.4 (r=.7) to 1.48 (r=0) if the path loss increases at a rate of 40 dB/decade, and in the order of 1.95 (r=.7) to 2.2 (r=0) if the path loss increases at a rate of 20 dB/decade (see Fig. 3.2-4).

The use of diversity not only increases the range of a fixed power transmitter but also reduces the average duration of the fades, i.e., the fraction of time that the received signal is below threshold. Note that the average fade duration has the dimension of time and is not the same as the probability of the received signal being below threshold. However, they are both related as shown in Appendix III. The corresponding curves the product of the average fade duration, T_D, and the fade in radians per second, $2\pi f_D$, for the case of pure Rayleigh and Rayleigh-lognormal fading (with σ = 8 dB) are shown
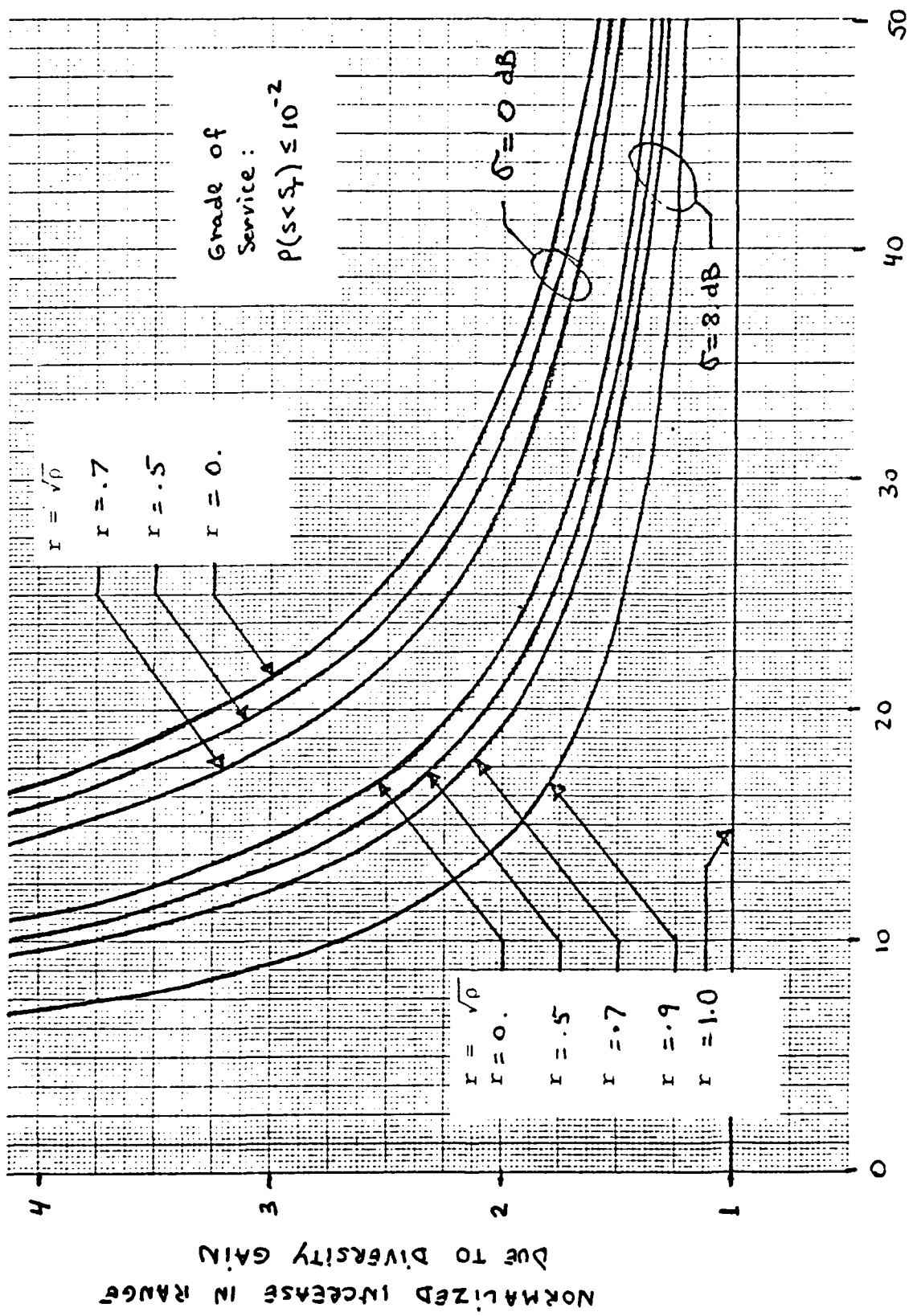
FIGURE 3.2-4 Increase in Range due to Diversity Gain as a Function of Path Loss Rate (Power Law) and Correlation

in Figures 3.2-5 an 3.2-6 as a function of the correlation, $r = \sqrt{\rho}$, and the median signal-to-noise ratio, $\tilde{S}_O/S_T$. The fading rate, f_D, depends on the frequency and the velocity at which the receiver is moving relative to the transmitter and is given by [Jakes, 1974]

$$f_D = \frac{v}{\lambda} = f\frac{v}{c} \qquad (3.2\text{-}10)$$

where λ is the wavelength and c is the speed of light. Note that if the transmitter and receiver are stationary, the fade rate is zero and the average fade duration is either zero or infinite depending on whether the received signal level is above or below threshold.

Thus, in a fixed power link with median signal-to-noise ratio, $\tilde{S}_O/S_T$, of 20 dB, the fade durations are reduced by a factor of 2 when dual selection diversity with correlation between the branches as high as .9 is used and the fading is pure Rayleigh. When the mean signal level also fades ($\sigma = 8$ dB), the fade duration is reduced by a factor of 1.5 if the correlation between the branches is .7 and by a factor of 1.6 if the branches are uncorrelated ($r=0$).
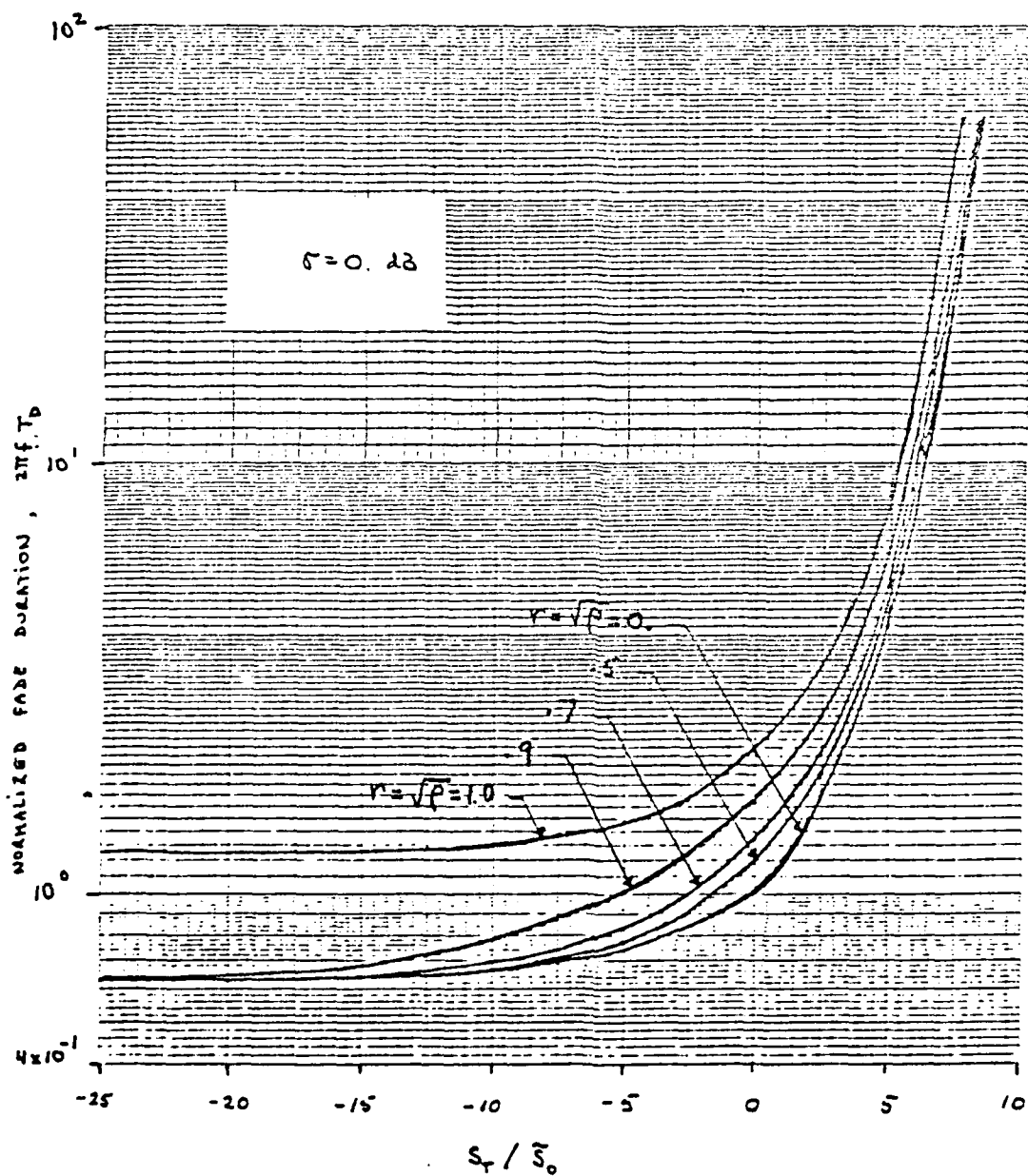
FIGURE 3.2-5   Normalized Fade Duration, T_D, vs. Threshold Level, S_T, for Correlated Dual Selection in Pure Rayleigh Fading
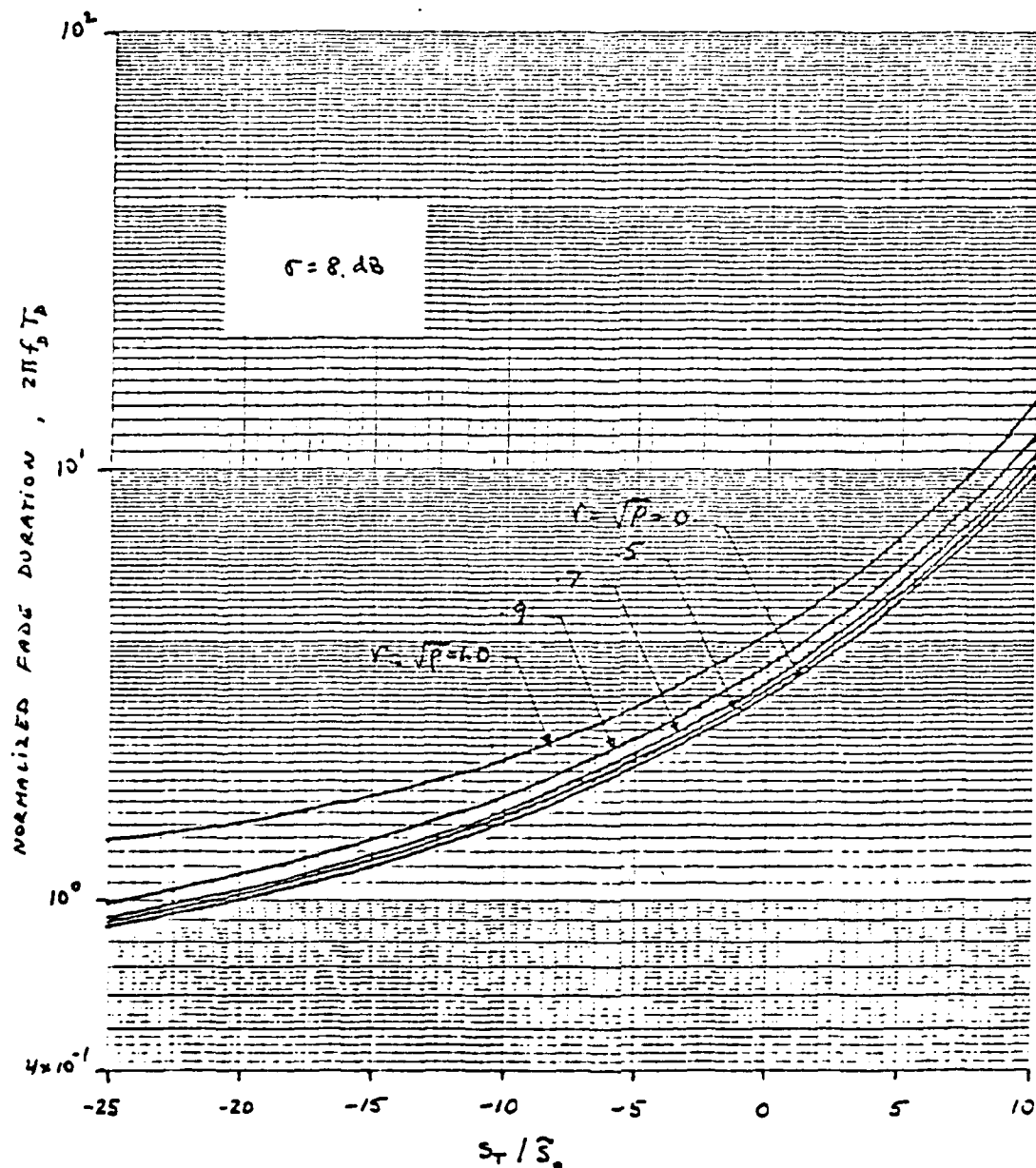
FIGURE 3.2-6 Normalized Fade Duration, T_D, vs. Threshold Level, S_T, for Correlated Dual Selection Diversity in Rayleigh-Lognormal Fading

3.3   Extension of Existing Path Loss Model

In this section we make use of the results of our measurements described in earlier sections to extend the current data base in the literature. A number of prediction methods for estimating the propagation path loss at VHF and UHF over irregular terrain have been reported in the literature. These may be broadly classified as empirical, [Egli, 1957] and [Okumura, 1968], and semitheoretical [Edwards and Durkin, 1969] and [Blomquist and Ladell, 1974]. Path loss prediction techniques for receivers located in urban and suburban areas are not well documented however. Of the previously mentioned techniques, only Okumura's [1968] model, which is empirical in nature, is, in our opinion, useful as a propagation prediction technique for receivers located in urban and suburban areas. This model is intended for use with tall (base station) antennas far from the receiver. The basic method involves the reading of values from numerous correction curves and adding or subtracting these, depending upon the context, to the free space propagation loss. The methods of determining the various correction factors are limited to applications involving radio links operating at frequencies above 150 MHz and over ranges greater than approximately 10 Km. Thus we will use the results of our measurements and Okumura's curves to derive new extended curves to predict path loss between low elevation antennas (2 meters) at frequencies between 30 MHz and 1000 MHz and for distances ranging from 100 meters to several kilometers.

The Okumura model basically predicts path loss according to the formula

$$L(f,d) = L_o(f,d) + A_m(f,d) - H_b(h_t,d) - H_m(h_r,f)$$

$$- K_{ac} - K_{so}$$
$$al$$

(3.3-1)

where all quantities are in dB, and

$L_o(f,d)$ is the free space propagation loss as defined in Eq. (3.1.1-2).

$A_m(f,d)$ is the median attenuation relative to free space in an urban area where the effective base station antenna height, h_t, is 200 meters and the receiver antenna height, h_r, is 3 meters. These values are expressed as a function of distance and frequency and can be obtained from Fig. 3.3-1.

$H_b(h_t,d)$ is the base station height-gain factor expressed in decibels relative to a 200-meter-high base station antenna in an urban area. This function is dependent upon range and has been plotted in Fig. 3.3-2.

$H_m(h_r,f)$ is the mobile height-gain factor expressed in decibels relative to a 3-meter-high mobile antenna. This factor is dependent upon frequency and has been plotted in Fig. 3.3-3.

$K_{\binom{ac}{a\ell}}$ is "the along or across street correction factor" for urban areas. This factor is dependent upon range and is plotted in Fig. 3.3-4.

K_{s0} is the correction factor for suburban and open terrain which is plotted in Figs. 3.3-5a and 3.3-5b.

In order to determine whether Okumura's prediction curves can be extended to shorter distances, lower frequencies and lower elevation antennas, we need to first compare his prediction curves with our results at a common point, e.g., at a frequency of 446 MHz, distance of 1 Km, and between 2 m high
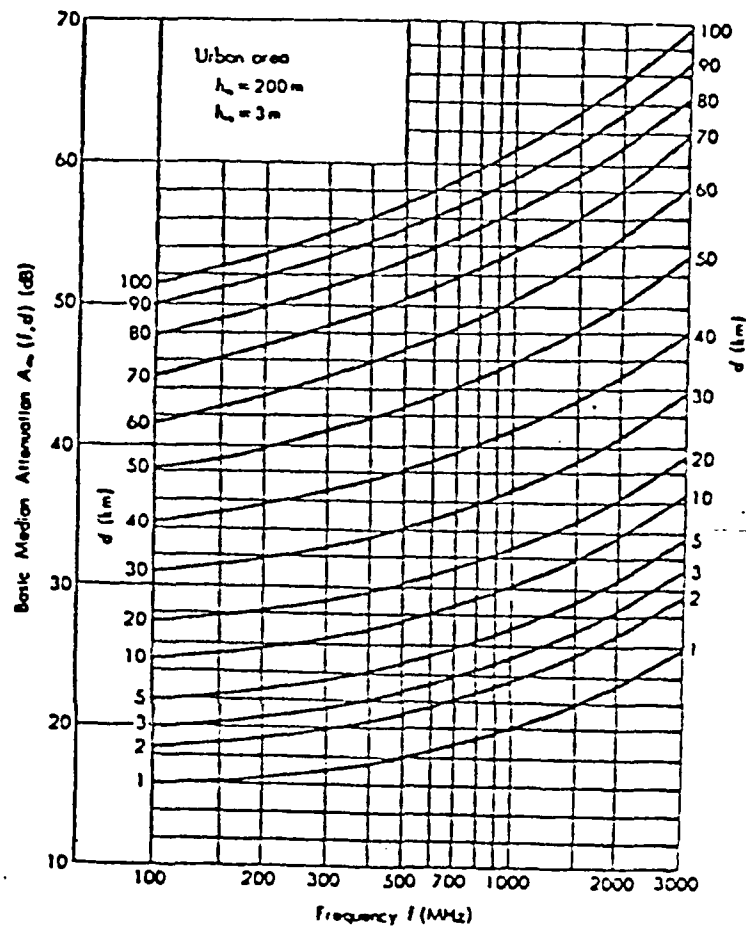
FIGURE 3.3-1 Prediction Curve for Basic Median Attenuation
Relative to Free Space in Urban Area Over
Quasi-smooth Terrain, Referred to h_{te}=200 m
h_{re}=3 m

(from Okumura, 1968)
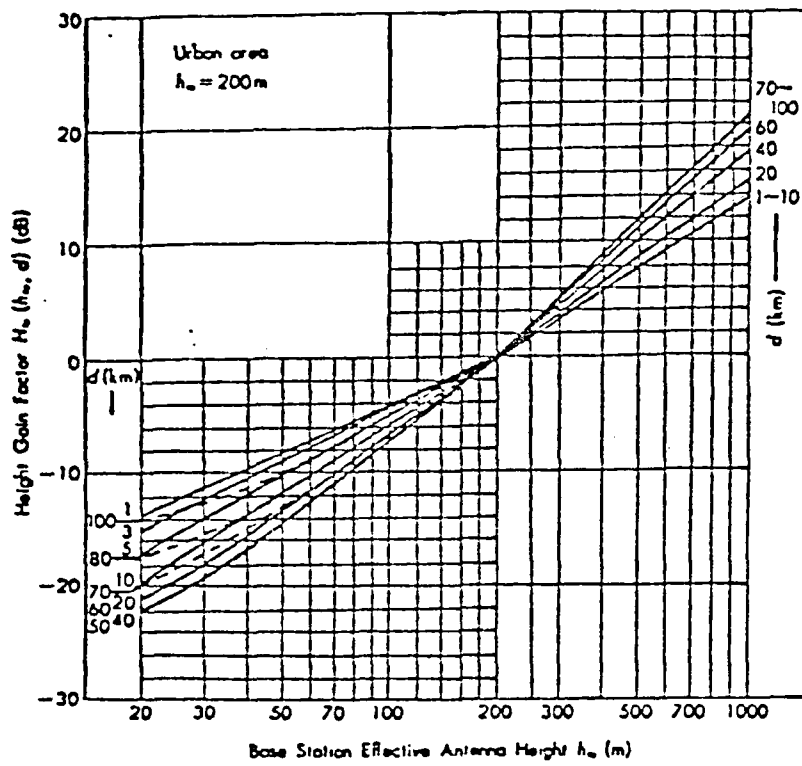
FIGURE 3.3-2   Prediction Curves for Base Station Antenna
Height Gain Factor Referred to h_{te}=200 m,
as a function of distance

(from Okumura, 1968)
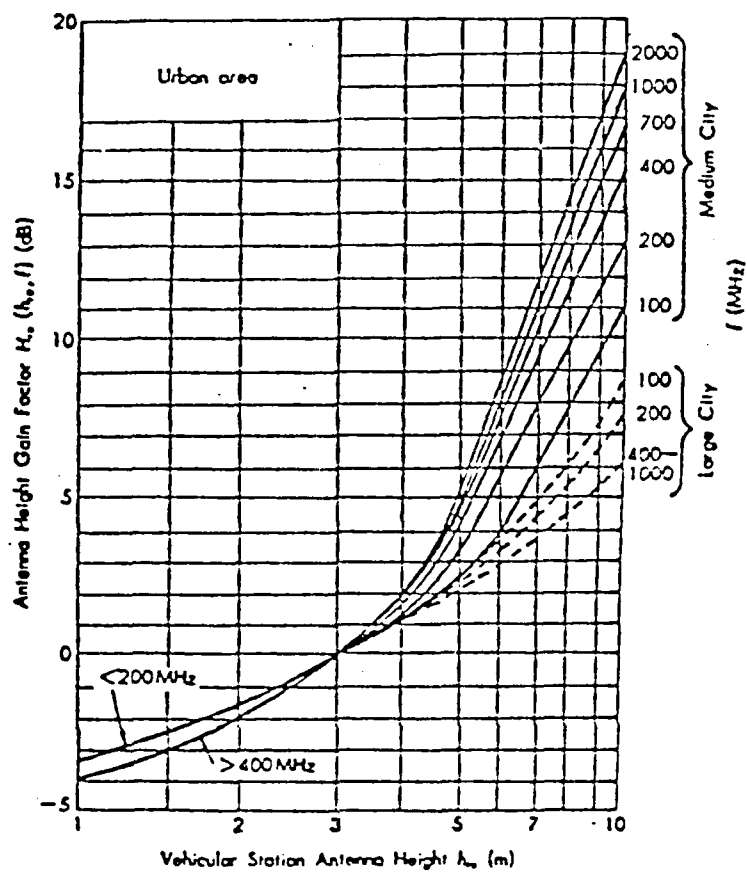
FIGURE 3.3-3   Prediction Curves for Mobile Antenna Height
Gain Factor in Urban Area

(from Okumura, 1968)
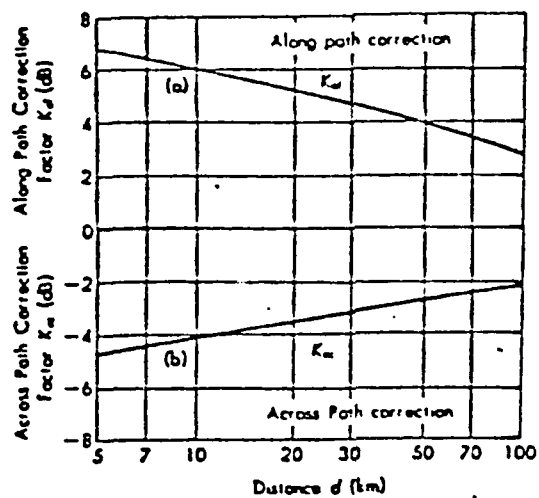
FIGURE 3.3-4   Prediction Curves for Along and Across Path
Correlation Factor in Urban Areas

(from Okumura, 1968)
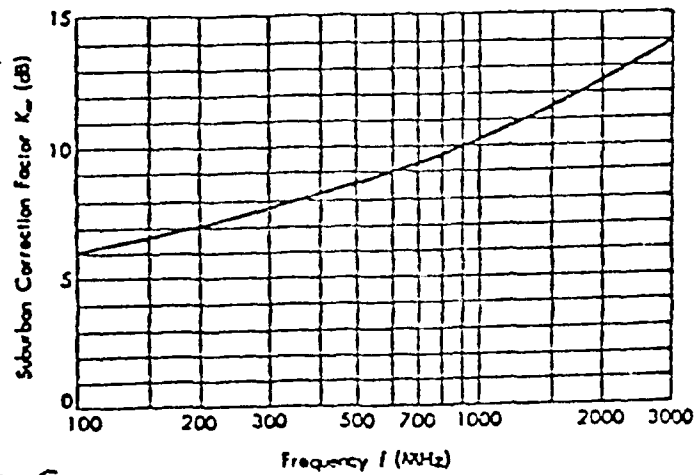
FIGURE 3.3-5a   Prediction Curve for "Suburban Correction Factor"
                as a Function of the Frequency (from Okumura, 1968)
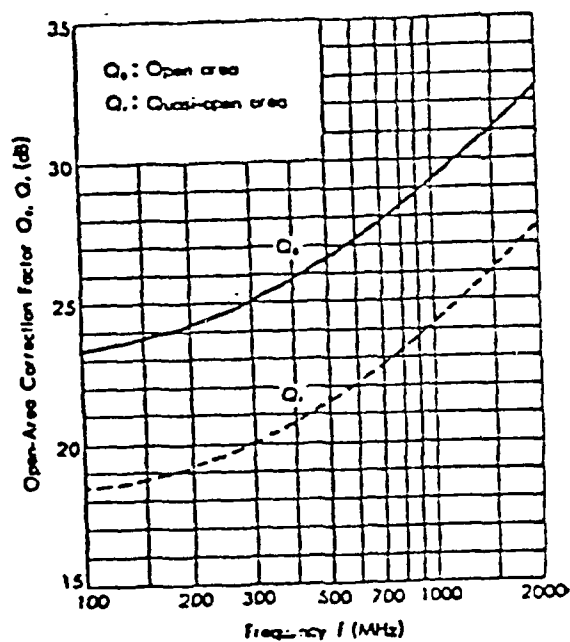
FIGURE 3.3-5b   Prediction Curves of "Open-Area Correction Factor"
                as a Function of the Frequency (from Okumura, 1968)

antennas. Since Okumura's curves give the median path loss
for all locations at a given distance and frequency, we have
averaged the path loss for all five urban and suburban 'runs'
described in Section 3.1 and in Figures 3.1.1-1 to 3.1.1-6.
The path loss averaged over all locations is shown in Figure
.-6 at the three test frequencies. Thus, we can see from
Fig. 3.3-6 that the average path loss at 446 MHz at a distance
of 1 km is 131 dB (or 45.6 dB above the free space loss).
From Okumura's curves we get that A_m = 17.8 dB, H_b = 27.2 dB
(by extrapolating curve for a = 1 Km to a base station antenna
height of 2 m), and H_m = -2.0 dB, so that the path loss pre-
dicted by Okumura's model is 47.0 dB above the free space
loss. Thus, our path loss curve at 446 MHz is well in agree-
ment with Okumura's prediction. At frequencies below 150 MHz,
the curves of Okumura give a constant attenuation above the
e space loss. This implies that the path loss decreases
with the square of the frequency (see Eq. (3.1.1-2)), or in dB
at a rate of 20 dB/decade, so that the difference in path loss
at 400 MHz and 40 MHz is 20 dB. Our results do not exhibit
such marked frequency dependence but a rather weak one. The
reason for the discrepancy is the difference in antenna heights
' ween our measurements and those of Okumura. When the base
station antenna height is much greater than the wavelength
(as is the case in Okumura's curves) and the distance is short
enough, the path loss is more likely to be equal to the free
space loss plus some additional diffraction loss due to the
presence of buildings around the receiving (mobile) antenna.
However, as the base station antenna height decreases to a
height below that of the immediate surroundings, then there
is likely to be more than one diffraction path between the
base station and the receiving antenna resulting in a path
loss which exhibits weak frequency dependence and a 40 dB/
c ade increase in path loss with distance as exhibited by
our measurements.
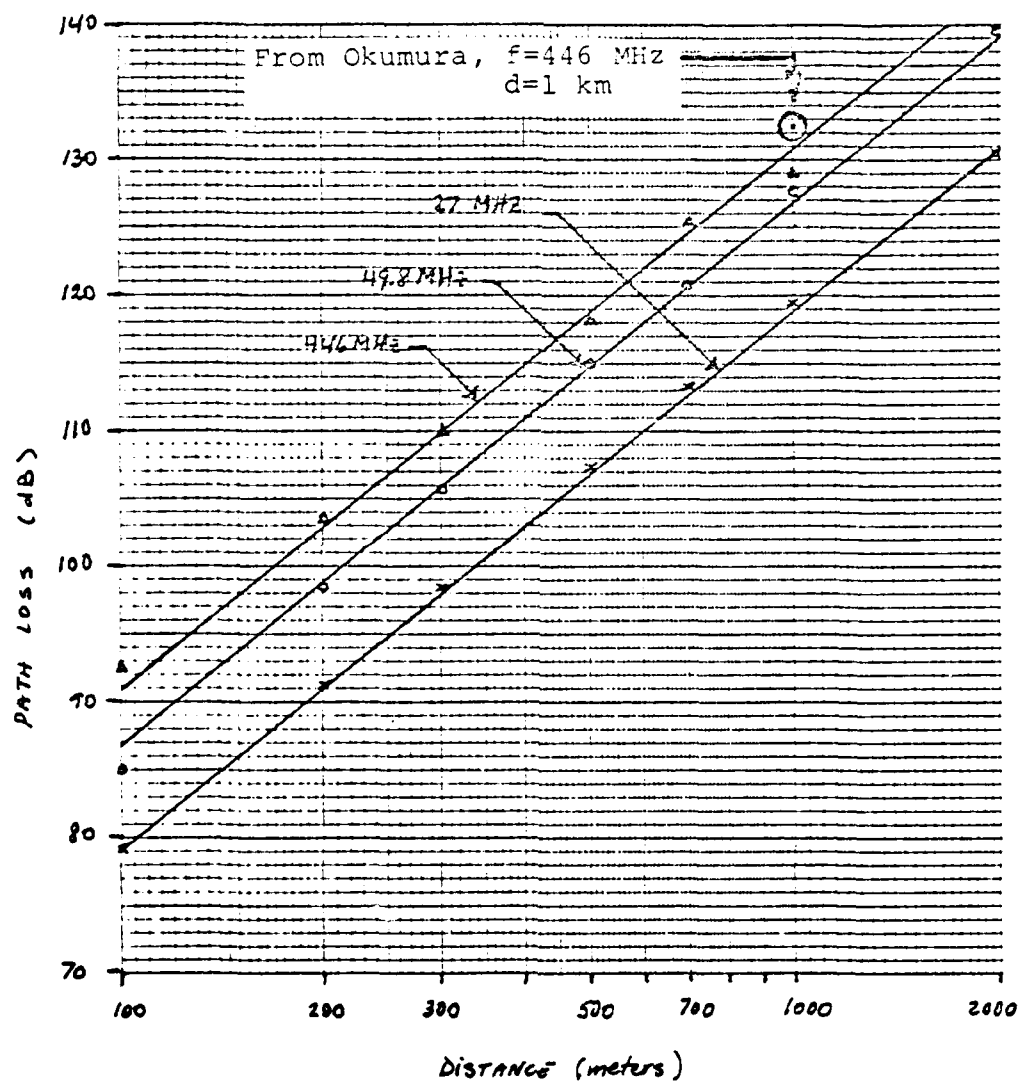
FIGURE 3.3-6   SIGNATRON Data for the Average Path Loss
at 27 MHz, 49.8 MHz, and 446 MHz in Built-
up Areas

3-87

From these arguments, we have concluded that the path
loss in urban and suburban areas between low elevation antennas
is better approximated by the formula

$$L = L_p(d) + L_D(f) - H_t(h_t,f) - H_r(h_r,f) \qquad (3.3-2)$$

$$+ K_{u,s}(f,d) + L_B(f)$$

where all quantities are in dB and,

$L_p(d)$ is the plane-earth path loss between two
antennas each 2 m high and which is defined
by Eq. (3.1.1-1).

$L_D(f)$ is an environmental clutter factor which
varies with frequency and accounts for the
average effect of the buildings and trees.
Our estimate of this factor from our data is
shown in Fig. 3.3-7.

$H_t(h_t,f)$ and $H_r(h_r,f)$ are the transmitting and receiving
antenna height gain factors expressed in dB
relative to 2 meter transmitting and receiving
antenna heights, h_t and h_r respectively.
These factors also depend on the frequency
and are shown in Fig. 3.3-8.

$K_{u,s}(f,d)$ is a highly-built-up area (urban) or medium-
built-up area (suburban or along street urban
transmission) correction factor. The highly-
built-up area correction factor K_u is inde-
pendent of frequency but varies depending on
whether both the transmit and receive location
are on a sidewalk or not. The medium-built-up
area correction factor K_s also applies to the
case of transmission along urban streets and
varies with frequency. These correction factors
have been obtained from our data and are shown
in Fig. 3.3-9.
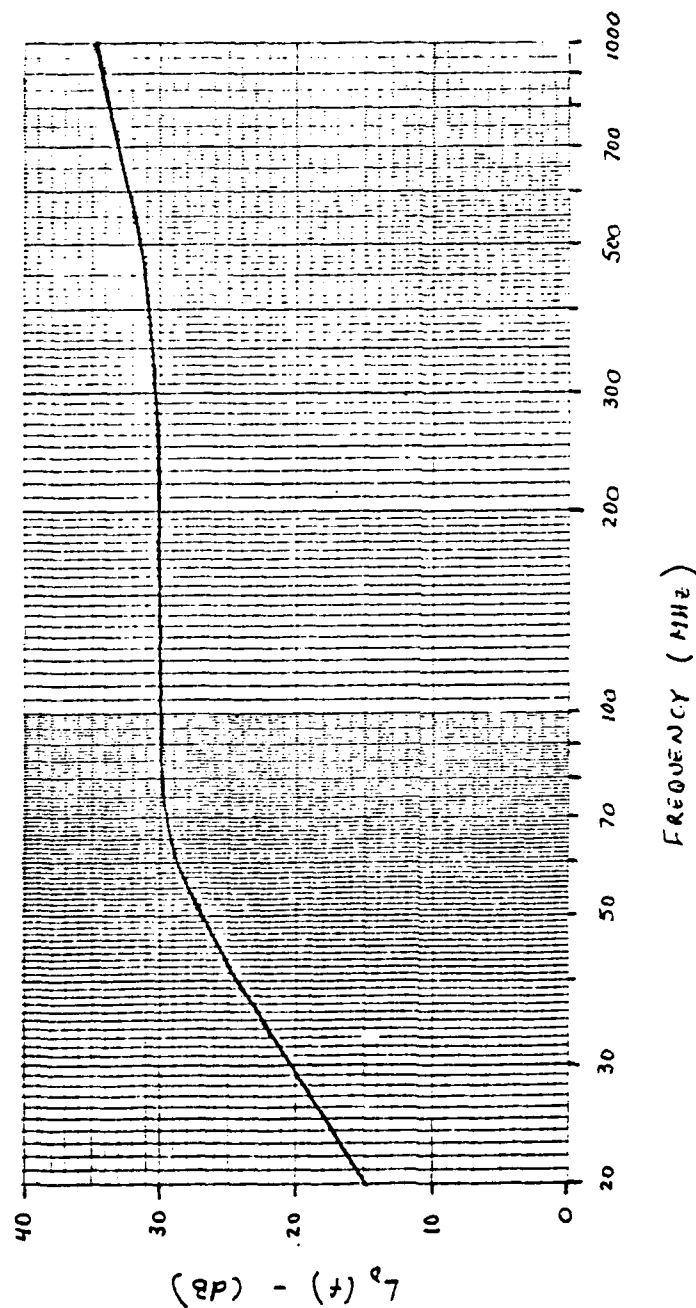
FIGURE 3.3-7 Environmental Clutter Factor for VHF and UHF Propagation
in Built-up Areas (Poorly Conducting Soil) and for
Antenna Heights of 2 Meters (from SIGNATRON Data)
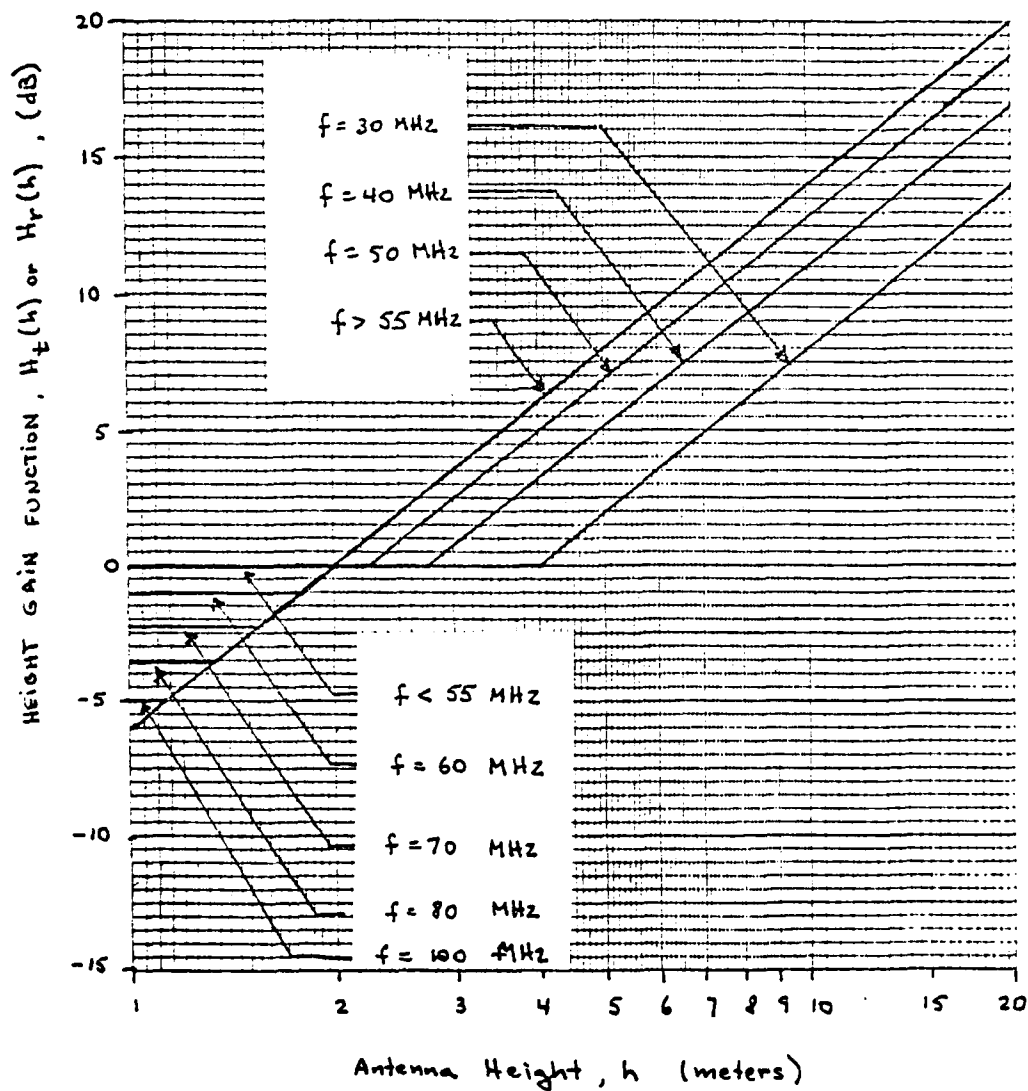
FIGURE 3.3-8 Height Gain Function Relative to 2 Meters
vs. Antenna Height for Various Frequencies
in Built-up Areas (Poorly Conducting Soil)
(from Bullington, 1957)
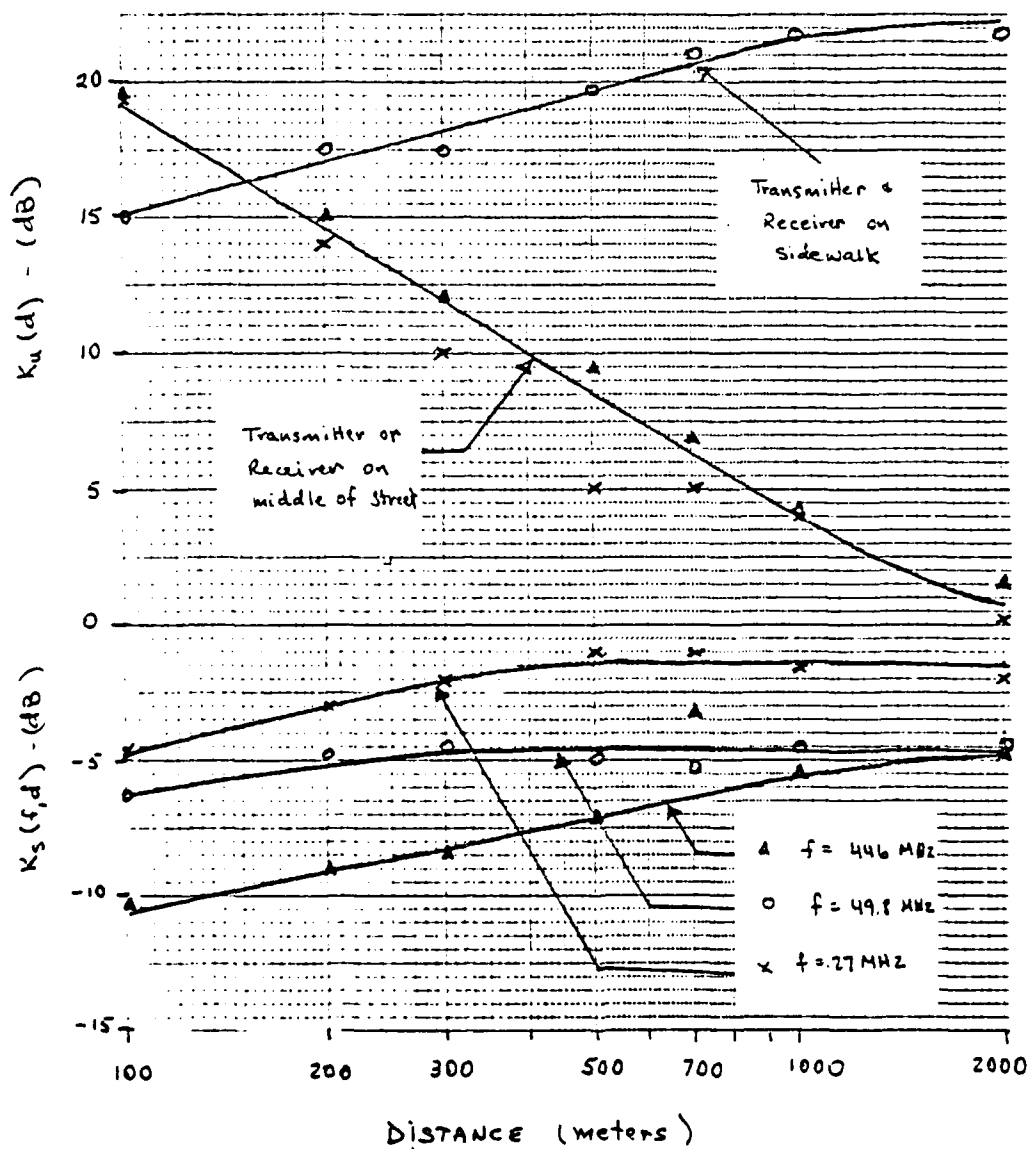
FIGURE 3.3-9 Urban (K_u) and Suburban (K_s) Correction Factors
(from SIGNATRON Data)

$L_B(f)$ is a correction factor for the case in which the transmitter or receiver is located inside a building and accounts for the building penetration loss. It varies with frequency and is given by Eq. (3.1.2-1) when the transmitter (or receiver) is in a basement; Eq. (3.1.2-2) when it is in an above-ground floor but not near a window; and by Eq. (3.1.3-3) when it is in an above-ground floor close to a window.

The distance dependence of the path loss is essentially the plane earth path loss, $L_p(d)$, which is 40 dB/decade with some minor corrections introduced by the urban and suburban correction factors, K_u and K_s respectively. The basic path loss above the plane-earth loss has been derived from the data in Fig. 3.3-6 and is given by the environmental clutter factor, $L_D(f)$. This factor is seen to be constant (30 dB) in the 70 to 300 MHz range. Above 300 MHz, it increases at a 10 dB/ decade rate because at these frequencies the terrain variations, tree heights, and mean building heights in the area become much larger than the wavelength and diffraction due to these obstacles becomes significant. At frequencies below 60 MHz, the clutter factor decreases significantly with frequency. The reason for this effect is that at these frequencies there is a surface or ground wave which propagates along the ground and whose attenuation increases with frequency. At lower VHF and lower frequencies, this wave is stronger (or less attenuated) than the waves diffracted over and around buildings. This is the main reason for the difference in the path losses at 27 MHz, 49.8 MHz, and 446 MHz shown by Fig. 3.3-6. The effects of changing the antenna height are determined from Fig. 3.3-8. These curves have not been derived from our data but we have used theoretical considerations as well as the data of Okumura to determine them. The height gain is basically 20 dB/decade and is the same as that exhibited by the plane

earth path loss (theoretical consideration). The frequency dependence is due to the presence of the surface or ground wave and its height gain effects have been discussed in a previous report [Ehrman and Parl, 1977]. Finally, the urban and suburban correction factors have been derived from our data and account for the difference in the path losses encountered between the three urban and two suburban paths where we made our measurements. The suburban correction factor also applies to urban paths where both transmitter and receiver are on a radial distance along the same street. The urban correction factor applies to the case where both transmitter and receiver are surrounded by structures (buildings) many wavelengths high. At lower VHF, this condition implies that the buildings must be on the average at least 5 to 6 stories high, where as at lower UHF the buildings need only average two to three stories for the condition to be met. Thus, this condition may also be met by some suburban areas at lower UHF. This model is very much similar to that proposed by Allsebrook and Parsons [1977] but it is more complete in the sense that it includes correction factors for the different environments. A more detailed discussion of the Allsebrook-Parsons model is given in the literature update presented in Section 4.

As a last remark, it should be added that these prediction curves only apply when both antenna heights are below the top of the buildings and other structures in the area. Thus, a practical limit to the antenna height is 10 to 20 meters. When one of the antenna heights is greater than this limit, the curves of Okumura may be extrapolated to obtain a prediction of the path loss.

3.4   Summary

Summarizing the results presented in this section, we have analyzed the data presented in Section 2 and determined the path or transmission loss (in dB) for the various types

of propagation conditions investigated. The path or transmission
loss was determined by obtaining a least-squares-fit to the
received signal data (in dBm) and then subtracting the effects
of the antenna gains and transmitted power. In addition to the
th or transmission loss, we also have done a correlation
analysis of the data and determined the field correlation co-
efficient (whip vs. loop correlation) at 27 MHz and 49.8 MHz as
well as the spatial correlation coefficient at 49.8 MHz (at
distances of 3 m and 4.5 m) and at 446 MHz (at distances of
50 cm and 100 cm).

The path losses for each of the street-to-street pro-
pagation paths tested are given in Figures 3.1.1-1 through
3.1.1-6. These path loss curves exhibit the following features:

- The path loss for the various locations tested
  exhibits distance dependence ranging from 20 dB/
  decade to 47 dB/decade. The distance dependence
  for the average path loss (over all locations)
  is 40 dB/decade at the three test frequencies
  (see Figure 3.3-6).

- The path loss in general increases with frequency
  at all locations tested. The difference between
  path losses at 27 MHz and 49.8 MHz ranges from
  2 to 12 dB, with the average path loss difference
  being 8 dB (Fig. 3.3-6). Similarly, the difference
  between the path losses at 27 MHz and 446 MHz
  ranges from 3 to 27 dB, with the average path
  loss difference being 12 dB. The difference
  between path losses at 49.8 MHz ranges from 0 to
  27.5 dB, with the average path loss difference
  being 4 dB (Fig. 3.3-6 and Fig. 3.3-7).

3-94

- The difference in path loss between a medium-built-up area and a highly-built-up area ranges from 2.5 to 30 dB with the smallest difference occurring at distances greater than 1 Km and the largest at distances less than 100 meters (see Fig. 3.3-9).

- When both transmitter and receiver are in a highly-built-up area and are surrounded by tall buildings, the path loss can be up to 20 dB greater if both transmitter and receiver are on the sidewalk (i.e., near a high wall) rather than if either transmitter or receiver is moved away from the wall to the middle of the street (see Fig. 3.3-9).

- Raising the antenna height above the ground results in a decrease in the path loss. The height gain is 6 dB/octave (i.e., 20 dB/decade) as shown in Fig. 3.3-8.

- All these trends and effects have been used in deriving a path loss prediction model in Section 3.3.

The transmission losses for the street-to-building measurements are given in Figures 3.1.2-1 and 3.1.2-2. The difference between the transmission loss curves and the free space loss in dB is defined as the building penetration loss. The following conclusions about the penetration losses are reached from these curves:

- The building penetration losses in general decrease as the frequency increases. However, since the free space loss increases with frequency, the total street-to-building transmission loss has a minimum at a frequency estimated to be around 50 MHz.

3-95

- The building penetration losses vary from floor to floor (i.e., receiver floor location) in a random manner so that no height gain (decrease in the penetration loss as the receiver floor level increases) is observed.

- The street-to-basement penetration loss in a concrete wall building is 67.5 dB at 27 MHz, 58 dB at 49.8 MHz, and 52 dB at 446 MHz.

- The street-to-above-ground-floor penetration loss in a concrete wall building ranges from 54 dB to 80 dB at 27 MHz, from 54 dB to 68 dB at 49.8 MHz, and from 38 to 48 dB at 446 MHz.

- The building penetration loss is greater the farther the receiver is inside the building.

- For a building with outer cinder block walls and inner gypsum walls, the penetration loss is 61 dB at 27 MHz, 44 to 48 dB at 49.8 MHz, and 40 to 58 dB at 446 MHz. The rate of increase in the path loss as the receiver location inside the building is farther away from the transmitter is 0 dB/decade at 27 MHz (i.e., there is no additional loss due to inside walls), 20 dB/decade at 49.8 MHz, and 80 dB/decade at 446 MHz.

The transmission losses for the building-to-building measurements are given in Figures 3.1.3-1 and 3.1.3-2. Defining the two-building penetration loss as the difference between the building-to-building transmission loss and the free space loss in dB, we reach the following conclusions:

- The two-building penetration loss exhibits no height dependence, i.e., on the average it is independent of the difference in floor levels at the transmitting and receiving ends.

- The two-building penetration loss ranges from 57.5 to 86 dB at 27 MHz, from 65 to 77 dB at 49.8 MHz, and from 58 to 64.5 dB at 446 MHz.

- Since the transmit location in one of the buildings was near a window we can get an estimate of the (one building) penetration loss when the receiver (or transmitter) is near a window by subtracting the (one) building penetration loss (for the concrete wall building) from the two-building penetration loss. We find that it ranges from 4 to 32 dB at 27 MHz, from 1 to 15 dB at 49.8 MHz, and from 10 to 25 dB at 446 MHz.

The transmission losses for the various intrabuilding measurements are given in Figures 3.1.4-1 to 3.1.4-7. From these curves we reach the following conclusions:

- The transmission loss (in dB) along corridors varies linearly with distance. The rate of increase in the transmission loss with distance varies with the dimensions of the corridor, whether the corridor is straight or not, the material composition of the corridor walls, and also the transmission frequency.

- The transmission losses for various corridors at 27 MHz and at a distance of 20 meters are: 108 dB for a corridor with one turn (at a distance of 15 meters) and gypsum walls, 84 dB for a straight corridor with gypsum walls, 70 dB for a corridor with a turn (at a distance of 10 meters) and cinder

block walls, and 64 dB for a straight corridor with cinder block walls.

● The transmission losses and the loss rate decrease with frequency when the corridor has one or more turns. However, the converse is true when the corridor is straight. Comparing the transmission losses at a distance of 20 meters for a straight corridor (A) and a winding corridor (B), both with cinder block walls, we find: a transmission loss of 64.5 dB for corridor A and 70 dB for corridor B at 27 MHz; a transmission loss of 63 dB for corridor A and 68.1 dB for corridor B at 49.8 MHz; and a transmission loss of 51.8 dB for corridor A and 82.5 dB for corridor B at 446 MHz. At longer distances the transmission loss increases at the following rates: 6.9 dB/10 meters in corridor A and 8.3 dB/10 meters in corridor B at 27 MHz; 6.9 dB/10 meters in corridor A and 9.8 dB/10 meters in corridor B at 49.8 MHz; and 5.4 dB/10 meters in corridor A and 10.2 dB/10 meters in corridor B at 446 MHz.

● The transmission loss (in dB) between above-ground floors increases linearly with the log of the number of floors transmitted through. The loss due to transmission through one floor is 83 dB at 27 and 49.8 MHz and 88 dB at 446 MHz. For transmissions through a greater number of floors, the transmission loss increases at a rate of 51.3 dB/decade at 27 MHz, 25.5 dB/decade at 49.8 MHz, and 30.2 dB/decade at 446 MHz, where a decade is a ten-fold increase in the number of floors transmitted through.

- The transmission loss (in dB) between above-ground floors and the basement also increases linearly with the log of the number of floors transmitted through. The loss due to transmission from the first floor to the basement is 77 dB at 27 MHz, 83 dB at 49.8 MHz, and 82 dB at 446 MHz. For transmissions to or from higher floors, the transmission loss increases at a rate of 56 dB/decade at 27 MHz, 44.5 dB/decade at 49.8 MHz, and 50 dB/decade at 446 MHz. These rates are higher than those for transmissions between above-ground floors.

- The transmission loss (in dB) in stairwells increases linearly with the log of the number of floors transmitted through. The loss due to transmission from one floor to the next in the stairwell is 40 dB at 27 MHz, 45.6 dB at 49.8 MHz, and 59.4 dB at 446 MHz. These losses are about half of the transmission loss through one floor at VHF and two thirds at UHF. For transmissions to or from higher floors, the loss increases at a rate of 60 dB/decade at 27 MHz, 27.5 dB/decade at 49.8 MHz, and 38 dB/decade at 446 MHz. Surprisingly, the loss rates are higher for transmission in stairwells compared to transmissions through the floors.

- The transmission loss between floors and near elevator shafts increases linearly with the number of floors transmitted through at VHF (i.e., 27 MHz and 49.8 MHz) and linearly with the log of the number of floors transmitted through at UHF (446 MHz). The loss due to transmission through one floor is 64.4 dB at 27 MHz, 73.3 at 49.8 MHz, and 52 dB at

3-99

446 MHz. For transmission through a greater number
of floors, the loss increases at a rate of 3.4 dB/
floor at 27 MHz, 4.3 dB/floor at 49.8 MHz, and
52.6 dB/decade (ten-fold increase in number of
floors) at 446 MHz.

● Thus we conclude that transmissions between floors
are best when both transmitter and receiver are in
a stairwell and worst if neither transmitter nor
receiver is near a stairwell or an elevator shaft.

Having summarized the results of our path or transmission
loss analysis, we now give the results of our correlation analysis.
The correlation analysis is divided into field correlation (whip
vs. loop receiving antenna correlation or equivalently E-Field
vs. H-Field correlation) analysis at 27 MHz and 49.8 MHz, and
spatial correlation analysis at 49.8 MHz and 446 MHz.

The field correlation coefficients for the various types
of propagation conditions tested for are given in Tables 3.2-1
through 3.2-4. From these we conclude the following:

● The field correlation coefficient in urban and sub-
urban street-to-street propagation has an average
value of .74 at 27 MHz and .61 at 49.8 MHz.

● In the case of street-to-building propagation,
the field correlation coefficient has an average
value of .79 at 27 MHz and .87 at 49.8 MHz.

● For the building-to-building propagation measure-
ments the average value of the field correlation
coefficient is .63 at 27 MHz and .48 at 49.8 MHz.

● The lowest field correlation coefficients are those
of the intrabuilding propagation measurements
which have an average value of .39 at 27 MHz and
.65 at 49.8 MHz.

The spatial correlation coefficients for the various types of propagation are given in Tables 3.2-5 through 3.2-11. From these tables, we conclude the following:

- In the case of the street-to-street propagation measurements, the spatial correlation at 49.8 MHz has an average value of .35 for antennas 3 meters apart. At 446 MHz, the spatial correlation has an average value of .52 for antennas 50 cm apart and .27 for antennas 100 cm apart.

- In the case of the street-to-building propagation measurements, the spatial correlation of 446 MHz has an average value of .25 for antennas 50 cm apart and -.01 for antennas 100 cm apart.

- In the case of the building-to-building propagation measurements, the spatial correlation at 49.8 MHz for antennas 4.5 meters has an average value of .19. Similarly the spatial correlation at 446 MHz has an average of .33 for antennas 50 cm apart, and .20 for antennas 3.5 meters apart.

- Finally in the case of the intrabuilding measurements, the spatial correlation at 49.8 MHz for antennas 4.5 meters apart has an average value of .32. Similarly, the spatial correlation at 446 MHz has an average value of .29 for antennas 50 cm apart and .20 for antennas 100 cm apart.

The correlation coefficients yielded by the VHF measurements indicate that there is sufficient decorrelation between the E-Field and H-Field components of the received signal to warrant the implementation of a field diversity VHF receiving system. Similarly, the spatial correlation coefficients yielded by the UHF measurements warrant the implementation of a spatial diversity UHF receiving system. The gains that may be expected by implementing such systems are:

- Increase in the transmitter range by at least a factor of 1.4 and up to a factor of 1.8 times the range of a no-diversity system.

- And a reduction in the fade duration by a factor of 1.5 to 2 times that of a no-diversity system.

While no field diversity measurements were made at 446 MHz, we would expect that field diversity would also be applicable at UHF. As a 50 cm space-diversity antenna separation might be awkward for a manpack radio, a practical UHF diversity receiver might also be implemented using a loop antenna.

REFERENCES FOR SECTION 3

Allsebrook, K., J.D. Parsons (1977), "Mobile Radio Propagation
   in British Cities at Frequencies in the VHF and UHF
   bands", IEEE Trans. On Vehicular Tech., Vol. VT-26,
   No. 4, pp 313-323.

Blomquist, A., L. Ladell (1974), "Prediction and Calculation
   of Transmission Loss in Different Types of Terrain",
   NATO AGARD Conf. Publ. CP144, 1974, Research Institute
   of National Defense, Dep 3, S-10450, Stockholm 80,
   Sweden, pp 32/1-32/25.

Bullington, K. (1977), "Radio Propagation for Vehicular
   Communications", IEEE Trans. on Vehicular Tech., Vol.
   VT-26, No. 4, pp 295-308.

Clarke, R.H. (1968), "A Statistical Theory of Mobile Radio
   Reception", Bell Syst. Tech. J., V47, pp 957-1000.

Edwards, R., J. Durkin (1969), "Computer Prediction of
   Service Areas for VHF Mobile Radio Networks", Proc.
   IEEE, V. 116, No. 9, pp 1493-1500.

Egli, J.J. (1957), "Radio Propagation Above 40 Mc Over
   Irregular Terrain", Proc. IRE, Vol. 45, No. 10,
   pp 1387-1391.

Ehrman, L., S. Parl (1977), "Communications Data Base Analysis
   for Military Operations in a Built-up Area (MOBA/COBA)",
   Interim report, SIG. A-223 prepared for U.S. Army
   Research Office by SIGNATRON, Inc., Lexington, Mass.

Gans, M.J. (1972), "A Power-Spectral Theory of Propagation
   in the Mobile Radio Environment", IEEE Trans. on
   Vehicular Tech., Vol. VT-21, No. 1, pp 27-38.

Jakes, W.C. (1974), Microwave Mobile Communications, Wiley-
   Interscience, New York, 1974.

Longley, A.G. (1976), "Location Variability of Transmission
Loss - Land Mobile and Broadcast Systems", O.T. Report
76-87, U.S. Dept. of Commerce, Office of Telecommunications.

Okumura, Y., et al. (1968), "Field Strength and its Variability
in VHF and UHF Land Mobile Service", Rev. Elec. Commun.
Lab., Vol. 16, pp 825-873.

Papoulis, A. (1965), Probability, Random Variables, and
Stochastic Processes, McGraw-Hill, Inc., New York, 1965.

SECTION 4
MOBA/COBA DATA - BASE UPDATE

4.0 Introduction

This section is basically independent from Sections 2 and 3. However, the topics covered are related to the MOBA/ COBA communications problem and together with the VHF/UHF propagation measurements and the data-base analysis performed in a previous report [Ehrman and Parl, 1977] present a complete picture of the present state of VHF/UHF communications in built-up areas and the potential for improvement.

The topics covered are diverse and have been divided into three sub-sections: Section 4.1 is a summary of a series of meetings held with European researchers during the week of October 24 - October 31, 1978 with the purpose of incorporating their findings into the MOBA/COBA data-base; Section 4.2 summarizes the recent work which has appeared in the literature (since our previous report) and which is related to the problem at hand; and Section 4.3 is concerned with the design of an active loop antenna for the implementation of a VHF field diversity system.

Among the recently published work are the results of propagation measurements made in British cities by a group of British workers [Allsebrook and Parsons, 1977] at frequencies in the VHF and UHF range using medium elevation antennas (20 to 50 meters). Their measurements exhibit the same distance dependence as ours (inverse fourth power law) and further reinforce our prediction model. In addition we also report on some man-made (ignition) noise measurements made by the same group of workers [Parsons and Sheikh, 1978]. The other work reported on deals with the analysis of the performance of

a two-branch equal-gain combining diversity receiver (as opposed to selection diversity) with applications to mobile communications [Lee, 1978].

Our active antenna work was motivated in part by the success which a group of German scientists have had in applying _ to mobile diversity (spatial) reception [Flachenecker, 1978]. But the most important reason is that an active loop antenna offers several advantages over a multi-turn loop (MTL) antenna. One is that active antennas in general can be designed to be very broadband (and thus require no tuning) while a multi-turn loop antenna is inherently very narrow band and requires automatic tuning. The automatic tuning makes the multi-turn loop antenna extremely bulky and heavy for use with man-pack radios. This further emphasizes another advantage of an active antenna, namely its low profile (much less than a quarter wave antenna) d small size and weight.

4.1 MOBA Communications Meetings with European Researchers

4.1.1 Introduction

The measurements reported in Section 2 and analyzed in Section 3 as well as our Interim Report, Communications Data se Analysis for Military Operations in a Built-up Area (MOBA/COBA) by Dr. L. Ehrman and Dr. H. Parl (Report A068.1, 9 Dec 1977), have been part of an effort to improve the knowledge of urban communications. In addition, contacts have been made with European researchers in this field, in order to incorporate their findings into the data base. In October 1978, Dr. Leonard Ehrman of SIGNATRON met with researchers in Great Britain, Sweden, and Germany to discuss their latest researches.

The remainder of this section documents visits made to four research groups.

4.1.2 Summary of Results

Visits were made to four organizations. The principal contact, and the name of each organization, follows:

1. Dr. P. R. M. Whittlestone
    T1 Division
    Royal Signals and Radar Establishment
    Malverne, Worcs., England

2. Mr. J. D. Parsons
    Department of Electronics and Electrical
                Engineering
    The University of Birmingham
    P.O. Box 363
    Birmingham B15 2TT England

3. Mr. Gösta Carlson
    National Defense Research Institute
    Department 3
    Communications Laboratory
    Box 1165
    581 11 Linköping, Sweden

4. Dr. G. Flachenecker
    Hoshschule der Bundeswehr Munchen
    Fachbereich Elektrotechnic,
                Hochfrequenztechnik
    Werner-Heisenberg-Weg 39
    8014 Neubiberg
    Munich, Germany

All of the experiments which have been performed in Europe show that the received signal level (RSL) in an urban environment follows an inverse fourth-power distance law, i.e., if the transmitter-receiver separation doubles, the RSL decreases by $1/2^4$, or by 12 dB. They also have found that over small areas the received signal will fade, with the envelope having a Rayleigh probability distribution. The Birmingham and Munich groups are both working on diversity combiners for use with mobile radios, as they believe diversity is a practical and inexpensive means of improving performance in Rayleigh fading. The Swedish researchers are not working on diversity at this time, although they are well aware of it.

The researchers at Birmingham, NDRI Linköping, and Munich all believe tactical VHF communications utilizing low height, low power radios would be extremely range limited in an urban environment. All of these, plus RSRE, consider UHF would be unusable due to range limitations.

RSRE takes the viewpoint that tactical urban radio communications can be maintained by one of two means. The first would employ elevated antennas, with field wire being used to connect a remotely located user's hand set to the radio; all the British VHF and UHF radios are designed for this mode of operation. The second means is to employ HF, instead of VHF, in urban communications. RSRE considers groundwave propagation in the low HF band (1.5 - 5 MHz) to be suited for short range MOBA use, although it might be excessively noisy. At this low a frequency, however, they expect there would be little or no fading, hich might be a mitigating factor. RSRE considers the high HF band (20 - 30 MHz), to be an alternative, although the frequency usage would have to vary diurnally with the MUF.

All researchers agree that care should be used in extrapolating either U.S. or European measurements to a MOUT (Military ᐤperations in Urban Terrain) environment. All consider auto-ᴡobiles and other vehicular traffic to be the prime source of VHF RF noise. European cities are considered to have a noise level 10 to 20 dB below U.S. cities, but military vehicles are claimed to produce significantly more radio noise than do civilian vehicles. In addition, it is expected that in a battle environment there will be a significant amount of both co-channel and adjacent-channel interference from other radio nets. As a result, urban range is expected to be reduced by factors of 2 or 4 below that measured in a peacetime environment.

Of the four groups listed above, only Dr. Flachenecker's is working in the field of active antennas. Active antenna research and development have been going on in Germany since the mid 1960's, and active whip antennas for cars are now commercially available products in Germany in both whip and windshield configurations. If active loop antennas were to be used with man-pack radios, as either low-profile receiving antennas or field diversity (H-field) antennas, a development effort would be required.

All of the groups visited are doing significant work, and liaison with their researchers should be maintained. With the exception of RSRE, all of the groups visited have mobile laboratories which they use for performing their propagation research, and recording their data. The experimental data are then reduced off-line on digital computers. The start-up expense is undoubtedly high, and software development is probably a never-ending project, but these facilities enable them to run large scale experiments in an efficient manner.

4.2 Literature Study

4.2.1 Allsebrook-Parsons VHF/UHF Path Loss Prediction Model

A path loss prediction model for VHF and UHF propagation in urban areas has recently been proposed by Allsebrook and Parsons [1977]. The model is based on measurements of the received signal envelope magnitude at frequencies of 85 MHz, 167 MHz, and 441 MHz. In all cases, unmodulated carrier waves were radiated from antennas atop tall buildings or prominent terrain features and detected using a vehicle mounted receiver. The effective height of the antennas at the three frequencies were 35 m, 20 m, and 50 m above local ground for the cities of Birmingham, Bath, and Bradford, England, respectively.

The path loss prediction model proposed by Allsebrook and Parsons is based on the following equation for the path loss in dB:

$$L = L_F(f,d) + \{[L_p(h_t,h_r,d) - L_F(f,d)]^2 + L_{DF}^2\}^{1/2}$$

$$+ L_{FC} + \gamma(f) \qquad (4.2-1)$$

where all quantities are in dB

$L_F(f,d)$ is the free-space loss as defined by Eq. (3.1.1-2).

$L_p(h_t,h_r,d)$ is the plane-earth path loss which depends on the transmitting and receiving antenna height and range and is given by Eq. (3.1.1-1).

L_{DF} is the diffraction loss over terrain obstacles such as ridges and hills.

L_{FC} is the flat-city correction factor which accounts for the loss due to diffraction over the buildings nearest to the receiver.

$\gamma(f)$ is a UHF correction factor to L_{FC} and is plotted in Figure 4.2-1.

From the definition of the path loss, L, we see that the terms $L_f + \{\ldots\}^{1/2}$ in (4.2-1) represent a modified loss for hilly terrain where the modification to the free-space loss, L_F, is the rms value of the loss due to a ground reflection, i.e., $L_p - L_F$, and the loss due to diffraction over terrain obstacles such as mountains or ridges, L_{DF}.

When the terrain is relatively flat compared to the heights of the buildings, L_{DF} is negligible and (4.2-1) reduces to

4-6
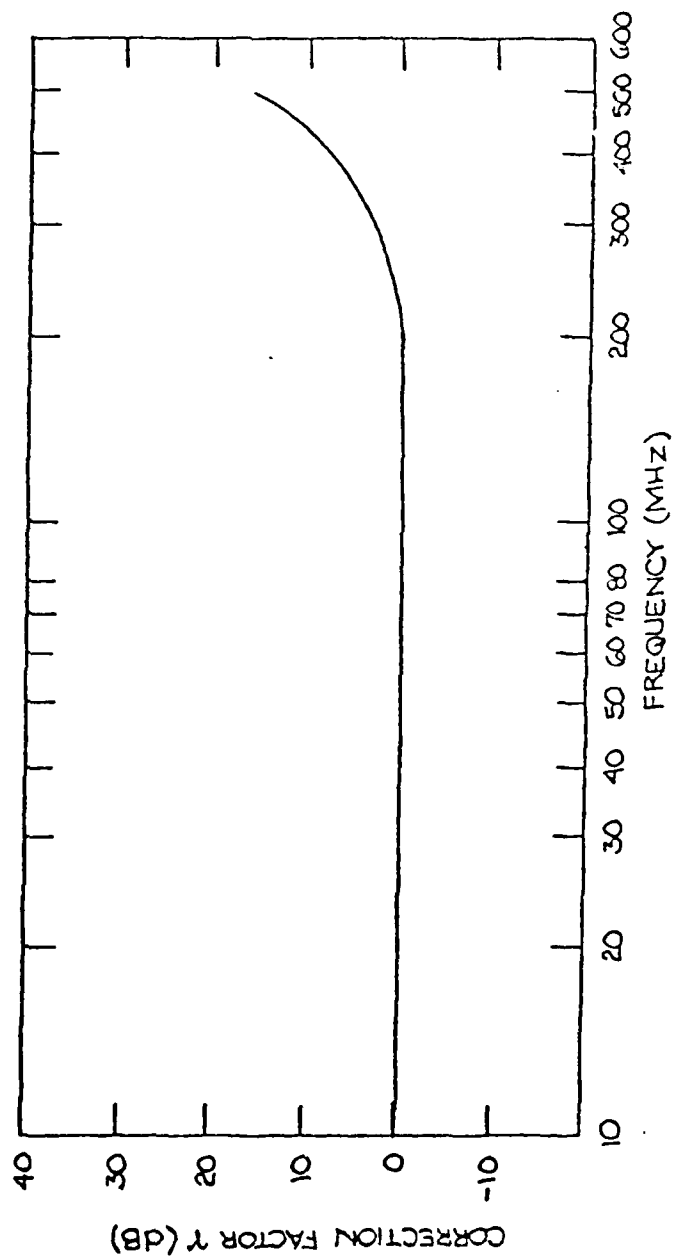
FIGURE 4.2-1 UHF Correction Factor (γ) (from Allsebrook and Parsons)

$$L = L_p(h_t, h_r, d) + L_{FC} + \gamma(f) \qquad (4.2-2)$$

which Allsebrook and Parsons [1977] refer to as the flat-city model as opposed to the hilly-city prediction model described by (4.2-1).

Note that the flat-city model is similar to the model which we have proposed (Eq. (3.3-2)) if we set the Allsebrook-Parsons correction factors, $L_{FC} + \gamma$, equal to urban clutter correction factor, L_D, proposed by us. The flat-city correction factor proposed by Allsebrook and Parsons [1977] is based on single-knife-edge diffraction theory, so that

$$L_{FC} = 20 \log_{10} \left(2\pi \frac{h_o - h_r}{\sqrt{\lambda d_o}} \right) \qquad (4.2-3)$$

where d_o is the distance from the closest building to the mobile receiver and h_o is the height of the building. This was found to be a good approximation to the excess loss above free-space loss at the two VHF frequencies but not at the UHF frequency, probably as a result of ignoring the thickness of the buildings, which at UHF is many wavelengths.

The flat-city correction factor defined in (4.2-3) was appropriate for the Allsebrook-Parsons measurements because their transmitting (base-station) antennas were mounted on roof tops so that the only significant obstacles were those nearest to the receiver. However, when the height of the transmitting antenna is well below the top of the buildings, the single-knife-edge diffraction theory may not be appropriate, at least if h_o and d_o are taken to be the actual height and istance to the nearest obstacle. Our factor, $K_{us}(f,d)$ is an empirical term which implicitly includes the parameters

of importance in L_{FC}, but is more oriented to the use of man-pack radios with low elevation antennas than is L_{FC}.

4.2.2 Man-Made Noise in Urban and Suburban Areas at 80 MHz

The results of man-made noise measurements in British urban and suburban areas at a frequency in the low VHF band ave recently appeared in a report by J.D. Parsons and A.U.H. Sheikh [1978]. The sources of the noise measured were primarily vehicle ignition noise and to a lesser extent power line noise and industrial noise. In order to fully characterize the noise, experiments were conducted to measure the following four parameters:

a. Amplitude Probability Distribution (APD)
b. Average Crossing Rate (ACR) at various threshold levels.
c. Time of Arrival Statistics or Pulse Interval Distribution (PID)
d. Pulse Width Distribution (PWD).

Measurements of these four parameters in a 20 kHz bandwidth are presented in graphical form for different locations (streets) typical of British urban and suburban areas: New Street (urban); Bristol Road South (suburban); an expressway 5; and other locations. We have reproduced these results in Figures 4.2-2 through 4.2-13. These curves and others given in the original report indicate that both traffic density (in the units of vehicles/minute) and traffic pattern (stop and go city driving vs. expressway traffic) have an effect on the shape of the Amplitude Probability Distribution (APD) curve as well as Average Crossing Rate (ACR). The high probability (background) noise levels range from a few dB above thermal kT_oB) in light traffic to as much as 20 dB above thermal in ....avy urban (New Street) traffic. The low probability, high ....plitude, impulsive (ignition) noise occurs at lower noise ....els the heavier the traffic as one might expect.
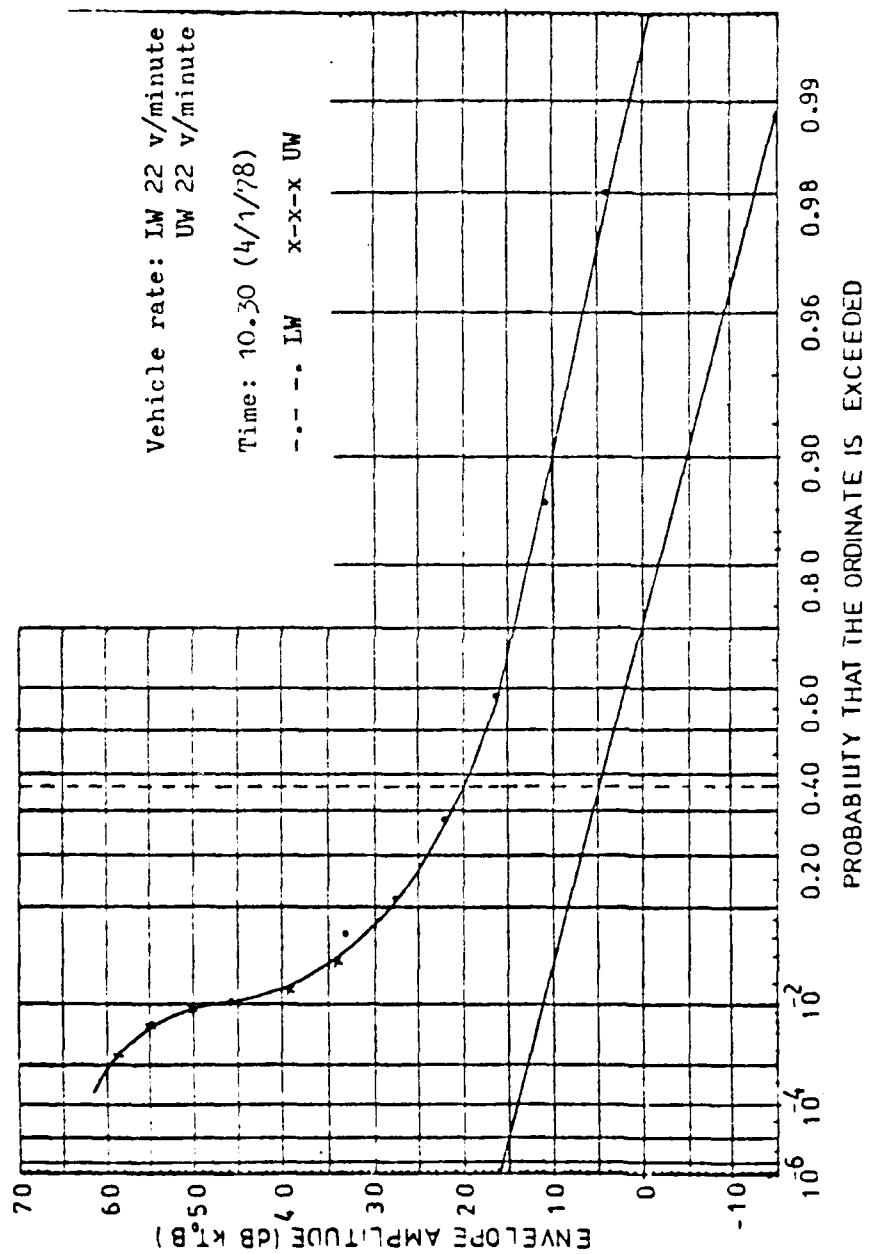
FIGURE 4.2-2 APD for New Street
Bandwidth 20 kHz

Time: 10.30 (4/1/78)

ENVELOPE AMPLITUDE (dBκ_TB)

AVERAGE NUMBER OF CROSSINGS PER SECOND

60 50 40 30 20 10 0

10   100   1000   10000   100000
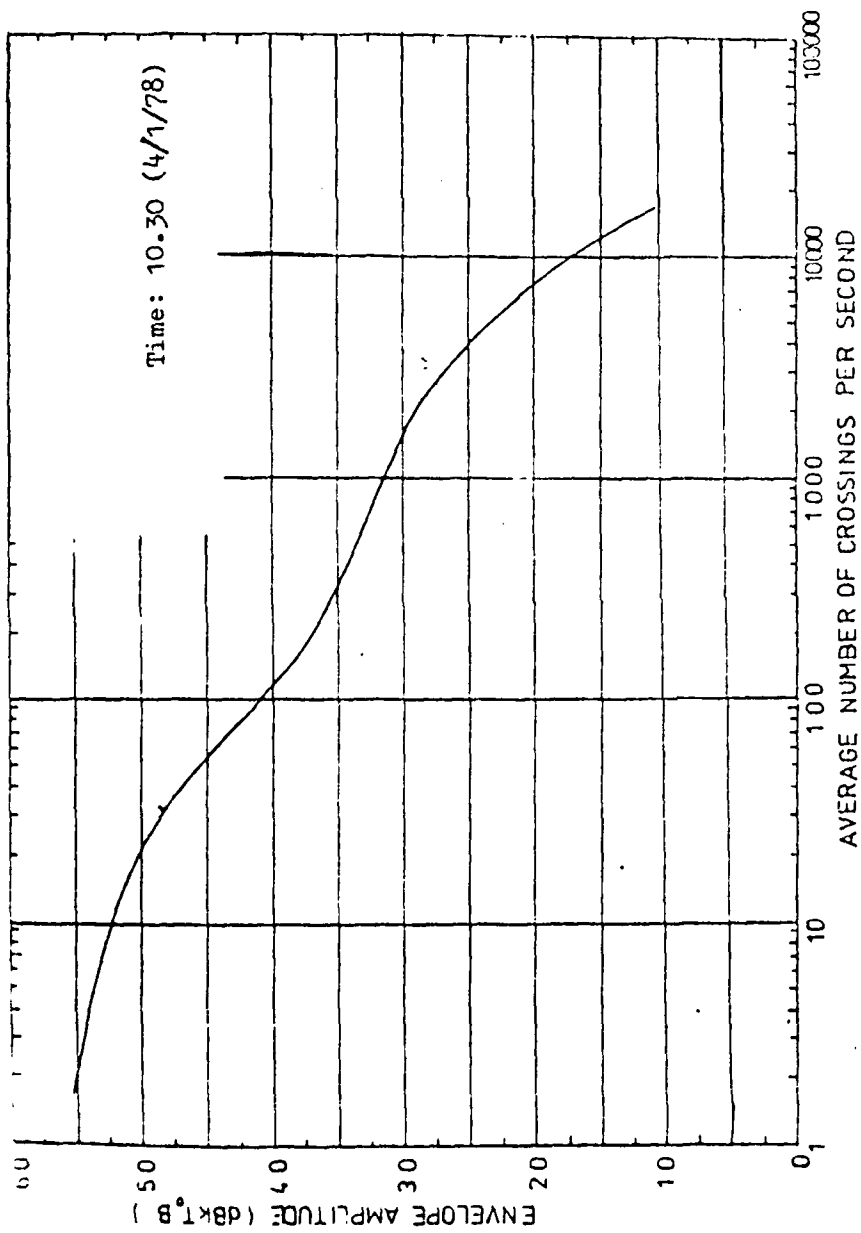
FIGURE 4.2-3   ACR for New Street
Bandwidth 20 kHz

Time: 10.30 (4/1/78)

—·—·—	11dB	—o—o—	20dB
—·—·—	30dB	—x—x—	40dB
—△—△—	50dB	————	55dB

(thresholds measured with respect to kT_oB)

PROBABILITY THAT ORDINATE IS EXCEEDED

PULSE WIDTH (µsec)

0.99 0.98 0.96 0.9 0.8 0.7 0.5 0.3 0.1 10^2 10^1

1000   100   10   1   0.1   0.01

10^{-6}
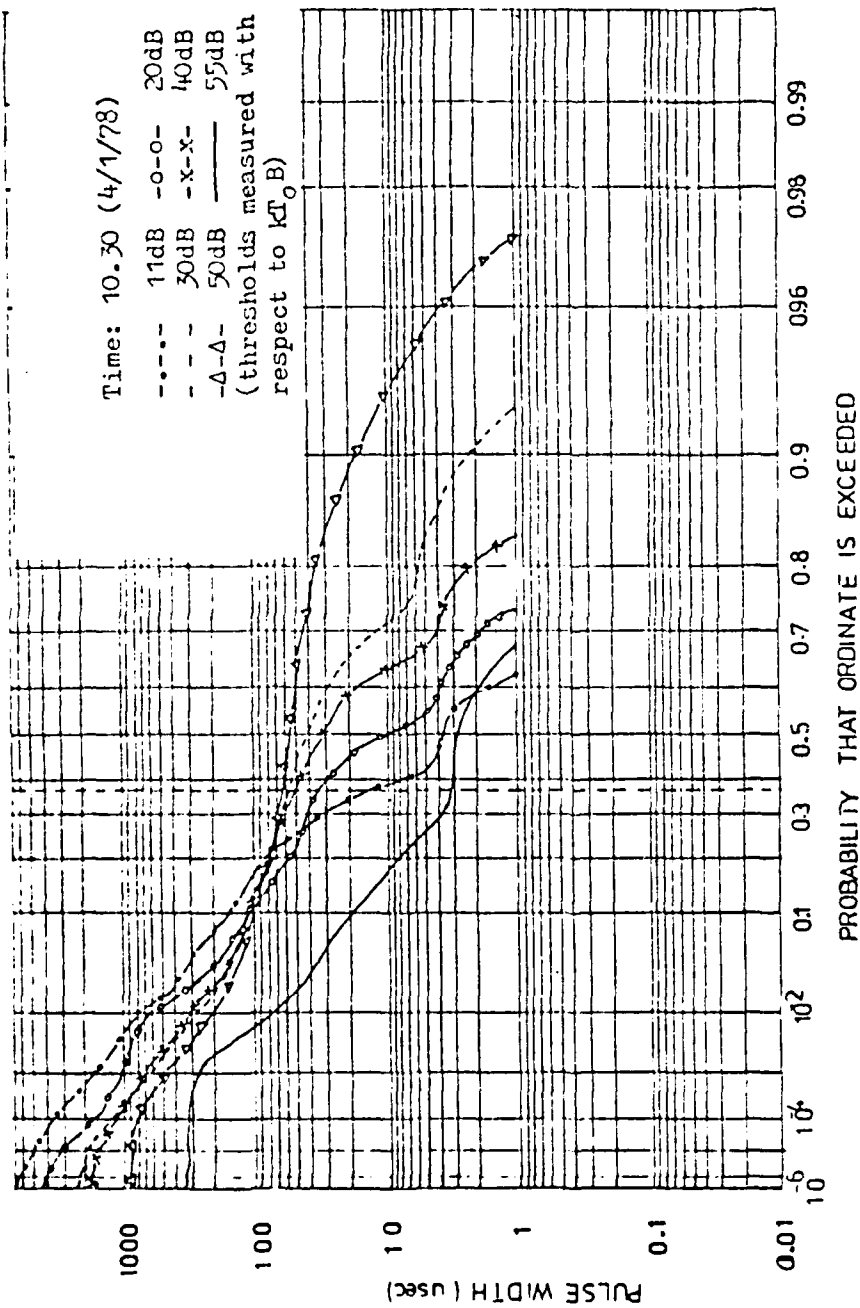
FIGURE 4.2-4   PWD for New Street
Bandwidth 20 kHz
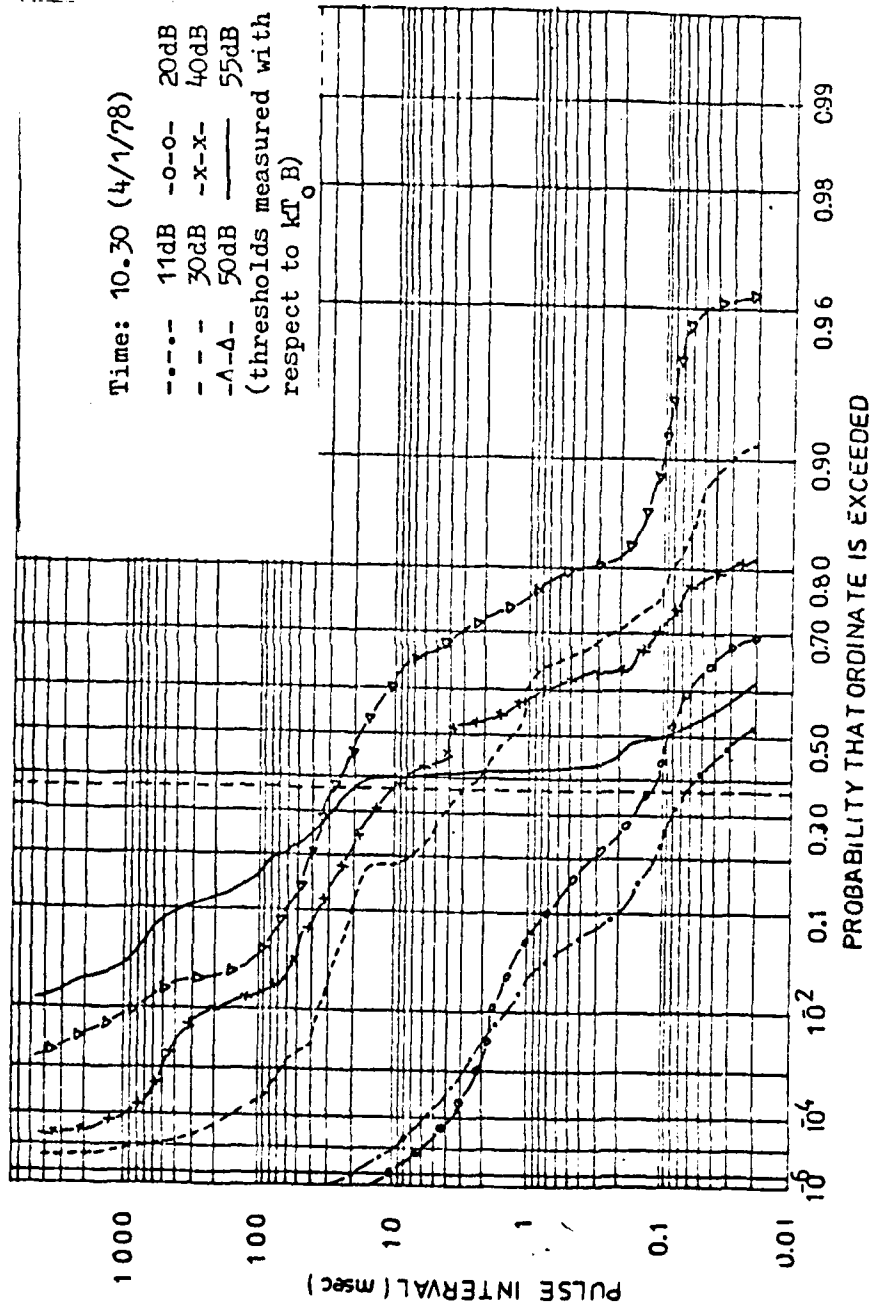
FIGURE 4.2-5   PID for New Street
Bandwidth 20 kHz

Vehicle rate: LW 17 v/minute
UW 17 v/minute

Time: 10.30 (6/1/78)

-.-.-. LW   -x-x-x UW

ENVELOPE AMPLITUDE (dB kT₀B)

70 60 50 40 30 20 10 0 -10

10⁻⁶ 10⁻⁴ 10⁻²

0.20 0.40 0.60 0.80 0.90 0.96 0.98 0.99

PROBABILITY THAT THE ORDINATE IS EXCEEDED
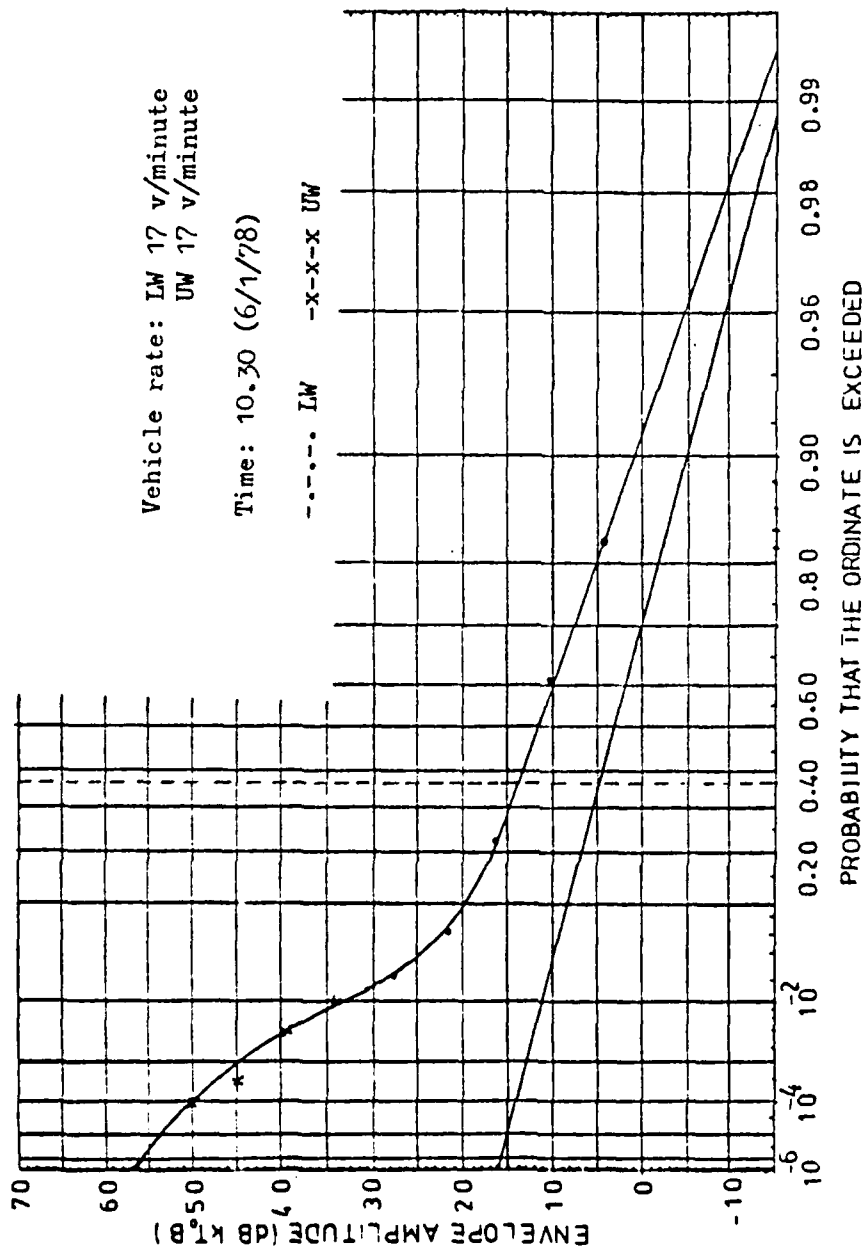
FIGURE 4.2-6   APD for Bristol Road South
Bandwidth 20 kHz
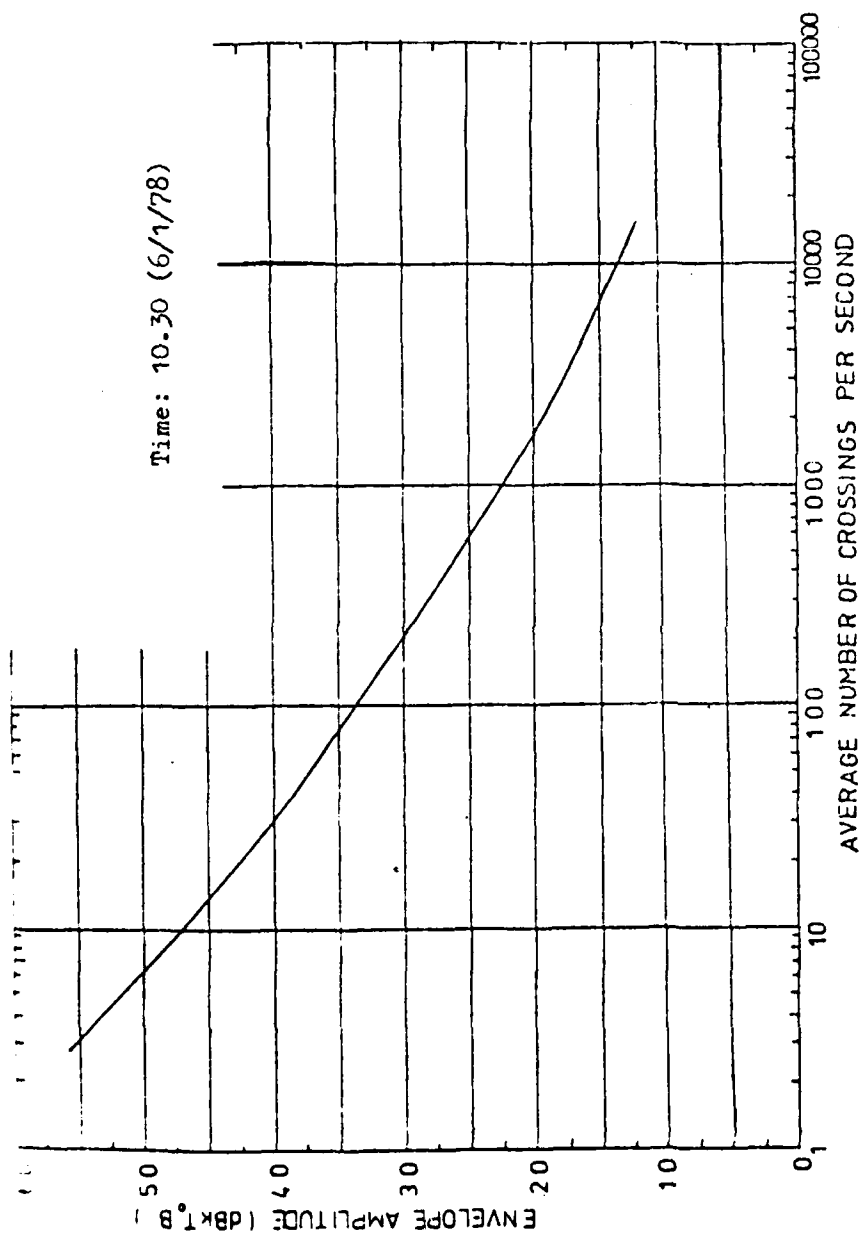
FIGURE 4.2-7   ACR for Bristol Road South
Bandwidth 20 kHz
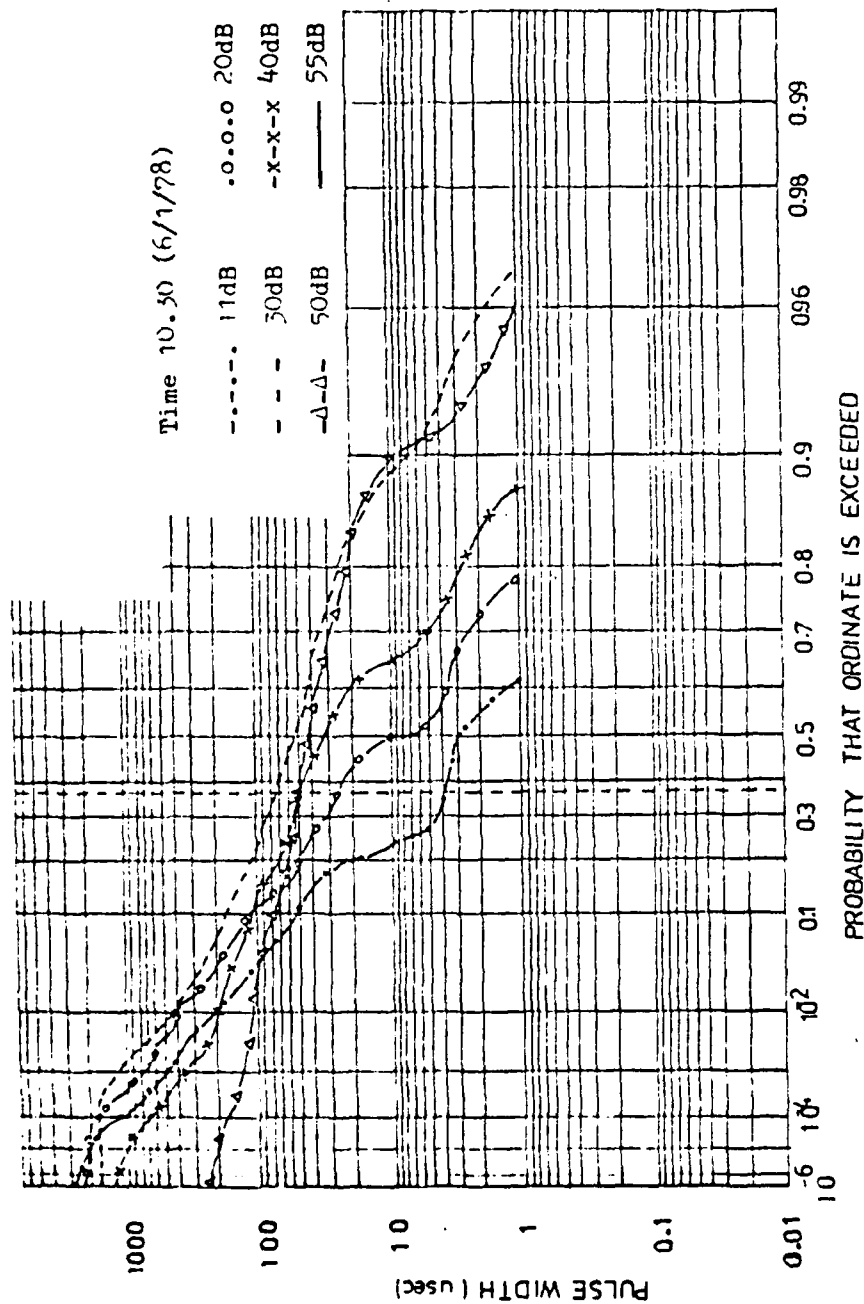
FIGURE 4.2-8 PWD for Bristol Road South
Bandwidth 20 kHz
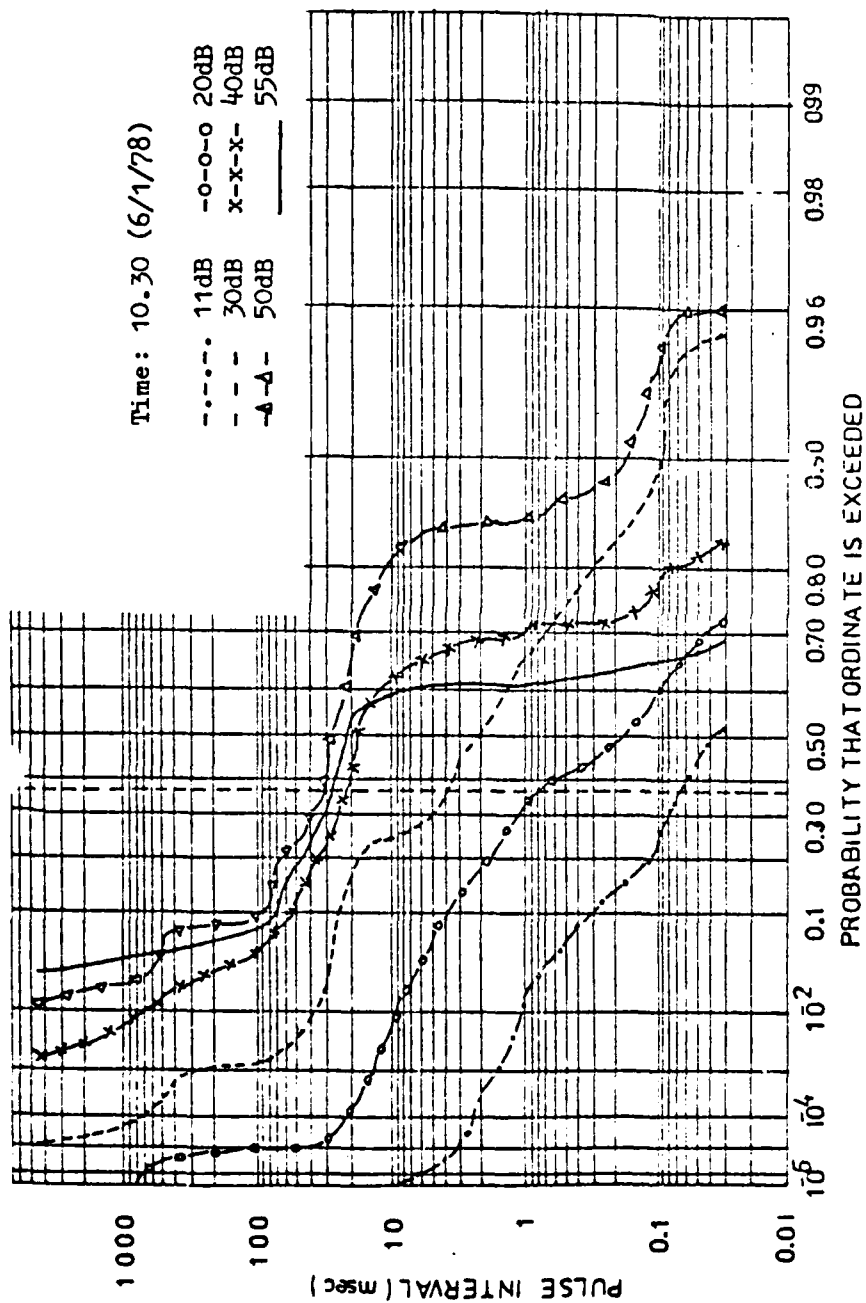
FIGURE 4.2-9 PID for Bristol Road South
Bandwidth 20 kHz
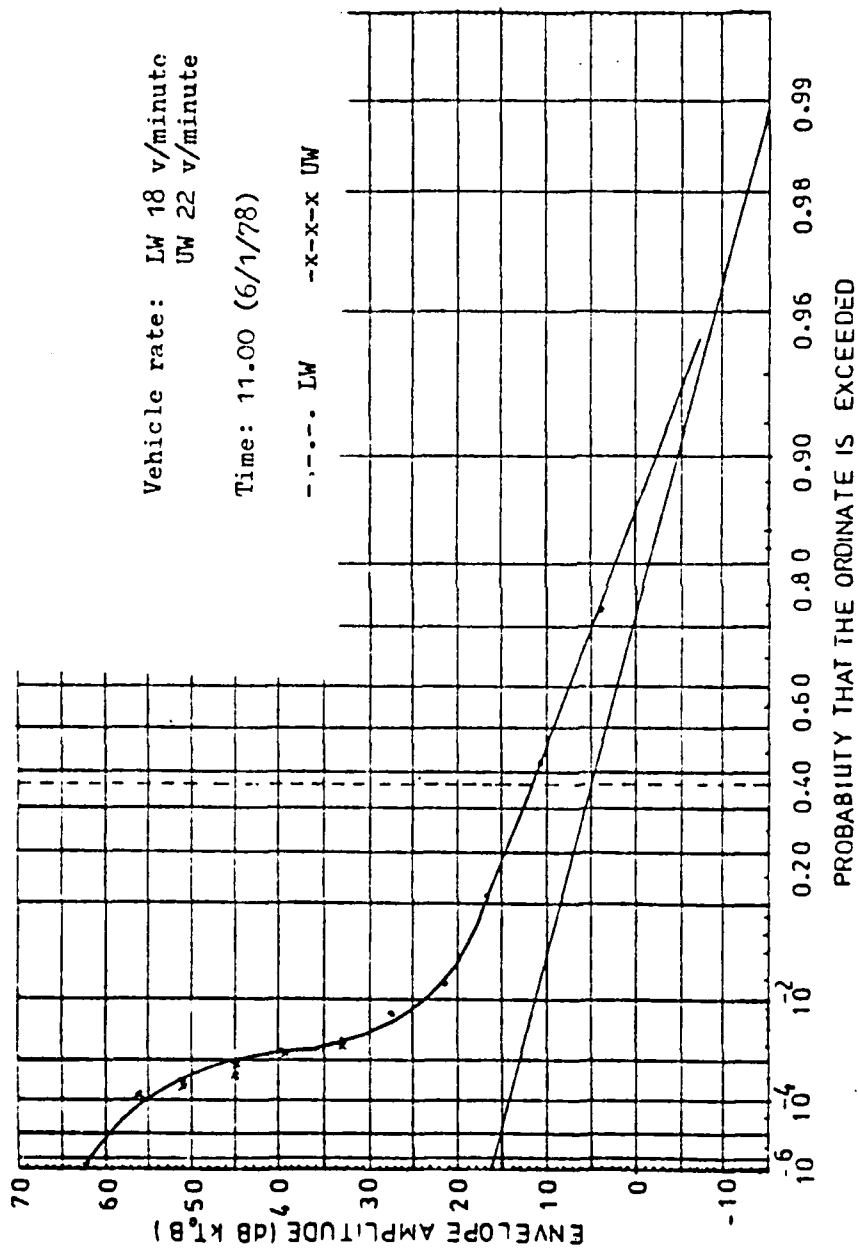
FIGURE 4.2-10 APD For M5
Bandwidth 20 kHz
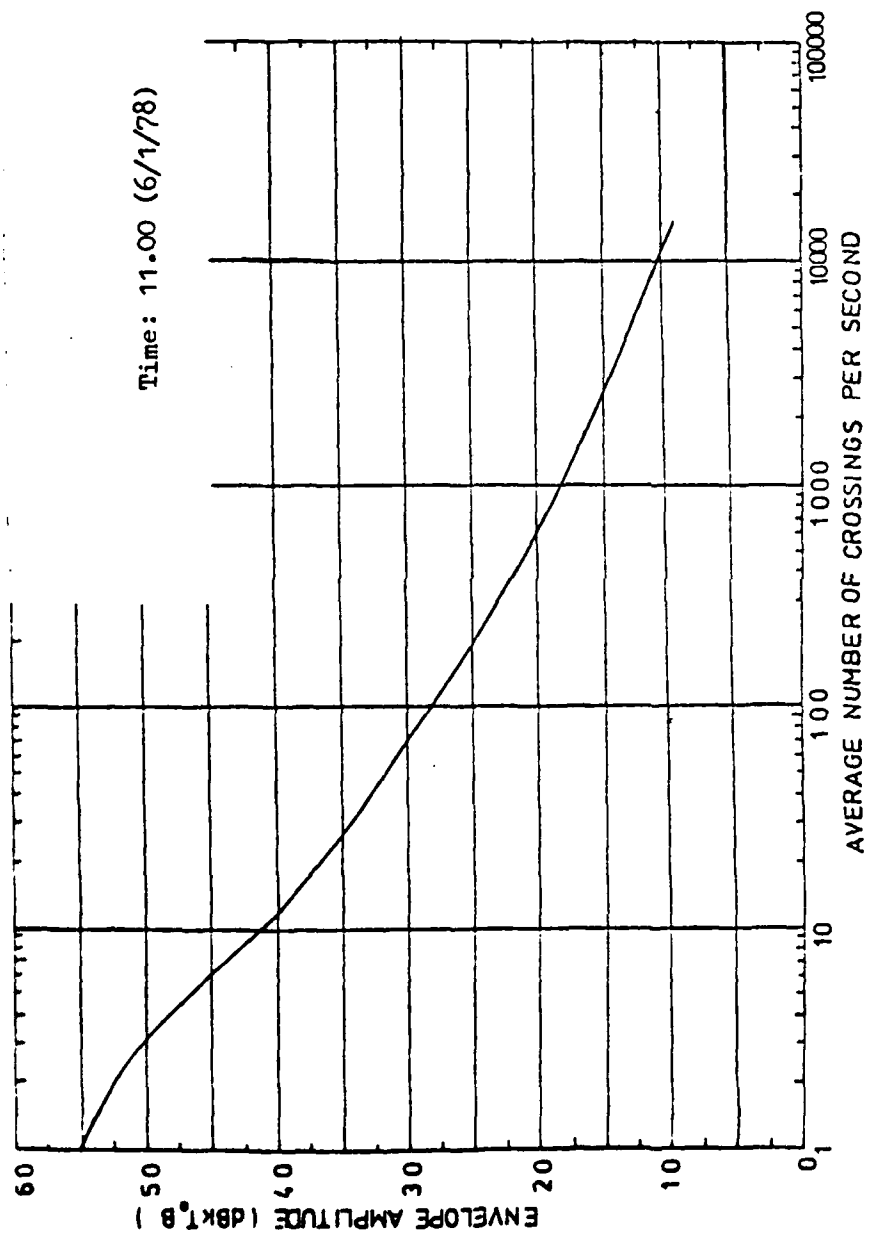
FIGURE 4.2-11   ACR for M5
Bandwidth 20 kHz
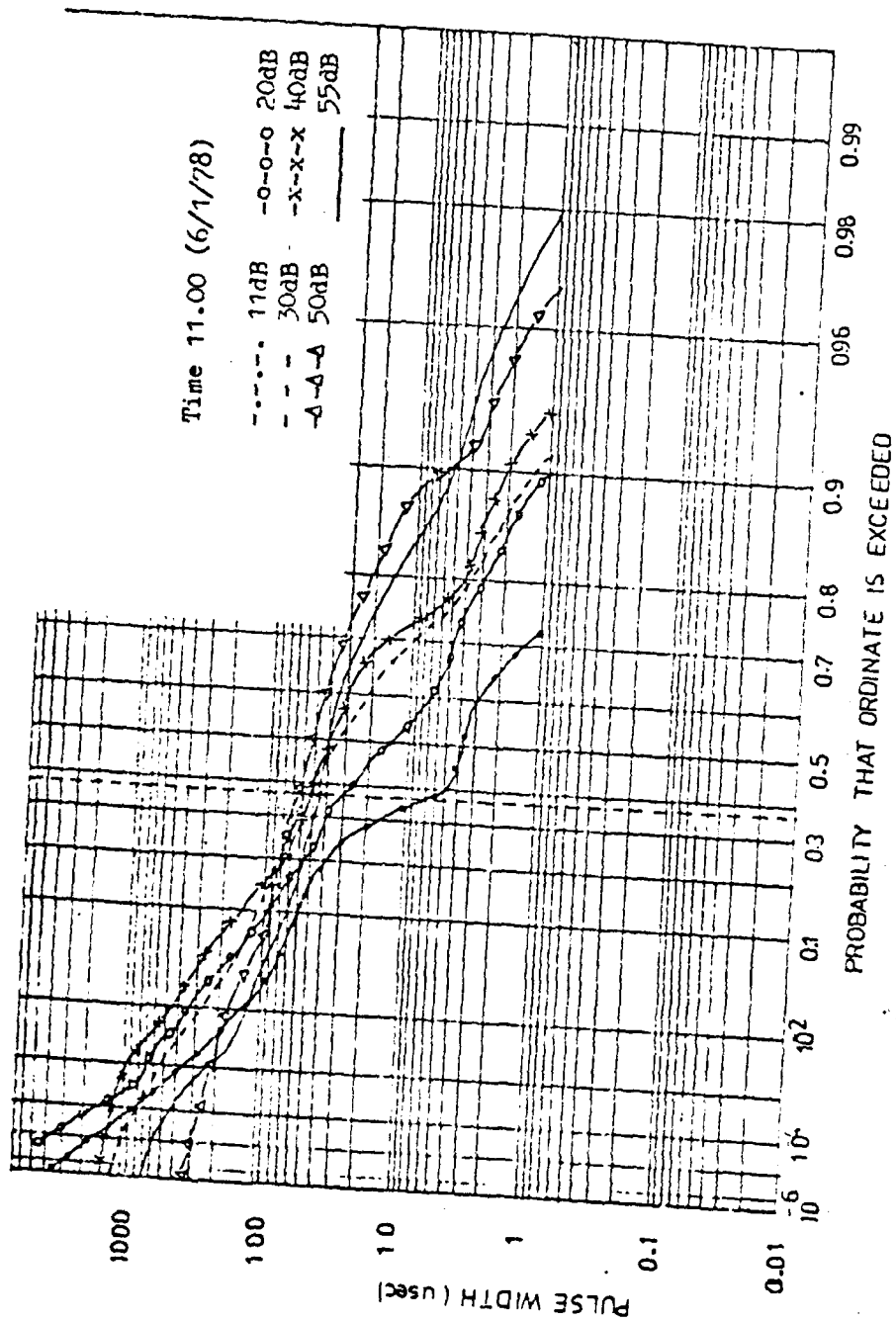
FIGURE 4.2-12 PWD for M5
Bandwidth 20 kHz

4-21
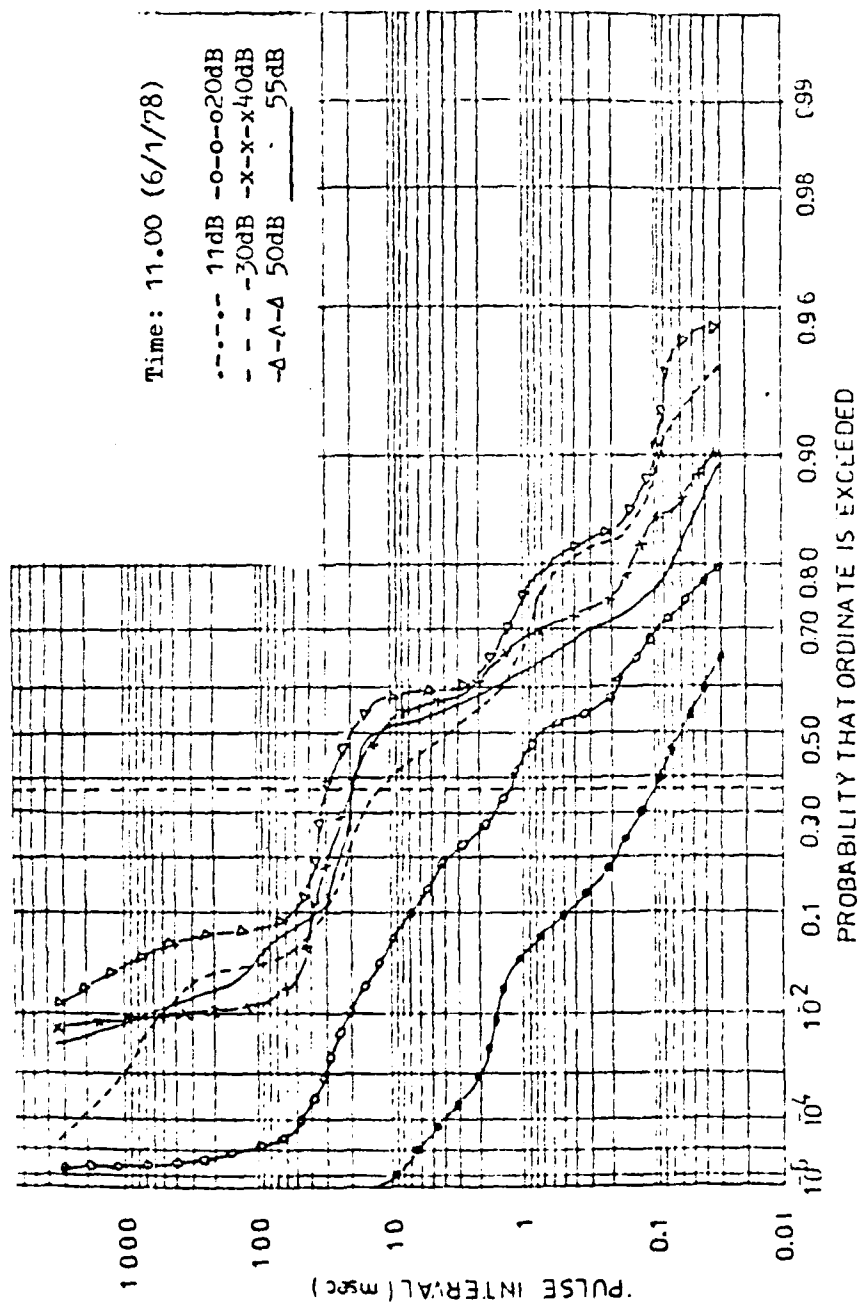
FIGURE 4.2-13   PID for M5
Bandwidth 20 kHz

The pulse width distributions show the spread of pulse-widths which occur at any threshold level. The important point on the vertical axis is 50 μsecs, which represents the reciprocal of the post-detector bandwidth (20 kHz). If there were no overlapping of noise impulses, then pulse widths greater than 50 μsecs would not occur, and the extent of their occurrence is a measure of the amount of overlapping which exists. The pulse interval distributions (PID) also indicate the existence of overlapping noise impulses by the fact that the PID's for different levels cross each other.

Although these measurements were made at a single frequency, 80 MHz, we may extrapolate the median noise level (i.e., APD $\leq$ 50%) by using the following empirically derived frequency dependence of man-made noise in the Birmingham, England, area [Bailey, 1976]:

$$N = 67 - 28 \log_{10} f \qquad (4.2-4)$$

where the units of N are dB above kT_oB and f is the measurement frequency in MHz. At 80 MHz, the median level for all locations is about 13.7 dB above kT_oB. The values predicted by (4.2-4) are about 10 dB lower than those measured in the USA [CCIR, 1974].

4.2.3 Two-Branch Equal Gain Diversity Combining Receiver

The theoretical performance of a two-branch equal gain diversity combining receiver with correlated signals has recently been described in the literature [Lee, 1978]. The performance is analyzed from the cumulative probability distributions of the output of the diversity combiner as well as the level crossing rates and duration of the fades. Lee shows that the probability that the instantaneous carrier-to-noise ratio, γ, at the output of a two branch equal-gain combiner is below the threshold level, x, in a pure Rayleigh fading

4-23

environment is given by

$$P(\gamma \le x) \simeq 1 + \frac{(1- \sqrt{\rho})e^{-2ax/\Gamma} - (1+ \sqrt{\rho})e^{-2bx/\Gamma}}{2 \sqrt{\rho}} \qquad (4.2\text{-}5)$$

where Γ is the average carrier-to-noise ratio in each branch, ρ is the correlation between the two branches, and a and b are constants which vary with ρ. Figure 4.2-14 shows how the diversity gain of the two-branch combined signal varies as a function of the correlation between the two branches. These curves, when compared with those we have derived for a two-branch selection diversity combiner (Figure 3.3-1), show that the equal-gain combiner is slightly superior to the selection combiner. For instance, for a desired performance level $P(\gamma \le x) = 10^{-2}$, the required average CNR with an equal gain combiner is 11.2 dB below that of a single channel receiver compared to 10.2 dB for a selection diversity receiver (from Figure 3.3-1) when the branches are uncorrelated ($\rho = 0$). This difference disappears as correlation increases. If the branches have correlation $\rho = .7$, then the diversity gain is 8.75 dB with an equal gain combiner, compared to 8.7 with a selection diversity combiner.
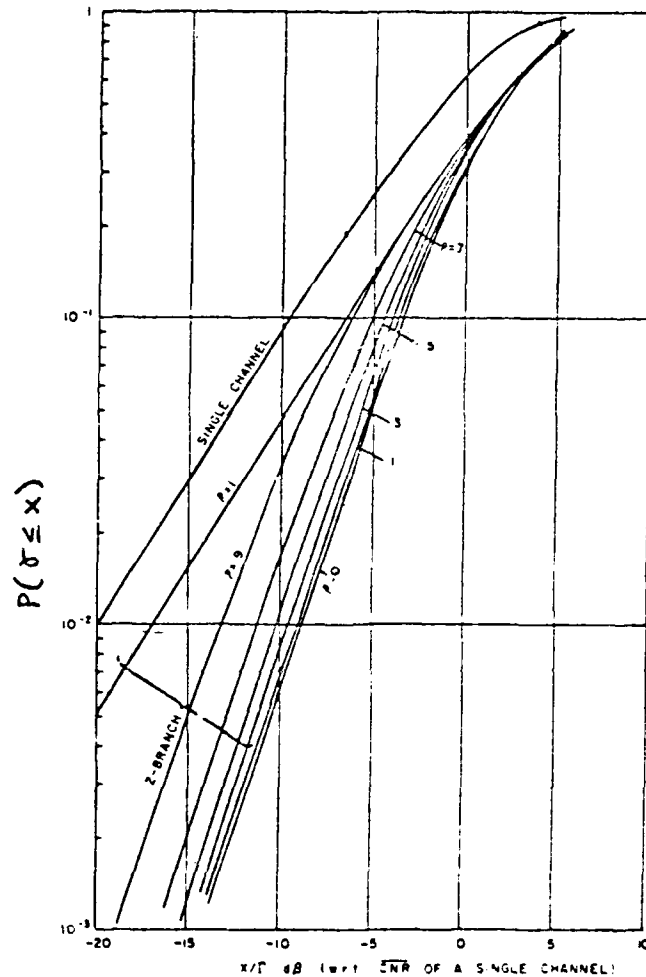
FIGURE 4.2-14   Cumulative Probabili* Distribution of a
                Two-Branch Equal-Gai   mbiner in Pure
                Rayleigh Fading [From Lᴄ , 1978]

4.3 Active Antenna for Field Diversity Implementation

4.3.1 Background and Scope

This analysis is intended to support the design, construction, and testing of an active loop antenna. Together with the existing design for a vertical whip antenna, the active loop could be used to implement a prototype diversity receiver for mobile communication in the 30 to 80 MHz portion of the VHF band.

Appendix IV contains the initial investigation of the subject of active antennas. It gives a broad overview of their published properties and summarizes in a systematic manner the rationale motivating their use and the salient features of the performance parameters. The two major areas of application that were encountered and the principal features of active antenna performance are:

- ### Single Element (Receive Only)

    By integrating the antenna directly into the matching network of the preamplifier transistor, ohmic losses, system noise temperature, and gain loss are minimized as are the detuning effects encountered when attempting to achieve inherently narrowband matching to a 50 or 75 ohm cable that connects to a remote preamplifier. System signal-to-noise ratio and bandwidth are major performance parameters. The unilateral property of the transistor provides decoupling of the antenna from the feed line. This is important at frequencies when the antenna is electrically small and is parameterized by the improved match (Γ_{in}) and bandwidth achieved by the transistor resulting in the active antenna.

- <u>Array</u>

Active antennas reduce mutual coupling effects in transmit and receive arrays because of the reverse isolation or unilateral buffering the transistor can provide as an active device. Increased bandwidth and improved impedance matching as well as improved SNR for receive only applications are realized and are the quantitative measure of performance. Because of the unilateral property, distinct active antenna designs and elements are required for transmit and receive. Receive only applications appear to have been the area of most interest.

In this report, the factors pertinent to the single receive only element are addressed to a level of detail approaching that which is necessary for the design of an active loop antenna. Specific items are:

- Preliminary Transistor Selection

    Table 4.3-1 gives a preliminary summary of the bipolar - FET tradeoff considerations.

- Quantitative characterization of the S-parameters and noise figure for a specific transistor (2N5943).

- Quantitative characterization of the electrically small loop antenna for impedance, efficiency, and antenna noise temperature.

- Performance calculations for the transistor/loop

        Stability
        Gain
        Noise Figure and Noise Temperature
        System signal-to-noise ratio (SNR).

    The approach enables these parameters to be plotted as circular contours (overlayed) on the Smith Chart impedance coordinates. This facilitates the matching network specification and design as well as providing simple yet comprehensive display that accommodates a wide range of antenna and matching network variations.

Table 4.3-1

Preliminary Bipolar - FET Trade Off

VHF Active Loop Antenna

Transistor	Comment
Bipolar NPN 2N 5943	• Good Stability • Reasonable match to low impedance typical of loop • Good noise figure and low detuning sensitivity • Optimized for CATV band • Low intermodulation distortion
Bipolar NPN 2N 2857 2N 3039	• Well characterized S-Parameters and Noise Figure • Appears optimized for above 100 MHz • Poor stability and unilateral figure of merit below 100 MHz • High mismatch below 100 MHz
FET N channel Silicon Junction 2N 1823	• Very high input and output impedance requires significant matching • Low noise figure • Poor noise figure characterization

The analysis outlined above provides us with a well defined, repeatable, quantitative approach for the design of an active antenna. Modification for an active whip antenna would be straightforward. Active whip antennas for reception have been designed, tested, and produced [Meinke,1977] with attention given to optimal SNR. The analysis offered here for the performance calculations and the optimal design of the active loop is believed to be a new application. One prior investigation of active loops of which the authors are aware was restricted to impedance matching and power gain considerations [Ramsdale, 1971].

Design level topics that have not yet been addressed at this time are:

- Matching network design for the input and output circuits

- Measurement and instrumentation aspects of transistor/ matching network selection and design

  S-parameters (match and gain)

  Noise Figure

  Experimental Optimization.

- More comprehensive transistor selection.

The following numerical results and discussion are for a specific transistor which is the low noise, low power model (2N5439) given in the first entry of Table 4.3-1. Although some effort was expended to select a transistor with suitable characteristics for performance calculation purposes, this should be considered only as the current baseline candidate against which future choices may be compared.

4-29

4.3.2 Summary

The objective of the calculations is to relate the measured characteristics of a transistor (S-parameters and noise figure parameters F_{min}, R_n, Y_0) to the

- Stability
- Gain
- Noise Figure/Temperature
- System SNR

as a function of the impedance of the input and output matching networks in which it is embedded. The approach and concepts are essentially the same as those that have been developed for RF amplifiers. The distinctive feature of the active antenna is that the antenna is an integral part of the matching network circuitry. The S-parameter/Smith Chart display approach chosen here facilitates the display of the complete range of performance levels using readily constructed circular contours on the Smith Chart whose coordinates represent the load or source impedance of the embedding circuitry of the transistor. This simple yet elegant geometrical construction as shown in Figure 4.3-1 enables the effect and sensitivity of the embedding circuitry to be determined readily. The design goal for an active antenna is to achieve an SNR that is but minimally degraded from that obtained with a lossless $\eta = 1$, noiseless $F_n = 1$, receiver, which is $SNR_{MX} = DS_0/KT_A B$. This measure is represented by a parameter which is independent of the system bandwidth [Radjy and Hansen, 1979]

$$\gamma = \frac{SNR}{SNR_{MX}} = \frac{T_A \eta}{T_A \eta + T_0 (F_n - \eta)} \qquad 4.3\text{-}1)$$

4-30
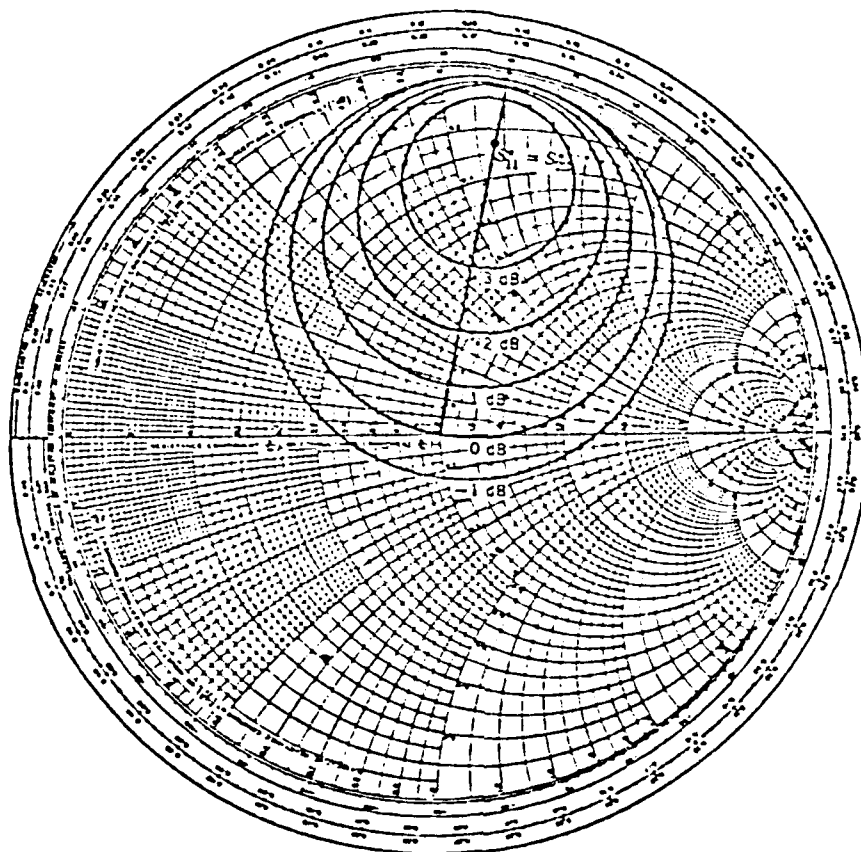
Figure 4.3-1 Circular gain contours on a Smith Chart

4-31

Table 4.3-2 summarizes the results of the detailed calculations for the active loop synthesized with a 2N5943 bipolar NPN transistor in Section 4.3.3. The most significant parameter is γ which is entered in the bottom lines. In a very noisy environment the external antenna noise contribution is so great that the -27 to -14 dB ohmic losses in the antenna and matching network are of no consequence. The SNR performance is the same as if the antenna and network were lossless and the receiver was noiseless ($\eta = 1$ and $\Delta_T = 0$). In a moderate (suburban) noise scenario these inefficiencies begin to affect the performance. In a very quiet noise scenario where the only antenna noise contribution is from that of the galactic background, the antenna and matching network ohmic losses begin to introduce appreciable degradation.

The performance levels of Table 4.3-2 are realized over the entire band without any adjustments. The 129° constant phase shift network that has been assumed to achieve the performance discussed above is not unique for implementation. Although the effects of its finite losses have been estimated it has not been designed. These results are intended as a baseline for future design effort.

Table 4.3-2

8" Active Loop Antenna 30 to 80 MHz

Numerical Example Summary

2N5943 Bipolar NPN

Assumed 129° Constant Phase Shift Network

$Q_M = 50$ $-.13$ dB Loss

Parameter	REFER TO FIGURE:	Comment
Stability	4.3-4 4.3-5	• Unconditional below 140 MHz • Potential instability 140 to 950 MHz for certain phases of Γ when VSWR > 12:1
Gain	4.3-6 to 4.3-10	• Nominal transistor gain of 16 dB • Active Loop Gain varies from -9 to + 3 dB due to efficiency variation from -27 to - 14 dB
Noise Figure	4.3-11, -12	6 to 7 dB
γ = SNR/SNR$_{MX}$	4.3-12	0 dB Noisy Urban -3.0 to -1.5 Moderate Suburban -17 to -13 Quiet Galactic

4-33

This section presents the performance contours that were computed for the stability, gain, noise figure, and SNR of an 8" active loop antenna in the 30 to 80 MHz band. The transistor chosen to obtain these results is a bipolar NPN, low-noise, low power model (2N5943) that, to the extent initial calculations indicate, appears to be suitable.

Its catalog description indicates low noise, low intermodulation distortion for broadband use in CATV applications. These same features appear appropriate for a broadband active loop. The impedance level of this transistor also appears to be commensurate with that of the loop antenna. Other transistors had a much higher impedance at low frequencies.

Figure 4.3-2 reproduces the catalog S-parameter and noise figure data [Motorola, 1978] from which the calculated results were derived. Since the S-parameter data is given for frequencies only down to 100 MHz (probably because of the limit of the particular model of Automatic Network Analyzer used) the procedure used to obtain the 30 to 80 MHz data for the band of interest here was to plot the available 100 to 1000 MHz data and extrapolate. Table 4.3-3 gives the approximating algorithms used to implement this and the values calculated in the extrapolated region. These algorithms and the values determined from them were used in a program coded for a large scale digital computer to obtain the results that are discussed in the following subsections.

The noise figure parameters F_{min}, R_N, and $G_0 = RE\,Y_0$ were determined from the three values of the noise figure in the graph
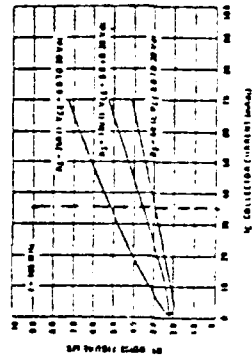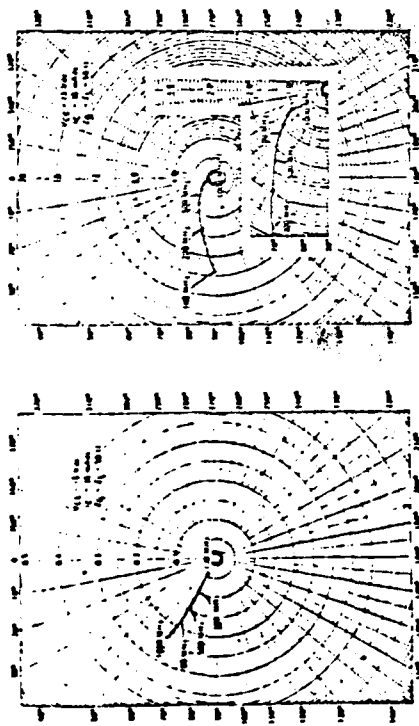
G_s mJ	$R_s - \Omega$	F dB	
20	50	3.0	(2.01)
10	100	3.6	(2.29)
4	250	5.2	(3.31)

(M) MOTOROLA Semiconductor Products Inc.

Figure 4.3-2 Catalog S-parameter and noise figure data for a bipolar NPN
low distortion transistor 2N5943, [Motorola,1978]

Table 4.3-3

Approximating Algorithms and Extrapolated Values

BIPOLAR NPN 2N5943 CHARACTERIZED FOR CATV APPLICATIONS.
FMIN=1.96 RN=8. RGO=33.

R11(X)=23.+0.*X
X11(X)=-1200./X+.021*X
R22(X)=92.-SQRT(X/1000.)*70.
X22(X)=-27.5-X/100.
AS21(X)=28.-9.*ALOG10(X)
PS21(X)=(97.2-.072*X)*DRAD
AS12(X)=.04*(X/100.)**.8
PS12(X)=(60.+.0*X)*DRAD

S-PARAMETERS   50 OHMS, POLAR FORM-AMP/DEG

F-MHZ	S11	S22	S21	S12
10.	0.875/ -44.	0.323/ -27.	19.000/ 96.	0.006/ 60.
20.	0.694/ -75.	0.314/ -29.	16.291/ 96.	0.011/ 60.
30.	0.576/ -96.	0.307/ -31.	14.706/ 95.	0.015/ 60.
40.	0.506/-111.	0.302/ -33.	13.581/ 94.	0.019/ 60.
50.	0.463/-122.	0.297/ -34.	12.709/ 94.	0.023/ 60.
60.	0.436/-131.	0.293/ -36.	11.997/ 93.	0.027/ 60.
70.	0.418/-138.	0.290/ -37.	11.394/ 92.	0.030/ 60.
80.	0.406/-143.	0.287/ -39.	10.872/ 91.	0.033/ 60.
90.	0.397/-148.	0.284/ -40.	10.412/ 91.	0.037/ 60.
100.	0.390/-152.	0.282/ -42.	10.000/ 90.	0.040/ 60.
110.	0.386/-156.	0.280/ -43.	9.627/ 89.	0.043/ 60.
120.	0.382/-159.	0.278/ -45.	9.287/ 89.	0.046/ 60.
130.	0.379/-161.	0.277/ -46.	8.975/ 88.	0.049/ 60.
140.	0.377/-164.	0.276/ -47.	8.685/ 87.	0.052/ 60.
150.	0.375/-166.	0.275/ -49.	8.415/ 86.	0.055/ 60.
160.	0.374/-168.	0.274/ -50.	8.163/ 86.	0.058/ 60.
170.	0.373/-170.	0.274/ -51.	7.926/ 85.	0.061/ 60.
180.	0.372/-172.	0.274/ -53.	7.703/ 84.	0.064/ 60.
190.	0.371/-173.	0.274/ -54.	7.491/ 84.	0.067/ 60.
200.	0.371/-175.	0.274/ -55.	7.291/ 83.	0.070/ 60.

of Figure 4.3-2 for I_c = 35 mAdc. By assuming different values
of G_0 and plotting F versus $X' = X(1000) = |G_s-G_0|^2/G_s$ (m℧) in
Figure 4.3-3, it was determined that the best straight line
fit of the three experimental points to the IRE Standard Noise
Figure Representation [1960] obtains for G_0 = 30m℧. The values of
the intercept (F_{min}), slope (R_N), and R_0 are given in the lower
right hand corner of figure. Since no experimental data was
given for $B_0 = Im [Y_0]$, the calculations of this report assumed
as a first approximation that B_0 is the power gain conjugate
match admittance. This conjecture is supported by inspection of
the experimentally measured Γ_0 and power gain conjugate match
data for a microwave FET transistor [Hewlett-Packard, 1977].
The optimal noise figure reflection coefficient had a smaller
amplitude and lagged in phase about 20° behind the power gain
conjugate match reflection coefficient.

4.3.3.1 Stability

Figure 4.3-4 plots the magnitude of the stability parameters
for the source impedance (S) and the load impedance (L) and
composite. The following features of the calculations are dis-
cussed in detail.

1)   Unlike gain and noise figure calculations, the
potential for instability and therefore the analysis, is not
limited to inband frequencies (30 to 80 MHz). The range of
10 to 1000 MHz is analyzed.

2)   Below 140 MHz the stability parameters all exceed unity
and are unconditionally stable. Between 140 and 950 MHz the
stability parameter decreases below unity indicating that the
potential exists for instability with certain phases of Γ that
exceed a minimal, threshold value.
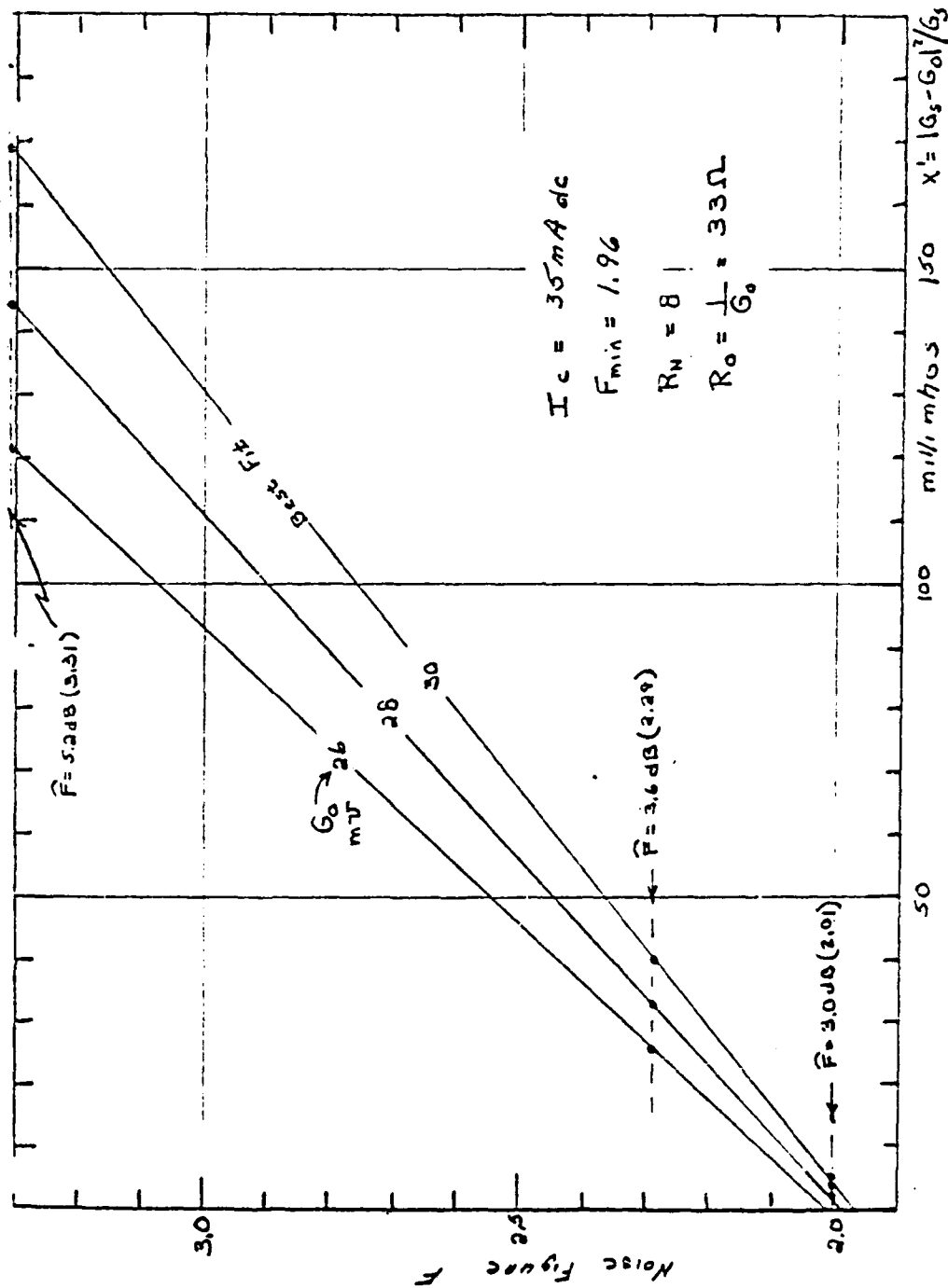
Fig. 4.3-3 Graphical determination of the noise figure parameters for 2N5943 per data of Fig. 4.3-2.
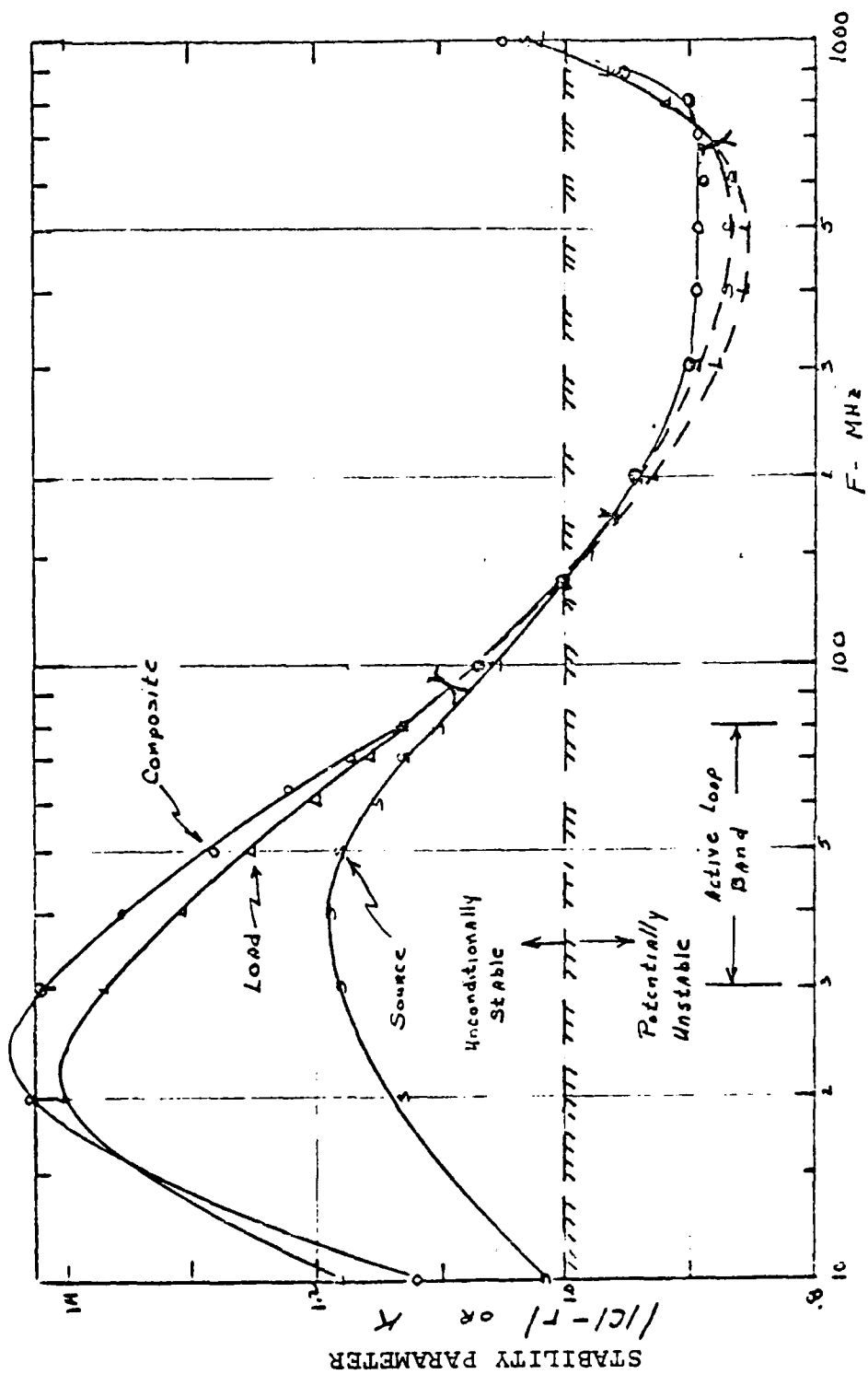
Figure 4.3-4 Stability parameters for 2N5943 over the 10 to 1000 MHz band

3) The minimal value of 0.85 for all three curves in Figure 4.3-4 suggests that so long as the magnitude of the coefficient is everywhere less than 0.85, then instability will be avoided under any circumstances. This is the basis for the $|\Gamma_L| = 0.85$ and 12.3:1 VSWR limit shown in the Γ-plane interpretation of Figure 4.3-5. This leads to the conclusion that if the matching networks at the input and output port of the transistor can everywhere ensure a VSWR of less than 10:1, then no instabilities will occur. However, reflections whose SNR's exceed 10:1 can also produce stable amplification provided they are of the appropriate phase.

4) Inspection of Figure 4.3-4 indicates there may also be a potential for instability below 10 MHz. However, this region represents over one decade of extrapolation below the 100 MHz measurement limit and should be verified by calculations using directly measured S-parameter data.

5) In the process of verifying the values of some of the machine calculations, it was found that apparently small deviations in the values of the S-parameters used had considerable effect on the magnitudes of the stability parameters. This sensitivity suggests that stability may change appreciably from transistor to transistor because of the normal dispersion of values encountered in any production sample.
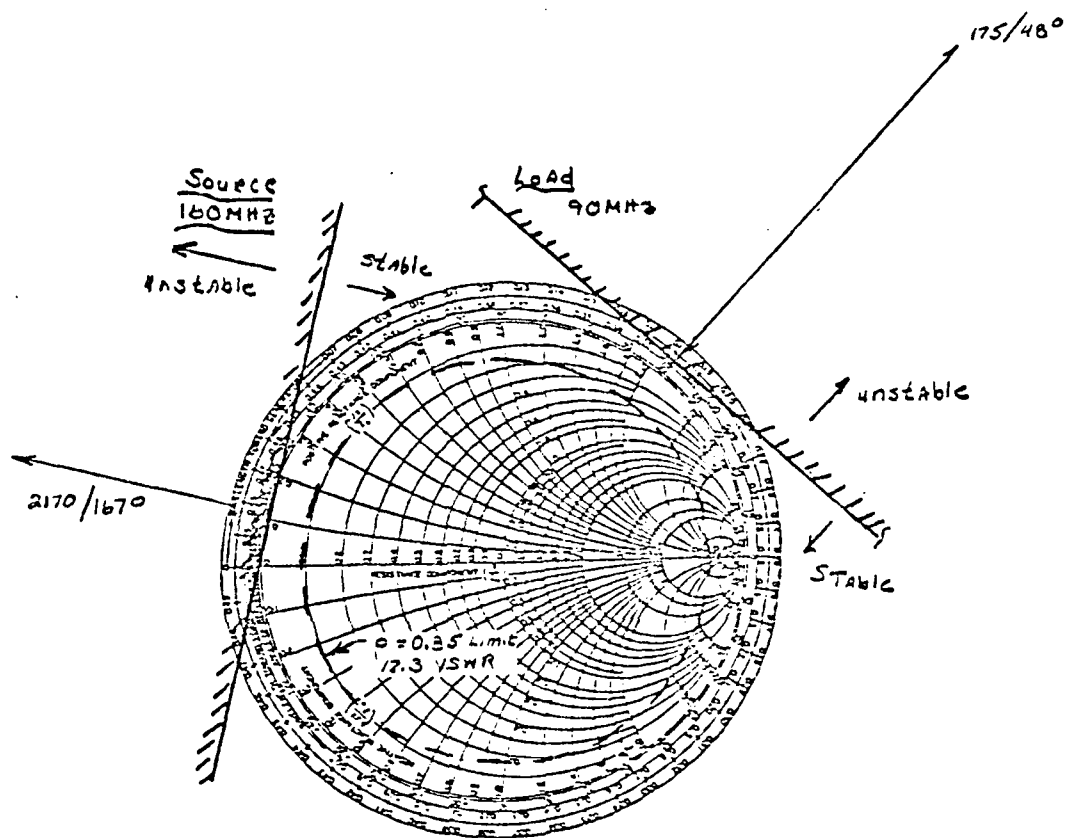
Figure 4.3-5   Stability contours of 2N5943 on the Smith Chart

4-41

4.3.3.2 Gain

Figure 4.3-6 shows the gain loss of the 2N5943 that is inherent with increasing frequency. This analysis will address the gain at three discrete frequencies 30,55,and 80 MHz. In order to achieve a gain that is flat across the band the relative gains of the matching networks G_{Mi} must be -3, -1, and 0 dB at the design frequencies. Inspection of Table 4.3-3 indicates that the magnitude of S_{22} is essentially constant at 0.3 across the band with $\hat{G}_{M2} = 0.4$ dB. The input reflection coefficient has much greater variation. Therefore the gain flatness compensation will be designed into the input matching network.

We shall first consider the case shown in Figure 4.3-7 that produces a gain that is very nearly maximal by allowing 1 dB (.794) of gain loss from each the matching networks at the input and output at the high edge of the band at 80 MHz. From the S-parameter data of Table 4.3-3 we compute [Carson, 1975; Hewlett-Packard, 1968 and 1972].

$$G(80) = \frac{.794}{1-(.406)^2} (10.87)^2 \frac{.794}{1-(.287)^2} \qquad 4.3-2)$$

$$= (.951)(118.16)(.865)$$

$$= 97.23 \qquad\qquad (19.9 \text{ dB})$$

The 80 MHz contour in Figure 4.3-7 is labeled -1 dB. Additional calculations not reproduced here indicate unilateral gains of 20.2 and 20.4 dB at 55 and 30 MHz for the -2 and -4 dB contours for a nominal wideband gain of +20 dB. Also shown in the upper right hand quadrant of the Smith chart is the impedance locus of the 8" loop over the band. The matching

4-42
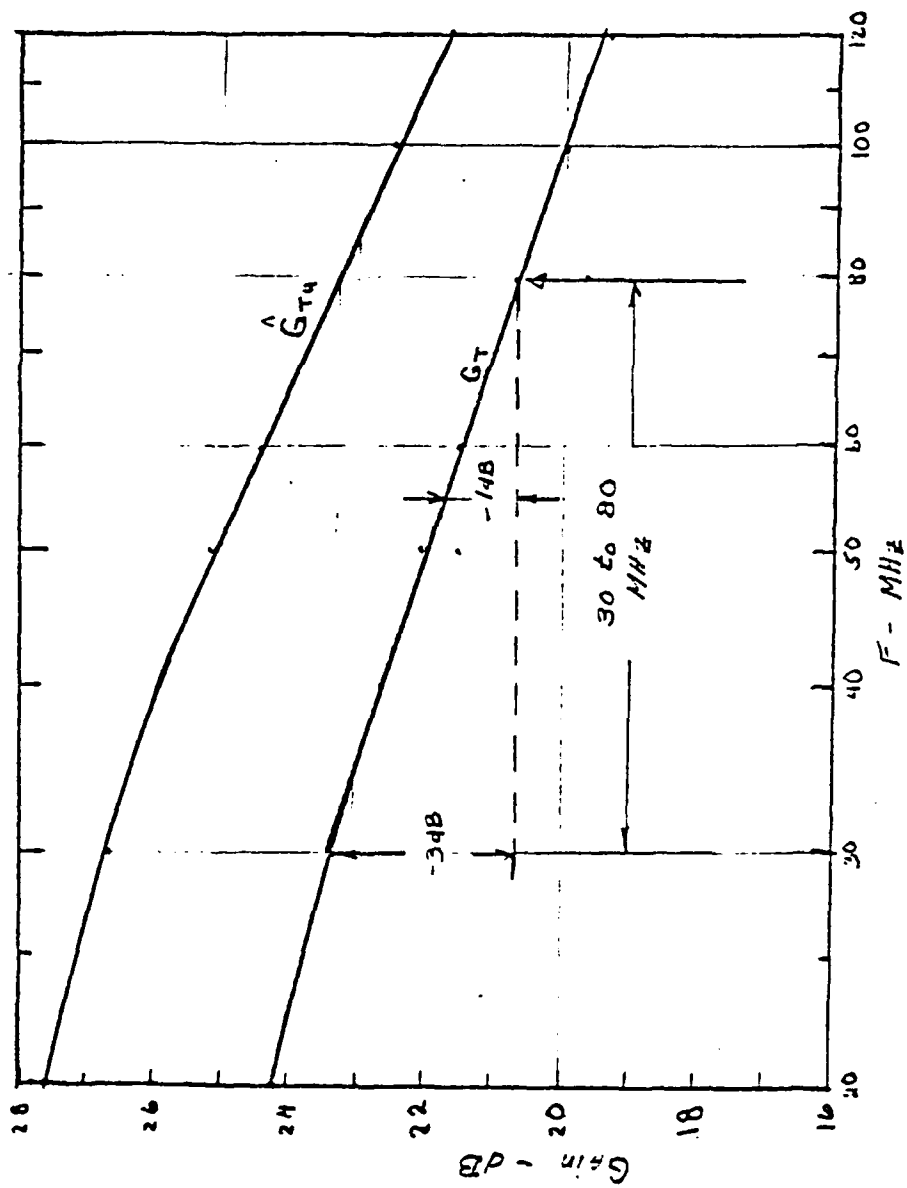
Figure 4.3-6 Transducer gain (G_T) and maximum gain G_p for conjugate match of 2N5943 extrapolated over the 30 to 80 MHz.
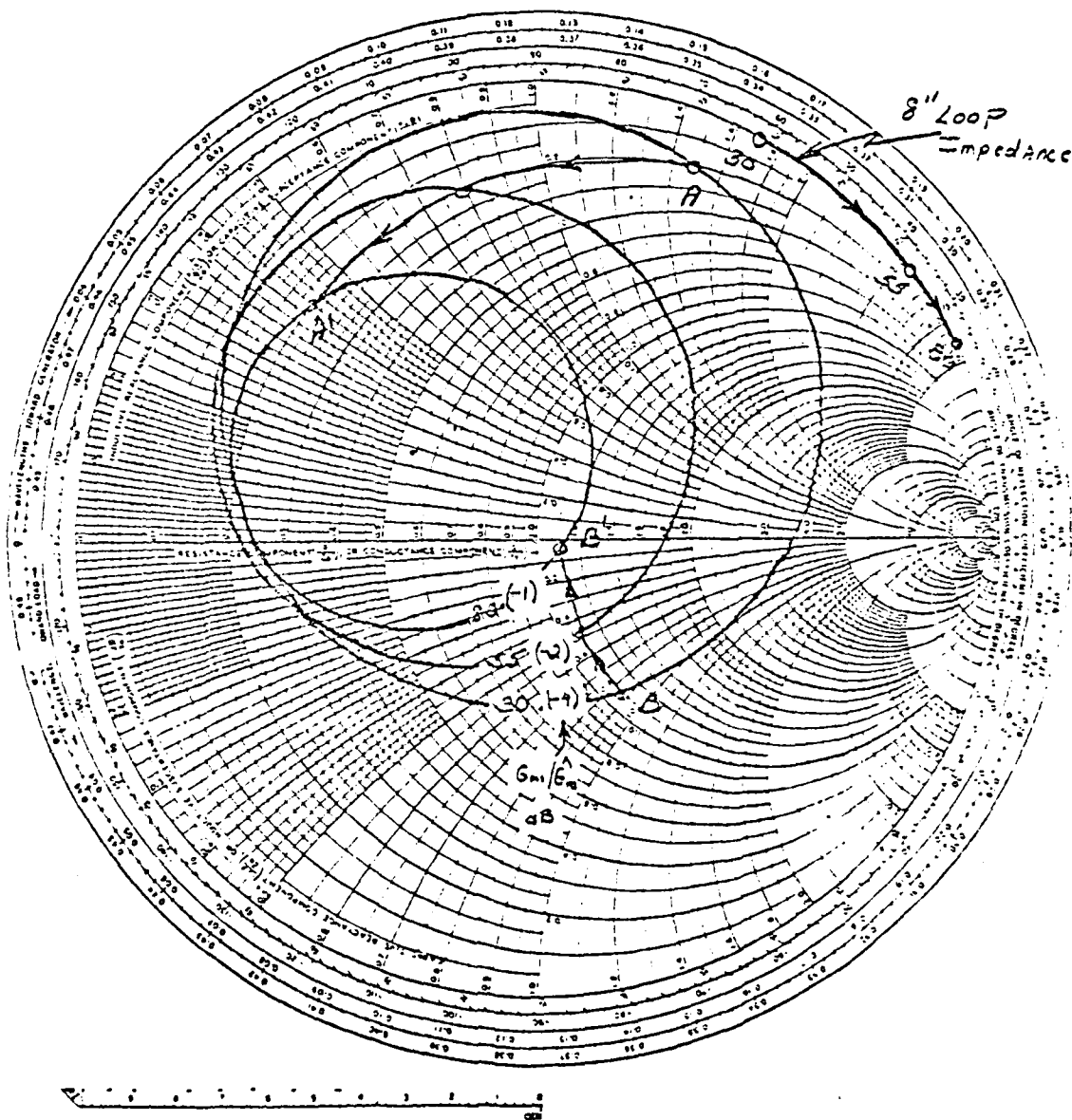
Figure 4.3-7   Input matching contours $f(S_{11}^*)$ for nominal 20 dB
gain with the 2N5943 over the 30 to 80 MHz band.

network design goal is to transform the 30, 55, and 80 MHz points
onto the appropriate contours. Temporarily bypassing the ques-
tion of physical realizability in a strict mathematical sense
or practical engineering sense, possible locii are AA' along
the r = 0.2 contour and BB' along r = 1.1. Neither of these
appear practically feasible at first glance. The AA' locus re-
quires a counterclockwise frequency variation that is directly
opposite to clockwise variation that occurs naturally with in-
creasing frequency. The BB' locus requires a large resistive
component that would appear impossible to achieve with acceptable
efficiency from the high Q loop that is essentially a pure in-
ductive reactance.

Figures 4.3-8 and -9 plot the countours for a nominal 19
and 16 dB gain. At the expense of a 4 dB gain loss, the latter
case appears to offer reasonable matching potential for a high
Q input reactance. When the 8" loop locus is <u>uniformly shifted</u>
by adding $.358\lambda = 129^{\circ}$ of all pass phase delay <u>across the band</u>,
the new locus is given by the dashed line in the upper left
hand quadrant. If the network were perfectly lossless, the
transformed locus would still be on the outer limit with a
vanishingly small resistive component. However, ohmic losses
associated with the finite Q_M of the matching network will in-
crease the resistive component. This can be estimated once
the Q and the electrical length are specified by an approxima-
tion [Schelkunoff, 1943, p.85] relating the attenuation constant
α and propagation constant β in a low loss (high Q) medium

$$\alpha \approx \frac{\sigma}{2}\sqrt{\frac{\mu}{\epsilon}} = \frac{\sigma}{\omega\epsilon}\frac{\omega\sqrt{\mu\epsilon}}{2} = \frac{1}{2Q}\beta \qquad\qquad 4.3-3)$$

$$\therefore \ \alpha\ell = (\beta\ell)\frac{1}{2Q} .$$
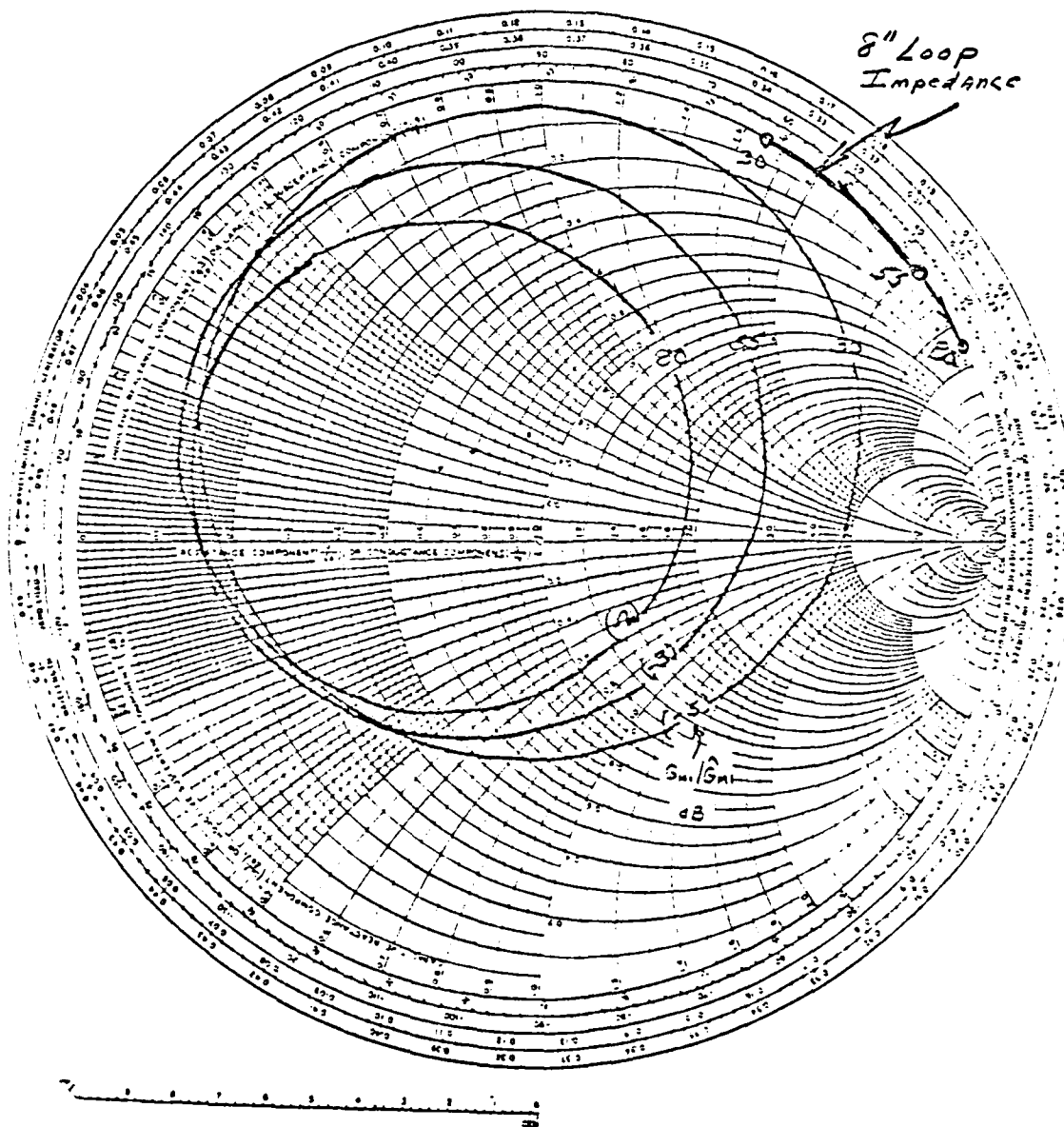
Figure 4.3-8 Input matching contours f(S_{11}^*) for nominal 19 dB
gain with the 2N5943 over the 30 to 80 MHz band

4-46
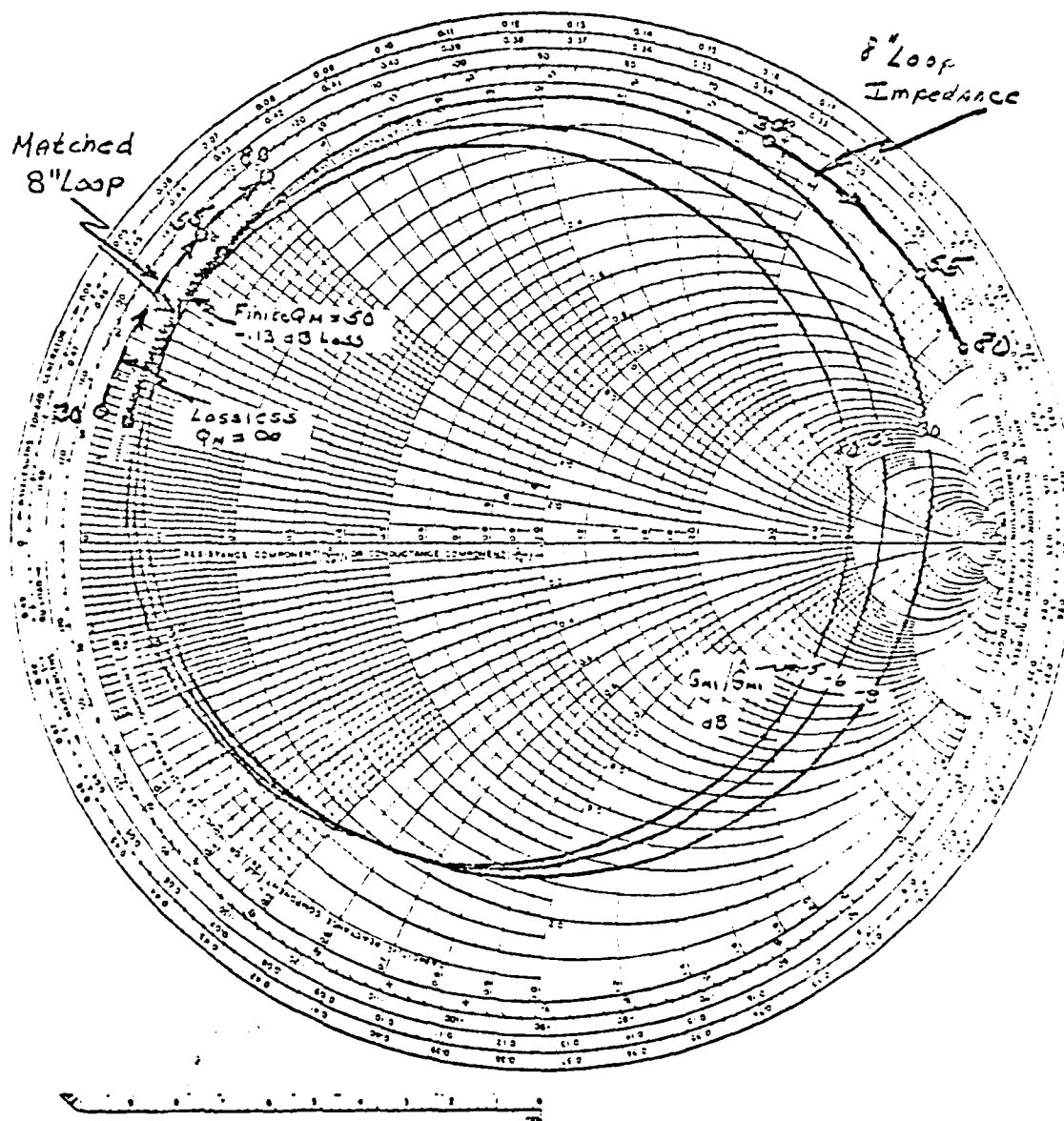
Fig. 4.3-9 Input matching contours $f(S_{11}^*)$ for nominal 16 dB gain with the 2N5943 over the 30 to 80 MHz band.

Table 4.?-4

8" Loop Antenna Parameters

ALL IMPEDANCES NORMALIZED TO 50 OHMS

ALL DIMENSIONS ARE INCHES

| FM	A	B	RRAD	ROHM	RTOT	EF1-DB	EF2-DB	X	Q_L
10.	0.125	4.	0.00000	0.00064	0.01202	-28.88	-41.64	0.57	
20.	0.125	4.	0.00001	0.00090	0.02367	-18.40	-32.55	1.14	
30.	0.125	4.	0.00007	0.00110	0.03531	-12.43	-27.24	1.71	
40.	0.125	4.	0.00021	0.00127	0.04701	-8.47	-23.48	2.28	1462
50.	0.125	4.	0.00051	0.00142	0.05884	-5.76	-20.58	2.85	1541
60.	0.125	4.	0.00107	0.00156	0.07091	-3.91	-18.23	3.41	1477
70.	0.125	4.	0.00198	0.00168	0.08333	-2.67	-16.25	3.98	1297
80.	0.125	4.	0.00337	0.00180	0.09622	-1.86	-14.55	4.55	1087
90.	0.125	4.	0.00540	0.00191	0.10974	-1.31	-13.08	5.12	880
100.	0.125	4.	0.00823	0.00201	0.12406	-0.95	-11.78	5.69	
110.	0.125	4.	0.01205	0.00211	0.13936	-0.70	-10.63	6.26	
120.	0.125	4.	0.01707	0.00220	0.15585	-0.53	-9.60	6.83	
130.	0.125	4.	0.02352	0.00229	0.17376	-0.40	-8.69	7.40	
140.	0.125	4.	0.03163	0.00238	0.19335	-0.31	-7.86	7.97	
150.	0.125	4.	0.04168	0.00246	0.21486	-0.25	-7.12	8.54	
160.	0.125	4.	0.05396	0.00254	0.23860	-0.20	-6.46	9.10	
170.	0.125	4.	0.06877	0.00262	0.26487	-0.16	-5.86	9.67	
180.	0.125	4.	0.08643	0.00270	0.29399	-0.13	-5.32	10.24	
190.	0.125	4.	0.10730	0.00277	0.32631	-0.11	-4.83	10.81	
200.	0.125	4.	0.13173	0.00284	0.36220	-0.09	-4.39	11.38	

work since the losses $\alpha\ell$ in equation (4.3-3) increase in direct proportion to the electrical length $\beta\ell$.

Table 4.3-5 compares the gains of a passive and active 8" loop that correspond to the efficiencies calculated above. It is assumed that the passive loop can be narrow band matched to 50 ohms with the same efficiency r_2 that was calculated for the transistor matching network. Because of the tremendous variation of the matching network efficiency r_2, minor variations of a dB or so in the transistor gain (because of imperfect matching network realization) do not appear to be particularly significant.

Table 4.3-5

Estimated 8" Loop Antenna Gains (dB)

f-MHz	Lossless* Loop	r_2	Narrow-Band * Passive Loop	G_T	Active Loop
30	1.8	-27	-25	+16	-9
55	1.8	-19	-17	+16	-1
80	1.8	-15	-13	+16	+3

* No mismatch loss included.

The transformed locus achieved by $129°$ of uniform delay across the band when the losses are included very nearly coincides with contours required for a uniform 16 dB gain in Figure 4.3-9. The design of a constant phase shift network is a classical network synthesis problem that has been analytically

formulated [Storer, 1957]. Another approach could be based on

numerical network synthesis algorithms programmed for a large

scale digital computer. However, this design aspect will not

be addressed here. The following calculations will proceed

assuming that the transformed impedances shown in Figure 4.3-9

f-MHz	$z = r + jx$
30	$.04 + j\ 0.15$
55	$.04 + j\ 0.39$
80	$.04 + j\ 0.50$

can be realized with the stated matching efficiency for a tran-

sistor gain of 16 dB. It is reiterated that the choice of the

locus in Fig. 4.3-9 is in no way unique. A comparable level

of gain flatness could be achieved in principle by a limitless

number of transformations. It is only by trial and error in

the actual matching network design that potential candidates

can be verified as practically realizable.

Although the proposed matching network locus of Figure

4.3-9 represents a high VSWR (32:1) that exceeds the 10:1

limit in the stability discussion, it occurs in the portion

of the band below 140 MHz where the transistor is unconditionally

stable. It is necessary to satisfy the 10:1 limit only above

140 MHz when the source phasing is such that the reflection co-

efficient is in the critical part of Smith chart. 10:1 VSWR's

outside that critical region may exist without initiating an

instability.

It is noted that the same reactance locus of the 129° con-

stant phase shifted 8" loop in Figure 4.3-9 could also be

achieved by reducing the loop diameter and reactance by a factor
of 8. However, this would increase the Q by $8^3 = 512$ and would
decrease the efficiency by 27 dB. This is not acceptable. In-
creasing the loop diameter to 10" would decrease the Q by 1/2
and increase the efficiency by about 3 dB.

Figure 4.3-10 shows -1 dB relative gain contours for the
output matching network at 30, 55, and 80 MHz. All nearly
coincide, and enclose the origin (50Ω) of the Smith chart. This
indicates that the output of the 2N5943 can be directly connected
to a reasonably well matched 50Ω cable (VSWR ≤ 1.47:1) and still
maintain its gain within the 1 dB matching loss assumed in the
calculation of equation 4.3-2. A transformation to 75Ω would
provide an improved match but may not be worth the effort.

Figure 4.3-11 gives the input matching network contours
for a noise figure that exceeds $F_{min} = 1.96$ (≈3 dB) by 1 dB.
The transformed loop locus will result in a noise figure that
exceeds this since it is outside the contours. The performance
measure that is more significant than noise figure for the
active antenna is the relative SNR ratio $\gamma = SNR/SNR_{MX}$. This
is related to the receiver noise figure F_n by the antenna noise
temperature and efficiency

$$\Delta T = T_A \eta \left(\gamma^{-1} - 1 \right) + T_0 (1 - \eta) \qquad\qquad 4.3-8)$$

$$F_n = \frac{\Delta T}{T_0} + 1$$

provided that $\Delta T \geq \Delta T_{min}$ of the transistor. Figure 4.3-12 gives
contours for the matching network that provide the relative SNR's
of Table 4.3-6. The relative SNR value is seen to depend greatly

4-52
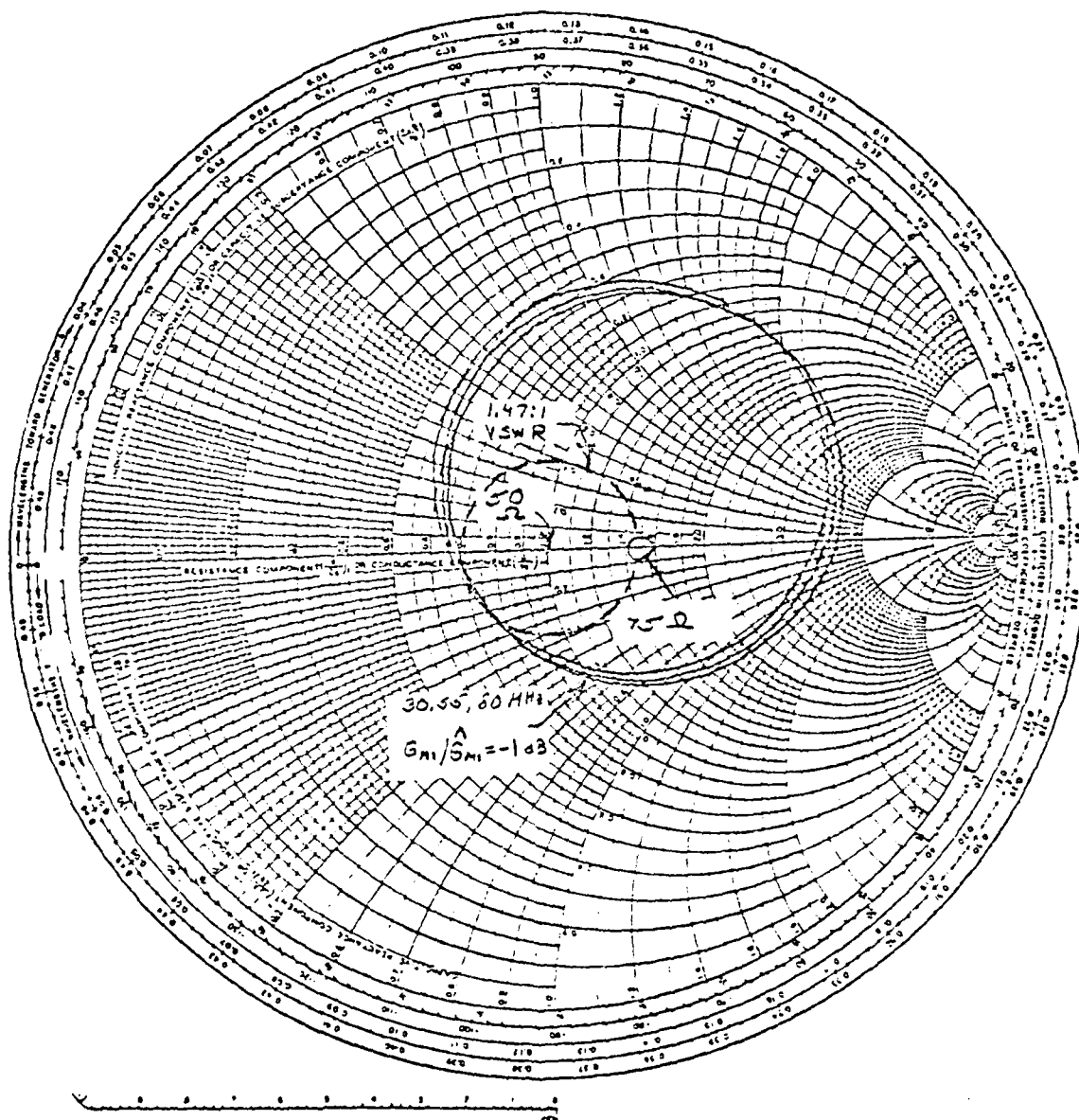
Figure 4.3-10   Output matching contours $f(S_{22}^*)$ for
                 -1 dB G_1 with the 2N5943 over the 30
                 to 80 MHz band
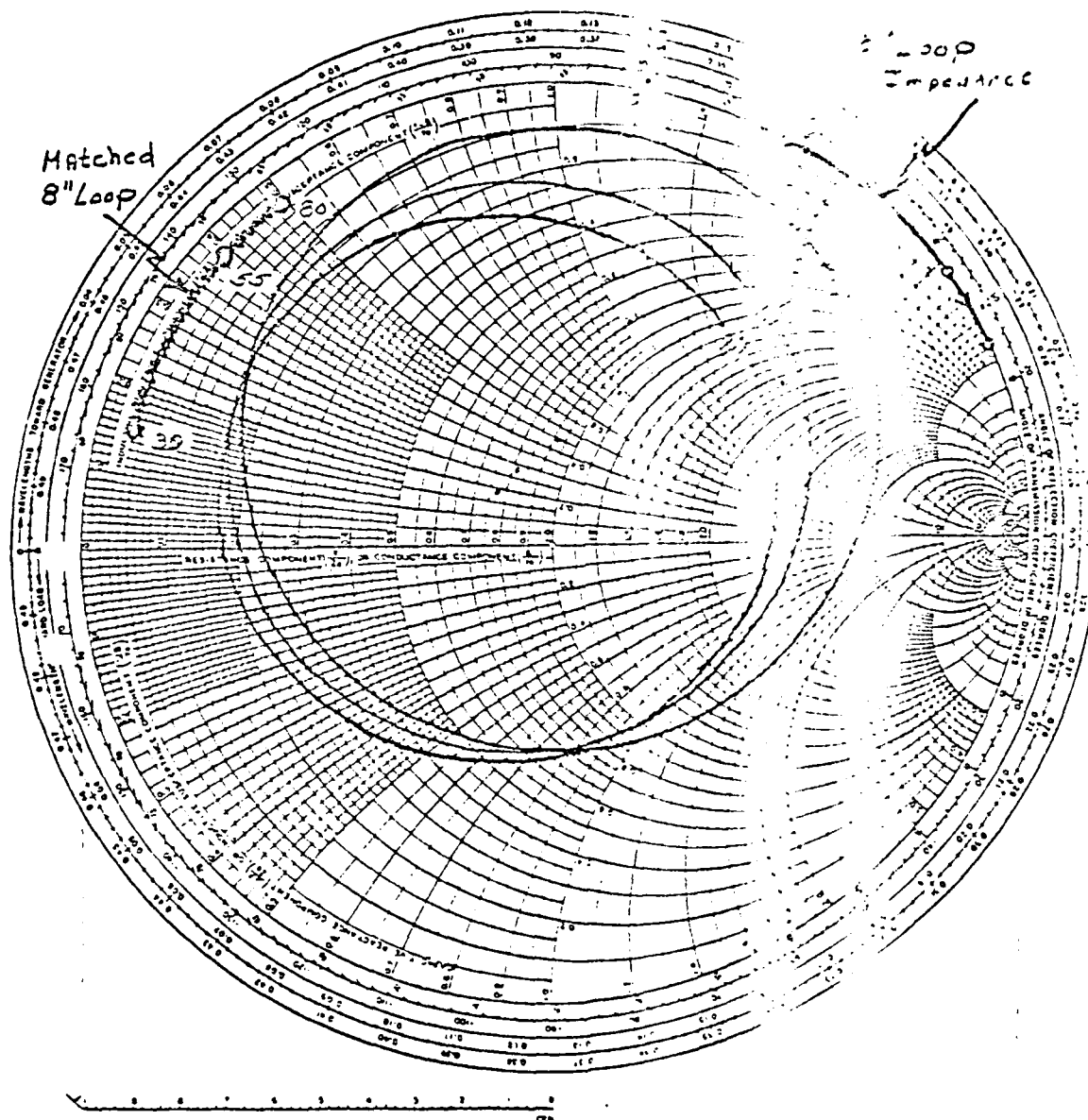
Figure 4.3-11   Input matching contours for F F_{min} + 1 dB = 4 dB noise figure of 2N5943
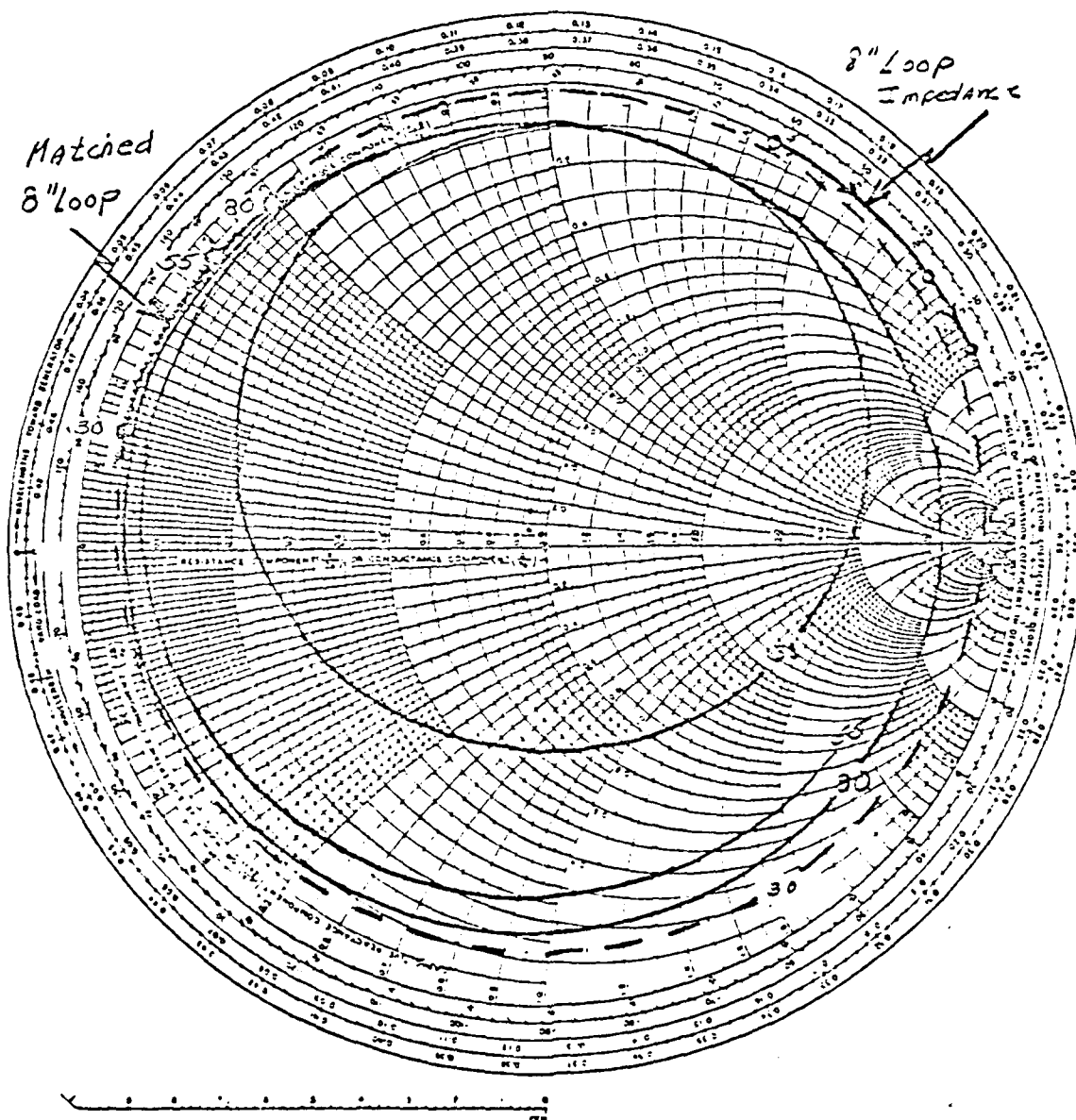
Figure 4.3-12   Input matching network contours for F and
$\gamma = SNR/SNR_{MX}$ values of Table 4.3-6

4-55

Table 4.3-6

Noise Figure and $\gamma = SNR/SNR_{Mx}$

2N5943

Matching Network Contours of Figures 4.3-11 and -12

f-MHz	Figure 4.3-11 $\widehat{F}$ – dB	Figure 4.3-12 $\widehat{F}$ – dB	$\overline{\gamma}$ – dB Noise Scenario Quiet	Moderate	Noisy
* ---	---	8	-17.1	-3.0	-0.1
30 —	4	4	-13.2	-1.4	-0.1
55	4	6	-13.3	-1.5	.0
80	4	7	-13.3	-1.5	.0

* --- Dashed line contour
 —— Solid line contour

4-56

on the noise environment. In a very noisy environment the degradation to the SNR is entirely negligible to that which would be obtained with a perfectly matched, noiseless receiver. In a modest suburban environment, the degradation for the matched 8" loop is only -1.5 dB at 55 and 80 MHz and -3.0 dB at 30. Only in a very quiet galactic noise background does the inefficiency of the loop and matching network seriously degrade the SNR. Per the values of Table 4.3-6 these degradations are -17, -13, and -13 dB at the design frequencies. Two contours (-- and ——) are given for the 30 MHz frequency in Figure 4.3-12.

Allsebrook, K., J.D. Parsons (1977), "Mobile Radio Propagation in British Cities at Frequencies in the VHF and UHF Bands", IEEE Trans. Vehic. Tech., Vol. VT-26, No. 4, pp. 313-323.

Bailey, K.R.G. (1976), "The Frequency Dependence of the Mean and Peak Levels of Radio Noise in the Birmingham Area", M. Sc. Dissertation, University of Birmingham, England.

Carson, R.S. (1975), High-Frequency Amplifiers, John Wiley.

CCIR Document 6/104-E (1974), "Man-made Radio Noise", Report 258-1, Study Program 21A-1/6.

Ehrman, L., S. Parl (1977), "Communications Data Base Analysis for Military Operations in a Built-up Area (MOBA/COBA)", Interim Report 15068.1 (SIG. A-223), prepared for U.S. Army Research Office by SIGNATRON, Inc., Lexington, MA.

Flachenecker, G. (1978), "MOBA-Receiving System with High Availability", Technical Report, U.S. Army European Research Office, May 1978.

Hewlett-Packard (1968), S-parameter Circuit Analysis and Design, Application Note 95.

Hewlett-Packard (1972), S-parameter Design, Application Note 154.

Hewlett-Packard (1977), Noise and Power Parameters for the HFET-1101, Application Bulletin 19.

IRE (1960), "IRE Standards on Methods of Measuring Noise in Linear Twoports", 1959, Proceedings IRE, January.

Lee, W.C. Y. (1978), "Mobile Radio Performance of a Two-Branch
        Equal-Gain Combining Receiver with Correlated Signals
        at the Land Site", IEEE Trans. Vehic. Tech., Vol.
        VT-27, No. 4, pp. 239-243.

Meinke, L. and Lindenmeier H. (1977), "Aktive Empfangsantennen",
        Lehrstuhl für Hockfrequenztechnik of the Technical
        University of Munich.

Motorola (1978), RF Data Manual.

Parsons, J.D., A.U.H. Sheikh (1978), "Mobile Impulsive Inter-
        ference: A Study of VHF Man-made Noise in Urban and
        Suburban Areas", Final Report on Home Office Directorate
        of Telecommunications Contract DT74/96/12, University
        of Birmingham, England.

Radjy, S.H. and Hansen, R.C. (1979), "S/N Performance of
        Aperiodic Monopoles", IEEE Trans. AP., March, pp. 259-
        261.

Ragan, G.L. (1949), "Microwave Transmission Circuits", MIT Rad.
        Lab. Series, McGraw-Hill.

Ramsdale, P.A. and MacLean, T.S. (1971), "Active Loop Dipole
        Aerials", Proc. IEEE, pp. 1698-1710.

Schelkunoff, S.A. (1943), Electromagnetic Waves, Van Nostrand.

Storer, J.E. (1957), Passive Network Synthesis, McGraw-Hill.

SECTION 5
CONCLUSIONS AND RECOMMENDATIONS

5.1   Conclusions

The following conclusions are based on the results of our propagation research.

1. Communications Range

The communications range in an urban or sub-urban environment is limited. If both the transmitter and receiver are located on a sidewalk, the VHF range may be less than 500 feet in highly-built-up areas (average building height of 5 stories or more), while UHF is unusable. If both the transmitter and receiver are in the center of the street, the range may be as great as one mile for both VHF and UHF. The urban area has a shorter communications range than the suburban area. For a given transmitter power, the communication range can be extended by a factor of approximately 1.4 to 1.8 if diversity reception is used.

2. Communications Between and Within Buildings

Communications within a building are possible at both VHF and UHF, with the communications range being dependent on the corridor structure, building material, and number of floors separating the transmitter and receiver. Communications between the street and a building are possible at VHF and UHF, although the attenuation increases rapidly at UHF when one terminal moves into the interior of the building. Communications between two adjacent buildings is not possible unless one terminal is near a window. Communications inside a building along a straight corridor is better at UHF than at VHF, but the converse is true when the corridor has turns. Communications be-

5-1

tween floors is enhanced at both VHF and UHF if within
a stairwell or near an elevator.

3. Path Loss Prediction Model

When low elevation antennas are used, our
experimental data indicate that the path loss in dB can
be approximated by Eq. (3.3-2):

$$L = L_p(d) + L_D(f) - H_e(h_t, f) - H_r(h_t, f) \quad (3.3-2)$$
$$+ K_{u,s}(f,d) + L_b(f)$$

where L_p is the plane-earth path loss for 2-meter antenna
height and separation d; $L_D(f)$ is a frequency-dependent
environmental clutter factor; H_t and H_r are antenna
height-gain factors; $K_{u,s}(f,d)$ is a frequency and distance
dependent urban/suburban clutter factor; and $L_b(f)$ is a
frequency dependent building penetration loss, applicable
when one terminal is within a building and the other is
in the street. This model is in excellent agreement with
that of Okumura at 446 MHz, but shows less of a frequency
dependence than his at VHF. It is similar to the Allsebrook
and Parsons model, but more complete in the inclusion of
$K_{u,s}$ and L_b.

4. Propagation Phenomenological Model

The path loss measured in urban and suburban
environments showed distance relations from inverse square-
law to inverse fourth-power law. The inverse square-law
is associated with a single predominant diffraction path,
and the inverse fourth-power is associated with (near)
equal strength multiple reflected (or diffracted) signals.

The single diffraction path is important when a terminal is located on the sidewalk, next to a building; however, the diffraction loss may be so great that the received signal is unusable. The multiple-reflected (or diffracted) signal case, which is the more reliable means of communication, requires that one of the terminals be away from the building.

5. Selection of MOBA Radio Operating Frequency

The measurements show, and the modeling explains, that communications are best when the building heights are small compared to a wavelength. This implies that urban communications would be better, from a path-loss point of view, at HF than at VHF. It further implies that UHF should not be considered for MOBA use by the Army in highly built-up areas as it requires that radio operators be in exposed positions. However, use of UHF in suburban areas (average building height of two stories or less) may be more desirable than VHF if antenna profile (height) is a factor.

6. Fading and Correlation Properties of the Received Signal

The received signal has been shown by our measurements, as well as by the measurements made by numerous other researchers, to be a fading signal. Thus, improved performance can best be achieved by diversity reception. Our correlation measurements show that both field diversity, using collocated loop and whip antennas, and space diversity, using two whip antennas spaced approximately one-half wavelength apart, are possible. From a practical point of view, only the field diversity approach is feasible for a manpack VHF radio.

5-3

7.   Antenna Developments

Active antennas appe⁻⁻ to have significant
application to military radios. First, because they are
broadband, they can be used as auxiliary receiving antennas
in diversity receivers without requiring additional tuning
sections. Secondly, because they are physically small, they
have good low-profile capabilities. Third, because they are
decoupled from their environment by the unilateral transistors,
they do not require ground planes and, when used in arrays,
they do not cross-couple. An active loop antenna would be
a practical means of implementing an appliqué for a
diversity VHF receiver.

5.2 Recommendations

The following recommendations are based on
the conclusions of this study.

1.   A development program be started to
     build and test a VHF diversity receiver
     using an active loop antenna as the
     auxiliary antenna.

2.   A research program be started to de-
     termine means of extending the range
     of MOBA radio communications. This
     should include both consideration of
     relay techniques and the use of other
     frequencies, most notably HF.

3.   Consideration should be given to ex-
     ternally deployed antennas for use
     with radios in the interior of a
     building.

APPENDIX I
IF Detector Circuit Diagram

APPENDIX I
IF Detector Circuit Diagram

In this appendix we give the circuit diagram of an
80 dB range detector designed to be used in conjunction with
the AN/PRC-77 and the KENWOOD TR-8300 to make the measure-
ments at 49.8 MHz and 446 MHz. The circuit diagram of the
detector is shown in Figure I-1. The input to the detector
is the IF signal from the radio and the output is a DC
voltage which can be read with a voltmeter. The IF fre-
quency of the PRC-77 was 11.5 MHz as shown in Figure I-1.
However, the first IF frequency of the KENWOOD TR-8300 was
10.7 MHz. Hence the detector of Figure I-1 was modified
to accommodate such an IF frequency by replacing the
11.5 MHz bandpass filters of Figure I-1 with the 10.5 MHz
bandpass filters of Figure I-2. In either case, the de-
tector has two 40 dB ranges: a high input (IF) signal
40 dB range denoted by point A in Figure I-1 and a low
input signal 40 dB range denoted by point B.
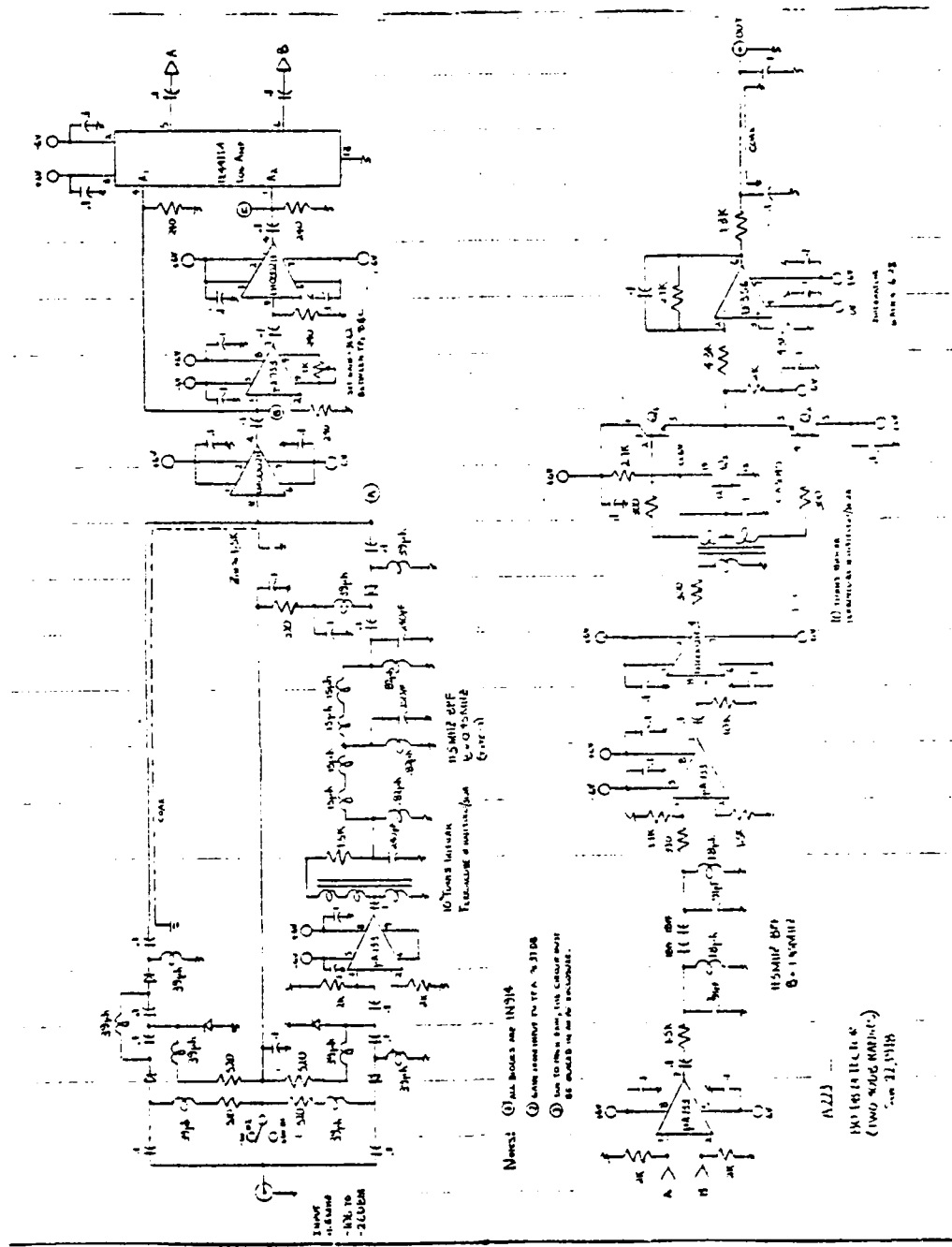
FIGURE I-1   Detector Circuit Schematic

I-3
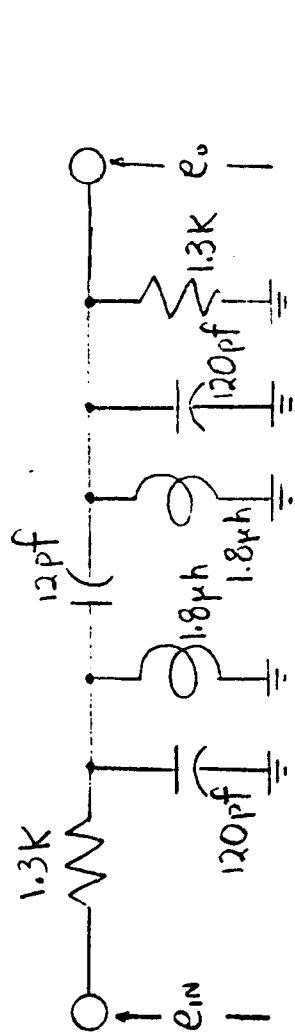
10.5 MHZ BPF
B = 1.81 MHZ
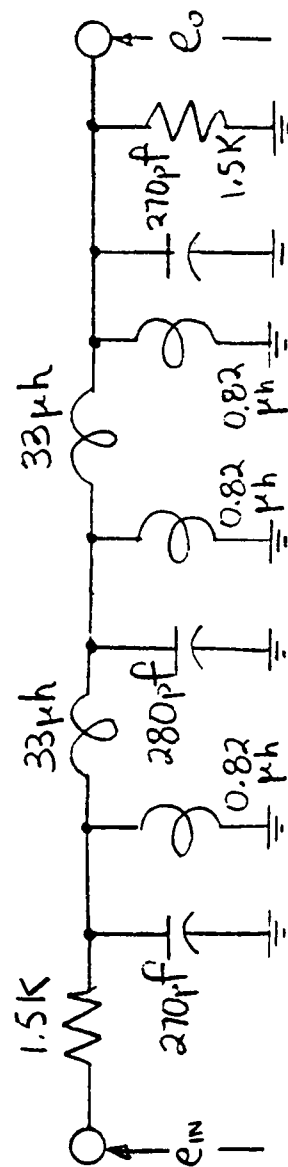
10.5 MHZ BPF
B = 0.33 MHZ

FIGURE I-2   Bandpass Filters used with KENWOOD TR-8300

APPENDIX II

Multiturn Loop Antenna Design for VHF Radio

APPENDIX II
MULTITURN LOOP ANTENNA DESIGN FOR VHF RADIO

1. Introduction

In this appendix, we will be concerned with the design of a multiturn loop antenna (MTL) for VHF communications in the 20-80 MHz band. Thus, the appendix will be divided into two subsections. In Section 2 we give a general description of the MTL antenna and in Section 3 we give the specific design of the MTL antenna used to make the propagation measurements at 27 MHz and 49.8 MHz.

2.   The Multiturn Loop Antenna

An overview of the important characteristics of the multi-turn loop antenna (MTL) as they apply to design for VHF mobile communications is presented here. Although the antenna is an electrically small element with regard to its volumetric dimensions, it uses about a quarter to a half wavelength of conductor. The antenna is mounted on an aluminum disk to help isolate the antenna from its surroundings as shown in Figure 1.

The basic schematic representation of the MTL antenna over a ground plane is shown in Figure 2(a) [1]. From the tuning standpoint the MTL may be considered as a lumped inductance. Using the configuration shown below, where the conductor in the antenna is always less than $\lambda/2$ in length, the antenna has inductive input impedance. This allows the use of low loss capacitive matching elements, C_M and C_T. The capacitor C_T is used to bring the tank circuit to the desired frequency of operation and C_M matches this combination to the feed cable (50 Ω, for example). If the leakage capacitance C_L between each antenna loop and the ground plane is sufficiently small, the input impedance of the MTL plus tuning and matching elements may be determined from the circuit schematic of Figure 2(b) where R is equal to the radiation resistance, R_r, plus the skin resistance, R_{ac}, of the MTL and L is the inductance of the MTL. It can readily be determined that

$$Z_{in}(\omega) = R_{loop}(\omega) + j\, x_{loop}(\omega) - j\,\frac{1}{\omega C_M} \tag{1}$$

where

$$R_{loop}(\omega) = \frac{R}{\left(1 - \frac{\omega^2}{\omega_r^2}\right)^2 + \left(\frac{R}{\omega_r L}\right)^2 \frac{\omega^2}{\omega_r^2}} \tag{2}$$
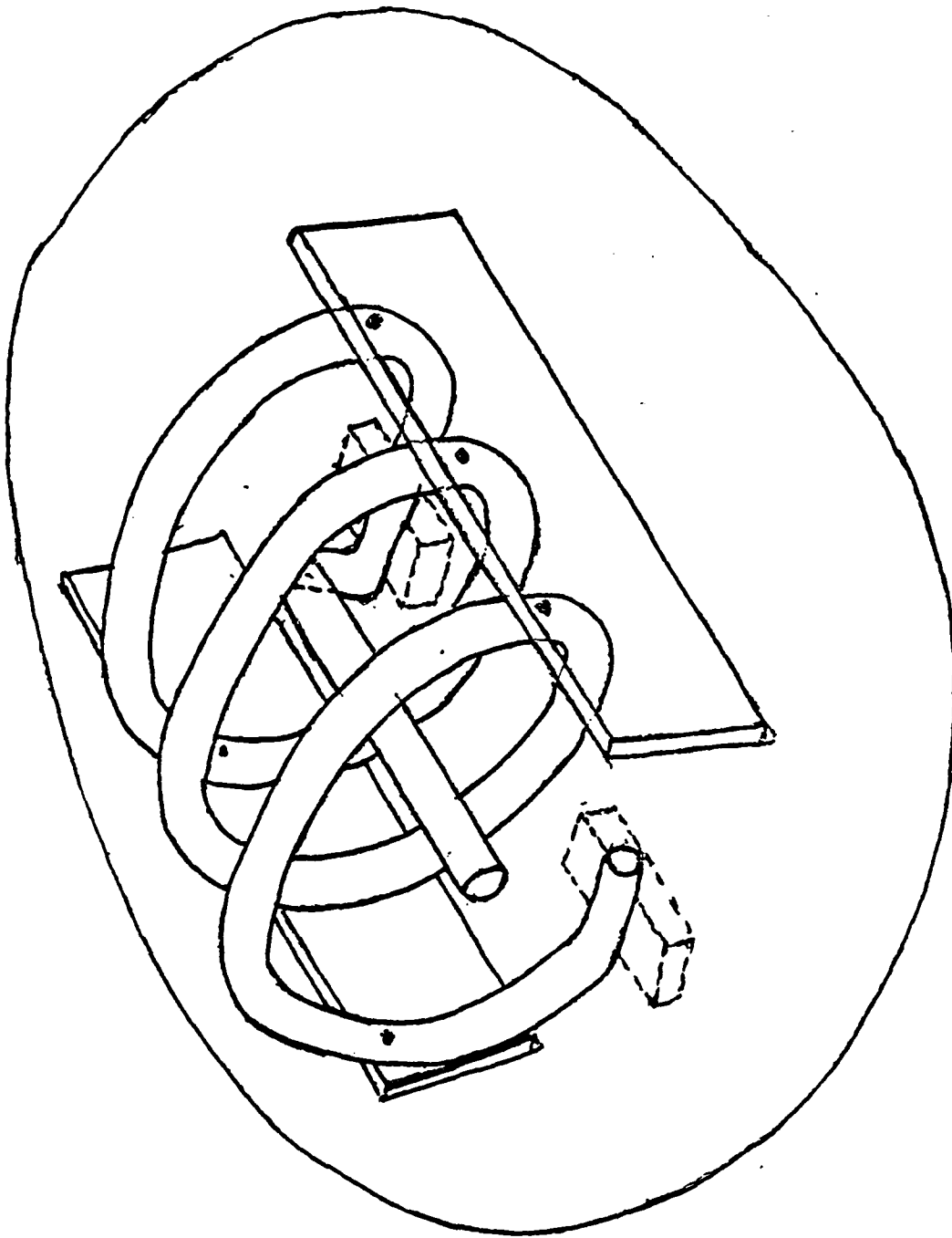
FIGURE 1   Typical MTL Antenna Mounted on a Ground Plane
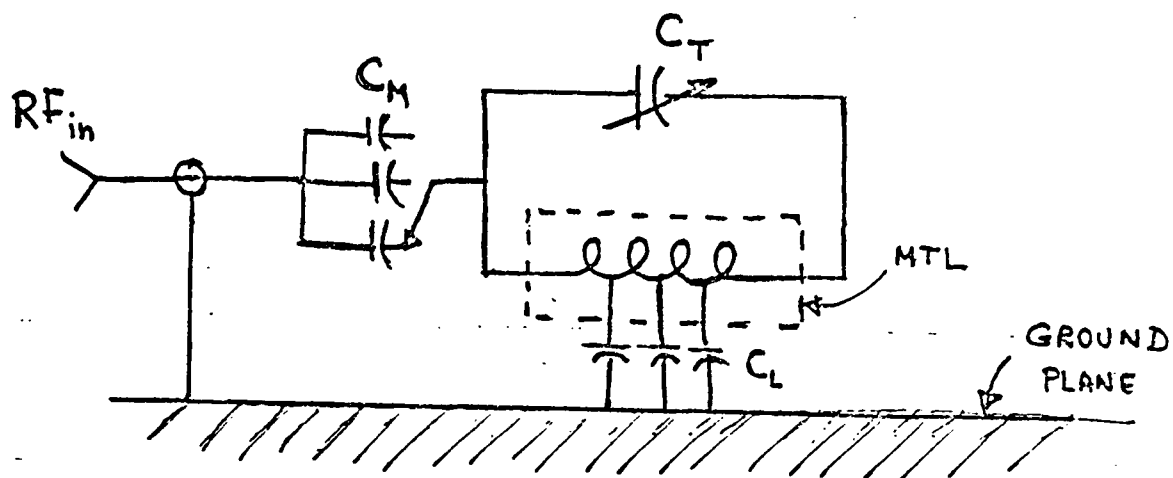
FIGURE 2(a)   Schematic Representation of MTL Antennas and
              Tuning and Matching Network
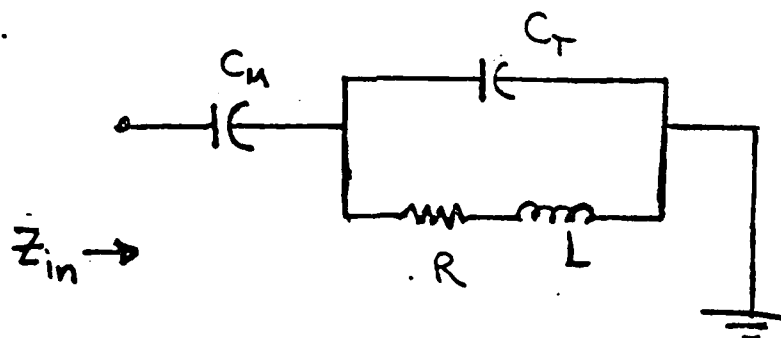
FIGURE 2(b)   Simplified Circuit Description of MTL Input
              Impedance Including Matching Elements

$$X_{loop}(\omega) = \omega L \frac{1 - \omega^2/\omega_r^2 - \left(\frac{R}{\omega_r L}\right)^2}{\left(1 - \frac{\omega^2}{\omega_r^2}\right)^2 + \left(\frac{R}{\omega_r L}\right)^2 \frac{\omega^2}{\omega_r^2}} \tag{3}$$

$$\omega_r = \sqrt{\frac{1}{LC_T}} = 2\pi f_r \tag{4}$$

A typical MTL characteristic input impedance is shown in Fig. 3 as a function of frequency. For fixed values of C_T and L, the highest frequency of operation for the MTL will be restricted to the lowest-resonant frequency, f_r, as defined in Eq. (4). The actual frequency of operation will always be less than f_r as shown in Fig. 3. By increasing or decreasing the parallel capacitance, C_T, one can adjust the resonant frequency, f_r, so that the real part of the input impedance is, say, 50 ohms at a desired operating frequency. The ratio of the operating frequency, f_o, to the required resonant frequency, f_r, so that $R_{loop}(f_o) = 50$ ohms, say, is plotted in Fig. 4 as a function of the ratio $R/R_{loop}(f_o)$ for various parametric values of $R/2\pi f_o L$. The values $f_o/f_r = 1$ are attained when the desired input loop resistance, $R_{loop}(f_o)$, is equal to resistance of the circuit at resonance, $R_{loop}(f_r) = \omega_r^2 L^2/R$ as shown in Fig. 3.

The matching capacitance, C_M, can then be selected so that

$$X_{loop}(\omega_o) = \frac{1}{\omega_o C_M} . \tag{5}$$

II-6
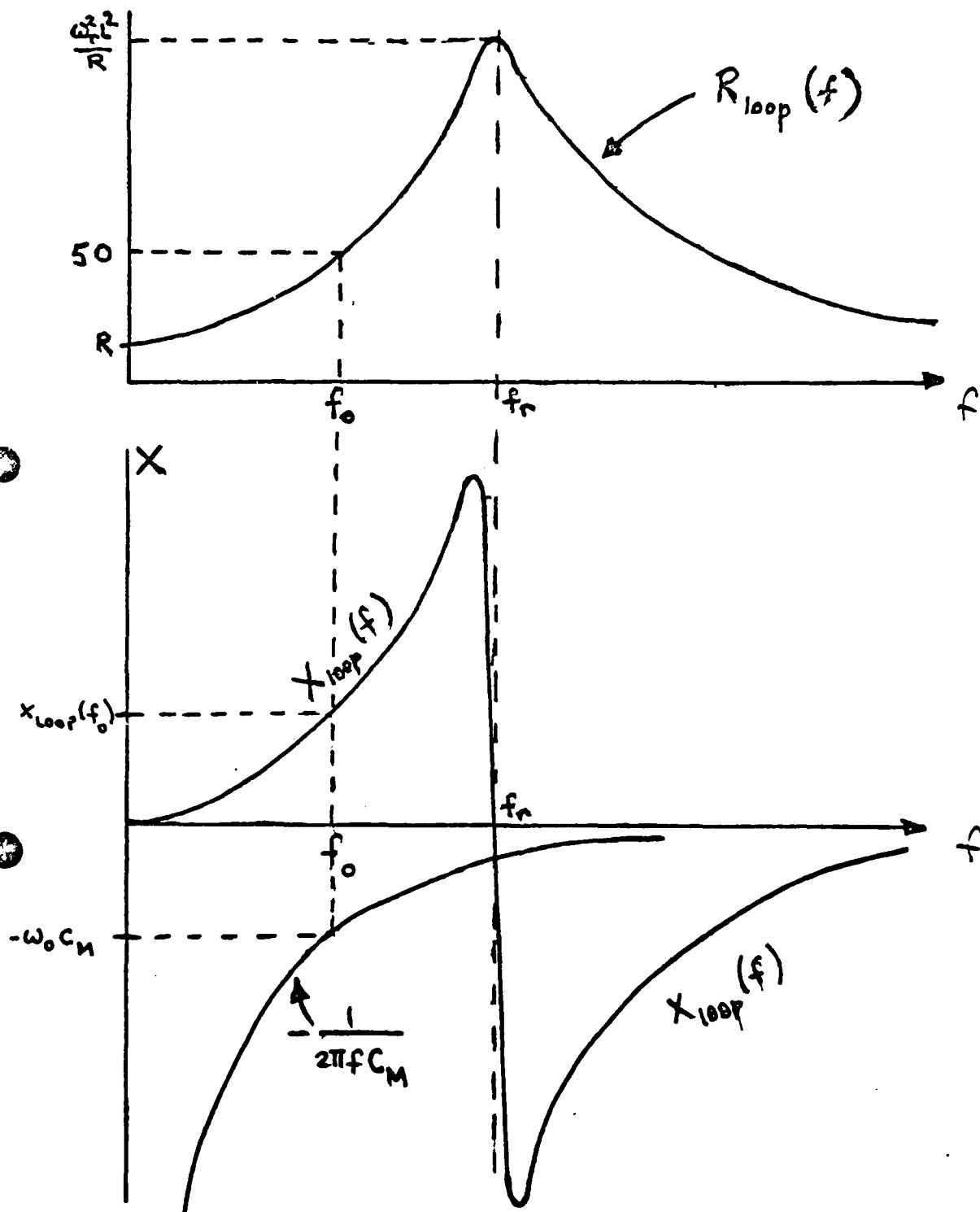
FIGURE 3 Typical Input Impedance of MTL Antenna

II-7
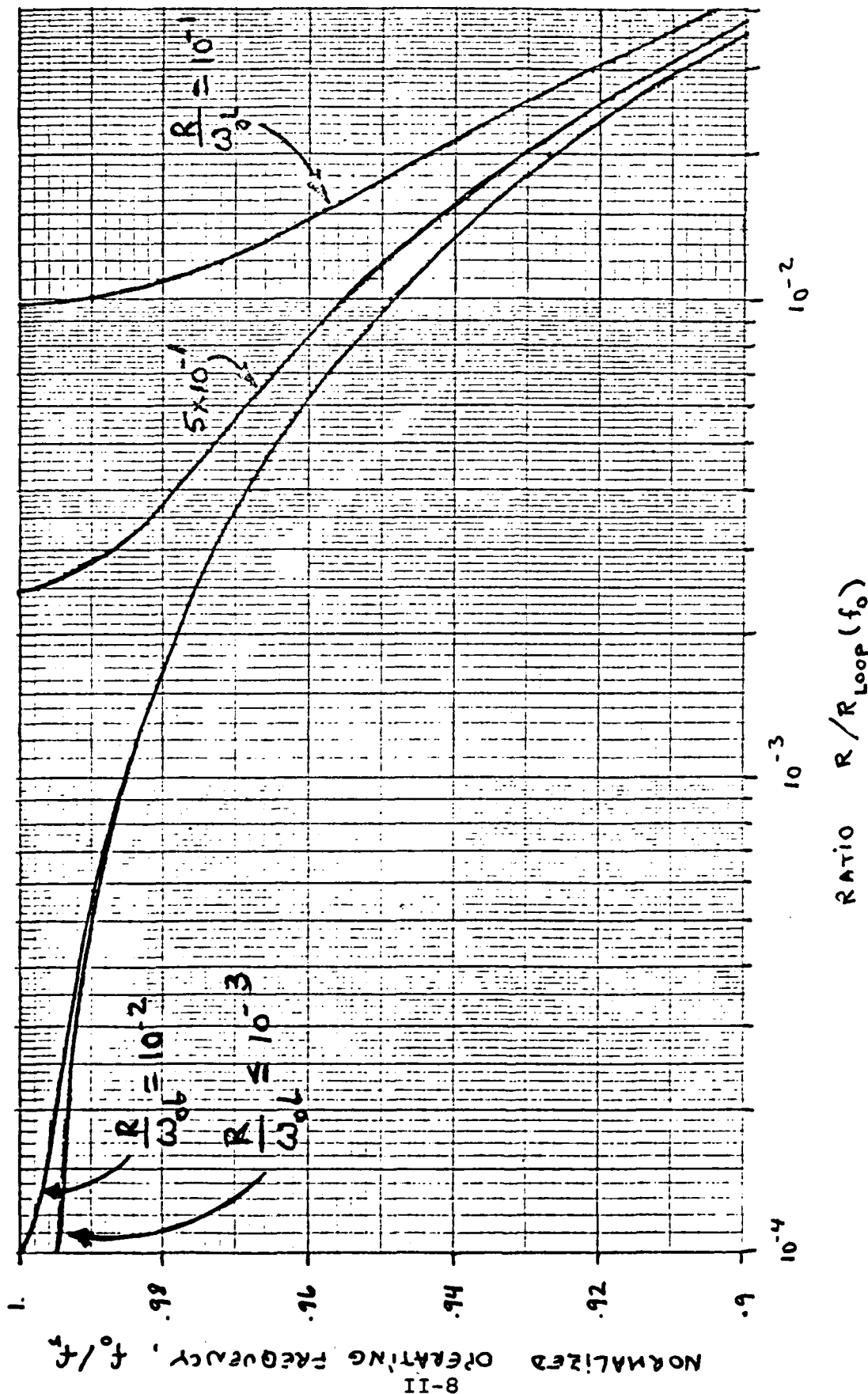
FIGURE 4   Ratio of Operating Frequency, f_0, to Resonant Frequencies, f_r, as a Function of Normalized Resistance R of the Loop

II-8

Equations (3) and (5) have been combined to plot, in Fig. 5, the normalized matching capacitance, $\omega_o^2 L C_M$, as a function of the ratio f_o/f_r for various parametric values $R/\omega_o L$. Hence having knowledge of the tank circuit resistance, R, inductance, L, and operating frequency, f_o, one can determine the required values of C_T and C_M from Figs. 4 and 5 (and Eq. (4)), respectively.

The resistance, R, and inductance, L, are determined by the physical dimensions of the MTL. The total resistance is equal to the sum of the radiation resistance and skin resistance of the antenna [2].

The radiation resistance is given by [3]

$$R_r = 20\pi^2 N^2 \left(\frac{2\pi b}{\lambda}\right)^4 \tag{6}$$

where b is the radius of each loop and N is the number of loops.

The ohmic or skin resistance is approximately given by [4]

$$R_{ac} = \frac{Nb}{a} \left(\frac{2\pi f \mu_o}{2\sigma}\right)^{\frac{1}{2}} \left(1 + \frac{R_p}{R_o}\right) \tag{7}$$

where a is the radius of the wire, σ is its conductivity, μ_o is the permeability of free space, and R_p/R_o is a correction term due to proximity effects between each loop. When the turn spacing, d, is $d \geq 8a$, then the proximity effect $R_p/R_o \ll 1$ [3]. Plots of the skin resistance when $R_p/R_o \ll 1$ for a copper conductor are shown in Fig. 6 as a function of frequency for various antenna dimensions, N, b and a. Plots of the total normalized resistance $R/R_{ac} = 1 + R_r/R_{ac}$ are shown in Fig. 7 as a function of frequency for various MTL dimensions. Hence we can determine the total resistance of a MTL antenna
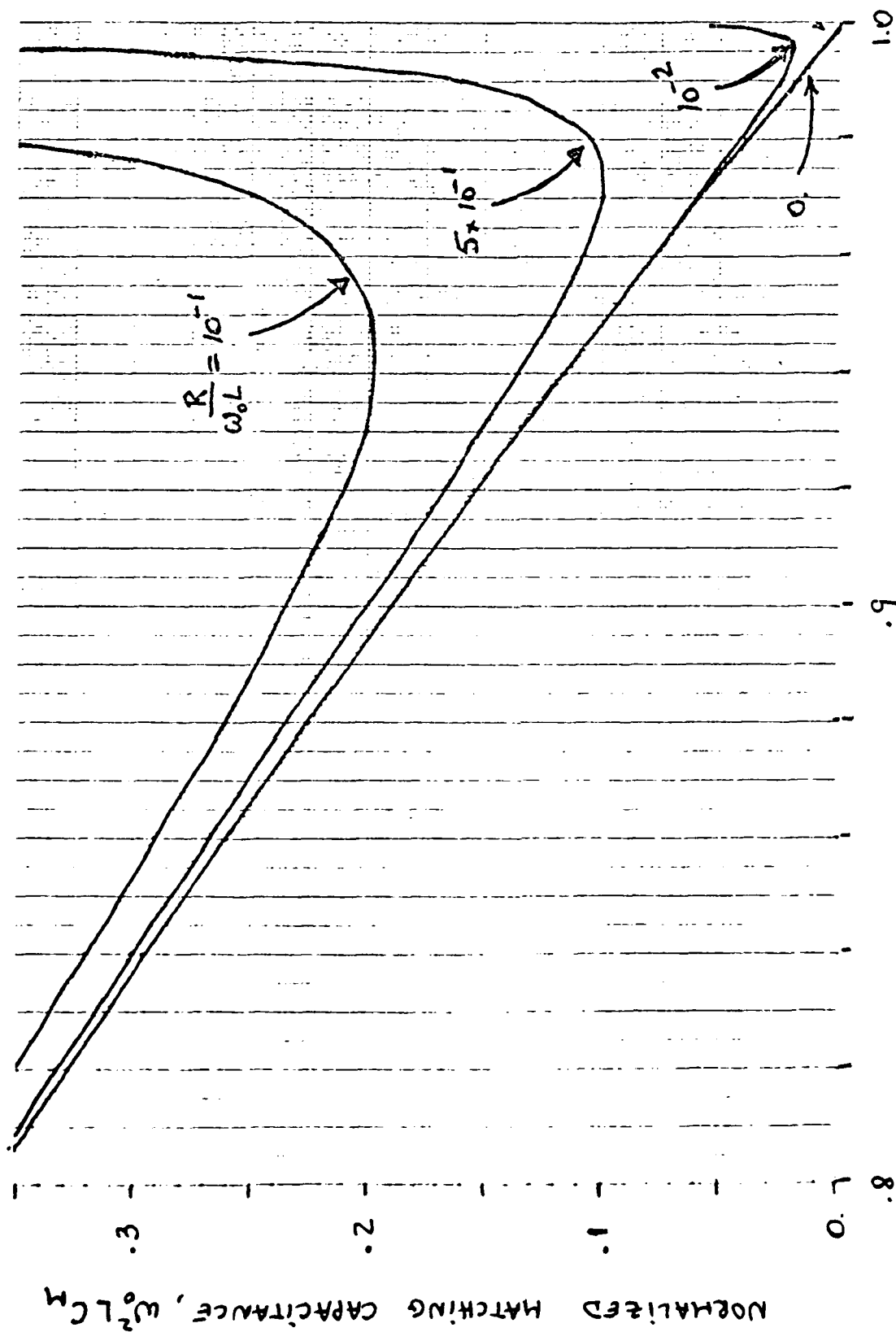
FIGURE 5   Normalized Matching Capacitance, C_M, as a Function of Operating Frequency, f
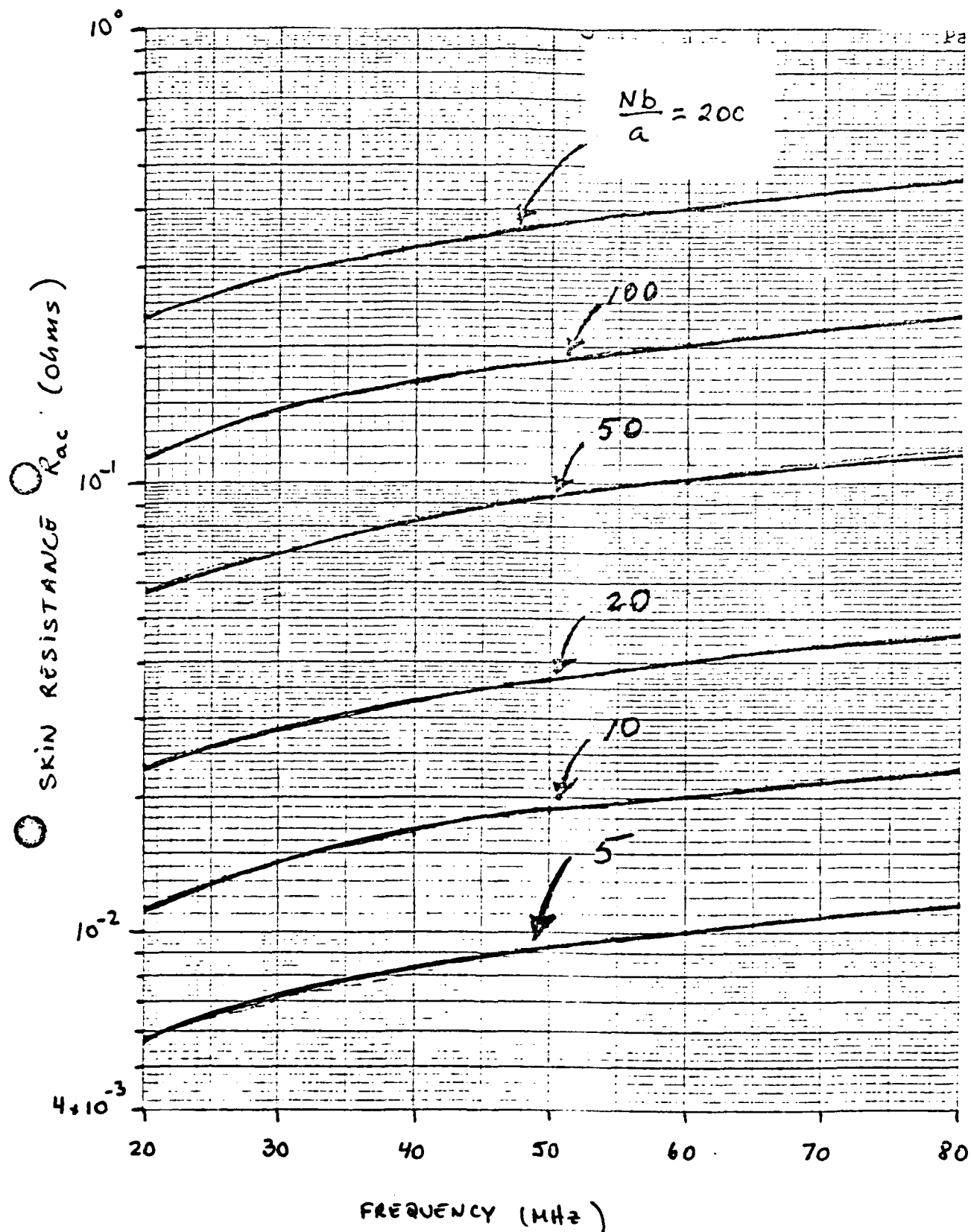
FIGURE 6   Skin Resistance of MTL Antenna as a Function of
Operating Frequency

II-11
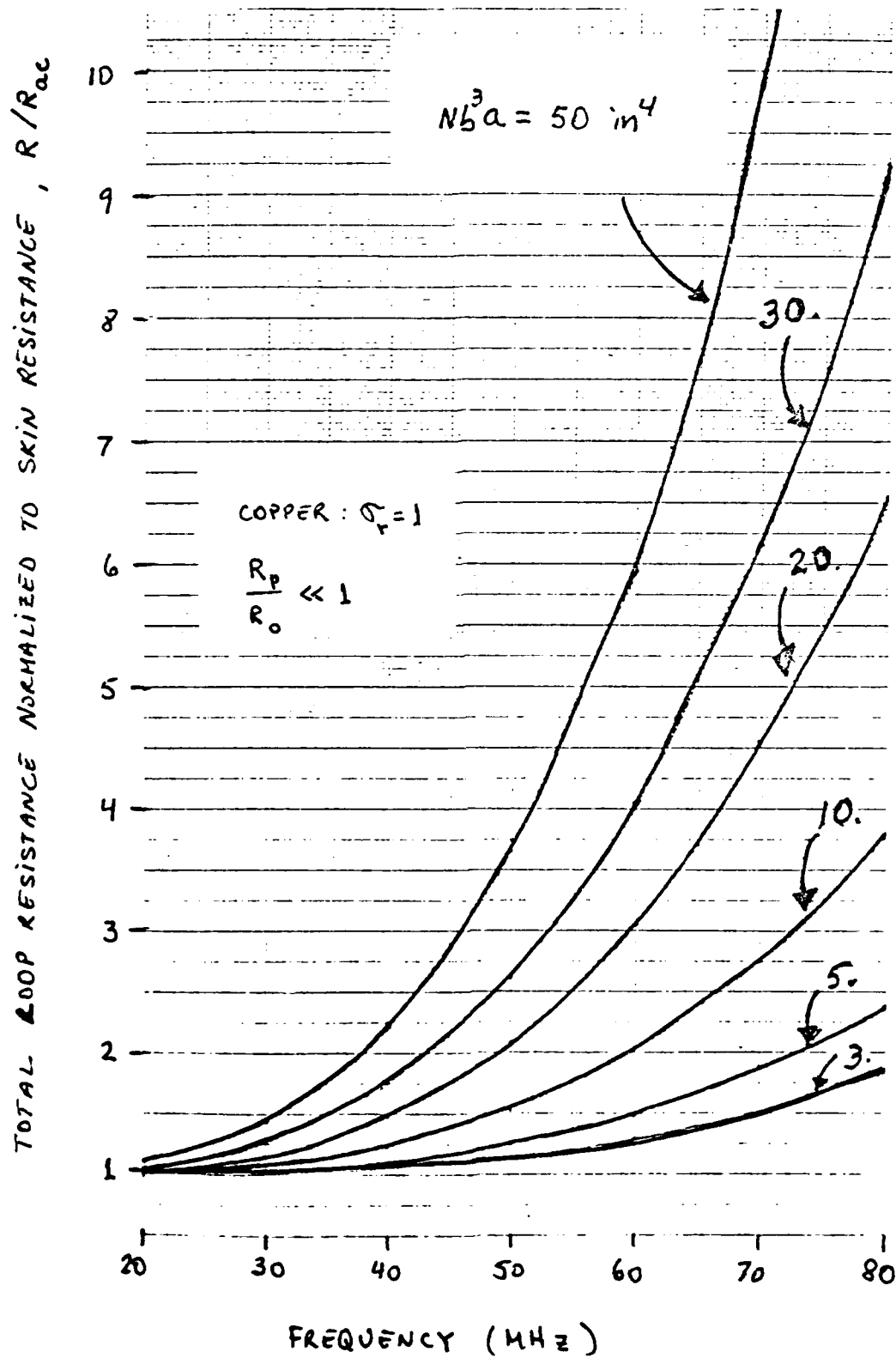
FIGURE 7 Total Loop Resistance, R, as a Function of Operating Frequency

from knowledge of the wire radius, a, loop radius, b, and number of turns, N from Figs. 6 and 7, provided the turn spacing, d, satisfies $d \geq 8a$.

The inductance of the MTL in microhenries is given by[5]

$$L = \frac{2bN^2}{18 + \frac{20 \ell_a}{b}}$$

(8)

where the length of the MTL antenna, ℓ_a, and b are in inches. A plot of $L/2bN^2$ as a function of $8b/\ell_a$ is shown in Fig. 8.

The optimum dimensions of the MTL antenna are selected so as to maximize the efficiency of the antenna. The efficiency of the antenna may be expressed as

$$E_a = \frac{R_r}{R_r + R_{ac}}$$

(9)

Hence from (6), (7) and (9), the theoretical efficiency of the MTL antenna is found to be given by

$$E_a = \left[1 + \frac{8.48 \times 10^{-10} \sqrt{f_{MHz}} \, \sigma_r}{N \left(\frac{b}{\lambda}\right)^3 \left(\frac{a}{\lambda}\right)} \left(1 + \frac{R_p}{R_o} \right) \right]^{-1}$$

(10)

where σ_r is the ratio of the conductivity of the loop wire to that of copper and f_{MHz} is the operating frequency in MHz. Eq. (10) has been plotted in Fig. 9 as a function of frequency for various loop dimensions and serves as the basis for the design of the MTL antenna.

Thus it is possible to maximize the efficiency of the antenna at a chosen frequency by selecting the parameter Nb^3a
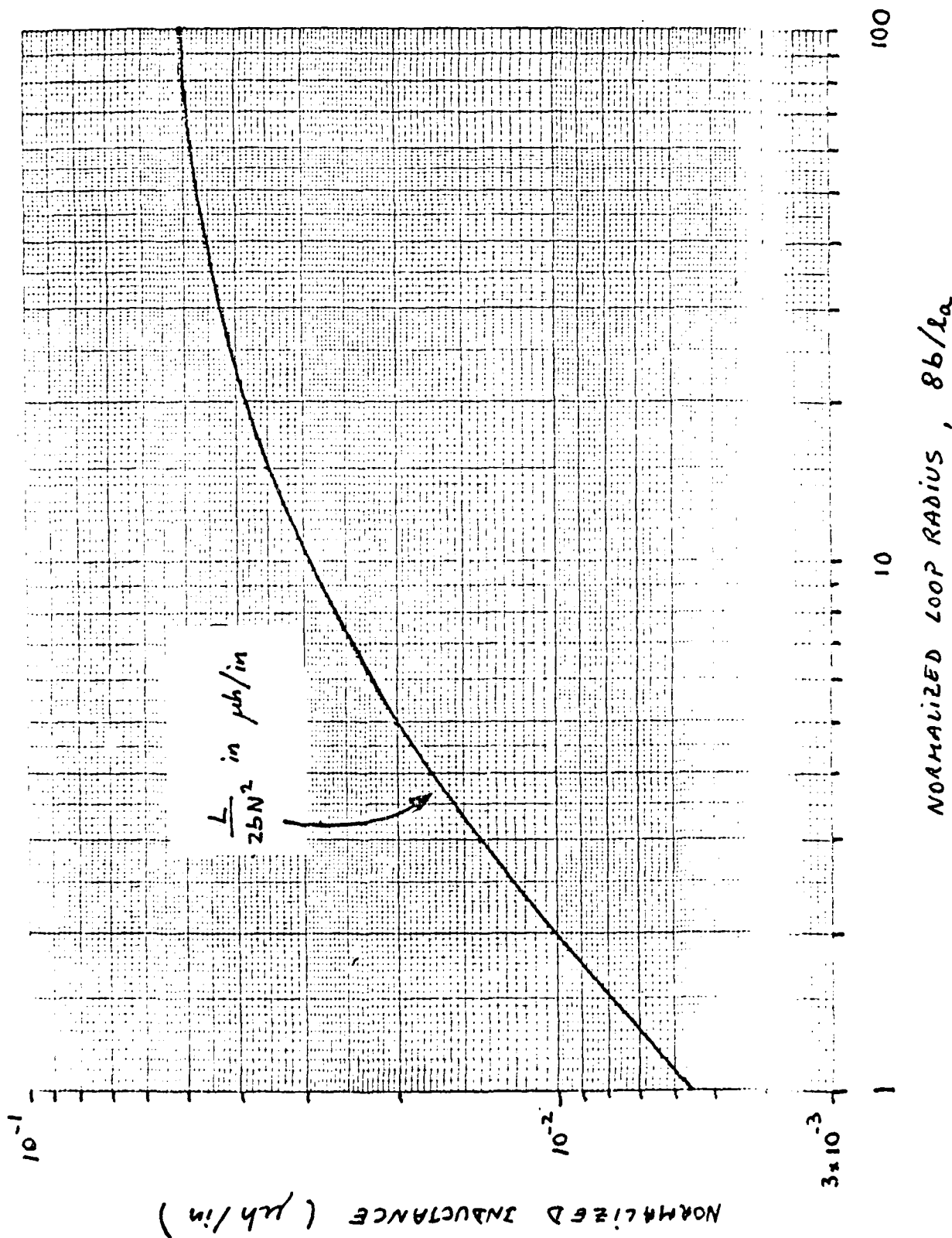
FIGURE 8 MTL Inductance as a Function of Loop Radius Normalized to the Length of the Coil (MTL)
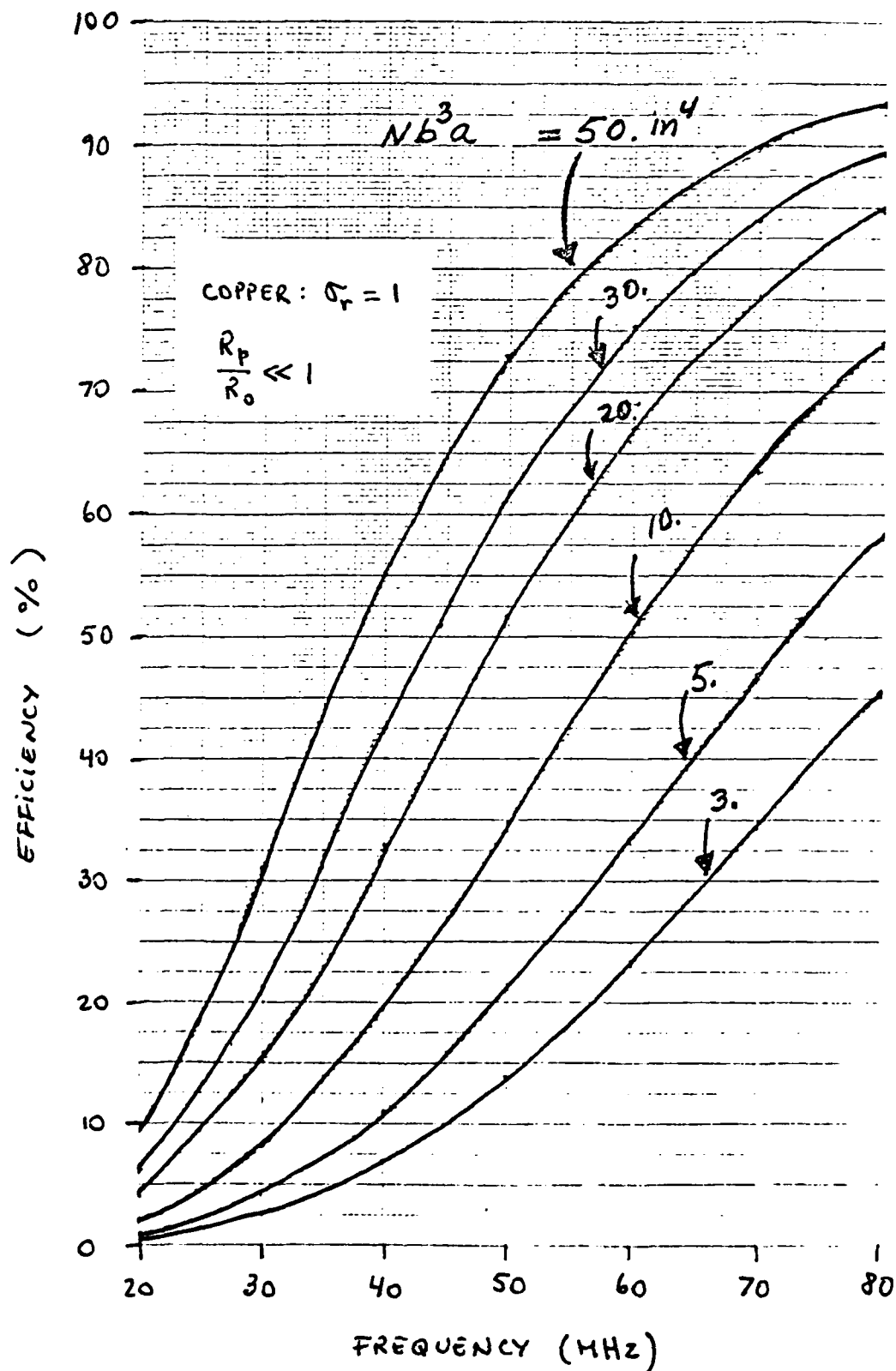
FIGURE 9   Efficiency of MTL as a Function of Operating
Frequency for Various Antenna Sizes

II-15

from Fig. 9. The tuning and matching capacitances may then theoretically be obtained from Figs. 4 - 8. However, it should be kept in mind that the analysis leading up to Figs. 4 and 5 was done assuming an infinite ground plane. When the ground plane is less than about $\lambda/2$ in diameter reduced efficiencies should be expected.

3.   MTL Antenna Design for Use at 27 MHz - 80 MHz

Since the efficiency of the MTL for a given physical size increases with frequency we selected the dimensions of the MTL so that a minimum efficiency of 10% would be acceptable at 30 MHz. Then, from Fig. 9 we have that the minimum size of the antenna must be $N b^3 a > 10$ in^4. Furthermore, if we select 1/2" copper tubing (i.e., $2a = 1/2$") for the antenna, pick loop diameters of 5.6" and 5" we can compare two antenna designs having the following dimensional parameters:

	a	b	N	ℓa	Nb^3a	Nb/a	E_a at 30 MHz
Design 1	1/4"	2.8"	5	8"	27.44 in^4	56	20%
Design 2	1/4"	2.5"	4	6"	15.63 in^4	40	12%

From Fig. 8 we find that the inductances of Design 1 and Design 2 are $L_1 = 1.862$ μh and $L_2 = 1.212$ μh, respectively.

The tank circuit resistance values and tuning and matching capacitances for each design for operating frequencies in the 30 - 80 MHz band are found from Figs. 4 to 8 and are summarized in Table 1 for the desired input resistance $R_{loop} = 50$ ohms.

The actual dimensions used to build the MTL antenna used in the 27 MHz measurements were those of Design 1. The MTL antenna used to make the measurements at 49.8 MHz was a 3 turn loop antenna (of equal diameter and copper tubing size) developed by Ohio State for the AN/PRC-77 and described in Reference [1].

f_o	R/R_{ac}	$R_{ac}\,\Omega$	$R\,\Omega$	$\dfrac{R}{\omega_o L}$	$\dfrac{f_o}{f_r}$	$\omega_o^2 L C_M$	C_M pf	C_T pf
30	1.24	.076	.094	2.7×10^{-4}	.978	.041	.620	14.8
	1.1	.057	.063	2.8×10^{-4}	.983	.032	.743	22.8
40	1.7	.088	.150	3.2×10^{-4}	.973	.053	.451	8.28
	1.37	.064	.088	2.9×10^{-4}	.979	.040	.522	12.8
50	2.48	.102	.253	4.3×10^{-4}	.964	.070	.381	5.25
	1.8	.074	.133	3.5×10^{-4}	.974	.050	.418	8.14
60	3.8	.114	.433	6.2×10^{-4}	.952	.094	.355	3.60
	2.55	.081	.207	4.5×10^{-4}	.967	.065	.377	5.61
70	5.75	.125	.718	8.8×10^{-4}	.937	.122	.339	2.60
	3.63	.087	.316	5.9×10^{-4}	.960	.078	.333	4.10
80	8.6	.130	1.120	1.2×10^{-3}	.922	.150	.319	1.96
	5.2	.093	.484	7.9×10^{-4}	.949	.099	.323	3.44

Table 1

References

(1) Davis, R. J., "The Development of a Multiturn Loop Antenna for the AN/PRC-77", Technical Report 3824-1, December 1974, The Ohio State University ElectroScience Laboratory, Department of Electrical Engineering.

(2) DeVore, R., and P. Bohley, "The Electrically Small Magnetically Loaded Multiturn Loop Antenna," IEEE Trans. on Antennas and Propagation, VAP-25, No. 4, July 1977, pp. 496-505.

(3) Jasik, Antenna Engineering Handbook, McGraw-Hill, 1961, pp. 6-2.

(4) Smith, "Radiation Efficiency of Electrically Small Multiturn Loop Antennas," IEEE Trans. Antennas & Propagation, V AP-20, No. 5, Sept. 1972, pp. 656-657.

(5) ITT Reference Data for Radio Engineers, 4th Edition, p. 112.

APPENDIX III

PERFORMANCE OF A DUAL-DIVERSITY SELECTION COMBINER
IN CORRELATED RAYLEIGH-LOGNORMAL FADING

APPENDIX III

PERFORMANCE OF A DUAL-DIVERSITY SELECTION COMBINER
IN CORRELATED RAYLEIGH-LOGNORMAL FADING

In this Appendix we investigate the effects of the
variability of the mean signal level in each branch of a
correlated dual-diversity selection combiner on the per-
formance of the combiner. The performance of the combiner
is primarily determined by the diversity gain which is
generally defined as the difference between the average
signal-to-noise ratio (in dB) required to achieve a certain
'grade of service' with the diversity system compared to
the average signal-to-noise ratio (in dB) required to achieve
the same level of performance when no diversity is used.
This diversity gain can be determined from the cumulative
probability distribution function of the output of the
combiner. The cumulative probability distribution function
of the output of a dual-diversity selection combiner is
well known for the case in which the signals in the two
diversity branches are Rayleigh fading and correlated.
However, signals in urban and suburban areas have been
found to exhibit rapid fluctuations (Rayleigh fading)
about a mean signal level which is also varying (but much
more slowly). Thus, we will be primarily concerned with
determining the effect of variations in the mean signal
level (in each branch) on the diversity gain of a dual-
diversity selection combiner.

In addition we will also determine the effect of
correlation between the branches on the diversity gain and
the average fade duration at the output of the combiner.

The effects of correlation between the branches is important
when the antenna spacing (in a space diversity situation)
is less than a wavelength or when the antenna heights are
well above the buildings and other obstacles in the immediate
surroundings [Lee, 1977]. The antenna spacing in a mobile
communications link will necessarily be less than a wave-
length when the frequency is in the lower VHF range (30-80 MHz)
or lower, while the antenna height will be above the sur-
rounding obstacles when diversity is used at the base-
station.

1. Cumulative Probability Distribution

The cumulative probability distribution is defined as
the probability that the signal level at the output of the
selection combiner, S, is below some threshold level, S_T.
In an environment dominated by ambient (atmospheric or man-
made) noise such as urban and suburban areas at VHF and
lower UHF, the threshold level is usually defined as the
average ambient noise level. In this case, the average
signal-to-noise (SNR) ratio in each diversity branch is
independent of the receiving antenna gain as long as the
received signal level at the antenna input port remains
above the receiver thermal noise level. Furthermore, if
that is the case, then we can assume that the mean signal
levels in the two diversity branches are the same.

When the envelopes of the signals in the two diversity
branches are correlated and each is Rayleigh distributed
with equal mean power (i.e., mean-squared amplitude) level
S_o, the cumulative distribution of the output of the
selection combiner is given by [Schwartz, Bennett and
Stein, 1966]

$$P(S \leq S_T/S_O) = 1 - \exp(-S_T/S_O) [1-Q(a,\rho a) - Q(\rho a,a)]; \qquad (1)$$

where

$$a = \left[\frac{S_T}{S_O(1-\rho^2)} \right]^{1/2} \qquad (2)$$

and $Q(a,b)$ is the Marcum Q-function defined as

$$Q(a,b) = \int_b^\infty \exp\left\{-\frac{a^2 + x^2}{2}\right\} I_O(ax) \, x \, dx. \qquad (3)$$

When the transmitting and receiving stations are both fixed or moving within a small area, the mean signal power level is constant (and known). Then the cumulative distribution of the output of the selection combiner is exactly that given by (1). However, when either the transmitting and/or receiving stations are moving within an area of radius greater than a few wavelengths, then the mean signal level tends to fluctuate randomly due to variations in the shadow losses caused by the buildings and trees in the area. In this case, an additional averaging over the variability of the mean signal level is required when computing the (mean) cumulative distribution. Thus, the (mean) cumulative distribution is better defined as

$$P(S \leq S_T) = \int_{-\infty}^\infty P(S \leq S_T/S_O) \, p(S_O) \, dS_O \qquad (4)$$

where $p(S_O)$ is the probability density function of the mean signal level, S_O.

III-4

The large area variations in the mean signal level, S_o, have been found to be lognormally distributed about a 'global' mean also known as the median signal level, $\tilde{S}_o$ [Longley, 1976, and Okumura, 1968]. Hence,

$$p(S_o) = \frac{10 \log_{10} e}{\sqrt{2\pi}\, \sigma\, S_o} \exp\left\{ -\left(10 \log_{10} \frac{S_o}{\tilde{S}_o}\right)^2 / 2\sigma^2 \right\}, \quad S_o \geq 0 \qquad (5)$$

where σ is the standard deviation of the mean signal level about the median in dB.

If we substitute equations (1) and (5) in Eq. (4), we can then solve for the cumulative distribution numerically. Plots of $P(S \leq S_T)$ as a function of $S_T/\tilde{S}_o$ for various correlation values ρ and standard deviations $\sigma = 0$ dB and $\sigma = 8$ dB are given in Section 3 (Figs. 3.2-1 and 3.2-2). The case $\sigma = 0$ corresponds to a situation in which transmitter and receiver are fixed and the mean signal level is constant and known (pure Rayleigh fading). A variability of $\sigma = 8$ dB is, on the other hand, more typical for a mobile urban radio link.

2. Diversity Gain

The diversity gain as defined in the introduction, may be interpreted as a reduction in the transmitted power required to achieve a certain 'grade of service', e.g., $P(S \leq S_T) \leq 10^{-2}$. Thus, in a 'pure' Rayleigh fading ($\sigma = 0$ dB) situation we can see (Fig. 3.2-1) that a system using dual selection diversity will require (for $P(S \leq S_T) = 10^{-2}$) a median SNR, $\tilde{S}_o/S_T$, that is 10.2 dB lower than that required when no diversity is used ($\rho = 1$), if the two branches are uncorrelated ($\rho = 0$), and 8.8 dB lower SNR (or transmitted

power) if the correlation between the branches is .7. When
the variability in the mean signal level is 8 dB (i.e.,
σ = 8 dB), the diversity gain is 6.8 dB if the branches
are uncorrelated (ρ = 0) and 5.8 dB if the correlation
between the branches is 0.7. The effect of the variability
of the mean signal level is then to reduce the diversity
gain (by about 3 dB). However, the diversity gain is still
significant even if the correlation between the branches is
0.7.

The diversity gain may be interpreted as an increase
in the range of the transmitter for a given transmitter
power. The reason is that the median SNR at the receiver,
$\tilde{S}_o/S_T$, decreases with transmitter-receiver separation so
that the minimum acceptable median SNR corresponds to the
maximum allowable transmitter-receiver separation (range).
Thus a decrease in the minimum acceptable SNR (due to di-
versity gain) corresponds to an increase in the range of
the transmitter. The increase in range due to the diversity
gain is shown in Fig. 3.2-3 as a function of the rate of
increase of the path loss and for various correlation
values and variability in the mean signal level. When
the path loss increases at a rate of 40 dB/decade, the range
of a system employing dual selection diversity will increase
by a factor of 1.8 if the two branches are uncorrelated and
by a factor of 1.66 if the correlation is .7 provided there
is no variability in the mean signal level (σ = 0 dB).
When the variability is 8 dB, the increase in range is in
the order of 1.4 (ρ = 0.7) to 1.48 (ρ = 0).

3. <u>Average Fade Duration and Level Crossing Rate</u>

The average duration of fades below a threshold level
$\tilde{S} = S_T$ has been shown to be given by [Jakes, 1974]

$$T_D(S_T) = \frac{P(S \leq S_T)}{N(S_T)} \tag{6}$$

where $N(S_T)$ is the average level crossing rate defined as the expected rate at which the envelope of the output of the selection combiner crosses the specified threshold level, S_T, in the positive direction. In general, it is given by [Rice, 1948]

$$N(r) = \int_0^\infty \dot{r}\, p\, (r,\dot{r})\, d\dot{r} \tag{7}$$

where $r = \sqrt{2S}$ is the amplitude of the envelope at the output of the combiner, $\dot{r}$ is its rate of change, and $p(r,\dot{r})$ is the joint probability density of the envelope and its rate of change.

The joint probability diversity $p(r,\dot{r})$ for a dual-diversity selection combiner can be obtained from its joint distribution function

$$F(\xi,\eta) = P(r \leq \xi, \dot{r} \leq \eta)$$

$$= P(r_1 > r_2)\, P(r_1 \leq \xi, \dot{r}_1 \leq \eta / r_1 > r_2) \tag{8}$$

$$+ P(r_2 > r_1)\, P(r_2 \leq \xi, \dot{r}_2 \leq \eta / r_2 > r_1)$$

since

$$p(r,\dot{r}) = \left. \frac{\partial^2 F(\xi,\eta)}{\partial \xi\, \partial \eta} \right|_{\substack{\xi = r \\ \eta = \dot{r}}} \tag{9}$$

where r_1 and r_2 are the envelopes in the two branches.

III-7

Hence, using (8) and (9) in (7) we find that the average level crossing rate for a dual-diversity selection combiner is given by

$$N(r) = \int_0^\infty \int_0^r \dot{r}\, p(r_1=r, r_2, \dot{r}_1=\dot{r})\, dr_2\, d\dot{r}$$

$$+ \int_0^\infty \int_0^r \dot{r}\, p(r_1, r_2=r, \dot{r}_2=\dot{r})\, dr_1\, d\dot{r}. \qquad (10)$$

Based on a theoretical model of the urban channel [Jakes, 1974], Lee [1978] has shown that the envelopes and their derivatives in each of the branches are independent, i.e., $p(r_1, r_2, \dot{r}_1, \dot{r}_2) = p(r_1, r_2)\, p(\dot{r}_1, \dot{r}_2)$. Hence, it follows that

$$p(r_1, r_2, \dot{r}_1) = p(r_1, r_2)\, p(\dot{r}_1)$$

$$(11)$$

$$p(r_1, r_2, \dot{r}_2) = p(r_1, r_2)\, p(\dot{r}_2)$$

where $p(r_1, r_2)$ is the joint density of the envelopes in the two correlated diversity branches, and $p(\dot{r}_1)$ and $p(\dot{r}_2)$ are the densities of their time derivatives.

When the two envelopes are Rayleigh fading with equal mean signal level, S_o, and are also correlated, their joint density function is given by (e.g., [Jakes, 1974])

$$p(r_1, r_2 / S_o) = \frac{r_1 r_2}{S_o^2 (1-\rho^2)} \exp \left\{ - \frac{r_1^2 + r_2^2}{2 S_o (1-\rho^2)} \right\} \qquad (12)$$

$$I_o \left(\frac{\rho}{1-\rho^2} \frac{r_1 r_2}{S_o} \right)$$

Furthermore, since the two diversity signals have been assumed to have equal mean power, S_o, they are identically distributed and so are their derivatives [Jakes, 1974]. Thus,

$$p(\dot{r}_1/S_o) = p(\dot{r}_2/S_o) = p(\dot{r}/S_o) = \frac{\exp\{-\dot{r}^2/2\, S_o (kv)^2\}}{\sqrt{2\pi S_o}\ (kv)} \tag{13}$$

where $k = 2\pi/\lambda$, λ is the wavelength and v is the velocity of the receiver relative to the transmitter. The ratio v/λ is the fading rate.

Since the joint density $p(\dot{r}_1, \dot{r}_2)$ is symmetric in the two variables and $p(\dot{r}_1) = p(\dot{r}_2)$, then (10) may be written as

$$N(r/S_o) = p(r/S_o) \int_0^\infty \dot{r}\ p(\dot{r}/S_o)\ d\dot{r} \tag{14}$$

where:

$$p(r/S_o) = \frac{2r}{S_o^2\ (1-\rho^2)} \int_0^r dr_1 \left[r_1\ \exp\ \left\{-\left(\frac{r_1^2 + r^2}{2S_o\ (1-\rho^2)}\right)\right\}\right.$$

$$\left. I_o \left(\frac{\rho}{1-\rho^2}\ \frac{r\, r_1}{S_o}\right)\right] = \frac{2r}{S_o}\ e^{-r^2/2S_o}\ [1-Q(\rho a', a')], \tag{15}$$

and where:

$$a' = \frac{r}{\sqrt{(1-\rho^2)S_o}}\ . \tag{16}$$

Substituting (13) and (15) in (14), we find that the average level crossing rate for a given mean signal level, S_O, is

$$N(r/S_O) = \frac{2\,kvr}{\sqrt{2\pi S_O}}\ e^{-r^2/2S_O}\ [1-Q(\rho a', a')].\qquad(17)$$

When the mean signal level is also fluctuating randomly, the average level crossing rate is given by

$$N(r) = \int_O^\infty N(r/S_O)\ p(S_O)\ dS_O.\qquad(18)$$

If the desired level is the threshold level, S_T, then we set $r = \sqrt{2S_T}$ in (18) and $a' = a$ in (16). Then, the average duration of the fades below S_T can be obtained from a numerical evaluation of the cumulative distribution and the average level crossing rate $N(r = \sqrt{2S_T})$. Plots of the average fade duration $T_D(S_T)$ as a function of $S_T/\tilde{S}_O$ for various correlation values ρ and standard deviations $\sigma = 0$ dB and $\sigma = 8$ dB are given in Section 3 (Figs. 3.2-4 and 3.2-5). The case $\sigma = 0$ dB corresponds to a situation in which the mean signal level is constant (pure Rayleigh fading). From these curves (Fig. 3.2-4) we see that even a small amount of decorrelation ($\rho = .9$) reduces the average fade duration significantly provided the median signal-to-noise ratio $\tilde{S}_O/S_T$ is greater than 10 dB. When the two signals are uncorrelated ($\rho = 0$), the averaged fade duration is half of what it would be if no diversity were used ($\rho = 1$). From the curves of Fig. 3.2-5 we see that variations in the mean signal level increase the average fade duration for a given median signal-to-noise ratio, $\tilde{S}_O/S_r$, as one might expect. In either case, the average fade duration decreases as the fading

rate, v/λ, increases. Note that as the relative velocity
of the receiver approaches zero so does the fading rate,
and the average fade duration becomes indeterminate. In
this limiting case the fade duration is either zero or
infinite depending on whether the received signal level is
above or below threshold.

4. Conclusions

We have shown in this appendix that dual-diversity
reception in an urban channel using a selection combiner
results in a significant diversity gain even when the
correlation between the branches is as large as $\rho = .7$.
The diversity gain, in the form of a lower power require-
ment or range increase, decreases as the variability
(standard deviation σ) in the mean signal level, S_o,
increases. The maximum tolerable variability for a
diversity gain greater than 5 dB with correlation $\rho = .7$
and grade of service $P(S \leq S_T) = 10^{-2}$ is in the order of
$\sigma \approx 10$ dB. Similarly, we have also shown that diversity
reception reduces the average fade duration by a factor
of 2 when there is no variability in the mean signal
level ($\sigma = 0$ dB) and by a factor of 1.3 ($\rho = .7$) to 1.4
($\rho = 0$) when the variability in the mean signal level is
$\sigma = 8$ dB.

References

Jakes, W.C. (1974), Microwave Mobile Communications,
Wiley-Interscience, New York, 1974.

Lee, W.C.Y. (1977), "Mobile Radio Signal Correlation Versus
Antenna Height and Spacing", IEEE Trans. Vehicular
Tech., Vol. VT-25, No. 4, pp 290-292.

Lee, W.C.Y. (1978), "Mobile Radio Performance for a Two-
Branch Equal-Gain Combining Receiver with Correlated
Signals at the Land Site", IEEE Trans. Vehicular
Tech., Vol. VT-27, No. 4, pp 239-243.

Longley, A.G. (1976), "Location Variability of Transmission
Loss-Land Mobile and Broadcast Systems", O.T. Report
76-87, U.S. Dept. of Commerce, Office of Telecommuni-
cations.

Okumura, Y., et al. (1968), "Field Strength and its Vari-
ability in VHF and UHF Land Mobile Service", Rev.
Elec. Commun. Lab., Vol. 16, pp 825-873.

Rice, S.O. (1948), "Distribution of the Duration of Fades
in Radio Transmission", Bell Syst. Tech. J., p 109.

Schwartz, Bennett, and Stein (1966), Communication Systems
and Techniques, McGraw-Hill, Inc., New York, 1966,
pp 468-475.

APPENDIX IV

Active Antennas for Mobile Receivers

1.0 Introduction

In order to assess the potential for active antennas in mobile communication systems, the subject is reviewed with the objective of identifying their major performance and design parameters. Active antennas have been reported in the literature for a number of applications:

1) Extremely wideband optimization of system signal-to-noise ratio (SNR) in the VHF frequency range and lower.

2) Reduction of mutual coupling effects in arrays for transmit and receive. This implies an increased bandwidth.

3) Increased bandwidth of transmit and receive antennas.

The results summarized in this introduction emphasize the wideband receive SNR optimization of item 1) that has application to mobile communications in the 30 to 80 MHz band. Additional technical details in support of this item and the other items cited above will be subsequently addressed. The articles on the subject of active antennas that have been published are of a restricted scope and use varying notational conventions. For that reason an overall summary is developed before discussing particular publications in the last section.

The elements in the block diagram of Fig. 1 represent a conventional receive communication system. Optimal operation requires that the system noise temperature be kept minimal. The distinctive features of the configuration are the remoteness of antenna and tuning network from the first amplifier stage the intervening 50 ohm cable. Consequently the antenna and

IV-2

Small Antenna — 50Ω Match — 50Ω Line — Receiver

η, T_A

F_N, G Matched to 50Ω

High Q Tuning

Narrowband Match to 50Ω

Efficiency $\eta = \dfrac{R_a}{R_A + R_L} \ll 1$

$$T_{sys} = \eta T_A + (F_N - \eta) T_o$$

$$\frac{S}{N} = \frac{DSb}{kT_A B} \frac{\dfrac{T_A \eta}{T_A \eta + T_o(F_N - \eta)}}{\gamma} \implies \frac{\eta}{F_N} \cong k \frac{T_A}{T_o}$$
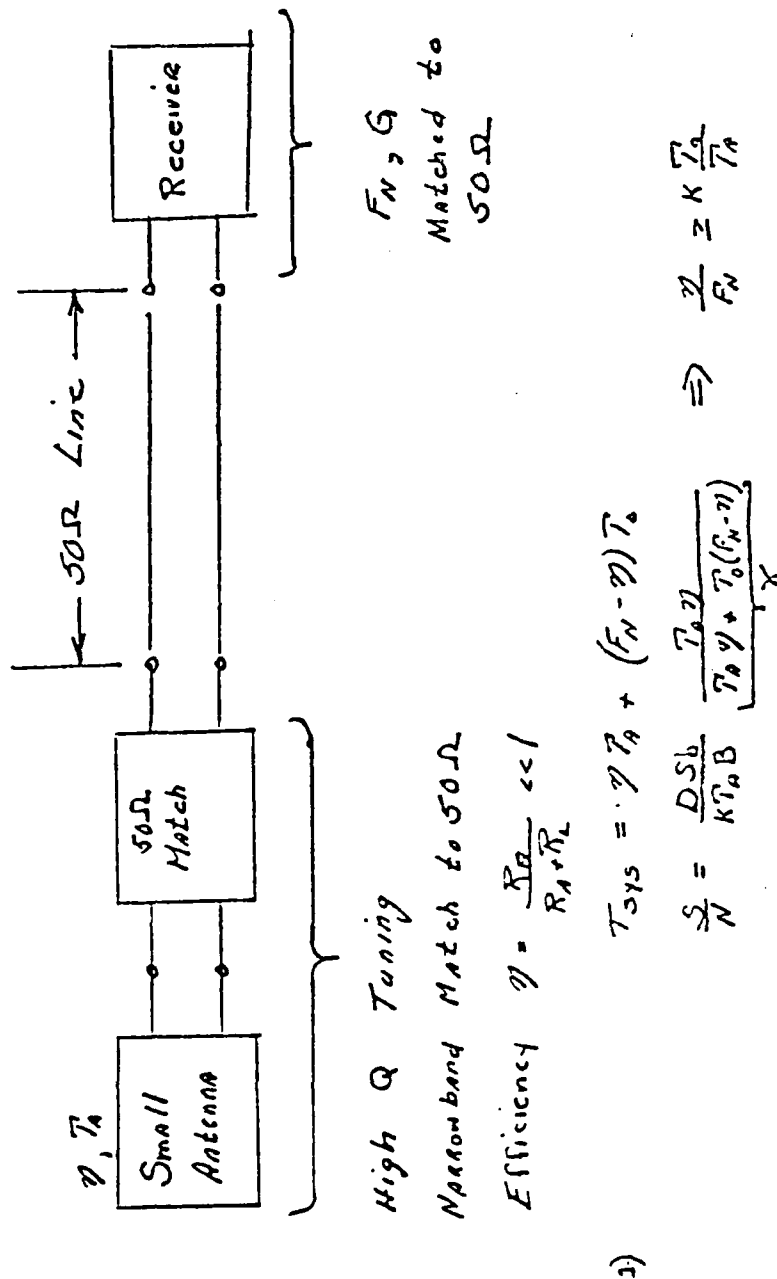
Fig. 1 Conventional remote antenna and receiver configuration that are separately matched into 50 ohms

tuning network must be matched into 50 ohms. For electrically small antennas that often occur in the lower part of the VHF band and at lower frequencies, this results in high Q, narrow-band matching in order to maintain acceptable efficiencies. Even when the preamp is brought right up to the base of the antenna, 50 ohm matching at the interface still imposes narrow-band operation. Wideband operation exceeding a few percent is achieved only at the expense of manual or mechanized switching or variation of the tuning network.

The system noise temperature of the configuration in Fig. 1 depends on the external or antenna noise temperature T_A, the efficiency η of the antenna and matching network, and the receiver noise figure F_N as shown by the equation in the lower part of the figure. Since T_0/T_A is often very much less than unity, a certain amount of inefficiency can be tolerated with little degradation to system performance. Usually the system cannot tolerate the additional mismatch losses incurred over wide bandwidths without retuning. The effect of any intervening transmission line between the antenna and matching network is to amplify the frequency variation of the antenna impedance and mismatch. This is demonstrated by the loci on the three Smith charts a), b), and c) of Fig. 2. In a) the locus is that of a one foot monopole observed at its base ($\ell_1 = 0$) when the frequency is increased from f_1 to f_2 (30 to 80 MHz). For the electrically small antenna as occurs here, the reactance ratio x_1/x_2 is in direct proportion to f_2/f_1. In the case of b), one eighth wavelength of 80 MHz line has been added. The reactance ratio $x_1/x_2 = 3.2/.85 = 3.76$ now exceeds $f_2/f_1 = 80/30 = 2.67$. In case c) where one half wavelength of 80 MHz line has been added, the impedance variation has become quite complex, going
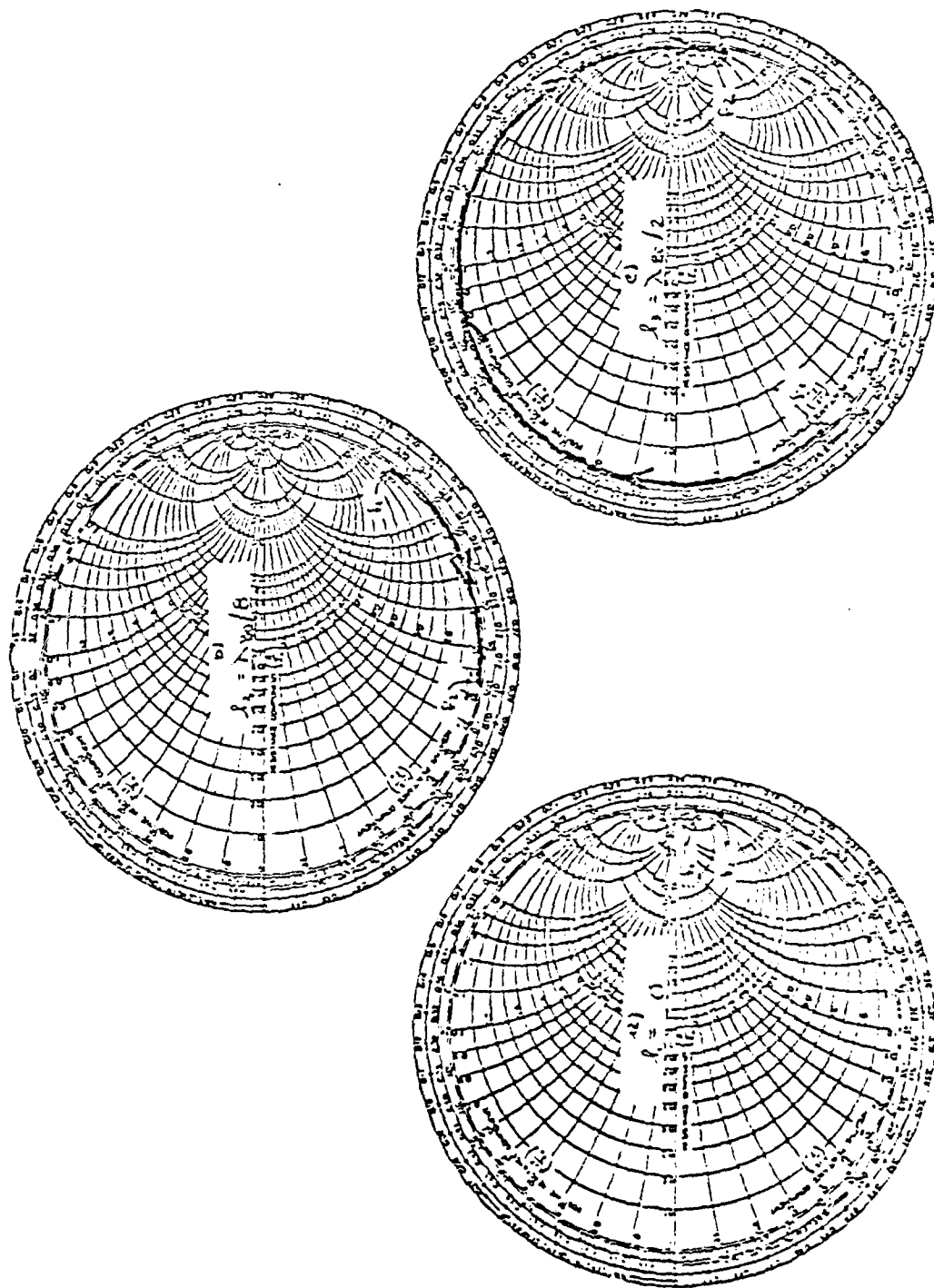
IV-4

Fig. 2   Impedance plots of electrically short monopole as viewed through different
lengths of line

from capacitive to inductive and back to capacitive as the frequency is increased from f_1 to f_2.

The basic idea behind the active antenna as a receiving element shown in the block diagram of Fig. 3 is that the antenna element can be integrated directly into the input matching network (Ml) of the transistor. This eliminates the 50 ohm interface requirement that had been the major cause of the narrowband limitation previously encountered. For this circuit integration, the electrically short antenna is representable by a series capacitance C_A and a frequency dependent resistance R_A. These and related parameters are summarized in Table I for an arbitrary monopole electrical height ($k_0 h$) and for the particular case of a 12 inch monopole at 30 and 80 MHz.

Table I

Short Monopole Impedance Parameters

$$\nu_0 = 3 \times 10^8 \text{ m/s} = 11.8 \times 10^9 \text{ in/s}$$

Parameter	$k_0 h = \dfrac{2\pi f h}{\nu_0}$	h=12" 30 MHz	h=12" 80 MHz
C_A - pfd	$85\, h^{in}/Z_{0A}$	4.0.	4.0
Z_{0A} - Ω	$60(\ln h/a - 1)$	255	255
X_A - Ω	$-\dfrac{1}{\omega C_A} = - Z_{0A}/k_0 h$	-1327	-500
R_A - Ω	$10(k_0 h)^2$	0.37	2.61
$Q = \lvert X_A \rvert / R_A$	$\dfrac{Z_{0A}}{10(k_0 h)^3}$	3586	191

IV-6

30-50 Mhz
1' Dipole

$R_a \approx 1\Omega$

$C_s = 4\,pfd$

$X_a = -1K\Omega$

$e_n = \sqrt{4KT_nB}$

$\frac{T_n}{T_a} \approx 3 \text{ to } 3\times10^6$

M1

unilateral →

Active Element G_2, F_N

$[\delta T]$

M2

50Ω

$R_s, \; S_{22}^{ni} = f(S_{11}^*)$

$S_{11}^{n2} = f(S_{22}^*)$

$T_{sys} = \eta T_n + (F_n - \eta) T_a$

$\frac{S}{N} = \frac{D S_a}{KT_aB} = \frac{T_a \eta}{T_a \eta + T_a(F_n - \eta)}$ Degradation δ

$\Rightarrow \frac{\eta}{F_n} \geq K \frac{T_a}{T_n}$
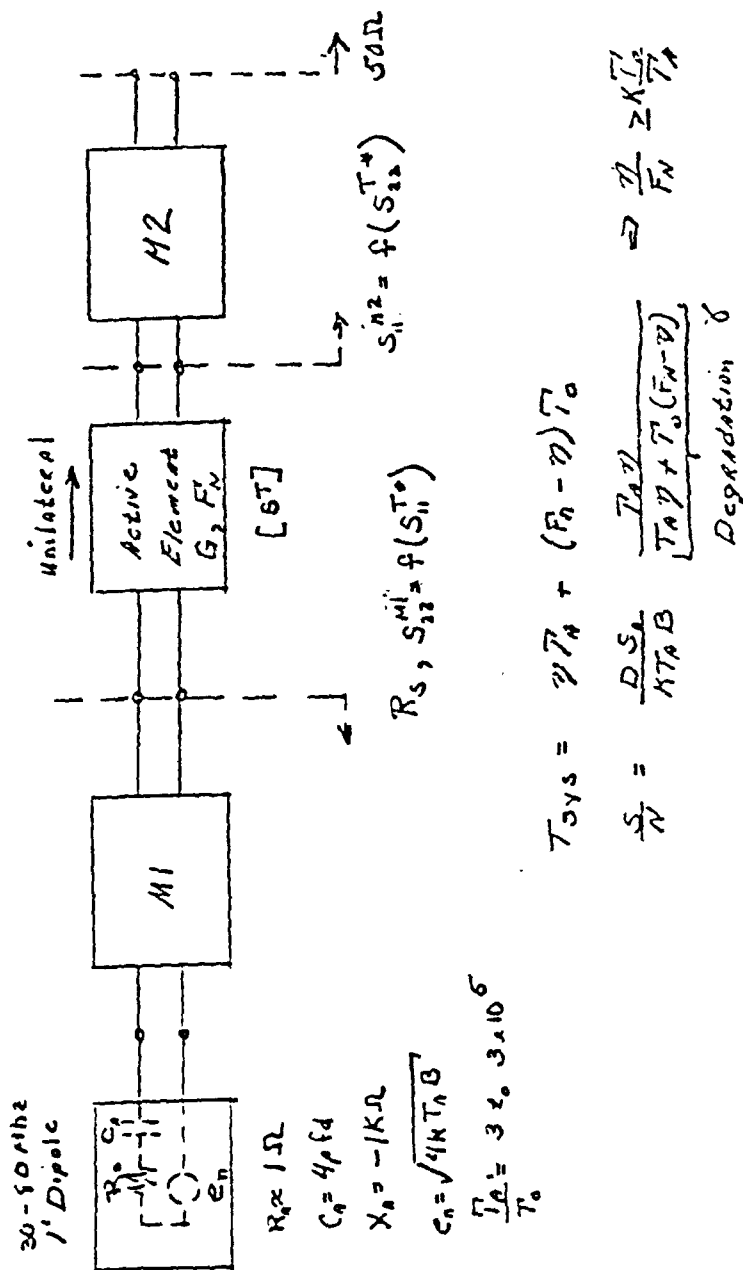
1) Optimize M1 for minimum noise ($R_s \approx 250\Omega$ Bipolar Silicon, $1M\Omega$ FET) and maximum efficiency η and gain.

2) Optimize M2 for maximum gain, gain flatness

Fig. 3 Active antenna configuration for receive only with minimum signal-to-noise

The design objectives for the output matching network M2 in Fig. 3 are the most straightforward. The conjugate match reflection $S_{11}^{M2} = f\left(S_{22}^{T*}\right)$ that M2 presents to the active element output is derived from gain and gain flatness considerations. However, the design of the input matching network M1 is considerably more constrained. Three conditions must be simultaneously satisfied in order to maximize the system signal-to-noise ratio. The design is a compromise between:

1) Minimizing the active element noise figure F_N by adjusting the source resistance R_S to minimize the combined thermal noise $(C_1 R_S)$ and shot noise $(C_2 R_S^{-1})$ of the transistor.

2) Obtaining some power gain by adjusting the reflection coefficient $S_{22}^{M1} = f(S_{11}^{T}*)$ as nearly as possible to the maximum power, conjugate match value. While maximum gain of the active element is not the primary design goal, sufficient gain is required of the first amplifier to eliminate subsequent contributions to the front end noise figure since

$$(2) \qquad F_N = F_{N1} + \frac{\left(F_{N2}-1\right)}{G_1} + \dots$$

3) Maximizing the efficiency η of the antenna and matching network.

There is no unique solution in practice to these multiple requirements. The general condition that must be satisfied for near optimal system signal-to-noise performance is that the degradation factor ν cited in Fig.1 must be as near unity as required. When η is much less than unity this requires

IV-8

(3) $$\frac{n}{F_N} \geq M \frac{T_0}{T_A} .$$

Values of the margin factor M are related to the degradation
γ in Table II.

Table II

Noise Figure Degradation γ
versus
Margin Factor M

γ-dB Loss	M
0.5	8.20
1.0	3.86
2.0	1.71
3.0	1.00
5.0	0.46
10.0	0.11

There are two distinctive features to the low frequency
behavior of electrically small (monopole) antennas and anten-
na noise that have in practice enabled extremely wideband, near
optimal integration into the transistor matching network. The
first is that over the entire low frequency range where the
monopole is less than $\lambda/12$, the reactive portion of the mono-
pole impedance is representable by a well-defined, frequency-
independent capacitance. Therefore, its reactive behavior
in the equivalent circuit of the matching network is simple
and amenable to wideband integration. The second feature is
that the cubic law decrease of the antenna Q with frequency and
increase in untuned efficiency are compensated in part by the de-
crease in the external or antenna noise temperature which is nearly

square law at 20 dB per decade. Thus the terms on both sides of equation (3), η/F_N and T_0/T_A decrease in roughly the same proportion over an extremely wide frequency range because the active element noise figure F_N usually decreases with frequency.

Because of the large reactance that the electrically small antenna presents to the transistor input, FET's with their very high input impedance have been found to be the most suitable for receive active antennas.

The design of the matching networks M1 and M2 for the case of the active transmit antenna as shown in Fig. 4 is much less constrained. The only active element parameter to be optimized is the gain. The matching networks M1 and M2 are derived solely from conjugate match considerations for power gain and gain flatness. The interface of M1 to the input signal must be matched to 50 ohms. Common emitter silicon bipolar transistors have been found to be compatible with the moderate 50 ohm input and high output impedance level requirements for active transmit antennas.

2.0 RF Transistor Amplifier Design

This section reviews some standard design procedures for optimizing the low noise and low power gain of RF transistor amplifiers. The assumption is that the design of an active receiving antenna, for example, is a low noise amplifier design with the additional constraint that the input matching circuit that normally assumes a 50 ohm source must now be designed to accommodate the highly reactive, low resistance source that is presented by an electrically small antenna. The total design is a trade-off between the net gain, noise figure, and antenna
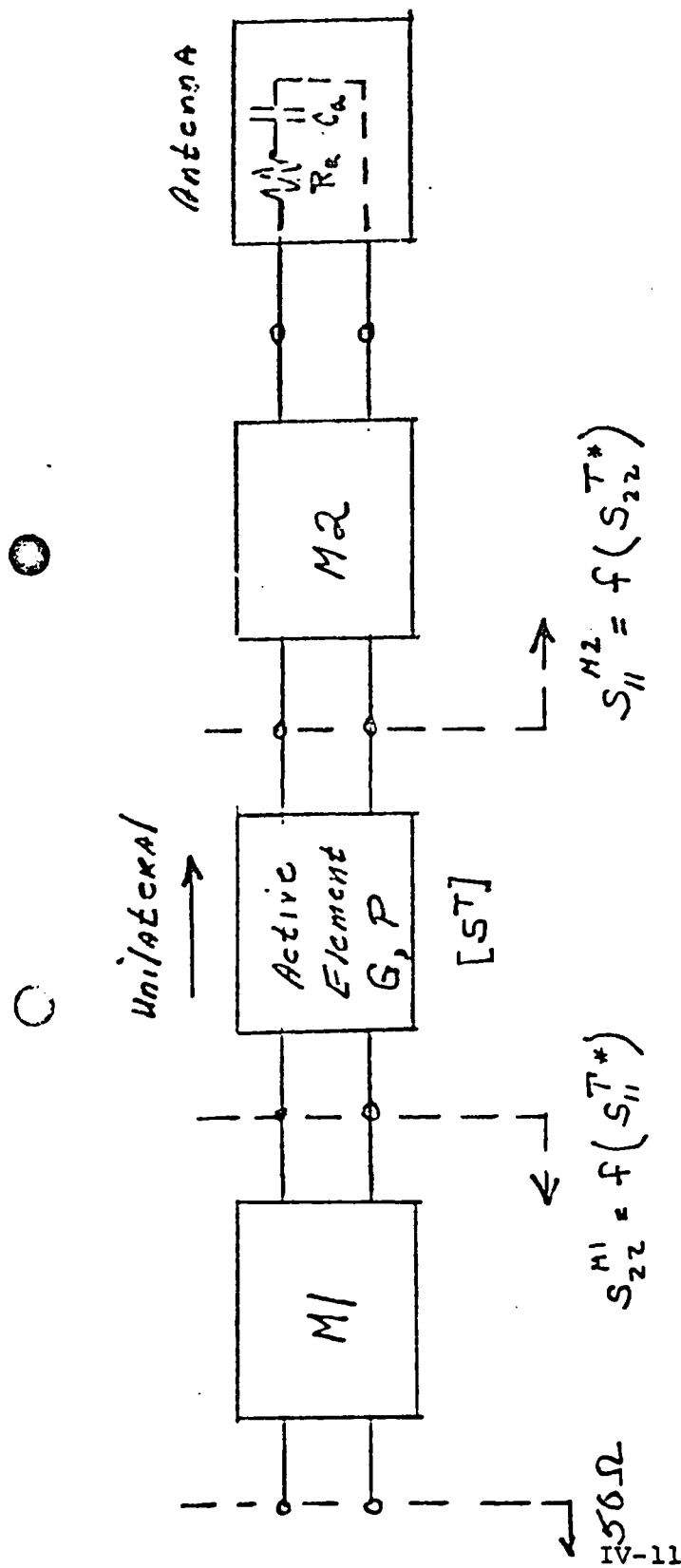
Fig. 4   Active antenna for transmit configuration with optimized output power

efficiency. Such a design is not unique and depends on the ambient noise temperature which at a single frequency can change by as much as 40 dB from electrically quiet to noisy environments.

The left hand side of Fig. 5 gives an idealized low frequency model of a junction transistor in the common base and common emitter configurations [1,10]. The common emitter form is perhaps the most often used because it has both voltage and current gain and input and output impedances that are more nearly compatible for cascading similar stages. The common base configuration has a very low input impedance and high output impedance with nearly unity current gain.

At RF frequencies, the effect of all the parasitic lead inductances, contact resistance, and mutual capacitances must be included. An example of an RF transistor equivalent circuit with all the parasitics included is shown on the right hand side of Fig. 5 [2]. A viable method for dealing with these unavoidable parasitics in the design of RF amplifiers is to characterize the transistor by a complete set of experimental data. In particular, S-parameters have proved to be best suited for RF measurements of transistors because all of the parameters are obtained with matched sources and terminations. This eliminates the possibility of spuriously induced oscillations [3].

The diagram and equations of Fig. 6 define the incident and reflected wave variables (a,b) that are the basis for the S-parameter representation. The matched condition requirement for the measurement of S_{11}, for example, follows from the fact that $a_2 = 0$ implies that port 2 is perfectly terminated. No reflection of the transmitted wave b_2 occurs to reenter the
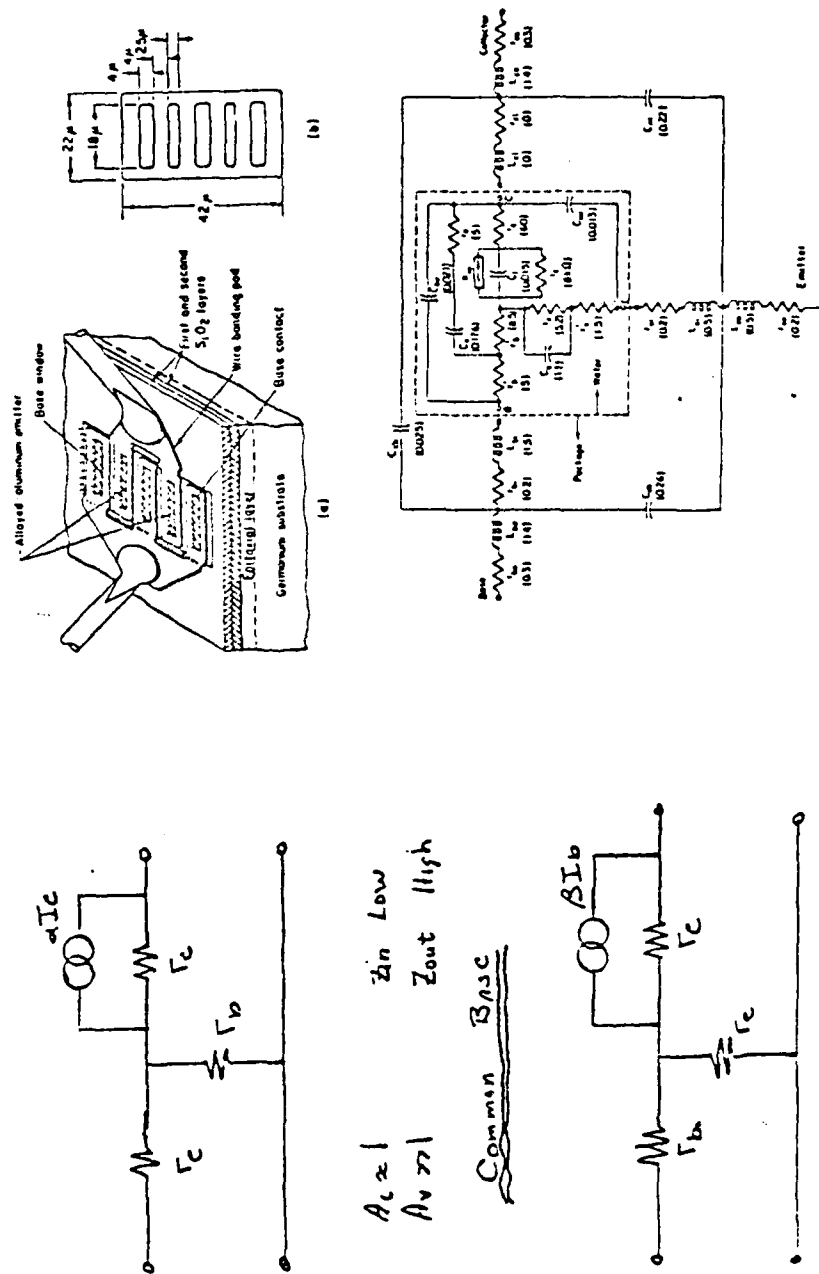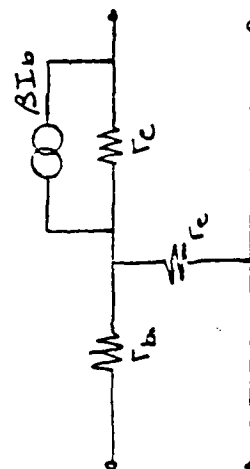
Fig. 5   Low frequency and RF equivalent circuits for bipolar transistor

Two sets of parameters, (a_1, b_1) and (a_2, b_2), represent the incident and reflected waves for the two-port network at terminals 1-1' and 2-2' respectively.

$$a_1 = \frac{1}{2}\left(\frac{V_1}{\sqrt{\bar{Z}_0}} + \sqrt{\bar{Z}_0}\, I_1\right)$$

$$b_1 = \frac{1}{2}\left(\frac{V_1}{\sqrt{\bar{Z}_0}} - \sqrt{\bar{Z}_0}\, I_1\right)$$

$$a_2 = \frac{1}{2}\left(\frac{V_2}{\sqrt{\bar{Z}_0}} + \sqrt{\bar{Z}_0}\, I_2\right)$$

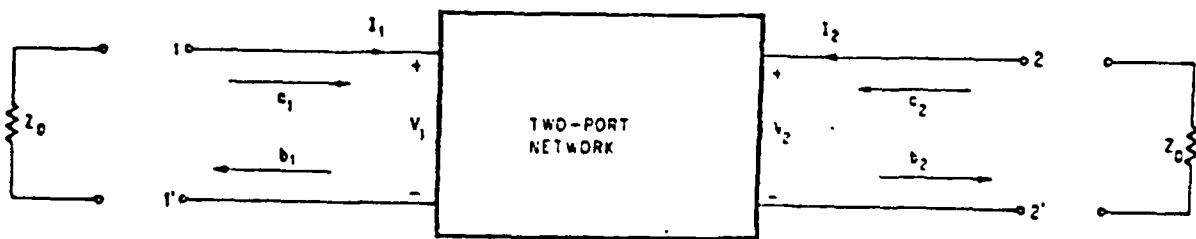$$b_2 = \frac{1}{2}\left(\frac{V_2}{\sqrt{\bar{Z}_0}} - \sqrt{\bar{Z}_0}\, I_2\right)$$

The scattering parameters for the two-port network are given by

$$b_1 = s_{11}\, a_1 + s_{12}\, a_2$$

$$b_2 = s_{21}\, a_1 + s_{22}\, a_2$$

$$s_{11} = \left.\frac{b_1}{a_1}\right|_{a_2 = 0} \qquad s_{12} = \left.\frac{b_1}{a_2}\right|_{a_1 = 0}$$

$$s_{21} = \left.\frac{b_2}{a_1}\right|_{a_2 = 0} \qquad s_{22} = \left.\frac{b_2}{a_2}\right|_{a_1 = 0}$$

Scattering parameters are defined by this representation of a two port network. Two sets of incident and reflected parameters (a_1, b_1) and (a_2, b_2) appear at terminals 1-1' and 2-2' respectively.

Fig. 6 [3]

network and perturb $b_1/a_1 = S_{11}$. The relation of the wave variables (a,b) to the circuit parameters (V,I) is also given in Fig. 6.

Figure 7 presents the measured S-parameters of a small signal, low power, low noise transistor [4]. It is observed that at the low end of the frequency band (100 MHz) the input resistance is slightly less than 50 ohms and has a capacitive reactance. The output impedance level is much higher for both the real and reactive parts. The corresponding forward transmission coefficient S_{21} is around 8. The reverse transmission coefficient S_{12} is about 0.03. The extent to which $|S_{12}S_{21}| << 1$ for a transistor represents the unilateral approximation. This simplifies the amplifier design procedure and enables the transistor to buffer impedance mismatches.

Power Gain Design [3]

Appendix A summarizes the S-parameter relationships that have been developed for the design of RF transistor amplifiers. The major features of that summary are:

- Unilateral Approximation
- Unilateral Figure of Merit – U
- Unilateral Transducer Power Gain.
  This is valid to the extent U is small.
  When it is valid one has

$$G_{TU} = G_{M1} \ G_T \ G_{M2}$$

(4)
$$= \frac{1 - |\Gamma_{M1}|^2}{|1 - S_{11}^T \Gamma_{M1}|^2} \ |S_{21}^T|^2 \ \frac{1 - |\Gamma_{M2}|^2}{|1 - S_{22}^T \Gamma_{M2}|^2} \ .$$

IV-15
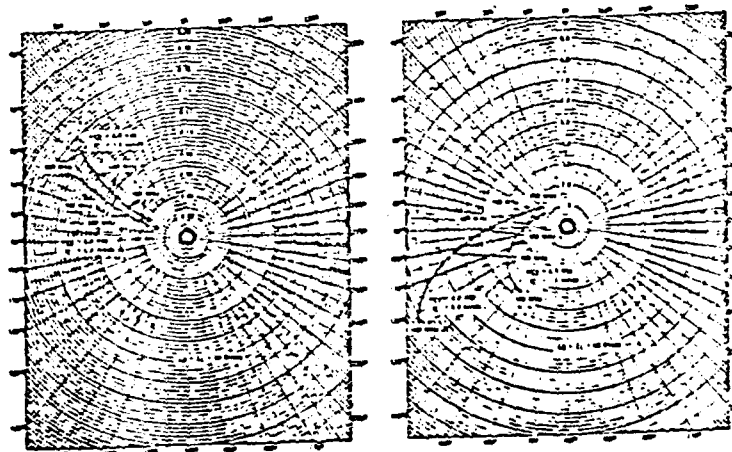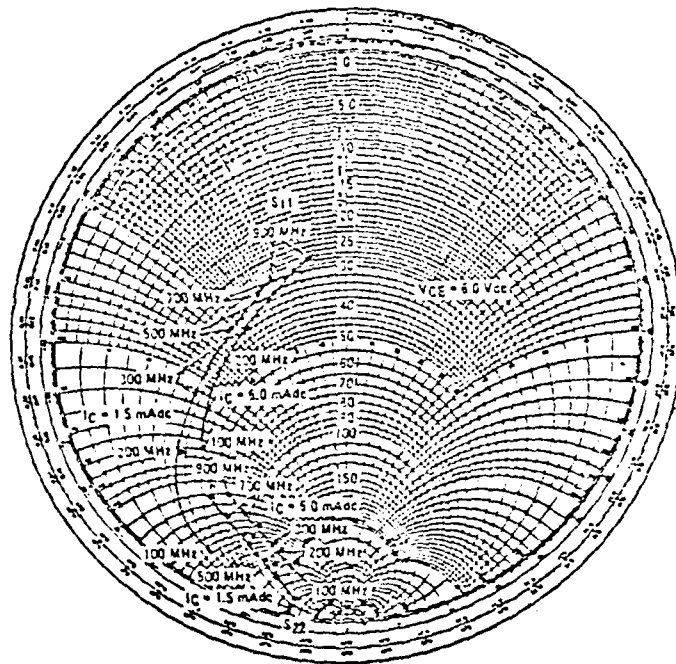
Fig. 7 Silicon RF small signal characteristics,
2N3839 NPN, Motorola RF Data Manual 1978

- Constant Gain Circles on the Smith Chart
- Stability Conditions
- Source and Load for Simultaneous Match.

It is noted that the unilateral power gain as defined by Eq. (4) can exceed the gain of the transistor into a 50 ohm load $G_T = |S_{21}|^2$. When M1 and M2 are conjugate matches one has

$$(5) \quad G_{TU}^{Max} = \frac{G_T}{(1-|S_{11}^T|^2)(1-|S_{22}^T|^2)} \gg G_T.$$

An amplifier designed with a transistor of the S_{21} characteristics shown in Fig. 7 could have a low frequency power gain that exceeds $8^2 = 64$ (18 dB).

The unilateral gain for the characteristics of the transistor displayed in the upper part of Fig. 8 monotonically decrease from a low frequency maximum of 29 dB to 0 dB at 10 GHz. It represents the maximum power that could be obtained when the proper conjugate match impedance is provided at each frequency. Often it is desired to obtain a uniform gain across a frequency band rather than the maximum possible, but monotonically decreasing, gain with frequency. In this case the matching network impedance locus is determined by inspection of the constant gain contours of the conjugate match impedances. The concept of determining the impedance locus from parametric contours on the Smith Chart has been generalized by Meinke et al [9] for noise figure performance and will be reviewed in Section 5.
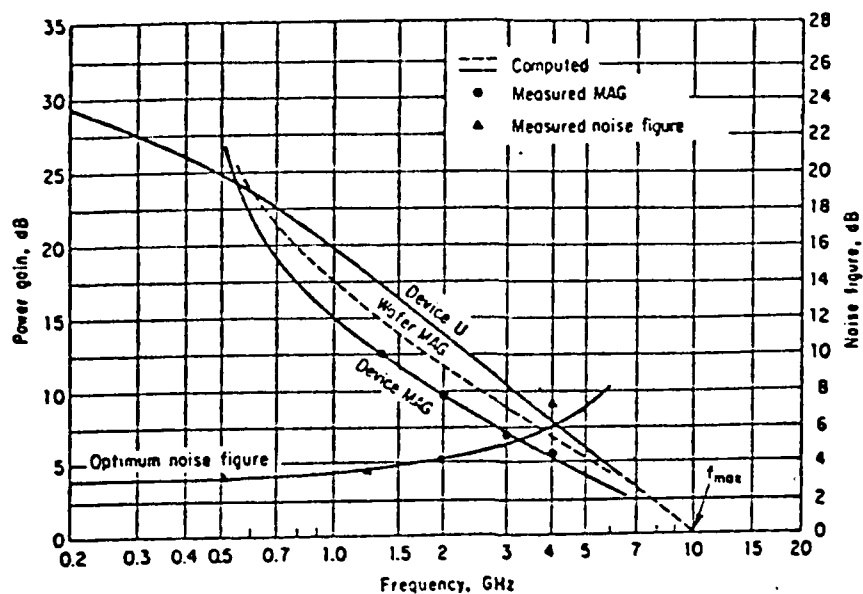
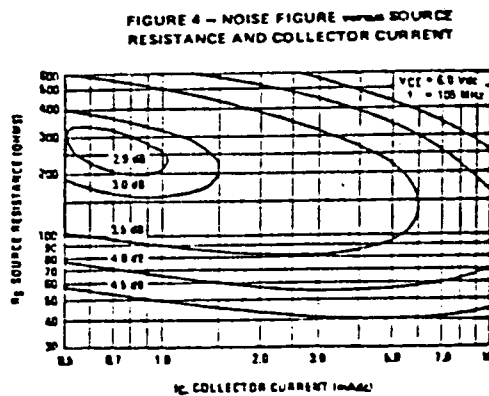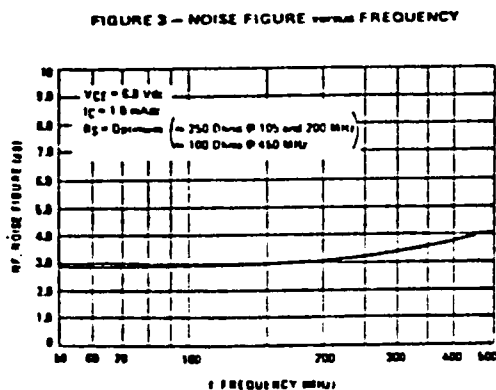Characteristics of microwave transistor as a function of frequency.

FIGURE 3 — NOISE FIGURE versus FREQUENCY

FIGURE 4 — NOISE FIGURE versus SOURCE RESISTANCE AND COLLECTOR CURRENT

Fig. 8   Gain and noise figure characteristics of microwave transistor [2,4]

IV-18

Low Noise Design

The noise performance of a junction transistor has been modeled by Neilson [4]. The expression for the noise figure is

$$
(6) \quad F = 1 + \frac{r_e}{2R_S} + \frac{r_b'}{R_S} + \left[\frac{\left(R_S + r_e + r_b' \right)^2}{2\beta_0 R_S r_e} \right] \left[1 + (\beta_0 + 1)\left(\frac{f}{f_{ab}} \right)^2 \right] .
$$

The noise figure has been shown to be essentially the same for common base and common emitter configurations [6]. It depends on the emitter and base resistances r_e and r_b' and the source resistance R_S in addition to the current gain β_0 and the frequency relative to the common base cut-off frequency f/f_{ab}. Equation (6) represents the effects of two different sources of noise. The first is thermally generated (Johnson) noise that is proportional to an effective resistance

$$
(7) \quad e_n = \sqrt{4kTRB}
$$

and a shot or recombination noise that is proportional to the dc current (and is inversely proportional to R)

$$
(8) \quad i_n = \sqrt{2q \, I_{dc} B} .
$$

Thus as shown by the graph in the lower part of Fig. 8, there is a value of source resistance that minimizes the total noise generated. For the 105 MHz family of curves shown the source resistance for minimum noise is 250 ohms. The other graph shows the frequency dependent increase that becomes evident at around 200 MHz.

This section will summarize selected characteristics of electrically small, low frequency antennas that are pertinent to the design of active antennas. These characteristics are the self-impedance of electric and magnetic dipoles, mutual coupling effects for transmit and receive arrays, and the antenna noise temperature.

3.1 Electric Monopole Impedance

For electrically short heights $k_0 h$, the series impedance of an electric monopole is represented by a frequency dependent resistance R_A and a capacitive reactance X_A [5]

$$(9) \qquad Z_A = R_A + jX_A$$

$$R_A = 10(k_0 h)^2$$

$$X_A = -Z_{0A}\, \cot k_0 h \approx -\frac{Z_{0A}}{k_0 h} = -\frac{1}{\omega C_A}$$

$$(10) \qquad C_A = \frac{h}{\nu_0 Z_{0A}} \quad , \quad C_A\,(\text{pfd}) = \frac{85 h^{in}}{Z_{0A}}$$

$$Z_{0A} = 60\left(\ln\frac{h}{a} - 1\right)$$

$$\nu_0 = 3 \times 10^8\, \text{m/s} = 11.8 \times 10^9\, \text{in/s} \ .$$

For monopoles of heights of 1 to 3 feet and diameters (2a) of 1/16 to 1/8 inch the characteristic impedance Z_{0A} is typically 250 to 350 ohms. The capacitive reactance X_A is adequately

modeled by a capacitance C_A that is of the order of 4 to 3 pfd per foot of length. The short monopole parameters presented in Table I of the Introduction follow from equations (9) and (10) directly. For a dipole antenna R_A, X_A, Z_{0A} and $1/C_A$ are double the corresponding monopole value.

Any antenna illuminated by an incident electric field E^{inc} develops an open circuit voltage that is proportional to its effective length $V^{oc} = E^{inc} \ell_e$ where for short dipoles $\ell_e = h/2$.

3.2 Magnetic Dipole Impedance

A single turn loop antenna of diameter 2R and conductor diameter 2a has a series impedance

(11) $R_A = 200 \, (k_0 R)^4$

$$X_A = \omega \, R\mu_0\left(\ell n \frac{8R}{a} - 2\right) = Z_{0L} (k_0 R) \; ; \; Z_{0L} = \eta_0\left(\ell n \frac{8R}{a} - 2\right).$$

The voltage developed by a small loop antenna is $V^{oc} = \pi R (k_0 R) E^{inc}$.

For small electric and magnetic dipoles the untuned efficiency η is inversely proportional to the Q and is cubic law dependent

(12) $\eta = \dfrac{R_A}{|Z_A|} \approx \dfrac{R_A}{|X_A|} = \dfrac{1}{Q_A}$

$$\eta_A^L = \frac{200}{Z_{0L}} (k_0 R)^3 \; ; \qquad \eta_A^D = \frac{10}{Z_{0A}} (k_0 h)^3 .$$

Both types of dipoles appear to have the same potential for broadband active antennas although the proportionality factor of η differs somewhat.

3.3 Mutual Coupling

The mutual coupling properties of antennas will be analyzed in terms of the S-parameters of the System 1 two element array and System 2 remote probe shown in Fig. 9. In particular the effect of mutual excitations will be explicitly modeled and the equivalence of the transmit and receive impedance verified. In Fig. 9, it is noted that the parameters S_{ij} are measured in the array environment. Thus S_{11} represents the self impedance of antenna 1 in the presence of 2. It is not necessarily identical to S_{11} when 2 is removed and the measurement is repeated for the isolated element.

Transmit Impedance

Let System 1 with antennas 1 and 2 be the transmit system. The input impedance is to be determined for the condition that the excitations are related by a complex constant

(13)
$$a_2 = V_{21} a_1 .$$

The remote probe antenna is well terminated so that $a_3 \equiv 0$. It follows directly from the equation in Fig. 9 that

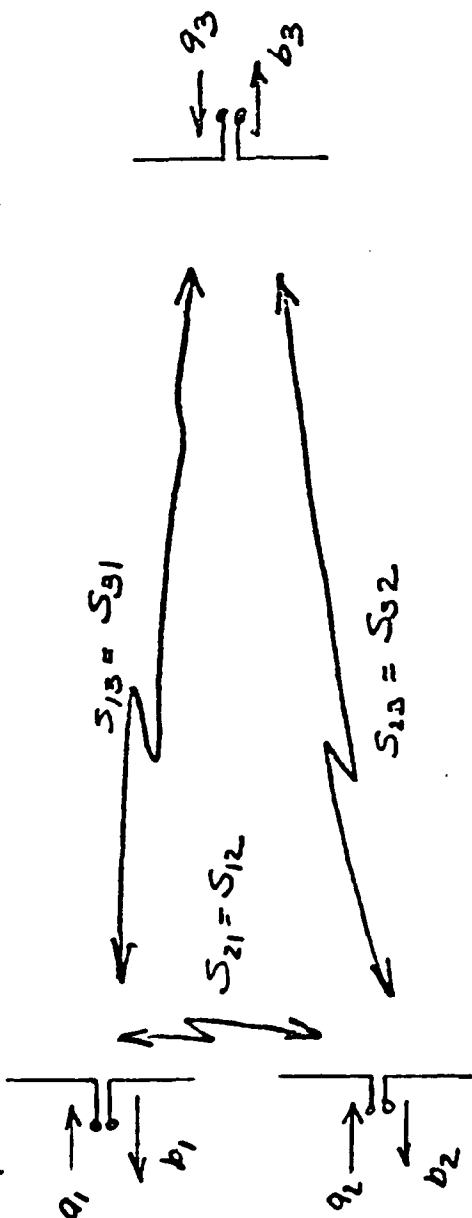(14)
$$\Gamma_{1T} = \frac{b_1}{a_1} = S_{11} + A_{12} V_{21}$$

$$\Gamma_{2T} = \frac{b_2}{a_2} = S_{22} + \frac{S_{21}}{V_{21}} .$$

The input impedance of antenna 1 for transmit is

(15)
$$z_{1T} = \frac{1 + \Gamma_{1T}}{1 - \Gamma_{1T}} = \frac{1 + S_{11} + S_{12} V_{21}}{1 - S_{11} - S_{12} V_{21}} .$$

System 2

a_3 b_3

Receive/Trans

System 1

$S_{13} = S_{31}$

$S_{21} = S_{12}$

$S_{23} = S_{32}$

a_1 b_1 a_2 b_2

Trans/Receive

$b_1 = S_{11} a_1 + S_{12} a_2 + S_{13} a_3$

$b_2 = S_{21} a_1 + S_{22} a_2 + S_{23} a_3$

$b_3 = S_{31} a_1 + S_{32} a_2 + S_{33} a_3$

$S_{ij} = \dfrac{b_i}{a_j}\bigg|_{\substack{a_k=0 \\ k \neq j}}$ $\Big\}$ All ports $k \neq j$ terminated in matched load.

Fig. 9. Transmit/receive system S parameters for array transmit and receive impedance analysis

IV-23

The mutual coupling coefficients $S_{21} = S_{12}$ and the relative excitation strengths V_{21} influence the input impedance as well as S_{11}. Had there been N elements in the array of System 1, the procedure outlined here for two elements could be extended in a straightforward manner without any significant change in the approach or concept.

Receive Impedance

If System 1 is now receiving a signal transmitted from the remote probe, then a_3 is an independent variable and

$$(16) \qquad a_i = \Gamma_i \, b_i \qquad i - 1,2 \, .$$

The source impedance of the Thevenin equivalent of any network is

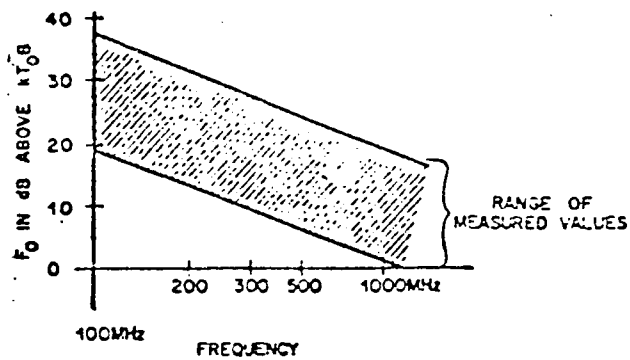$$(17) \qquad z_{iR} = z_{iS} = \frac{V_i^{OC}}{I_i^{SC}} - \frac{b_i^{OC}}{b_i^{SC}} \, .$$

For an open circuit $\Gamma_i = 1$ and for a short circuit $\Gamma_i = -1$. For antenna 1 we obtain

$$(18) \qquad b_i^{OC} = S_{11} \, b_1^{OC} + S_{12} \, V_{21} \, b_1^{OC} + S_{13} \, a_3$$
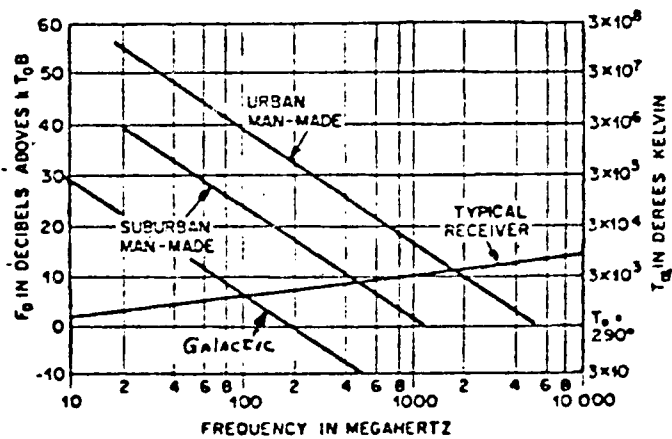
$$b_1^{OC} = \frac{S_{13} a_3}{1 - S_{11} - S_{12} V_{21}}$$

$$b_1^{SC} = \frac{S_{13} a_3}{1 + S_{11} + S_{12} V_{21}}$$

$$\therefore \quad z_{1R} = \frac{1 + S_{11} + S_{12} V_{21}}{1 - S_{11} - S_{12} V_{21}}$$

Composite urban average incidental man-made noise power.

ITT handbook average man-made noise power curves.

Fig. 10   Man-made noise levels

IV-26

80 MHz frequency band, the external noise can exceed the re-
ceiver noise from as little as 1 to 2 dB to as much as 45 dB.
It is noted that all the noise curves increase approximately
20 dB per decade as the frequency is decreased.

When the antenna is lossless, the antenna noise temperature
equals the ambient noise temperature. When the antenna is lossy
with an efficiency η the effective antenna temperature is

$$(20) \qquad T_A{}' = \eta T_A + (1-\eta) T_0.$$

If the ambient noise temperature is very high and is the dominant
source of noise, then the inefficiency of the antenna lessens
the noise as well as the signal.

4.0 System Noise Temperature [5]

When an antenna of noise temperature T_A and efficiency η
is connected to a receiver with a front end noise temperature
$T_R = (F_N-1) T_0$ the system noise temperature is

$$(21) \qquad T_{SYS} = \eta T_A + (1-\eta) T_0 + (F_N-1) T_0$$

$$= \eta T_A + (F_N-\eta) T_0.$$

The system signal-to-noise ratio is

$$(22) \qquad S = GS_0 = DS_0 \eta$$
$$N = KT_{SYS} B$$

$$\frac{S}{N} = \frac{DS_0}{KT_A B} \underbrace{\frac{T_A \eta}{T_A \eta + T_0 (F_N-\eta)}}_{\text{Degradation}}$$

IV-27

So long as $T_A\eta \gg T_0(F_N-\eta)$ the system signal-to-noise ratio will not be appreciably degraded beyond the fundamental limit imposed by the external noise.

5.0 Review of Selected Literature

It appears that the earliest publications of antennas as an integral part of a transistor preamplifier are due to J.R. Copeland. The references cited in his 1964 paper on antenna-fier arrays [7] begin in 1960. In the 1964 publication, the advantages of integrating the antenna into the transistor input matching circuitry to optimize the receive signal-to-noise ratio were discussed in very general terms such as eliminating losses and extra circuit elements. The extremely wideband potential of the integrated antenna transistor network in terms of similar antenna efficiency and external noise characteristics is not explicitly mentioned. Some experimental data is presented for the noise figure of an individual element and a four element array. Pattern measurements were made over a 25% bandwidth. Noise temperature data was presented only for frequencies in the band center near 150 MHz.

Since 1968 an extensive and continuous effort by H.Meinke and H.Lindenmeier of the Technical University of Munich has been in progress. They have systematically analyzed and reduced to practice the optimum wideband SNR potential of active antennas [8,9]. The distinctive feature of their analytical publications on the topic has been the use of contours (circles) of normalized power and SNR in the antenna impedance plane. The case of the constant power curves can be derived rather simply and will be presented as an introduction to their approach. For

the equivalent circuit on the left hand side of Fig.11, the power available to the load impedance Z from the source of impedance Z_S is

$$(23) \qquad P = \frac{V\,V^*\,R}{(Z+Z_S)\,(Z+Z_S)^*}$$

$$= \frac{V\,V^*\,R}{(R+R_S)^2 + (X+X_S)^2} \quad.$$

When $Z = Z_{opt} = Z_0^*$ the maximum power is $\hat{P} = VV^*/4R_0$. Thus

$$(24) \qquad \frac{P}{\hat{P}} = \frac{4R_0}{VV^*} \; \frac{VV^*R}{(R+R_0)^2 + (X-X_0)^2}$$

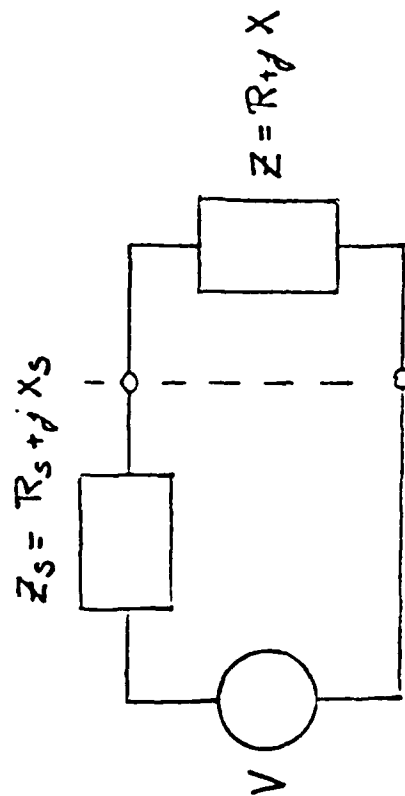$$\doteq \frac{1}{1 + \dfrac{|Z-Z_0|^2}{4R_0R}} \quad.$$

The 3 dB half power contour occurs when the second term in the denominator is unity.

$$(25) \qquad 4RR_0 = (R-R_0)^2 + (X-X_0)^2 \quad.$$

Solving equation (25) when $X = X_0$ yields the maximum and minimum resistance of the contour.
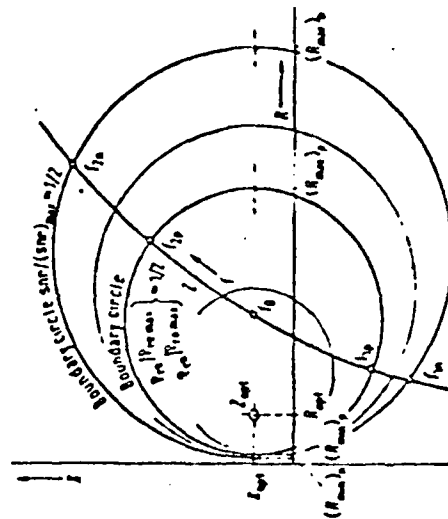
$$(26) \qquad \hat{R} = R_0 \; (3 + \sqrt{8})$$

$$\check{R} = R_0 \; (3 - \sqrt{8})$$

Circles of constant normalized power and are respectively in the antenna impedance plane; Z_{opt} impedance for optimum power and optimum ... respectively. X curve of antenna impedance. $(f_{2p} - f_{1p})$ and $(f_{2a} - f_{1a})$ are the width of the power transmission band and the ... transmission band respectively.

$Z_s = R_s + jX_s$

$Z = R + jX$

$Z_{optimum} = R_s - jX_s$

$P = |I|^2 R = \dfrac{VV^*R}{(R+Z_s)(Z+Z_s)^*}$

Fig. 11 Equivalent circuit for determination of constant power contours in the antenna impedance plane.

The normalized diameter of the contour is

$$(27) \qquad \delta_p = \frac{\hat{R} - \check{R}}{R_0} = 3 + \sqrt{8} - 3 + \sqrt{8} = 4\sqrt{2}.$$

This enables the 3 dB power contour on the right hand side of Fig. 11 to be constructed. In a similar manner Lindenmeier [8] has constructed contours of SNR using the fact that the transistor noise temperature can be represented by

$$(28) \qquad T_T = T_{min} + T_1 \frac{|Z - Z_0|^2}{R\, R_0}.$$

The result comparable to equation (24) for the power contour is

$$(29) \qquad \frac{SNR}{\hat{SNR}} = \frac{1}{1 + \dfrac{|Z - Z_0|^2}{\xi RR_0}}$$

$$\xi = \frac{1 + T_A/T_{min}}{T_1/T_{min}}.$$

The normalized diameter of the 3 dB contour is

$$(30) \qquad \delta_N = \xi\sqrt{1 + 4\xi^{-1}}.$$

Additional results have been derived to include the effects of loss in the antenna and matching network.

The formulation of Hansen [5] which defined the degradation factor ν introduced in Fig. 1 and equation (22) was found to be conceptually helpful. His article written from a system point

of view is brief, but lucid and self-contained. It does not, however, address any of the concepts pertinent to an actual design of the matching network or transistor characterization.

Anderson et al [10,11] appear to be the first to publish a common representation of the transistor and antenna characteristics [z parameters] which can analytically demonstrate the buffering or mutual impedance reduction for active elements in transmit and receive arrays. Experimental results have been published to substantiate the improved bandwidth obtained by the use of active elements for the separate cases of transmit and receive configurations.

Results have also been reported using active elements with loop antennas [12]. The effort was limited to analysis and experimental measurements of the impedance and radiation properties. Noise figure performance was not addressed.

REFERENCES

[1] P.E.Gray, _Introduction to Electronics,_ Wiley 1967

[2] H.A. Watson (Ed), _Microwave Semiconductor Devices and Their Circuit Applications_, McGraw-Hill, 1969

[3] S-Parameter Circuit Analysis and Design, H.P. Application Note 95, September 1968.

[4] Motorola RF Data Manual, 1978.

[5] S.H.Radjy and R.C.Hansen, S/N Performance of Aperiodic Monopoles, pp.259-261, IEEE Trans. AP,March 1979.

[6] A.van der Ziel, _Noise Sources, Characterization, Measurement_, Prentice-Hall, 1970.

[7] J.R.Copeland et al, Antennafier Arrays, pp.227-233, IEEE Trans. A.P.,March 1964.

[8] H.Lindenmeier, Optimum Bandwidth of Signal-to-Noise Ratio of Receiving Systems with Small Antennas, Archiv für Elektronik und Übertragungstechnik, Band 30, 1976.

[9] H.Meinke & H.Lindenmeier,Aktive Empfangsantennen,Lehrstuhl für Hockfrequenztechnk of the Technical University of Munich, March 1977.

[10] A.P.Anderson et al, Note on Transistor-Fed Active Array Antennas, pp 537-539, IEEE Trans. A.P.,July 1971

[11] A.P.Anderson and M.M.Dawoud, The Performance of Transistor Fed Monopoles in Active Antennas, pp.371-374, IEEE Trans. AP,May 1973

[12] P.A. Ramsdale and T.S.M.MacLean, Active Loop Dipole Aerials, pp.1698-1710, Proc.IEE, December 1971.

APPENDIX A

S-Parameter Relationships
for the Design of
RF Transistor Amplifiers

H.P.Application Note 95

Useful Scattering Parameter Relationships

TWO-PORT NETWORK
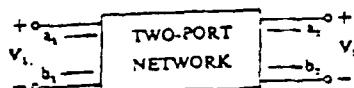
$$b_1 = s_{11}a_1 + s_{12}a_2$$
$$b_2 = s_{21}a_1 + s_{22}a_2$$

Input reflection coefficient with arbitrary Z_L

$$\Gamma_{11} = s_{11} + \frac{s_{12}s_{21}\Gamma_L}{1 - s_{22}\Gamma_L}$$

Output reflection coefficient with arbitrary Z_s

$$\Gamma_{22} = s_{22} + \frac{s_{12}s_{21}\Gamma_s}{1 - s_{11}\Gamma_s}$$

Voltage gain with arbitrary Z_L and Z_s

$$A_v = \frac{V_2}{V_1} = \frac{s_{21}(1 + \Gamma_L)}{(1 - s_{22}\Gamma_L)(1 + s'_{11})}$$

Power Gain $= \dfrac{\text{Power delivered to load}}{\text{Power input to network}}$

$$G = \frac{s_{21}^2(1 - |\Gamma_L|^2)}{(1 - |s_{11}|^2) + |\Gamma_L|^2(|s_{22}|^2 - |D|^2) - 2\,\mathrm{Re}(\Gamma_L N)}$$

Available Power Gain $= \dfrac{\text{Power available from network}}{\text{Power available from source}}$

$$G_A = \frac{s_{21}^2(1 - |\Gamma_s|^2)}{(1 - |s_{11}|^2) + |\Gamma_s|^2(|s_{11}|^2 - |D|^2) - 2\,\mathrm{Re}(\Gamma_s M)}$$

Transducer Power Gain $= \dfrac{\text{Power delivered to load}}{\text{Power available from source}}$

$$G_T = \frac{|s_{21}|^2(1 - |\Gamma_s|^2)(1 - |\Gamma_L|^2)}{|(1 - s_{11}\Gamma_s)(1 - s_{22}\Gamma_L) - s_{12}s_{21}\Gamma_L\Gamma_s|^2}$$

Unilateral Transducer Power Gain ($s_{12} = 0$)

$$G_{Tu} = \frac{|s_{21}|^2(1 - |\Gamma_s|^2)(1 - |\Gamma_L|^2)}{|1 - s_{11}\Gamma_s|^2|1 - s_{22}\Gamma_L|^2}$$

$$= G_0 G_1 G_2$$

$$G_0 = |s_{21}|^2$$

$$G_1 = \frac{1 - |\Gamma_s|^2}{|1 - s_{11}\Gamma_s|^2}$$

$$G_2 = \frac{1 - |\Gamma_L|^2}{|1 - s_{22}\Gamma_L|^2}$$

Maximum Unilateral Transducer Power Gain when $|s_{11}| < 1$ and $|s_{22}| < 1$

$$G_u = \frac{|s_{21}|^2}{(1 - |s_{11}|^2)(1 - |s_{22}|^2)}$$

$$= G_0 G_{1\,max} G_{2\,max}$$

$$G_{i\,max} = \frac{1}{1 - |s_{ii}|^2} \qquad i = 1, 2$$

This maximum attained for $\Gamma_s = s^*_{11}$ and $\Gamma_L = s^*_{22}$

Constant Gain Circles (Unilateral case: $s_{12} = 0$)
— center of constant gain circle is on line between center of Smith Chart and point representing s^*_{11}

— distance of center of circle from center of Smith Chart:

$$r_i = \frac{g_i s_{ii}}{1 - s_{ii}^2(1 - g_i)}$$

— radius of circle:

$$\rho_i = \frac{\sqrt{1 - g_i}(1 - |s_{ii}|^2)}{1 - s_{ii}^2(1 - g_i)}$$

where: $i = 1, 2$

$$\text{and } g_i = \frac{G_i}{G_{i\,max}} = G_i(1 - |s_{ii}|^2)$$

Unilateral Figure of Merit

$$u = \frac{s_{11}s_{22}s_{12}s_{21}}{|(1 - |s_{11}|^2)(1 - |s_{22}|^2)|}$$

Error Limits on Unilateral Gain Calculation

$$\frac{1}{(1 + u)^2} < \frac{G_u}{G_{Tu}} < \frac{1}{(1 - u)^2}$$

Conditions for Absolute Stability

No passive source or load will cause network to oscillate if a, b, and c are all satisfied.

a. $|s_{11}| < 1$, $|s_{22}| < 1$

b. $\left| \dfrac{|s_{22} s_{11}| - |M^*|}{|s_{11}|^2 - |D|^2} \right| > 1$

c. $\left| \dfrac{|s_{11} s_{22}| - |N^*|}{|s_{22}|^2 - |D|^2} \right| > 1$

Condition that a two-port network can be simultaneously matched with a positive real source and load:

$K > 1$ or $C < 1$

$C =$ Linvill C factor

Linvill C Factor

$C = K^{-1}$

$K = \dfrac{1 + |D|^2 - |s_{11}|^2 - |s_{22}|^2}{2\,|s_{12} s_{21}|}$

Source and Load for Simultaneous Match

$$\Gamma_{mS} = M^* \left[\frac{B_1 \pm \sqrt{B_1^2 - 4\,|M|^2}}{2\,|M|^2} \right]$$

$$\Gamma_{mL} = N^* \left[\frac{B_2 \pm \sqrt{B_2^2 - 4\,|N|^2}}{2\,|N|^2} \right]$$

Where $B_1 = 1 + |s_{11}|^2 - |s_{22}|^2 - |D|^2$

$B_2 = 1 + |s_{22}|^2 - |s_{11}|^2 - |D|^2$

Maximum Available Power Gain

If $K > 1$,

$$G_{A\,max} = \left| \frac{s_{21}}{s_{12}} (K \pm \sqrt{K^2 - 1}) \right|$$

$K = C^{-1}$

$C =$ Linvill C Factor

(Use plus sign when B_1 is positive, minus sign when B_1 is negative. For definition of B_1, see 'Source and Load for Simultaneous Match' elsewhere in this table.)

$$D = s_{11} s_{22} - s_{12} s_{21}$$

$$M = s_{11} - D\,s^*_{22}$$

$$N = s_{22} - D\,s^*_{11}$$

s-parameters in terms of h-, y-, and z-parameters	h-, y-, and z-parameters in terms of s-parameters
$s_{11} = \dfrac{(z_{11}-1)(z_{22}+1) - z_{12} z_{21}}{(z_{11}+1)(z_{22}+1) - z_{12} z_{21}}$	$z_{11} = \dfrac{(1+s_{11})(1-s_{22}) + s_{12} s_{21}}{(1-s_{11})(1-s_{22}) - s_{12} s_{21}}$
$s_{12} = \dfrac{2 z_{12}}{(z_{11}+1)(z_{22}+1) - z_{12} z_{21}}$	$z_{12} = \dfrac{2 s_{12}}{(1-s_{11})(1-s_{22}) - s_{12} s_{21}}$
$s_{21} = \dfrac{2 z_{21}}{(z_{11}+1)(z_{22}+1) - z_{12} z_{21}}$	$z_{21} = \dfrac{2 s_{21}}{(1-s_{11})(1-s_{22}) - s_{12} s_{21}}$
$s_{22} = \dfrac{(z_{11}+1)(z_{22}-1) - z_{12} z_{21}}{(z_{11}+1)(z_{22}+1) - z_{12} z_{21}}$	$z_{22} = \dfrac{(1+s_{22})(1-s_{11}) + s_{12} s_{21}}{(1-s_{11})(1-s_{22}) - s_{12} s_{21}}$
$s_{11} = \dfrac{(1-y_{11})(1+y_{22}) + y_{12} y_{21}}{(1+y_{11})(1+y_{22}) - y_{12} y_{21}}$	$y_{11} = \dfrac{(1+s_{22})(1-s_{11}) + s_{12} s_{21}}{(1+s_{11})(1+s_{22}) - s_{12} s_{21}}$
$s_{12} = \dfrac{-2 y_{12}}{(1+y_{11})(1+y_{22}) - y_{12} y_{21}}$	$y_{12} = \dfrac{-2 s_{12}}{(1+s_{11})(1+s_{22}) - s_{12} s_{21}}$
$s_{21} = \dfrac{-2 y_{21}}{(1+y_{11})(1+y_{22}) - y_{12} y_{21}}$	$y_{21} = \dfrac{-2 s_{21}}{(1+s_{11})(1+s_{22}) - s_{12} s_{21}}$
$s_{22} = \dfrac{(1+y_{11})(1-y_{22}) + y_{12} y_{21}}{(1+y_{11})(1+y_{22}) - y_{12} y_{21}}$	$y_{22} = \dfrac{(1+s_{11})(1-s_{22}) + s_{12} s_{21}}{(1+s_{11})(1+s_{22}) - s_{12} s_{21}}$
$s_{11} = \dfrac{(h_{11}-1)(h_{22}+1) - h_{12} h_{21}}{(h_{11}+1)(h_{22}+1) - h_{12} h_{21}}$	$h_{11} = \dfrac{(1+s_{11})(1+s_{22}) - s_{12} s_{21}}{(1-s_{11})(1+s_{22}) + s_{12} s_{21}}$
$s_{12} = \dfrac{2 h_{12}}{(h_{11}+1)(h_{22}+1) - h_{12} h_{21}}$	$h_{12} = \dfrac{2 s_{12}}{(1-s_{11})(1+s_{22}) + s_{12} s_{21}}$
$s_{21} = \dfrac{-2 h_{21}}{(h_{11}+1)(h_{22}+1) - h_{12} h_{21}}$	$h_{21} = \dfrac{-2 s_{21}}{(1-s_{11})(1+s_{22}) + s_{12} s_{21}}$
$s_{22} = \dfrac{(1-h_{11})(1-h_{22}) + h_{12} h_{21}}{(h_{11}+1)(h_{22}+1) - h_{12} h_{21}}$	$h_{22} = \dfrac{(1-s_{11})(1-s_{22}) - s_{12} s_{21}}{(1-s_{11})(1+s_{22}) + s_{12} s_{21}}$

The h-, y-, and z-parameters listed above are all normalized to Z_0. If h, y, and z are the actual parameters, then

$z_{11}' = z_{11} Z_0$	$y_{11}' = \dfrac{y_{11}}{Z_0}$	$h_{11}' = h_{11} Z_0$
$z_{12}' = z_{12} Z_0$	$y_{12}' = \dfrac{y_{12}}{Z_0}$	$h_{12}' = h_{12}$
$z_{21}' = z_{21} Z_0$	$y_{21}' = \dfrac{y_{21}}{Z_0}$	$h_{21}' = h_{21}$
$z_{22}' = z_{22} Z_0$	$y_{22}' = \dfrac{y_{22}}{Z_0}$	$h_{22}' = \dfrac{h_{22}}{Z_0}$

Transistor Frequency Parameters

f_t = frequency at which $|h_{fe}|$

= $|h_{21}|$ for common-emitter configuration = 1

f_{max} = frequency at which $G_{A\,max}$ = 1